

# Resistive switching in polymer-metal oxide diodes for electronic memory applications

**Citation for published version (APA):**

Verbakel, F. (2008). *Resistive switching in polymer-metal oxide diodes for electronic memory applications*. [Phd Thesis 1 (Research TU/e / Graduation TU/e), Chemical Engineering and Chemistry]. Technische Universiteit Eindhoven. <https://doi.org/10.6100/IR633791>

**DOI:**

[10.6100/IR633791](https://doi.org/10.6100/IR633791)

**Document status and date:**

Published: 01/01/2008

**Document Version:**

Publisher's PDF, also known as Version of Record (includes final page, issue and volume numbers)

**Please check the document version of this publication:**

- A submitted manuscript is the version of the article upon submission and before peer-review. There can be important differences between the submitted version and the official published version of record. People interested in the research are advised to contact the author for the final version of the publication, or visit the DOI to the publisher's website.
- The final author version and the galley proof are versions of the publication after peer review.
- The final published version features the final layout of the paper including the volume, issue and page numbers.

[Link to publication](#)

**General rights**

Copyright and moral rights for the publications made accessible in the public portal are retained by the authors and/or other copyright owners and it is a condition of accessing publications that users recognise and abide by the legal requirements associated with these rights.

- Users may download and print one copy of any publication from the public portal for the purpose of private study or research.
- You may not further distribute the material or use it for any profit-making activity or commercial gain
- You may freely distribute the URL identifying the publication in the public portal.

If the publication is distributed under the terms of Article 25fa of the Dutch Copyright Act, indicated by the "Taverne" license above, please follow below link for the End User Agreement:

[www.tue.nl/taverne](http://www.tue.nl/taverne)

**Take down policy**

If you believe that this document breaches copyright please contact us at:

[openaccess@tue.nl](mailto:openaccess@tue.nl)

providing details and we will investigate your claim.

RESISTIVE SWITCHING  
IN POLYMER – METAL OXIDE DIODES  
FOR  
ELECTRONIC MEMORY APPLICATIONS



RESISTIVE SWITCHING  
IN POLYMER – METAL OXIDE DIODES  
FOR  
ELECTRONIC MEMORY APPLICATIONS

PROEFSCHRIFT

ter verkrijging van de graad van doctor aan de Technische Universiteit  
Eindhoven, op gezag van de Rector Magnificus, prof.dr.ir. C.J. van Duijn,  
voor een commissie aangewezen door het College voor Promoties in het  
openbaar te verdedigen op woensdag 16 april 2008 om 16.00 uur

door

Frank Verbakel

geboren te Helmond

Dit proefschrift is goedgekeurd door de promotoren:

prof.dr.ir. R.A.J. Janssen

en

prof.dr. D.M. de Leeuw

Copromotor:

dr. S.C.J. Meskers

Omslagontwerp: Frank Verbakel

Druk: Gildeprint Drukkerijen B.V. te Enschede

A catalogue record is available from the Eindhoven University of Technology Library

ISBN: 978-90-386-1238-6

This research forms part of the research programme of the Dutch Polymer Institute (DPI), Technology Area Functional Polymer Systems, DPI project #523.



# Table of contents

<b>Chapter 1</b>	<b>Introduction: resistive switching in polymers and inorganic materials</b>	
1.1	Introduction	2
1.2	Memory devices	2
1.3	Resistive switching	4
1.4	Semiconducting materials for resistive switching	6
1.5	Aim and outline of the thesis	12
1.6	References	13
<b>Chapter 2</b>	<b>Electronic memory effects in a sexithiophene poly(ethylene oxide) block copolymer doped with NaCl. Combined diode and resistive switching behavior</b>	
2.1	Introduction	20
2.2	Cyclic voltammetry and spectroscopic analysis	21
2.3	Current-voltage characterization	23
2.4	Electrical hysteresis	26
2.5	Electroluminescence	31
2.6	Conclusion	32
2.7	Experimental	32
2.8	References	33
<b>Chapter 3</b>	<b>Electronic memory effects in diodes from a zinc oxide nanoparticle –polystyrene hybrid material</b>	
3.1	Introduction	36
3.2	Current-voltage characterization	36
3.3	Resistive switching	37
3.4	Forming process	39
3.5	Conclusion	41
3.6	Experimental	42
3.7	References	42
<b>Chapter 4</b>	<b>Electronic memory effects in diodes of zinc oxide nanoparticles in a matrix of polystyrene or poly(3-hexylthiophene)</b>	
4.1	Introduction	46
4.2	Mobile charge carriers in ZnO	47
4.3	Diodes with ZnO:PS as active layer	50
4.4	Diodes with ZnO:P3HT as active layer	57
4.5	Discussion	60
4.6	Conclusion	61
4.7	Experimental	61
4.8	References	62
<b>Chapter 5</b>	<b>Surface modification of zinc oxide nanoparticles induces electronic memory effects in ZnO - polystyrene diodes.</b>	
5.1	Introduction	68
5.2	Diodes with various ligands	68
5.3	Frequency dependence	71
5.4	Temperature dependence	72
5.5	Conclusion	74
5.6	Experimental	74
5.7	References	74

<b>Chapter 6</b>	<b>Anomalous resistive switching at the percolation limit of ZnO nanoparticle – polymer diodes</b>	
6.1	Introduction	78
6.2	Monitoring ligand binding	79
6.3	Influence of surface modification on the morphology	82
6.4	Electronic properties of diodes with surface modified ZnO particles	83
6.5	Discussion	91
6.6	Conclusion	93
6.7	Experimental	93
6.8	References	95
<b>Chapter 7</b>	<b>Reproducible resistive switching in non-volatile organic memories</b>	
7.1	Introduction	100
7.2	Forming process	100
7.3	Al <sub>2</sub> O <sub>3</sub> layer thickness	102
7.4	Conclusion	105
7.5	Experimental	105
7.6	References	106
<b>Chapter 8</b>	<b>Switching dynamics in non volatile polymer memories</b>	
8.1	Introduction	108
8.2	Negative differential resistance	108
8.3	Switching dynamics	110
8.4	Conclusion	112
8.5	Experimental	113
8.6	References	113
<b>Chapter 9</b>	<b>Resistive switching in organic memories with a spin coated metal oxide nanoparticle layer</b>	
9.1	Introduction	116
9.2	Spin coated Al <sub>2</sub> O <sub>3</sub> nanoparticles	116
9.3	Various metal oxides nanoparticles	118
9.4	Conclusion	120
9.5	Experimental	121
9.6	References	121
<b>Chapter 10</b>	<b>Negative differential resistance and resistive switching in polymer - aluminum oxide diodes</b>	
10.1	Introduction	124
10.2	Voltage-current and current-voltage characteristics	124
10.3	Time domain measurements	127
10.4	Frequency domain methods	130
10.5	Filaments	134
10.6	Discussion	135
10.7	Conclusion	144
10.8	Experimental	145
10.9	References	145
Summary		
Samenvatting		
Curriculum Vitae		
Dankwoord		





# 1

**Introduction: resistive switching in  
polymers and inorganic materials**

## **1.1. Introduction**

Nowadays computers are used in almost every household and company. Various components in computers are used for data storage, for example hard drive, work memory (Dynamic random access memory, DRAM), USB stick (flash memory), CD, and DVD. Although all these devices are used to store data, the method of storages differs. Worldwide there is an enormous effort to develop new memory devices that combine the best properties of the leading technologies. This means high speed of DRAM, non-volatility of flash memory, and the low cost and high data density of hard drives. The targeted memory should be non-volatile with long retention time and high programming cycle endurance. Moreover, writing and reading should be fast and non-destructive. Its functionality should be based on resistive switching, since it offers the possibility for large current modulations and for downscaling.

In this chapter a short introduction on some commonly used data storage techniques will be provided. Novel types of memory cells involving inorganic materials and polymers currently under development will be discussed.

## **1.2. Memory devices**

Different types of digital electronic memory devices exist. Magnetic storage (Magnetoresistive Random Access Memory, MRAM) is used in the hard drive of the computer, but was also used in tape recorders for e.g. audio and video. The discovery of the giant magnetoresistance by Fert<sup>1</sup> and Grünberg<sup>2</sup> in 1988, for which they received the Nobel Prize in Physics in 2007,<sup>3</sup> increased the potential of this storage technique greatly. A very weak change in magnetic field gives rise to major differences in electrical resistance in these systems. A system of this kind is the perfect tool for reading data from hard disks when information registered magnetically has to be converted to electric current. MRAM<sup>4-8</sup> is also widely used in some specific applications, such as bank checks and payment cards.

The CD-ROM (Compact Disc – Read Only Memory) is a form of optical storage<sup>9</sup> and in fact is an improvement of the mechanical punch card memories. A laser is used to read the pits on a flat surface. The Digital Versatile Disc (DVD) and Blu-Ray are recent improvements, which allow for higher data densities. The rewritable “CD-ROM” uses a phase change alloy<sup>10-14</sup> to produce reflection differences, creating “1” and “0”. A disadvantage of MRAM and optical memories is the slow speed with which these memories can be addressed.

Electronic memories are also commonly used. DRAM and flash memory are some examples. DRAM stores a bit of data by charging a capacitor. Because these capacitors leak charge, the information eventually fades unless the capacitor charge is refreshed periodically ( $<100$  ms). Therefore this memory type is volatile. However, this type of memories is one of the fastest addressable types ( $\sim 20$  ns). Flash memory stores information in an array of floating-gate transistors. These gates can store their charge for a long time in contrast to capacitors and therefore this can be used as a non-volatile memory, but unfortunately the addressing is much slower than for DRAM.

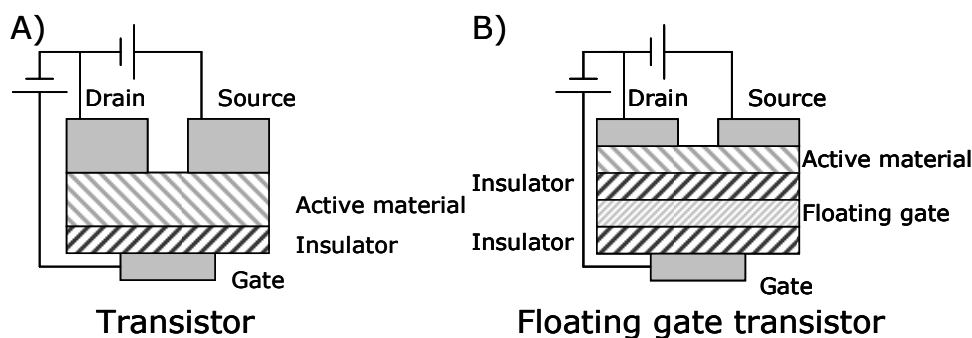


**Figure 1.1:** Schematic representation of a transistor (a) and a floating gate transistor (b) structure.

Flash memory uses transistors to store information. The transistor structure (Figure 1.1a) consists of three electrodes; source, drain and gate. An isolating material, often  $\text{SiO}_2$ , is used to enable the possibility to apply a field between gate and drain without current flowing. With this field between the gate and drain, the current between source and drain can be controlled. The active material can be either an  $n$ -type or  $p$ -type semiconductor.

In a floating gate transistor (Figure 1.1b), the charge introduced by the gate voltage can be stored in the floating gate.<sup>15</sup> The gate field will charge or discharge the floating gate. The charge will remain trapped until a gate field is applied. This makes this memory type non-volatile. The current between the source and drain is now controlled by the charge state of floating gate. In a "normal" transistor the gate field switches the current between the source and drain on or off. However, this is not a permanent change, when the field is removed the current is also reduced. In a floating gate transistor additional layers are required to retain the data.

Instead of a floating gate, a single layer of a ferroelectric material can be used to store charge. In ferroelectric memories (Ferroelectric Random Access Memory, FeRAM), the dielectric is replaced by a ferroelectric material. The dipole of this material can be switched by the gate field and remains in this state until another gate field is applied. Inorganic materials<sup>16-20</sup> and polymers can be used as ferroelectric material.

Polyvinylidene fluoride (PVDF) and its copolymers with trifluoroethylene (TrFE) are commonly used as polymeric ferroelectric.<sup>21-23</sup>

### 1.3. Resistive switching

In applications there is a continuing demand for higher densities in data storage. One approach to minimize the size or area needed for a single active memory cell is to use a device architecture which requires few electrodes, preferably fewer than the three used in transistor type memory cells as discussed above. A possibility which is currently being investigated intensively is to use a diode structure with just two electrodes (Figure 1.2). With this design, information has to be written, read and preferably also erased by application of voltage differences over the same two electrodes. A particular solution is to use materials that show *resistive switching*, i.e. materials whose electrical resistivity can be altered by applying high voltage pulses and read out using a low voltage.

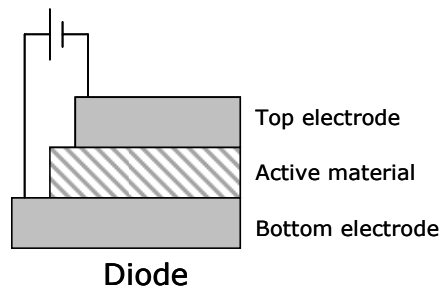


**Figure 1.2:** Schematic display of a diode structure.

The example of DNA<sup>24</sup> shows that high information densities are in principle possible by storing information at the molecular level. DNA contains the genetic instructions necessary for the development and functioning of all known living organisms. This prospect of data storage at the molecular level has inspired people to investigate very small resistive switching diodes in which single molecules act as the active element.<sup>25-28</sup> However, this development is still in a very preliminary stage. Many research efforts still focus on finding materials which show resistive switching in their 'bulk' state and on understanding the physical mechanism behind this peculiar effect. Also this thesis focuses on resistive switching in diodes with macroscopic lateral dimensions, leaving miniaturization as future challenge.

Resistive memories use a change in the resistance of the device by application of bias voltage.<sup>29</sup> Readout is usually performed using low voltages, and hence for a working memory electrical bistability is required. A high conductivity (ON) state and a low conductivity (OFF) state should be distinguishable, and, of course, the actual state of the diode should depend on the history of the device. The ratio between the measured

electrical currents upon application of the read voltage for the two different states is called the ON/OFF ratio. A resistive memory cell can be further characterized by several other parameters; *the switching time* is the minimal time required to induce a change to the other resistive state. *The retention time* is the time after preparation of the two different resistance states after which the states can no longer be differentiated from one another. Furthermore also the characteristic time scales needed to write, erase and read the memory states are of importance. Finally, we can distinguish between memories with destructive and non-destructive readout of the memory state, and between rewritable and write-once memories (e.g. WORM – Write Once Read Many memories).<sup>30,31</sup>

The most economic solid-state memory is a cross-point array or passive matrix array schematically presented in Figure 1.3. This layout achieves high density data storage.<sup>32-34</sup> The storage medium is sandwiched between two layers of electrodes. The row with the top electrodes is rotated 90° with respect to the row of bottom electrodes. The cross-section of the electrodes is the active cell area. The rows then form the word and bit lines. For the storage medium resistive switching is preferred as it has the advantage of high ON/OFF resistance ratios and non-destructive read-out. Using an unpatterned storage medium a passive matrix array is simple to make because it does not require strict alignment and is used in displays.<sup>35</sup> By selecting the appropriate word and bit line, the logic value of a cell may be read by sensing the resistance. The area required for a memory cell based on a diode structure (Figure 1.2) is smaller than for cells with in a transistor array. The density is optimal because each cell occupies an area of  $4f^2$ , where  $f$  is the smallest feature size that can be achieved with the particular fabrication method used (e.g. photolithography).<sup>36</sup> Memories that use these arrays are being explored.<sup>37,38</sup> This design poses additional requirements to the memory element. A very important prerequisite is a diode functionality and two states with different resistance at the read voltage under forward bias. The diode functionality ensures that there will be always one diode in the blocking direction in the cross talk loops, such that the current flowing via these loops is minimized. This then allows for selective readout of the resistance of an individual cell in the forward direction. Therefore the hysteresis in conductivity (ON and OFF state) should also be in forward bias.

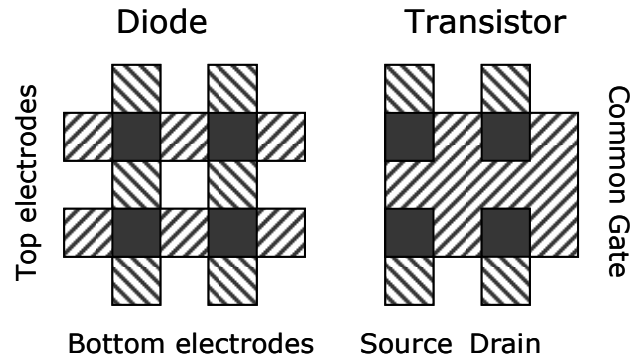


**Figure 1.3:** Top view of a passive matrix array of diode structure, showing 4 cells and the top view of a transistor structure, showing 2 transistors with a common gate.

This thesis focuses on the development of memory cells based on the diode structure and resistive switching. For resistive switching (semi)conducting materials are needed whose resistance can be switched.

#### 1.4. Semiconducting materials for resistive switching

A semiconducting material has an energy gap between the valence band (VB) and the conduction band (CB) (Figure 1.4). The VB is filled with electrons, while no electrons are present in the CB. When the band gap is reduced to zero, a metal is obtained and when the band gap is increased the material can eventually be called an insulator. For molecular materials the band picture is less appropriate because charge carriers are localized and move by hopping motion. In these materials there is generally a considerable energy gap between the highest occupied molecular orbital (HOMO) and the lowest unoccupied molecular orbital (LUMO) of the molecule making up the material. This gap corresponds to the band gap in inorganic semiconductors.

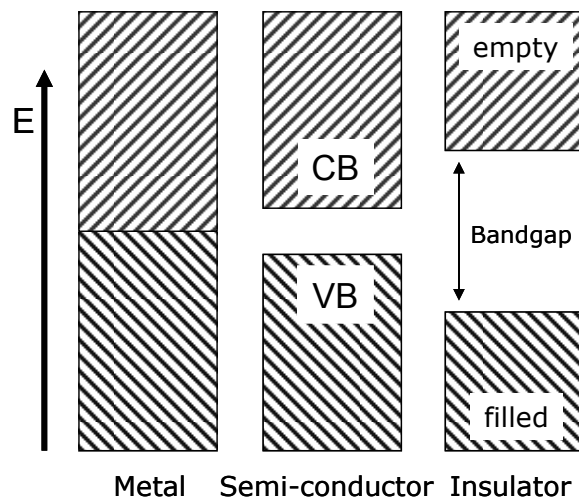


**Figure 1.4:** Band structure of a metal, semiconductor and an insulator, showing a filled valence band (VB) and an empty conduction band (CB).





### Polymer based memories

One of the first reported polymer based resistive switching memory cells is a metal-insulator-metal (MIM) diode with Pb electrodes and poly(divinylbenzene) as polymer.<sup>50</sup> These devices show resistive switching of orders of magnitude. The switching can be induced by pulses with a width of microseconds. A review of organic and polymeric devices showing resistance switching has been written by Scott et al.<sup>51</sup> Switching in various polymers<sup>52,53</sup> (e.g. polystyrene,<sup>54,55</sup> polyacetylene, polyaniline) has been observed already in the 1970s. In semiconducting polymers, like poly(vinylcarbazole),<sup>56</sup> poly(thiophene),<sup>57,58</sup> poly(spirofluorene)<sup>59</sup> and poly(phenylene vinylene)<sup>60</sup> similar switching is observed. Also small molecule semiconductors, such as anthracene,<sup>61</sup> pentacene,<sup>62</sup> Alq3,<sup>63,64</sup> TPD,<sup>65</sup> AIDCN,<sup>66</sup> have been incorporated in MIM diodes and show memory effects. Especially copper tetracyanoquinodimethane (CuTCNQ) has been studied extensively.<sup>67-73</sup> No general theory or explanation for the resistive switching in these polymers and molecular materials has been given in literature and the relationship between polymer or molecular chemical structure is not clear. Recently these memory effects have been related to the specific use of Al as top electrode.<sup>59,65,74,75</sup> The switching effects are then ascribed to native Al<sub>2</sub>O<sub>3</sub>, formed during evaporation.

For some  $\pi$ -conjugated polymer films that are doped with inorganic salts, memory effects have been reported.<sup>76-78</sup> For this particular class of polymer films, the effects can be interpreted in terms of movement of the inorganic ions, a notion that is supported by the observation of relatively slow and gradual changes in conductivity. Another type of conjugated polymer memories, for which a mechanistic explanation of the switching has been established are the polymer fuses.<sup>30,79</sup> Here the conductivity displayed by conducting polymers (e.g. PEDOT:PSS, polyaniline) can be reduced irreversibly by chemical degradation as a result of Joule heating. These memories classify as WORM.

The inclusion of nanoparticles of different types, like Al<sup>80,81</sup> or Au<sup>37,82-86</sup> and the incorporation of a metal inter layer sandwiched between organic or polymeric layers has been investigated as a means to induce memory effects.<sup>86-88</sup> In Figure 1.6 a typical current-voltage ( $J$ - $V$ ) characteristic is given, showing the bistability (ON and OFF-state) at low voltages, the threshold voltage ( $V_{th}$ ) above which the device is switched on. As well as the corresponding write ( $V_{ON}$ ) and erase bias voltages ( $V_{OFF}$ ) at which the device is switched on and off, respectively.

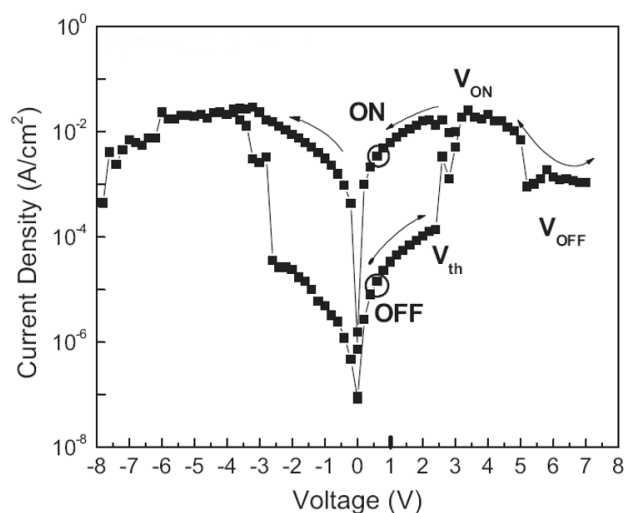


**Figure 1.6:** A typical  $J$ - $V$  characteristic of an organic device with nanoparticles, ITO/polymer: Au-np/Al by Bozano et al.<sup>37</sup>

Mechanisms to explain memory effects in polymer films with metal nanostructures have been proposed by various groups. The involvement of defects and pinholes in the deposited films in the switching has been proposed by Tang et al.<sup>65</sup> Isolated metal islands are then formed at or in these defects during the evaporation of the top electrode. The electrode material that is being deposited eventually seals off the crevices with the already formed metallic islands, preventing further growth of the islands (Figure 1.7). The transport is then explained by conduction pathways *via* the islands and the switching by a Coulomb blockade mechanism<sup>89,90</sup> where charge trapped or stored on an island can block the conduction.

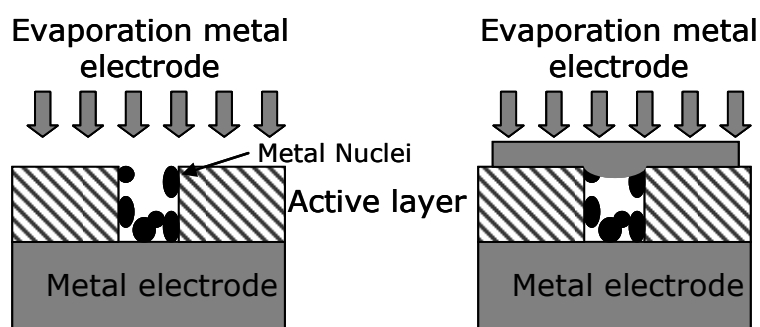


**Figure 1.7:** Schematic illustration of the formation of metal islands inside crevices by nucleation and growth of a thermally evaporated electrode.

Yang et al. argue that the memory effects in organic devices with metal nanoparticles added, are related to charge storage.<sup>86</sup> The critical material requirement is the existence of an energy barrier preventing recombination of charges even after the electric field has been removed. Among others, gold nanoparticles with a surface capping

layer to prevent charge recombination have been used in their experiments. The charge is then considered to be stored on the nanoparticle.

### **Metal oxides**

Metal oxides are a class of materials showing a large variation in their electrical properties. Some oxides are good conductors (e.g. indium tin oxide (ITO)), others are good insulators (e.g.  $\text{SiO}_2$  and  $\text{Al}_2\text{O}_3$ ) or semiconductors (e.g.  $\text{TiO}_2$  and  $\text{ZnO}$ ). Zinc oxide ( $\text{ZnO}$ ) for example is a *n*-type semiconductor even without intentional doping. Native defects such as oxygen vacancies and zinc interstitials are often assumed to be the origin of this.<sup>91-93</sup> With a band gap of 3.2 eV<sup>94,95</sup>,  $\text{ZnO}$  is usually classified as a semiconductor, while for example  $\text{Al}_2\text{O}_3$  with a band gap of 8.7 eV<sup>96,97</sup> is considered to be an insulator.

Nanoparticles of semiconductors show properties that differ from the bulk and that can often be controlled by the size of the particle. This creates opportunities for new applications.<sup>98</sup> Various semiconducting nanoparticles have been synthesized.<sup>99-102</sup> Also nanoparticles of metals oxides, like  $\text{ZnO}$  are widely studied and can be used in various applications,<sup>103-106</sup> for instance in hybrid photovoltaic devices in combination with  $\pi$ -conjugated polymers.<sup>95,107</sup>

### **Metal oxides based memories**

Resistive switching in  $\text{SiO}_x$  has already been investigated by Simmons and Verderber in the 1960s.<sup>108</sup> The switching, however, is not limited to this oxide, many binary metal oxides show resistive switching<sup>109</sup> (e.g.  $\text{Nb}_2\text{O}_5$ ,<sup>110,111</sup>  $\text{Al}_2\text{O}_3$ ,<sup>112</sup>  $\text{Ta}_2\text{O}_5$ ,<sup>113</sup>  $\text{TiO}_2$ ,<sup>114-116</sup>  $\text{NiO}$ ,<sup>117,118</sup>  $\text{Cu}_2\text{O}$ ,<sup>119</sup>  $\text{ZnO}$ ,<sup>120</sup>  $\text{ZrO}_2$ ,<sup>121</sup>  $\text{CeO}_2$ ,<sup>122</sup>  $\text{Y}_2\text{O}_3$ <sup>123</sup> and indium zinc oxide (IZO)<sup>124</sup>), but also ternary oxides exhibit switching.<sup>125,126</sup> In many of these materials, resistive switching is only observed after a forming process.<sup>127</sup> The forming is performed by application of a high voltage. This voltage is terminated immediately when the current reaches a predetermined compliance level. The forming is often related to the soft breakdown of these materials.<sup>128</sup> The stacking of oxide layers to create a resistive switching with diode behavior opens the possibility to use them in a passive matrix array.<sup>129</sup>

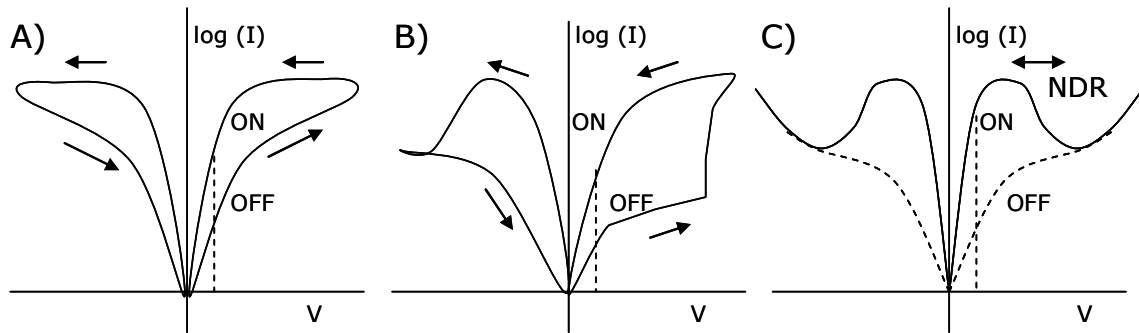


**Figure 1.8:** Schematic illustration of the three types of current versus voltage ( $J$ - $V$ ) curves reported for metal oxide memory devices.

Various types of resistive switching and memory effects can be observed (Figure 1.8), which may be characterized by the current – voltage ( $J$ - $V$ ) behavior of the diode. For some materials hysteresis is observed in the  $J$ - $V$  characteristic (A and B). Often a so-called negative differential resistance regime (NDR) (B and C) is also observed. In a negative differential resistance (NDR) regime, the current density decreases at increasing bias voltage. In this case not always hysteresis is obtained (C), however, resistive switching might still be possible.

The  $J$ - $V$  characteristics can be used to find appropriate voltages to induce resistive switching. Switching induced by voltage pulses of different polarity, is called bipolar switching. This switching can occur in a smooth manner (A) or at a sharp threshold (B). For example devices with  $\text{TiO}_2$ <sup>114</sup> (A) and  $\text{Pr}_{0.7}\text{Ca}_{0.3}\text{MnO}_3$ <sup>130</sup> (B) show this bipolar switching behavior. Sometimes pulses of the same polarity can be used to switch the memory state: unipolar switching, (C). In this case the pulses usually correspond to the local maximum (ON switching) and local minimum of the current (OFF switching) at the NDR.<sup>108,131</sup> Hysteresis can be observed in this plots, however, this is not necessary. Devices, e.g. with  $\text{Al}_2\text{O}_3$ <sup>112</sup> can be switched in this manner. The types are summarized in table 1.1.

**Table 1.1:** Description of the types of  $J$ - $V$  characteristics that can be observed in resistive switching memory devices (see also Figure 1.8).

Types of $J$ - $V$ characteristics that can be observed:			
(A)	Smooth hysteresis without a sharp threshold	No NDR	Bipolar
(B)	Switches on at a sharp threshold and back to off with opposite polarity, hysteresis is observed	NDR	Bipolar
(C)	Switches on at sharp threshold; may be switched off with a pulse of either polarity, hysteresis can be observed.	NDR	Unipolar and Bipolar

Various mechanisms to explain the resistive switching have been proposed.<sup>132</sup> Some will be discussed below. There is considerable evidence that the current density in many oxide devices is not homogeneous, but filamentary in nature. In some interpretations, the filamentary current densities are supposed to be supported by actual metal filaments in the oxide with a width of a few nanometers. Switching from a high to a low conduction state can then be interpreted in terms of rupture of the metal filament due to Joule heating. The switching from low to high conductivity is then related to reformation of the filament under influence in the applied electric field.<sup>127,133-135</sup> The equilibrium between larger, less resistive filaments rupturing, and thinner, more resistive ones carrying the current explains the NDR. Obviously these two processes require mass transport. This metal filament model might also be applicable to the organic or polymeric memories.<sup>136</sup>

Not only metal filaments are believed to be responsible for the resistive switching, but also the presence of intrinsic defects in the oxides. These defects consist partly of impurities having different oxidation states and vacancies (e.g. oxygen vacancies) in the material.<sup>137-139</sup>

Other groups explain the switching by trap-controlled tunneling in the gaps between filamentary chains of metal islands.<sup>140</sup> The traps are proposed to be oxygen vacancies. Simmons and Verderber explain many experimental observations, including NDR and the bistability by charge trapping.<sup>108</sup> This trapping of charges results in an inhibition of further charge injection. However there are some inconsistencies, most notable the fact that the OFF-state is observed the first time a voltage is applied, while the mechanism predicts that the initial absence of charge yields the ON-state.

Although many studies have been performed and complex arrays of oxide memory cells are being fabricated,<sup>141</sup> no general accepted mechanism for the resistive switching in metal oxides is available.

### **1.5. Aim and outline of the thesis**

Resistive switching in metal-insulator-metal (MIM) structures is an intriguing phenomenon. It is being investigated intensely, because of its potential application in data storage. However, the mechanism of this switching is still unknown. The goal of this thesis is to design, construct and electrically characterize novel polymer resistive switching memory cells with an active layer of organic-inorganic hybrid materials. The aim is to understand the mechanism of switching in these cells.

This thesis is organized as follows. In Chapter 2 the electronic memory effects in a polymer (sexithiophene - poly(ethylene oxide) block copolymer) doped with NaCl are investigated. Hysteresis in the current density is observed. In these devices switching is

induced by the migration of salt ions under influence of the applied electrical field. As will turn out, the low mobility of these ions results in a low switching speed. An experimental section is included at the end of each chapter.

The following chapters describe two different approaches to increase the switching speed and with this the overall performance of the memory.

Zinc oxide nanoparticles (ZnO-np) show interesting electronic memory effect, which are explored in Chapter 3 to 6. By mixing these ZnO nanoparticles with polystyrene an interpretation is sketched in Chapter 3. In these devices resistive switching, induced by voltage pulses of milliseconds, is observed after a forming reaction, which is also studied in this chapter. Chapter 4 provides a more detailed investigation of the resistive switching in ZnO-np mixed with polymers. Controlling the aggregate of the ZnO nanoparticles by ligands the memory properties are altered drastically. In Chapter 5 and 6 these effects of ligand exchange on switching properties of the ZnO-nps are provided.

The thickness of an additional aluminum oxide ( $\text{Al}_2\text{O}_3$ ) layer affects the switching reliability, as will be shown in Chapter 7. Reproducible switching is observed when an oxide layer with a defined thickness of circa 20 nm, is included in these devices. In Chapter 8 the switching dynamics of these devices are discussed. These results could only be achieved by the high reproducibility of the samples, obtained by the production process. A "dead time" of milliseconds in which switching is inhibited is observed, while single switching can be induced by  $<1 \mu\text{s}$  voltage pulses. By solution-processing metal oxide nanoparticle layers instead of sputtering these oxide layers, the device fabrication can be simplified. Furthermore, it is demonstrated that the memory effects are not limited to devices with an  $\text{Al}_2\text{O}_3$  oxide layer but that also other metal oxides can be applied. Finally in Chapter 10 a novel switching mechanism will be presented.

## 1.6. References

- 1 M.N. Baibich, J.M. Broto, A. Fert, F. Nguyen van Dau, F. Petroff, P. Eitenne, G. Creuzet, A. Friederich, and J. Chazelas, *Phys. Rev. Lett.* **61**, 2472 (1988).
- 2 G. Binasch, P. Grünberg, F. Saurenbach, and W. Zinn, *Phys. Rev. B* **39**, 4828 (1989).
- 3 G. Brumfiel, *Nature* **449**, 643 (2007).
- 4 J.M. Daughton, *Thin Solid Films* **216**, 162 (1992).
- 5 S.S.P. Parkin, K.P. Roche, M.G. Samant, P.M. Rice, R.B. Beyers, R.E. Scheuerlein, E.J. O'Sullivan, S.L. Brown, J. Bucchigano, D.W. Abraham, Y. Lu, M. Rooks, P.L. Trouilloud, R.A. Wanner, and W.J. Gallagher, *J. Appl. Phys.* **85**, 5828 (1999).
- 6 S. Tehrani, E. Chen, M. Durlam, M. DeHerrera, J.M. Slaughter, J. Shi, and G. Kerszykowski, *J. Appl. Phys.* **85** 5822 (1999).

- 7 J.G. Zhu, Y.F. Zheng, and G.A. Prinz, *J. Appl. Phys.* **87** 6668 (2000).
- 8 S. Tehrani, J.M. Slaughter, E. Chen, M. Durlam, J. Shi, and M. DeHerren, *IEEE Trans. Mag.* **35**, 2814 (1999).
- 9 V.A. Barachevskii, *High Energy Chemistry* **40**, 131 (2006).
- 10 M. Wuttig, and N. Yamada, *Nature Mater.* **6**, 824 (2007).
- 11 N. Yamada, E. Ohno, K. Nishiuchi, N. Akahira, and M. Takao, *J. Appl. Phys.* **69** 2849 (1991).
- 12 A.N. Vasil'ev, A.D. Bozhko, V.V. Khovailo, I.E. Dikshtein, V.G. Shavrov, V.D. Buchelnikov, M. Matsumoto, S. Suzuki, T. Takagi, and J. Tani, *Phys. Rev. B* **59** 1113 (1999).
- 13 A.V. Kolobov, P. Fons, A.I. Frenkel, A.L. Ankudinov, J. Tominaga, and T. Uruga, *Nature Mater.* **3** 703 (2004).
- 14 M. Wuttig, *Nature Mater.* **4**, 265 (2005).
- 15 H.E. Katz, X.M. Hong, A. Dodabalapur, and R. Sarpeshkar, *J. Appl. Phys.* **91**, 1572 (2002).
- 16 S.Y. WU, *IEEE Trans. Electron Devices* **21**, 499 (1974).
- 17 J.T. Evans and R. Womack, *IEEE J. Solid-State Circuits* **23**, 1171 (1988).
- 18 G.H. Haertling, *J. Vac. Sci. & Techn. A* **9** 414 (1991).
- 19 H.N. Alshareef, O. Auciello, and A.I. Kingson, *J. Appl. Phys.* **77** 2146 (1995).
- 20 M.W.J. Prins, K.-O. Grosse-Holz, G. Müller, J.F.M. Cillessen, J.B. Giesbers, R.P. Weening, and R.M. Wolf, *Appl. Phys. Lett.* **68**, 3650 (1996).
- 21 R.C.G. Naber, C. Tanase, P.W.M. Blom, G.H. Gelinck, A.W. Marsman, F.J. Touwslager, S. Setayesh, and D.M. De Leeuw, *Nature Mater.* **4**, 243 (2005).
- 22 T.J. Reece, S. Ducharme, A.V. Sorokin, and M. Poulsen, *Appl. Phys. Lett.* **82**, 142 (2003).
- 23 G.H. Gelinck, A.W. Marsman, F.J. Touwslager, S. Setayesh, D.M. De Leeuw, R.C.G. Naber, and P.W.M. Blom, *Appl. Phys. Lett.* **87**, 092903 (2005).
- 24 A. Bird, *Genes & Develop.* **16**, 6 (2002).
- 25 Z.M. Liu, A.A. Yasseri, J.S. Lindsey, and D.F. Bocian, *Science* **302**, 1543 (2003).
- 26 Q. Li, G. Mathur, S. Gowda, S. Surthi, Q. Zhao, L. Yu, J.S. Lindsey, D.F. Bocian, and V. Misra, *Adv. Mater.* **16**, 133 (2004).
- 27 A.R. Pease, J.O. Jeppesen, J.F. Stoddart, Y. Luo, C.P. Collier, and J.R. Heath, *Acc. Chem. Res.* **34**, 433 (2001).
- 28 Y. Luo, C.P. Collier, J.O. Jeppesen, K.A. Nielsen, E. DeIonno, G. Ho, J. Perkins, H.R. Tseng, T. Yamamoto, J.F. Stoddart, and J.R. Heath, *ChemPhysChem* **3**, 519 (2002).
- 29 R. Bez and A. Pirovano, *Mater. Sci. Semicond. Process.* **7**, 349 (2004).
- 30 S. Moller, C. Perlov, W. Jackson, C. Taussig, and S.R. Forrest, *Nature* **426**, 166 (2003).
- 31 S. Smith and S.R. Forrest, *Appl. Phys. Lett.* **84**, 5019 (2004).
- 32 R.J. Luyken and F. Hofmann, *Nanotechnology* **14**, 273 (2003).
- 33 Y. Kijima, N. Asai, N. Kishii, and S.-I. Tamura, *IEEE Trans. Electr. Dev.* **44**, 1222 (1997).
- 34 F.L.E. Jakobsson, X. Crispin, and M. Berggren, *Appl. Phys. Lett.* **87**, 063503 (2005).
- 35 K. Mori, Y. Sakaguchi, Y. Iketsu, and J. Suzuki, *Displays* **22** 43 (2001).
- 36 J.C. Scott, *Science* **304**, 62 (2004).

- 
- 37 L.D. Bozano, B.W. Kean, M. Beinhoff, K.R. Carter, P.M. Rice, and J.C. Scott, *Adv. Funct. Mater.* **15**, 1933 (2005).
- 38 F.L.E. Jakobsson, X. Crispin, and M. Berggren, *Appl. Phys. Lett.* **87**, 063503 (2005).
- 39 S. Lai, and T. Lowrey, OUM – a 180nm Nonvolatile Memory Cell Element Technology for Standalone and Embedded Applications, *IEDM technical digest* (2002).
- 40 S.R. Ovshinsky, *Phys. Rev. Lett.* **21**, 1450 (1968).
- 41 Y. Yin, A. Miyachi, D. Niida, H. Sone, and S. Hosaka, *Jpn. J. Appl. Phys. Part 1* **45**, 3238 (2006).
- 42 C.W. Tang and S. A. VanSlyke, *Appl. Phys. Lett.* **51**, 913 (1987).
- 43 J.H. Burroughes, D.D.C. Bradley, A.R. Brown, R.N. Marks, K. Mackay, R.H. Friend, P.L. Burn, and A.B. Holmes, *Nature* **347**, 539 (1990)
- 44 R.H. Friend, R.W. Gymer, A.B. Holmes, J.H. Burroughes, R.N. Marks, C. Taliani, D.D.C. Bradley, D.A. Dos Santos, J.L. Brédas, M. Logdlund, and W.R. Salaneck, *Nature* **397**, 121 (1999).
- 45 C.D. Dimitrakopolous and P.R.L. Malenfant, *Adv. Mater.* **14**, 99 (2002).
- 46 H. Sirringhaus, P.J. Brown, R.H. Friend, M.M. Nielsen, K. Bechgaard, B.M.W. Langeveld-Voss, A.J.H. Spiering, R.A.J. Janssen, E.W. Meijer, P. Herwig, and D.M. de Leeuw, *Nature* **401**, 685 (1999).
- 47 A.R. Brown, A. Pomp, C.M. Hart, and D.M. de Leeuw, *Science* **270**, 972 (1995).
- 48 C.J. Brabec, V. Dyakonov, J. Parisi, and N.S. Sariciftci (Eds.), *Organic Photovoltaics: Concepts and Realization*, *Springer Series in Materials Science* **60** Springer-Verlag, London (2003).
- 49 W.U. Huynh, J.J. Dittmer, and A.P. Alivisatos, *Science* **295**, 2425 (2002).
- 50 L.V. Gregor, *Thin Solid Films* **2**, 235 (1968).
- 51 J.C. Scott and L.D. Bozano, *Adv. Mater.* **19**, 1452 (2007).
- 52 L.F. Pender and R.J. Fleming, *J. Appl. Phys.* **46**, 3426 (1975).
- 53 J. McGinness, P. Corry, and P. Proctor, *Science* **183**, 853 (1974).
- 54 H. Carchano, R. Lacoste, and Y. Segui, *Appl. Phys. Lett.* **19**, 414 (1971).
- 55 H.K. Hensch and W.R. Smith, *Appl. Phys. Lett.* **24**, 589 (1974).
- 56 Y.-S. Lai, C.-H. Tu, D.-L. Kwong, and J.S. Chen, *Appl. Phys. Lett.* **87**, 122101 (2005).
- 57 H.S. Majumdar, A. Bandyopadhyay, A. Bolognesi, and A.J. Pal, *J. Appl. Phys.* **91**, 2433 (2002).
- 58 H.S. Majumdar, A. Bolognesi, and A.J. Pal, *Synth. Met.* **140**, 203 (2004).
- 59 M. Cölle, M. Büchel, and D.M. de Leeuw, *Org. Electron.* **7**, 305 (2006).
- 60 M. Lauters, B. McCarthy, D. Sarid, and G.E. Jabbour, *Appl. Phys. Lett.* **89**, 013507 (2006).
- 61 A.R. Elsharkawi and K.C. Kao, *J. Phys. Chem. Solids* **38**, 95 (1977).
- 62 D. Tondelier, K. Lmimouni, D. Vuillaume, C. Fery, and G. Haas, *Appl. Phys. Lett.* **85**, 5763 (2004).
- 63 C.H. Tu, Y.S. Lai, and D.L. Kwong, *IEEE Electron Device Lett.* **27**, 354 (2006).
- 64 A.K. Mahapatro, R. Agrawal, and S. Ghosh, *J. Appl. Phys.* **96**, 3583 (2004).



- 65 W. Tang, H. Shi, G. Xu, B.S. Ong, Z.D. Popovic, J. Deng, J. Zhao, and G. Rao, *Adv. Mater.* **17**, 2307 (2005).
- 66 M. Terai, K. Fujita, and T. Tsutsui, *Jpn. J. Appl. Phys. Part 1* **45**, 3754 (2006).
- 67 R. Müller, S. De Jonge, K. Myny, D. J. Wouters, J. Genoe, and P. Heremans, *Appl. Phys. Lett.* **89**, 223201 (2006).
- 68 R.S. Potember, T.O. Poehler, and D.O. Cowan, *Appl. Phys. Lett.* **34**, 405 (1979).
- 69 E.I. Kamitsos, C.H. Tzinis, and W.M. Risen, *Solid State Commun.* **42**, 561 (1982).
- 70 C. Sato, S. Wakamatsu, K. Tadokoro, and K. Ishii, *J. Appl. Phys.* **68**, 6535 (1990).
- 71 T. Oyamada, H. Tanaka, K. Matsushige, H. Sasabe, and C. Adachi, *Appl. Phys. Lett.* **83**, 1252 (2003).
- 72 R. Müller, J. Genoe, and P. Heremans, *Appl. Phys. Lett.* **88**, 242105 (2006).
- 73 R. Müller, R. Naulaerts, J. Billen, J. Genoe, and P. Heremans, *Appl. Phys. Lett.* **90**, 063503 (2007).
- 74 A. Prakash, J. Ouyang, J.-L. Lin, and Y. Yang, *J. Appl. Phys.* **100**, 054309 (2006).
- 75 C.W. Chu, J. Ouyang, J.-L. Lin, and Y. Yang, *Adv. Mater.* **17**, 1440 (2005).
- 76 J.H.A. Smits, S.C.J. Meskers, R.A.J. Janssen, A.W. Marsman, and D.M. de Leeuw *Adv. Mater.* **17**, 1169 (2005).
- 77 J.H. Krieger, S.V. Trubin, S.B. Vaschenko, and N.F. Yudanov, *Synth. Met.* **122**, 199 (2001).
- 78 Q.X. Lai, Z.H. Zhu, Y. Chen, S. Patil, and F. Wudl, *Appl. Phys. Lett.* **88**, 133515 (2006).
- 79 A.W. Marsman, C.M. Hart, G.H. Gelinck, T.C.T. Geuns, and D.M. de Leeuw, *J. Mater. Res.* **19** 2057 (2004).
- 80 L.D. Bozano, B.W. Kean, V.R. Deline, J.R. Salem, and J.C. Scott, *Appl. Phys. Lett.* **84**, 607 (2004).
- 81 L.P. Ma, S.M. Pyo, J.Y. Ouyang, Q.F. Yu, and Y. Yang, *Appl. Phys. Lett.* **82**, 1419 (2003).
- 82 J. Ouyang, C.-W. Chu, D. Sieves, and Y. Yang, *Appl. Phys. Lett.* **86**, 123507 (2005).
- 83 J. Ouyang, C.-W. Chu, C. Szmanda, L.P. Ma, and Y. Yang, *Nat. Mater.* **3**, 918 (2004).
- 84 J. Ouyang, C.-W. Chu, R.J.-T. Tseng, A. Prakash, and Y. Yang, *Proc. IEEE* **93**, 1287 (2005).
- 85 A. Prakash, J. Ouyang, J.L. Lin, and Y. Yang, *J. Appl. Phys.* **100**, 054309 (2006).
- 86 Y. Yang, J.Y. Ouyang, L.P. Ma, R.J.H. Tseng, and C.W. Chu, *Adv. Funct. Mater.* **16**, 1001 (2006).
- 87 L.P. Ma, J. Liu, and Y. Yang, *Appl. Phys. Lett.* **80**, 2997 (2002).
- 88 L.P. Ma, J. Liu, S.M. Pyo, and Y. Yang, *Appl. Phys. Lett.* **80**, 362 (2002).
- 89 H. Nakashima, and K. Uozumi, *Jpn. J. Appl. Phys. Part 2* **34**, L1659 (1995).
- 90 M.C. Shin, S.J. Lee, K.W. Park, and E.-H. Lee, *Phys. Rev. B* **59**, 3160 (1999).
- 91 D.C. Look, J.W. Hemsky, and J.R. Sizelove, *Phys. Rev. Lett.* **82**, 2552 (1999).
- 92 A. van Dijken, E. A. Meulenkaamp, D. Vanmaekelbergh, and A. Meijerink, *J. Phys. Chem B* **104**, 1715 (2000).
- 93 P.V. Kamat and B. Patrick, *J. Phys Chem.* **96**, 6829 (1992).
- 94 S.J. Pearton, D.P. Norton, K. Ip, Y.W. Heo, and T. Steiner, *J. Vac. Sci. Technol. B* **22**, 932 (2004).

- 
- 95 W.J.E. Beek, *PhD thesis: Hybrid Polymer Solar Cells*, Technische Universiteit Eindhoven, (2005).
- 96 R.H. French, *J. Am. Ceram. Soc.* **73**, 477 (1990).
- 97 S.-D. Mo and W.Y. Ching, *Phys. Rev. B* **57**, 15219 (1998).
- 98 C. Burda, X. Chen, R. Narayanan, and M.A. El-Sayed, *Chem. Rev.* **105**, 1025 (2005).
- 99 B.L. Cushing, V.L. Kolesnichenko, and C.J. O'Connor, *Chem. Rev.* **104**, 3893 (2004).
- 100 Y. Yin and A.P. Alivisatos, *Nature* **437**, 664 (2005).
- 101 J.A. Dahl, B.L.S. Maddux, and J.E. Hutchison, *Chem. Rev.* **107**, 2228 (2007).
- 102 V.I. Klimov, *Semiconductors and Metal Nanoclusters*, Marcel Dekker Inc., New York (2004).
- 103 Z.L. Wang, *J. Phys. Condens. Matter* **16**, R829 (2004).
- 104 C. Klingshirn, *Chem. Phys. Chem.* **8**, 782 (2007).
- 105 V. Noack, H. Weller, and A. Eychmüller, *J. Phys. Chem. B* **106**, 8514 (2002).
- 106 M.H. Huang, S. Mao, H. Feick, H. Yan, Y. Wu, H. Kind, E. Weber, R. Russo, and P. Yang, *Science* **292**, 1897 (2001).
- 107 W.J.E. Beek, M.M. Wienk, and R.A.J. Janssen, *Adv. Mater.* **16**, 1009 (2004).
- 108 J.G. Simmons and R.R. Verderber, *Proc. R Soc. Lond. Ser. A* **301**, 77 (1967).
- 109 T.W. Hickmott, *J. Appl. Phys.* **88**, 2805 (2000).
- 110 W.R. Hiatt and T.W. Hickmott, *Appl. Phys. Lett.* **6**, 106 (1965).
- 111 T.W. Hickmott and W.R. Hiatt, *Solid-State Electron.* **13**, 1033 (1970).
- 112 T.W. Hickmott, *J. Appl. Phys.* **88**, 2805 (2000).
- 113 K. L. Chopra, *J. Appl. Phys.* **36**, 184 (1965).
- 114 F. Argall, *Solid-State Electron.* **11**, 535 (1968).
- 115 K. Tsunoda, Y. Fukuzumi, J.R. Jameson, Z. Wang, P.B. Griffin, and Y. Nishi, *Appl. Phys. Lett.* **90**, 113501 (2007).
- 116 B.J. Choi, S. Choi, K.M. Kim, Y.C. Shin, C.S. Hwanga, S.-Y. Hwang, S. Cho, S. Park, and S.-K. Hong, *Appl. Phys. Lett.* **89**, 012906 (2006).
- 117 J.F. Gibbons and W.E. Beadle, *Solid-State Electron.* **7**, 785 (1964).
- 118 M.-J. Lee, Y. Park, D.-S. Suh, E.-H. Lee, S. Seo, D.-C. Kim, R. Jung, B.-S. Kang, S.-E. Ahn, C. B. Lee, D.H. Seo, Y.-K. Cha, I.-K. Yoo, J.-S. Kim, and B.H. Park, *Adv. Mater.* **19**, 3919, (2007).
- 119 J.H. Jung, J.H. Kim, T.W. Kim, M.S. Song, Y.H. Kim, and S. Jin, *Appl. Phys. Lett.* **89**, 122110 (2006).
- 120 T. Hada, K. Wasa, and S. Hayakawa, *Jpn. J. Appl. Phys.*, **10**, 521 (1971).
- 121 K.C. Park and S. Basavaiah, *J. Non-Cryst. Solids* **2**, 284 (1970).
- 122 R. Fors, S.I. Khartsev, and A.M. Grishin, *Phys. Rev. B* **71**, 045305 (2005).
- 123 A.L. Pergament, V.P. Malinenko, O.I. Tulubaeva, and L.A. Aleshina, *Phys. Stat. Solidi A* **201**, 1543 (2004).
- 124 G.B. Stefanovich, C.-R. Cho, E.-H. Lee, and I.K. Yoo, *J. Non-Cryst. Solids* **353**, 956 (2007).
- 125 K. Szot, R. Dittmann, W. Speier, and R. Waser, *Phys. Stat. Sol. (RRL)* **1**, R86 (2007).
- 126 X. Chen, N. Wu, J. Strozier, and A. Ignatiev, *Appl. Phys. Lett.* **89**, 063507 (2006).

- 127 G. Dearnaley, A.M. Stoneham, and D.V. Morgan, *Rep. Prog. Phys.* **33**, 1129 (1970).
- 128 D.J. Dumin, *Oxide Reliability: A summary of silicon oxide wearout, Breakdown and reliability*, World Scientific Publishing Co. Pte. Ltd. Singapore (2002).
- 129 M.-J. Lee, S. Seo, D.-C. Kim, S.-E. Ahn, D.H. Seo, I.-K. Yoo, I.-G. Baek, D.-S. Kim, I.-S. Byun, S.-H. Kim, I.-R. Hwang, J.-S. Kim, S.-H. Jeon, and B.H. Park, *Adv. Mater.* **19**, 73 (2007).
- 130 M. Fujimoto, H. Koyama, Y. Nishi, and T. Suzuki, *Appl. Phys. Lett.* **91**, 223504 (2007).
- 131 L.D. Bozano, B.W. Kean, V.R. Deline, J.R. Salem, and J.C. Scott, *Appl. Phys. Lett.* **84**, 607 (2004).
- 132 R. Waser and M. Aono, *Nature Mater.* **6**, 833 (2007).
- 133 G. Dearnaley, D.V. Morgan, and A.M. Stoneham, *J. Non-Cryst. Solids* **4**, 593 (1970).
- 134 G.-S. Park, X.-S. Li, D.-C. Kim, R.-J. Jung, M.-J. Lee, and S. Seo, *Appl. Phys. Lett.* **91**, 222103 (2007).
- 135 K. Kinoshita, T. Tamura, M. Aoki, Y. Sugiyama, and H. Tanaka, *Appl. Phys. Lett.* **89**, 103509 (2006).
- 136 W.-J. Joo, T.-L. Choi, J. Lee, S. K. Lee, M.-S. Jung, N. Kim, and J. M. Kim *J. Phys. Chem. B* **110**, 23812 (2006).
- 137 A. Beck, J.G. Bednorz, Ch. Gerber, C. Rossel, and D. Widmer, *Appl. Phys. Lett.* **77**, 139 (2000).
- 138 J.-W. Park, J.-W. Park, D.-Y. Kim, and J.-K. Lee, *J. Vac. Sci. Technol. A* **23** 1309 (2005).
- 139 M. Janousch, G.I. Meijer, U. Staub, B. Delley, S.F. Karg, and B.P. Andreasson, *Adv. Mater.* **19**, 2232 (2007).
- 140 R.E. Thurstans, and D.P. Oxley, *J. Phys. D* **35**, 802 (2002).
- 141 I.G. Baek, D.C. Kim, M.J. Lee, H.-J. Kim, E.K. Yim, M.S. Lee, J.E. Lee, S.E. Ahn, S. Seo, J.H. Lee, J.C. Park, Y.K. Cha, S.O. Park, H.S. Kim, I.K. Yoo, U. Chung, J.T. Moon, and B.I. Ryu, *Electron Devices Meeting, 2005. IEDM Technical Digest.* 750 (2005).

# 2

## **Electronic memory effects in a sexithiophene-poly (ethylene oxide) block copolymer doped with NaCl. Combined diode and resistive switching behavior**

*Electrical transport in devices consisting of an electrode of a conducting polymer (poly(ethylenedioxythiophene): poly(styrenesulfonate), PEDOT:PSS), a layer of a sexithiophene –poly(ethylene oxide) (6T-PEO) block copolymer with an Al top electrode is investigated. These devices show diode behavior with the larger current density flowing when the PEDOT:PSS electrode is biased positive with respect to the Al electrode (forward bias). Introduction of inorganic salt (NaCl) in the PEDOT layer results in resistive switching behavior under forward bias while retaining the diode character. The switching allows for storage of information and rewritable memory operation is demonstrated for the diodes although the retention time of the information is still very short ( $\sim 10$  s). The reported combination of switching and diode behavior is an important requirement for passive matrix addressing of resistive switching memory cells in an array and shows that materials with combined ion and (electron) charge transport properties are interesting for information storage.*

This work has been published: F. Verbakel, S.C.J. Meskers, and R.A.J. Janssen, *Chem. Mater.* **18**, 2707 (2006).

## 2.1. Introduction

The possibility to use  $\pi$ -conjugated polymers in electronic memory elements is currently being explored by a large number of research groups.<sup>1-6</sup> One of the approaches being followed is to make diode-like structures for which the resistance at a particular 'read' voltage can be modified by application of a higher voltage.<sup>7-10</sup> One of the attractive features of these diodes is that they may be integrated into a matrix array of plastic memory elements relying on passive matrix addressing to read out the individual cells.<sup>11,12</sup> Forrest *et al.* have used a polymeric fuse in combination with an inorganic diode to make a passive matrix array of write-once read-many memory elements.<sup>13-15</sup> The incorporation of a diode is required for selective writing and reading of individual cells in the array, suppressing cross-talk between the cells in the matrix array. Recently they showed that also an inorganic-organic heterojunction can serve as a diode in memory cells.<sup>8</sup> In order to come to *rewritable* memory cells that can be integrated into a passive matrix array, many requirements have to be fulfilled. Important features of such memory elements are to exhibit diode character and to have two different resistance levels in forward bias.

It has been shown that the electrical properties of  $\pi$ -conjugated polymers doped with mobile ions can be modified by application of bias voltage stress.<sup>16-18</sup> This feature may allow for storage of information in a rewritable manner. For example, bias voltage stress applied to films of poly(*p*-phenylene vinylene) doped with mobile ions, sandwiched between two non-Ohmic contacts, induces the formation of a junction and results in diode-like current-voltage (*J-V*) characteristic.<sup>16-18</sup> After junction formation these cells can emit electroluminescence (light-emitting electrochemical cell, LEEC). The electrical response of these devices to positive and negative bias voltage stress is very similar and both types of stress induce a high conductivity state for probe voltages that have the same parity as the applied bias stress.<sup>16-18</sup> This latter property makes it difficult to use these structures as memory cells in a passive matrix array because a particular cell in the matrix array will experience reverse bias stress when trying to reduce the conduction level or when trying to raise the conduction level in another cell. This may result in creating a diode with the wrong polarity that makes it impossible to read out cells in the matrix array selectively.

Devices with one Ohmic and one Schottky contact feature the required asymmetric response to positive and negative bias stress voltages, but here the induced change in conductivity is mainly in the reverse bias regime.<sup>19</sup> Because modulation of the conduction level in forward bias is required for selective readout of cells in the matrix, these cells are not useful in arrays.

In this chapter, charge transport in a 6T-PEO block copolymer<sup>20</sup> that contains semiconducting blocks (sexithiophene, 6T) and ion transporting blocks (poly(ethylene oxide), PEO) alternating along the polymer chain (Figure 2.1) will be reported. The use of this alternating block copolymer ensures nanoscopic mixing of the electron and ion transporting components, resulting in unique properties. These films are contacted on one side with an electrode consisting of a conducting  $\pi$ -conjugated polymer (PEDOT:PSS), doped with an inorganic salt (NaCl) and a plasticizer (ethylene carbonate, EC), and on the other side with a vacuum deposited Al electrode. In this way a diode configuration is created for which the conductivity in forward direction can be modulated by application of forward and reverse bias stress. Thus, information can be stored in the cell in a reversible manner. Importantly, negative bias voltage stress does not raise the conduction level under the reverse bias. Therefore the cell meets an important requirement for passive matrix addressing, illustrating the potential of molecular engineering to design switchable electronic elements.

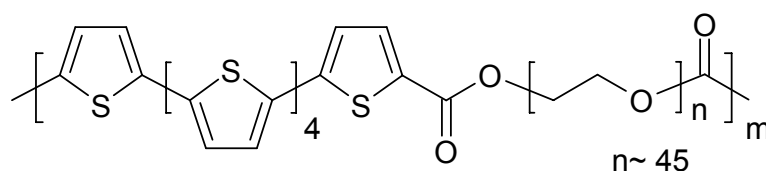


**Figure 2.1:** Chemical structure of the 6T-PEO block co-polymer.

## 2.2. Cyclic voltammetry and spectroscopic analysis

The cyclic voltammogram (CV) of 6T-PEO reveals that the first oxidation and reduction waves are chemically reversible (Figure 2.2). The first oxidation potential observed at +0.43 V vs.  $\text{Fc}/\text{Fc}^+$  is close to that of  $\alpha,\omega$ -dihexylsexithiophene (+0.42 V).<sup>21</sup> The first reduction of the 6T-PEO occurs at -2.09 V vs.  $\text{Fc}/\text{Fc}^+$ , i.e. less negative than for  $\alpha,\omega$ -dihexylsexithiophene (-2.23 V). This difference is attributed to the electron withdrawing effect of the ester moieties in 6T-PEO. The lower part of Figure 2.2 shows an approximate band level diagram of the devices under study featuring the HOMO and LUMO levels of the 6T block as determined from the cyclic voltammetry. The position versus the vacuum is calculated via  $\text{Fc}/\text{Fc}^+$ , which is positioned 5.1 eV below the vacuum level.<sup>22,23</sup> The work functions ( $\phi$ ) of PEDOT:PSS<sup>24</sup> and Al<sup>25</sup> are obtained from literature. The lowest barrier for charge carrier injection into 6T-PEO is for holes entering via the PEDOT:PSS electrode. The barrier at the opposite electrode is considerably higher and therefore, diode-like behavior is expected.

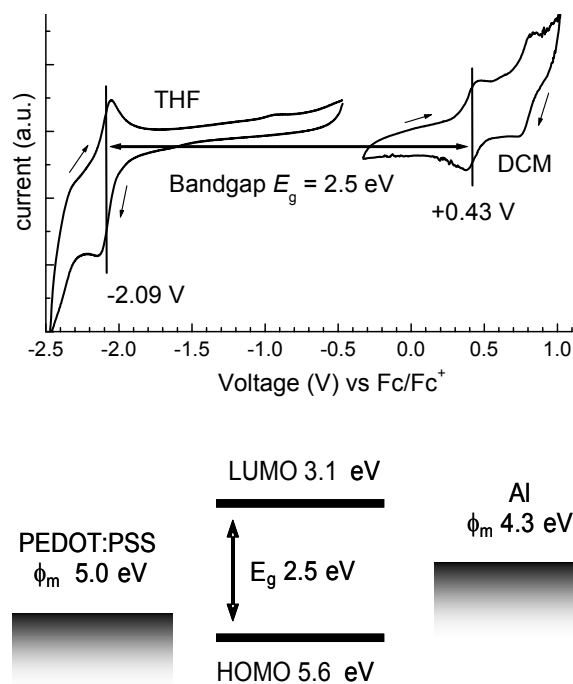


**Figure 2.2:** Cyclic voltammetry data for 6T-PEO in tetrahydrofuran (THF) and dichloromethane (DCM). The lower part represents a band level diagram for the devices under study with the work functions ( $\phi$ ) of PEDOT:PSS and Al and the position of the HOMO and LUMO of the polymer (calculated via Fc/Fc<sup>+</sup>) with respect to the vacuum.

The absorption spectrum of 6T-PEO in THF shows the absorption band associated with the optically allowed transition from the ground state ( $S_0$ ) to the lowest excited singlet state ( $S_1$ ) with a maximum at 2.8 eV in agreement with data for sexithiophene (Figure 2.3).<sup>26</sup> For a solid film of 6T-PEO on glass, the maximum absorption in the UV-vis spectrum shifts to higher photon energies (3.2 eV), while the onset occurs at lower energies. These changes are accompanied by a shift of the 6T-PEO photoluminescence to lower photon energies. These spectral changes indicate that the 6T units of 6T-PEO cluster in the solid state and form an H-type aggregate with the 6T moieties stacking in a cofacial or herringbone type fashion with their long axis almost perpendicular to the line joining the centers of the 6T units.<sup>27</sup> Similar spectral features have been observed upon crystallization of sexithiophene<sup>28-30</sup> and aggregation of a number of derivatives similar to 6T-PEO.<sup>27</sup>

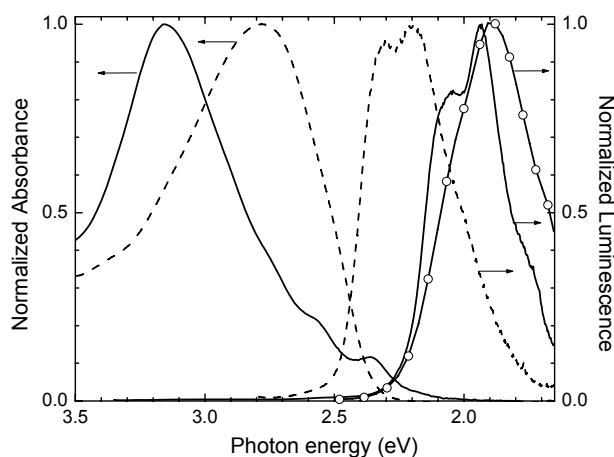


**Figure 2.3:** Normalized absorption and photoluminescence (excitation photon energy 3.5 eV) spectra of the 6T-PEO block copolymer as solid film spin cast from tetrahydrofuran (THF) solution (solid lines) and dissolved in THF ( $10^{-5}$  M) (dashed lines). Electroluminescence from a ITO/PEDOT:PSS(NaCl,EC)/6T-PEO/Al structure (solid line with open circles).

### 2.3. Current-voltage characterization

The current-voltage ( $J$ - $V$ ) characteristic of a ITO/PEDOT:PSS/6T-PEO/Al device without salt or plasticizer added to the PEDOT:PSS reveals a clear diode behavior (Figure 2.4a). At +4 V forward bias (Al electrode negatively biased with respect to the PEDOT:PSS electrode), the current density is approx. two orders of magnitude higher than at -4 V bias. Similar alternating block copolymers with oligothiophene blocks shorter than 6 thiophene units,<sup>31</sup> did not show diode behavior when tested under identical conditions. The observation of electrical conductivity in 6T-PEO in combination with the insulating properties of the PEO blocks, imply the presence of percolating pathways from one electrode to the other via adjacent 6T moieties enabling transport of charge carriers. This view is supported by the aggregation of the 6T blocks inferred from UV-vis absorption spectroscopy and supports the conclusion that phase separation of the two blocks occurs.



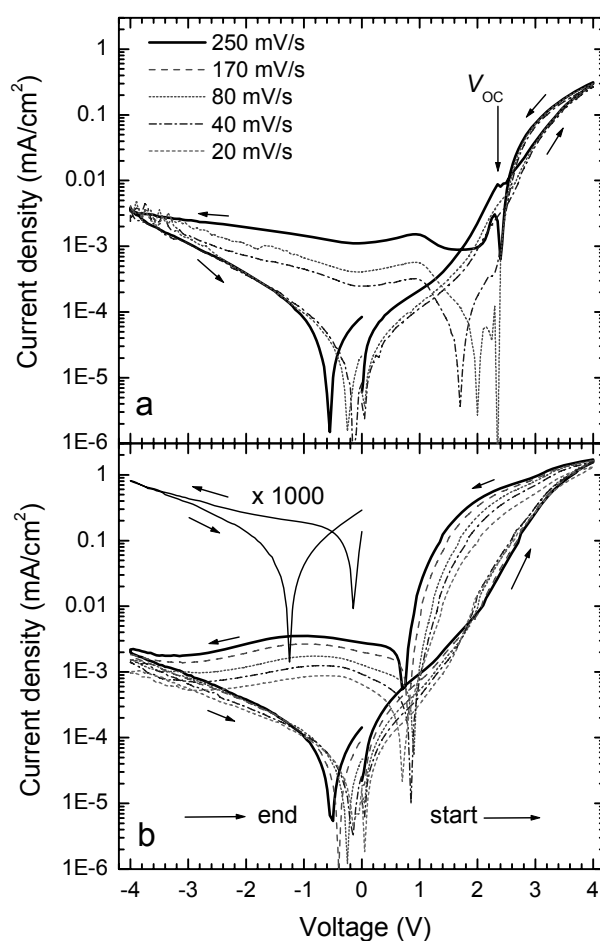


**Figure 2.4:** Current-voltage characteristics of ITO/PEDOT:PSS/6T-PEO/Al devices at different scan speeds. (a) no salt or plasticizer added. (b) with NaCl and EC added to PEDOT:PSS. The trace in the upper left corner of panel (b) pertains to a scan of only the reverse bias voltages and was taken directly after a 1 min. period of  $-4$  V bias stress (scan speed 170 mV/s).

In Figure 2.4a the scan direction of the  $J$ - $V$  characterization is indicated. When scanning back from positive bias towards negative bias, the current changes sign at  $+2.4$  V. In a separate experiment the open-circuit voltage ( $V_{oc}$ ) displayed by the cell after being biased at  $+6$  V for 60 s is determined (Figure 2.5a). This voltage amounts to  $+2.4$  V and this is virtually identical to the difference between oxidation and reduction potentials as determined from CV in solution (Figure 2.2). This correspondence, which has also been observed for LEECs,<sup>16-18</sup> indicates that  $V_{oc}$  originates from Faradaic charging facilitated by a small number of mobile ions originating from e.g. the PEDOT:PSS layer. Under forward bias, the undoped devices work similar to the charging of a battery. Oxidation of the neutral 6T block takes place at the PEDOT:PSS electrode and reduction of neutral 6T at the Al electrode. After charging for 60 sec at  $+6$ V, and subsequently short circuiting the device, electrical current flows spontaneously, decaying with time (Figure 2.5b). By integration over the time window of observation, it is found

that  $6 \times 10^{-5} \text{ C/cm}^2$  flows from the cell. When monitoring the current density while applying a constant bias voltage (Figure 2.5c), the current density reaches a maximum at  $\sim 6 \text{ s}$  after switching on the bias voltage. This indicates that the charging has reached completion, probably because the source of mobile ions is exhausted.

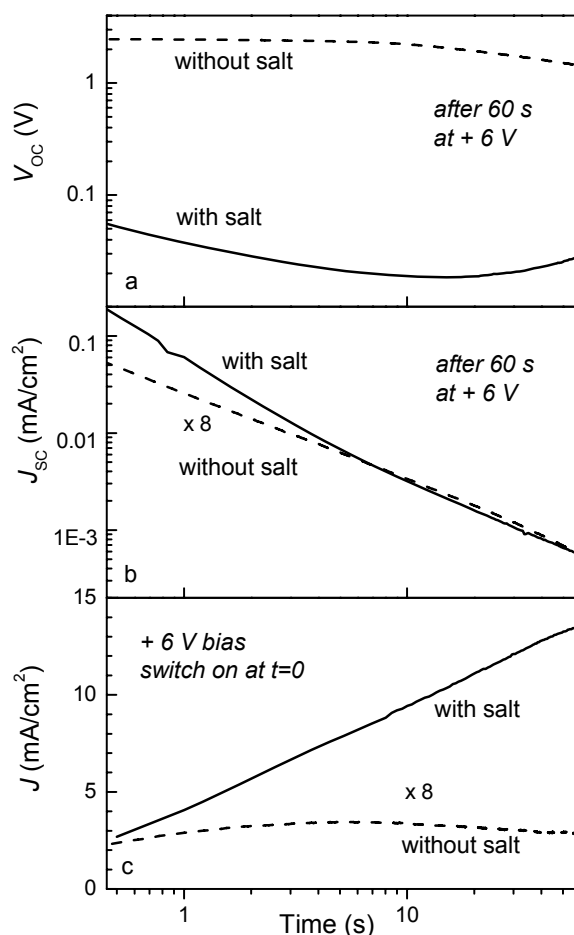


**Figure 2.5:** (a) Time dependence of the open-circuit voltage ( $V_{oc}$ ) measured directly after termination of a bias voltage stress (+6 V, 60 s) for a PEDOT:PSS/6T-PEO/Al diode (dashed line) and of a PEDOT:PSS(NaCl, EC)/6T-PEO/Al diode (solid line). (b). Short-circuit current ( $J_{sc}$ ) after bias stress (+6 V, 60 s). (c) Current density ( $J$ ) under +6 V bias stress started at  $t = 0$ .

ITO/PEDOT:PSS(NaCl,EC)/6T-PEO/Al devices to which salt and plasticizer have been added deliberately, show current densities under forward bias that are approximately one order of magnitude higher than for the undoped devices (Figure 2.4b). A large hysteresis is now observed in the  $J$ - $V$  characteristics which results from the interdependence of the field induced transport of ions towards the electrodes and electrochemical redox reactions of the 6T block of the polymer. This combination of processes is well known from research on LEECs.<sup>16-18</sup> The ion accumulation and electrochemical doping at the electrodes strongly reduces the barrier for charge injection.

This combination of processes results in a hysteresis with an anticlockwise direction. In contrast, the hysteresis in the cyclic voltammetry scan has a clockwise direction when the absolute value of the current is plotted (Figure 2.2). This underlines that the hysteresis observed for the diodes does not originate only from reversible redox reactions at the electrodes, but results from junction formation. The open-circuit voltage for the doped devices, measured directly after 60 s at +6 V bias stress drops below 0.1 V within 1 s after termination of the stress voltage (Figure 2.5a). While the devices without added salt show a saturation of the current density at about 10 sec after the turn on of the bias voltage, the devices with added salt do not show a clear saturation in the period of measurement (Figure 2.5c).

Interestingly, devices with added salt retain their diode characteristic. The current density under negative bias is three orders of magnitude lower than in the forward (Figure 2.4b). The application of reverse bias voltages does not raise the conduction level in the reverse bias regime. To confirm the absence of any ion induced electrode processes under reverse bias, the devices are biased for 60 s at -4 V and an  $J$ - $V$  scan of the negative bias region is performed. The result shown in the upper left corner of Figure 4b reveals no enhancement of the current density at negative bias. This indicates that migration of anions towards the interface with the Al electrode, leading to a built-up of negative space charge and allowing for facile hole injection through the Al electrode, does not take place. In principle, ion migration induced by an electrical field may not be fully reversible. However, no obvious signs of fatigue have been found and the cells can be cycled for at least 15 times without any significant changes in the  $J$ - $V$  characteristic.

### **2.4. Electrical hysteresis**

The response of the devices to pulses of positive and negative bias voltages has been analyzed in more detail. A bias voltage of +4 V was applied for 1 s and subsequently the conductivity of the diode was probed by applying multiple short ( $\sim 40$  ms) 'read' pulses of +1.5 V and monitoring the current density (Figure 2.6, upper panel, solid squares). In between the read pulses, the device was kept short circuited. Two transient components to the current density under the read voltage may be expected. The first is a Faradaic discharge current, which flows in a direction opposite to the steady state current under +1.5 V bias when the device has been stress at +4 V. The second transient contribution results from the enhanced injection of charge carriers at +1.5 V after modification of the barriers for injection by the motion of ions and the associated redox reactions resulting from the +4 V stress. This excess current flows in the same directions as the steady state current at +1.5 V bias. At times  $t < 1$  s after the write pulse, the Faradaic discharge current dominates while for times  $t > 1$  s, the current

density is enhanced due to the junction formation. When the +4 V bias is applied for a longer time interval (2, 5, or 10 s), the importance of the discharge current ( $t < 1$  s) is reduced while the excess current ( $t > 1$  s) due to junction formation increases. Figure 2.6 shows the response to a -4 V bias voltage pulses (open circles). Here, the discharge current has the same direction as the steady state current under +1.5 V bias. Therefore, the enhanced current densities in the first second after the -4 V pulse as observed for the 1, 2, and 5 s voltage pulses, may be ascribed to the discharge current. Consistent with the absence of junction formation under reverse bias as inferred from the  $J$ - $V$  scans, no significant reduction of the current density at the read voltage due to induction of a junction with opposite polarity by applying -4 V bias stress has been found.

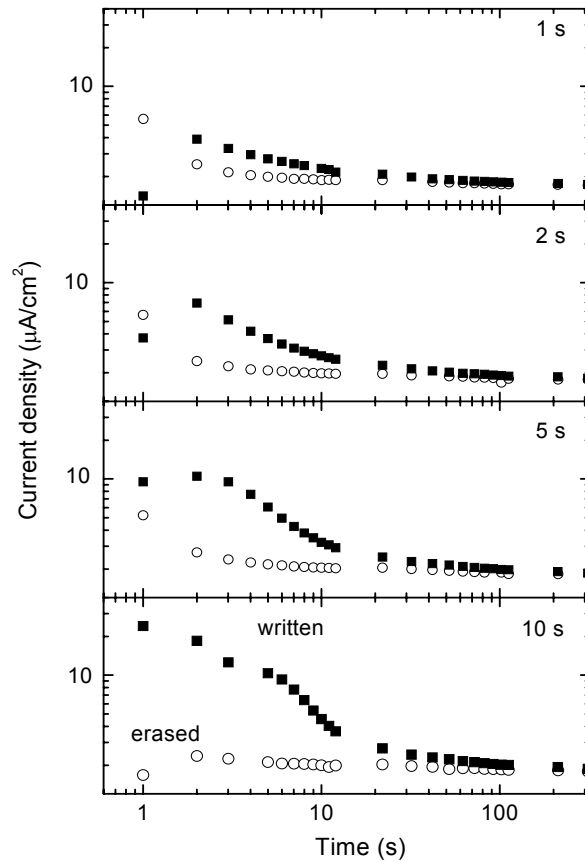


**Figure 2.6:** Time dependence of the current density of the ITO/PEDOT:PSS(NaCl, EC)/6T-PEO/Al at  $V = +1.5$  V after a +4 V write pulse (■) and after a -4 V erase pulse (○). The length of the write and erase pulses is systematically varied from 1, 2, 5, and 10 s. The read pulses have a temporal width of  $\sim 40$  ms and in between the read pulses the devices is kept at 0 V bias.

This asymmetric response of the diodes and the excess current density associated with the hysteresis allows us to temporarily store information in the cells in a reversible manner. The cells can be 'written' at +4 V, 'erased' at -4 V, and 'read' in forward bias at

+1.5 V. As can be seen from Figure 2.6, the excess current density allows one to distinguish a low conductivity state and a high conductivity state in the time window between 1 and 10 s when the write and erase pulses are  $\geq 5$  s. For delays larger than 10 s after the write/erase pulse, the current densities for the written and erased states quickly converge. Thus, the retention time of the information (10 s) is at present rather short. To improve on this, a block copolymer with a very steep dependence of the ion mobility on electric field is needed.

As mentioned above, the hysteresis in forward bias can be rationalized in terms of electrochemical doping at the electrodes induced by ion transport.<sup>16</sup> The effect of ion accumulation and electrochemical doping on the barriers for charge injection are illustrated schematically in Figure 2.7. Under application of forward bias stress, electrochemical doping of 6T occurs at both electrodes. Near the Al, reduction of the 6T is facilitated by migration of sodium ions towards the metal electrode (n-type doping). Oxidation of 6T occurs near the interface with the PEDOT:PSS electrode and is associated with migration of the chloride ions in the vicinity of the interface (p-type doping). This results in formation of a p-n junction.<sup>32,33</sup>

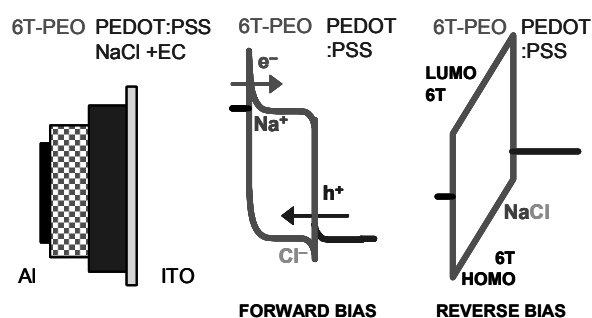


**Figure 2.7:** Schematic layout of the ITO/PEDOT:PSS(NaCl,EC)/6T-PEO/Al device (left) and a band level diagram for the diode under forward bias stress (middle) and reverse bias stress (right). The injection of negative ( $e^-$ ) and positive ( $h^+$ ) charge carriers into the semiconducting block of the copolymers is indicated.

This mechanism is supported by the temperature dependence of the  $J$ - $V$  characteristic. At low temperature, where motion of ions is inhibited, the hysteresis is strongly reduced (Figure 2.8). At the lowest temperature ( $T = 225$  K) no hysteresis in the  $J$ - $V$  characteristic could be observed. This is consistent with the view that hysteresis is induced by motion of ions and subsequent electrochemical processes. At  $T = 305$  K the hysteresis is reduced in magnitude compared to  $T = 275$  K. This may be explained by a high mobility of ions at this temperature, such that they are almost able to reach thermodynamic equilibrium in their positional motion during the scan time. When equilibration is rapid, no hysteresis can occur. Conversely, at high temperature, the

mobility of ions is higher and relaxation to the thermodynamically favored state is faster. Hence the hysteresis is suppressed as well.

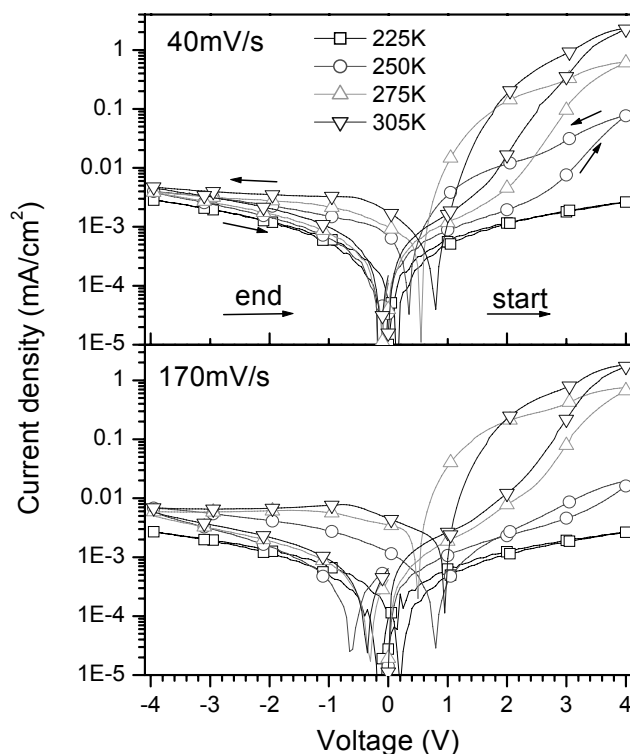


**Figure 2.8:** Temperature dependence of the current voltage characteristics of the PEDOT:PSS/6T-PEO/Al diode with the PEDOT:PSS layer doped with NaCl and ethylene carbonate. Results for two different scan speeds are shown, the upper panel pertains to a slow scan speed (40 mV/s) while the lower panel pertains to an almost fourfold higher speed (170 mV/s). Direction of the hysteresis, indicated in the upper graph, is the same at all temperatures and scan speeds. Measurements were performed in a vacuum cryostat.

As expected, the hysteresis remains when taking top metal contacts with different work functions (Figure 2.9). For all three metals used, the devices display some diode character. Using gold as metal electrode, the rectification is the lowest. With this metal, the barrier for hole injection in the molecular material through the metal electrode is lower, which can explain the higher current densities in at negative (reverse) bias and the lower rectification ratio observed for gold.

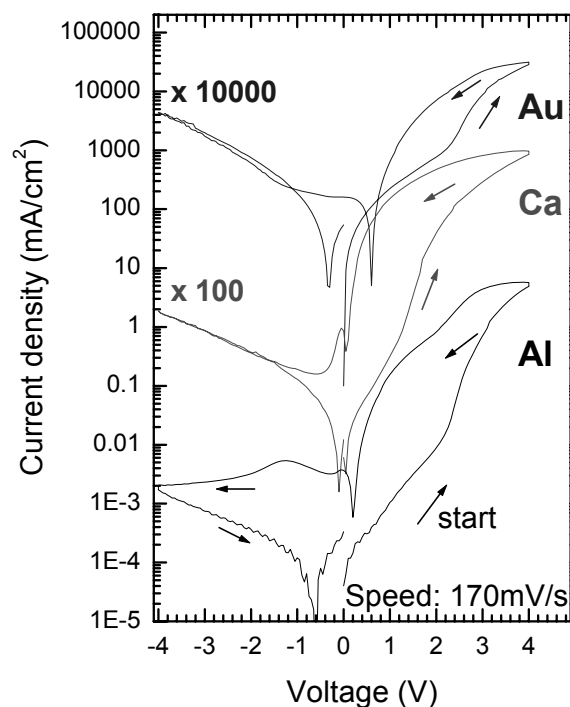


**Figure 2.9:** Current voltage characteristics of the PEDOT:PSS/6T-PEO/Metal diode with the PEDOT:PSS layer doped with 20 wt % NaCl and ethylene carbonate. Results for three different metal top electrodes are shown (Gold, Calcium and Aluminum) Scan speed 170 mV/s, room temperature. Diodes were stored and characterized in an inert atmosphere ( $O_2, H_2O \sim 1$  ppm).

In all three cases an anticlockwise hysteresis is observed under forward bias, which can be explained by a lowering of the barrier for charge carrier injection induced by motion of salt ions towards the electrodes with ensuing electrochemical processes. Under reverse bias, hardly any hysteresis is observed for Au and Ca electrodes and clockwise hysteresis is found for Al. In the latter case, the clockwise hysteresis can be attributed to the contribution of a Faradaic discharge current. This discharge current is driven by the energy stored in the device under forward bias stress. This assignment is confirmed by measurements of the current voltage characteristics in the reverse bias regime only (see Figure 2.2); here little hysteresis is observed in the -4V to -2V bias regime.

To account for the low open-circuit voltage after bias stress as observed for the diodes with salt, it is argued that a p-n junction is formed with a narrow depletion zone between the p and n doped regions. Such narrow widths are expected when extensive electrochemical doping occurs.<sup>34</sup> Because of the narrow depletion width, mobile electrons and holes on the 6T segments can recombine after diffusional motion, reducing any open-circuit voltage quickly after termination of the bias voltage.

## 2.5. Electroluminescence

The observation of electroluminescence (EL, Figure 2.3) allows us to analyze the junction formation in further detail. EL is observed for devices when the PEDOT:PSS layer is doped with either NaCl or Li:PSS. The EL shows an onset at +2.5 V (Figure 2.10a) which is delayed in time with respect to the start of the bias voltage (Figure 2.10b). In order to generate EL, electrons must be injected via the Al electrode, a process that is assisted by accumulation of small positive ions ( $\text{Na}^+$ ,  $\text{Li}^+$ ) near the Al electrode and after being transported through the block copolymer. The delayed onset of the EL with respect to the application of the bias voltage can then be interpreted in terms of the time needed for the transport of ion and the electrochemical doping processes.

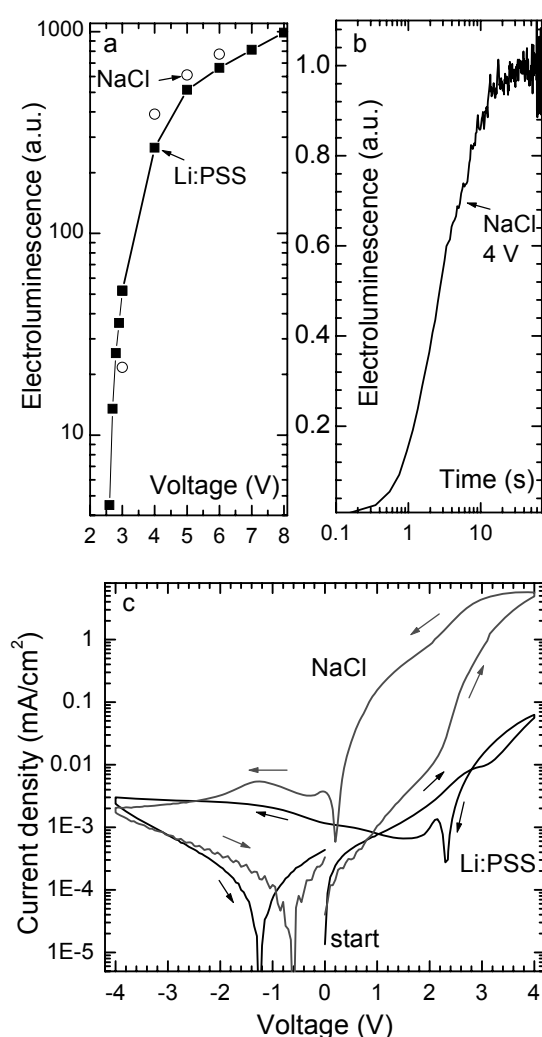


**Figure 2.10:** (a) Electroluminescence intensity as a function of applied voltage for ITO/PEDOT:PSS/6T-PEO/Al diodes doped with EC and either NaCl (open circles) or Li:PSS (20 wt %, solid squares). (b) Time dependence of the electroluminescence intensity for the diode with NaCl. At time  $t = 0$  s a constant bias voltage of +4 V was switched on. (c) J-V characteristics of the diodes with Li:PSS or NaCl. Scan speed 170 mV/s, room temperature.



Interestingly, for the devices with Li:PSS added, the hysteresis in the  $J$ - $V$  characteristic is strongly reduced in comparison with devices doped with NaCl (Figure 2.10c). Because of its bulkiness, the PSS polyanion will hardly migrate. The fact that EL is observed upon doping with Li:PSS in combination with the absence of a considerable hysteresis in the forward bias regime, indicates that the hysteresis observed with NaCl doping results from migration of the  $\text{Cl}^-$  anions to the vicinity of the PEDOT:PSS/6T-PEO interface resulting in an effective lowering of the barrier for hole injection. From the absence of enhanced current under reverse bias stress, it is inferred that the  $\text{Cl}^-$  anions are not transported through the block copolymer to the interface with the Al electrode. Had the chloride ions reached the close proximity of the Al electrode, electrochemical were to be expected resulting in an Ohmic contact for hole injection. In this interpretation the asymmetry of the diode in its response towards positive and negative bias stress results from selective transport of ions.

### **2.6. Conclusion**

In summary, it has been shown that block copolymers with a semiconducting and ion transporting block can be used to construct diodes displaying resistive switching in the current under forward bias without any appreciable modulation of the conductivity in the reverse bias regime. This type of behavior is required for integration of memory cells in passive matrix arrays. The asymmetry in the response is attributed to selectivity in the transport of ions by the block copolymer. Molecular engineering of block copolymers combining charge and ion transporting moieties therefore seems a promising tool to design switchable electronic elements.

### **2.7. Experimental**

The devices were built on a glass substrate with a transparent tin doped indium oxide (ITO) electrode. The substrates were first cleaned in a ultrasonic bath with sequentially acetone, a soap solution, water, and isopropanol. After a final UV-Ozone treatment (UV-Ozone Photoreactor PR-100) of 30 minutes, an aqueous dispersion of poly(ethylenedioxythiophene):poly(styrenesulfonate) (PEDOT:PSS, H.C. Starck, Baytron P VP Al 4083) containing NaCl (20 wt.-% relative to the weight of dry material in the dispersion) and EC (20 wt.-%) was spin coated on the ITO to create the bottom electrode. The resulting PEDOT:PSS(NaCl, EC) layer was dried (2 min 180 °C, thickness 0.07  $\mu\text{m}$ ) and a layer of 6T-PEO was deposited by spin coating from 15 mg/mL tetrahydrofuran (THF) solution (thickness 0.09  $\mu\text{m}$ ). The top metal contact was made by vapor deposition of Al at  $5 \times 10^{-6}$  mbar. The active area of the devices was 0.095  $\text{cm}^2$ . All solvents used are of AR quality and the chemicals are used as received. Devices were stored and measured in an inert atmosphere ( $\text{O}_2$ ,  $\text{H}_2\text{O} \sim 1$  ppm) using homemade Labview programs with a computer

controlled Keithley 2400 source meter. Cyclic voltammograms were recorded with a Autolab Potentiostat in an inert atmosphere with 0.1 M tetrabutyl ammonium hexafluorophosphate (TBAPF<sub>6</sub>) in dichloromethane (DCM) or THF as supporting electrolyte. Redox potentials were measured against an Ag/AgCl reference electrode referenced *in situ* against Fc/Fc<sup>+</sup>. UV-Vis measurements were performed on a Perkin Elmer Lambda 40 UV/Vis Spectrometer or a Perkin Elmer 900 UV/Vis/NIR Spectrometer. Fluorescence measurements were performed on a Edinburgh Instruments FS920 double monochromator luminescence using a Peltier-cooled red-sensitive photomultiplier.

## 2.8. References

- 1 S. Tal, B. Blumer-Ganon, M. Kapon, and Y. Eichen, *J. Am. Chem. Soc.* **127**, 9848 (2005).
- 2 R.C.G. Naber, B. de Boer, P.W.M. Blom, and D.M. de Leeuw, *Appl. Phys. Lett.* **87**, 203509 (2005).
- 3 M. Mushrush, A. Facchetti, M. Lefenfeld, H. E. Katz, and T.J. Marks, *J. Am. Chem. Soc.* **125**, 9414 (2003).
- 4 A. Facchetti, J. Letizia, M.-H. Yoon, M. Mushrush, H. E. Katz, and T. J. Marks, *Chem. Mater.* **16**, 4715 (2004).
- 5 J. He, L.P. Ma, J.H. Wu, and Y. Yang, *J. Appl. Phys.* **97**, 064507 (2005).
- 6 R.J. Tseng, J. X. Huang, J. Ouyang, R. B. Kaner, and Y. Yang, *Nano Lett.* **5**, 1077 (2005).
- 7 J.C. Scott, *Science* **304**, 62 (2004).
- 8 Y. Yang, L. Ma, and J. Wu, *MRS Bulletin* **29**, 833 (2004).
- 9 J. Ouyang, C.-W. Chu, R.J.-H. Tseng, A. Prakash, and Y. Yang, *Proceedings IEEE* **93**, 1287 (2005).
- 10 W.J. Yoon, S.Y. Chung, P.R. Berger, and S. M. Asar, *Appl. Phys. Lett.* **87**, 203506 (2005).
- 11 R.J. Luyken and F. Hofmann, *Nanotechnology* **14**, 273 (2003).
- 12 F.L.E. Jakobsson, X. Crispin, and M. Berggren, *Appl. Phys. Lett.* **87**, 063503 (2005).
- 13 S. Möller, C. Perlov, W. Jackson, C. Taussig, and S. R. Forrest, *Nature* **426**, 166 (2003).
- 14 S. Möller, S.R. Forrest, C. Perlov, W. Jackson, and C. Taussig, *J. Appl. Phys.* **94**, 7811 (2003).
- 15 S. Smith and S.R. Forrest, *Appl. Phys. Lett.* **84**, 5019 (2004).
- 16 L. Edman, M.A. Summers, S.K. Buratto, and A.J. Heeger, *Phys. Rev. B* **70**, 115212 (2004).
- 17 Q. Pei, G. Yu, C. Zhang, Y. Yang, and A.J. Heeger, *Science* **269**, 1086 (1995).
- 18 J.C. deMello, N. Tessler, S.C. Graham, and R.H. Friend, *Phys. Rev. B* **57**, 12951 (1998).
- 19 J.H.A. Smits, S.C.J. Meskers, R.A.J. Janssen, A.W. Marsman, and D.M. de Leeuw, *Adv. Mater.* **17**, 1169 (2005).
- 20 O. Henze and W.J. Feast, *J. Mater. Chem.* **6**, 1274 (2003).
- 21 A. Facchetti, M.-H. Yoon, C.L. Stern, G.R. Hutchison, M.A. Ratner, and T.J. Marks, *J. Am. Chem. Soc.* **126**, 13480 (2004).

- 22 D. Mühlbacher, M. Scharber, M. Morana, Z. Zhu, D. Waller, R. Gaudiana, and C. Brabec, *Adv. Mater.* **18**, 2884 (2006).
- 23 T. Johansson, W. Mammo, M. Svensson, M.R. Andersson, and O. Inganäs, *J. Mater. Chem.* **13**, 1316 (2003).
- 24 T.M. Brown, J.S. Kim, R.H. Friend, F. Caciallia, R. Daik, and W.J. Feast, *Appl. Phys. Lett.* **75**, 1679 (1999).
- 25 H.B. Michaelson, *J. Appl. Phys.* **48**, 4729 (1977).
- 26 R.S. Becker, J.S. de Melo, A.L. Maçanita, and F. Elisei, *J. Phys. Chem.* **100**, 18683 (1996).
- 27 P. Leclère, M. Surin, P. Viville, R. Lazzaroni, A.F.M. Kilbinger, O. Henze, W.J. Feast, M. Cavallini, F. Biscarini, A.P.H.J. Schenning, and E.W. Meijer, *Chem. Mater.* **16**, 4452 (2004).
- 28 F. Garnier, *Acc. Chem. Res.* **32**, 209 (1999).
- 29 M. Muccini, E. Lunedei, C. Taliani, D. Beljonne, J. Cornil, and J.L. Brédas, *J. Chem. Phys.* **109**, 10513 (1998).
- 30 M. Muccini, E. Lunedei, A. Bree, G. Horowitz, F. Garnier, and C. Taliani, *J. Chem. Phys.* **108**, 7327 (1998).
- 31 A.F.M. Kilbinger and W.J. Feast, *J. Mater. Chem.* **10**, 1777 (2000).
- 32 C.H.W. Cheng and M.C. Lonergan, *J. Am. Chem. Soc.* **126**, 10536 (2004).
- 33 K. Harada, A.G. Werner, M. Pfeiffer, C.J. Bloom, C.M. Elliott, and K. Leo, *Phys. Rev. Lett.* **94**, 036601 (2005).
- 34 J. Gao, and J. Dane, *J. Appl. Phys.* **98**, 063513 (2005).

# 3

## **Electronic memory effects in diodes from a zinc oxide nanoparticle – polystyrene hybrid material**

*Current-voltage characteristics of diode structures with an active layer of a zinc oxide nanoparticle – polystyrene hybrid material (1:2 by weight) deposited by spin coating from solution are investigated. Aluminum and poly(3,4-ethylenedioxythiophene):polystyrenesulfonate are used as electrodes. After a forming step, the conduction under reverse bias voltage can be raised or lowered in a gradual and reversible manner by applying forward and reverse bias voltages, respectively. Electrically induced switching between states with high and lower conductivity is possible on a timescale of 100 ms and the conduction levels remain stable for over 1 hour.*

This work has been published: F. Verbakel, S.C.J. Meskers, and R.A.J. Janssen, *Appl. Phys Lett.* **89**, 102103 (2006).

### 3.1. Introduction

In recent years electronic memory effects in molecular materials have been investigated, in particular field induced resistive switching in diodes.<sup>1,2</sup> Also diodes with an active layer of molecular materials containing inorganic nanoparticles or metal interlayers have been investigated.<sup>3,4,5</sup> In this chapter, memory effects in the electrical conduction through an organic-inorganic hybrid layer consisting of zinc oxide nanoparticles mixed with polystyrene (PS) polymer have been studied. This mixture is solution processable and high loadings of ZnO particles can be achieved allowing for conduction of charge via interparticle contacts. ZnO was chosen because this material is known to exhibit memory effects in bulk conduction,<sup>6,7</sup> an effect which is also known for many other metal oxides.<sup>8,9</sup>

### 3.2. Current-voltage characterization

The pristine devices, comprising ZnO nanoparticles and PS sandwiched between ITO/PEDOT:PSS and Al electrodes, have a current-voltage ( $J$ - $V$ ) characteristic that shows considerable rectification when scanned between  $-2$  V and  $+2$  V (Figure 3.1). Here, positive bias voltage refers to the PEDOT:PSS electrode being charged positive with respect to the Al electrode. The current density at  $+2$  V increases with the weight fraction of ZnO in the active layer. This indicates that the current is due to transport of electrons via a percolating network of inorganic particles in combination with a rectifying contact between the ZnO particles and the PEDOT:PSS and an Ohmic contact between ZnO and Al. Extending the range of the bias voltage sweep from  $\pm 2$  V to  $\pm 10$  V introduces some hysteresis in the  $J$ - $V$  characteristics but the diode behavior is largely retained. After further stressing the device by applying a  $+15$  V bias for 10 s, the conduction increases further and becomes almost Ohmic. After this forming step, the  $J$ - $V$  characteristic shows considerable hysteresis for negative bias voltages when performing a cyclic  $J$ - $V$  scan. The voltage required for the forming step increases with decreasing ZnO content and devices with only PS do not show any forming at all when applying  $+20$  V for 30 sec.

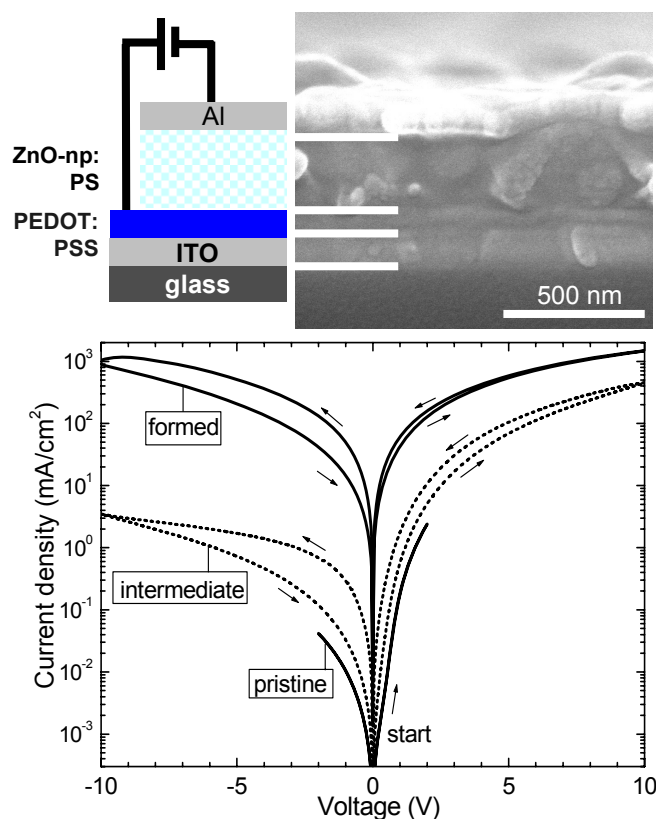


**Figure 3.1:** (Top) Schematic representation of the device structure and cross-sectional SEM image (ZnO:PS 1:2 wt). (Bottom)  $J$ - $V$  characteristic of the diode in the pristine state and in an intermediate conduction state reached by scanning the bias voltage from 0 V  $\rightarrow$  +10 V  $\rightarrow$  -10 V  $\rightarrow$  0 V. The uppermost curve shows the  $J$ - $V$  after forming for 10 s at +15 V bias voltage. Scan speed 170 mV/s.

### 3.3. Resistive switching

The hysteresis shown by the *formed* device implies that its resistance can be altered in a reversible manner by applying voltage pulses. Applying a +10 V pulse with a duration of either 0.1, 1 or 5 s to the diode, the conduction level can be raised while an ensuing -10 V pulse with the same temporal width reduces the conductivity again (Figure 3.2a-c). These high and low conduction states correspond to the two branches of the  $J$ - $V$  curve of the formed device as shown in Figure 3.1. In between these “write” and “erase” pulses the conductivity is probed by measuring the current under application of a series of short -0.5 V “read” pulses. During the time between the pulses the device is kept at zero bias. This cycle can be repeated many times.

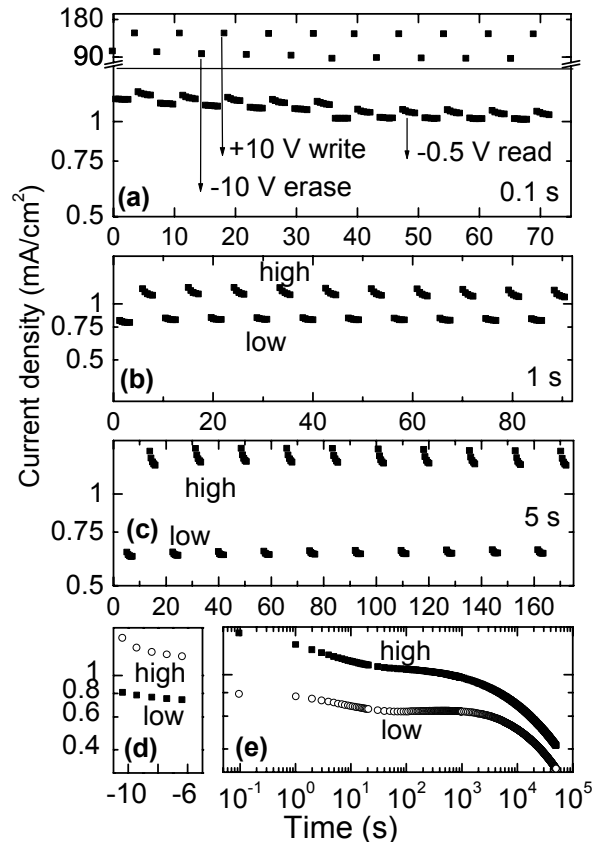


**Figure 3.2:** (a-c): Current density of the ZnO:PS (1:2 wt) device upon application of a cycle of voltage pulses: a  $-10$  V (erase) , five  $-0.5$  V (read) pulses, a  $+10$  V (write) and five  $-0.5$  V (read) pulses. Duration of the  $-0.5$  V pulses:  $0.1$  sec. Duration of the  $+10$  and  $-10$  V pulses is varied from  $0.1$  (a),  $1$  (b), to  $5$  s (c). In between the pulses the device is kept at zero bias voltage. (d-e): Preparation of the high and low conduction levels by application of a  $+10$  V ( $-10$  V) pulse for  $5$  s. The current densities upon application of  $-0.5$  V,  $0.1$  s pulses are shown (d). Subsequently, a  $-10$  V ( $+10$  V),  $5$  s pulse is applied to switch from high to low conductivity (or vice versa) and the time evolution of the conductivity is probed, applying  $-0.5$  V,  $0.1$  s pulses (e).

As can be seen in Figure 3.2, the ratio between the high and low conduction level (as probed at  $-0.5$  V) increases with the duration of the  $\pm 10$  V pulses and reaches a factor of 2 for pulses of  $5$  s. The stability of the high and low conduction level in time has been evaluated (Figure 3.2d-e). In order to monitor the preparation of the high conduction state, the device is first brought to the low conduction state and probed (Figure 3.2d). Subsequently, the high conduction state is prepared by applying  $+10$  V bias for  $5$  s and the time evolution of the conduction is then probed in the  $1 - 10^5$  s interval by applying a series of  $-0.5$  V,  $0.1$  s pulses (Figure 3.2e). In the first seconds after the  $+10$  V pulse, the conduction shows some decay, but in the  $10 - 1000$  s time window the level does not show any substantial change. The time evolution of the low conductivity state is probed in similar manner and shows some rapid initial decay after

the  $-10$  V pulse, remaining relatively stable up to 1000 s. On the timescale of several hours both the high and low conduction level decrease but are still much higher than the conduction level in the pristine device.

### 3.4. Forming process

The forming process and the associated memory effects may arise from modulation of the density of mobile electrons in the ZnO particles. For bulk ZnO, unintentional n-type doping is well known and is usually ascribed to native point defects such as oxygen vacancies and/or interstitial Zn atoms.<sup>10,11</sup> In addition, a number of extrinsic dopants are known (including Al and H). Further information on the forming process comes from experiments on the influence of molecular oxygen and ultraviolet (UV) illumination on the conduction (Figure 3.3). When the device is exposed to air after the formation step, the Ohmic conduction is strongly suppressed and the initial diode like characteristic is restored. Subsequent illumination with UV light results in Ohmic conduction, which can be quenched again by exposure to air. This effect of UV light is also observed for pristine films. After this UV treatment and O<sub>2</sub> exposure, the films can be formed again by application of a positive bias voltage. Thus the effects of UV illumination and positive bias stress on the conductivity seem indistinguishable.

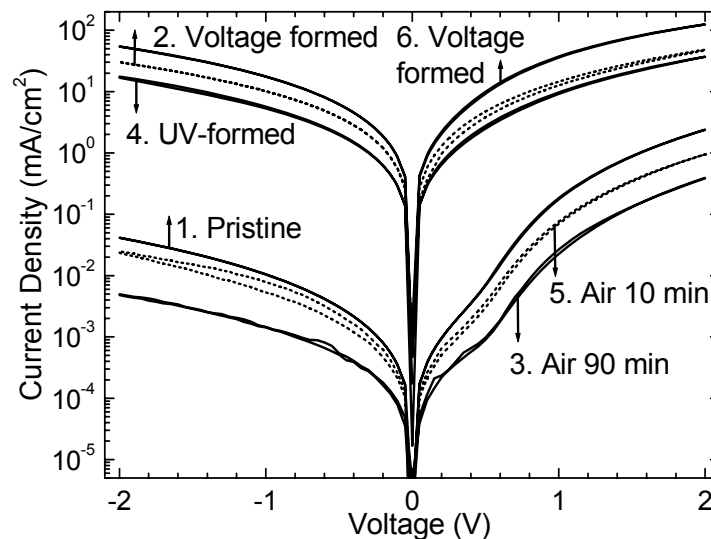


**Figure 3.3:** J-V characteristics of a ZnO:PS (1:2 wt) device in chronological order: (1) Pristine device. (2) After forming at +15 V bias voltage for 5 s. (3) After subsequent exposure to air for 90 min. (4) After illumination for 5 min with 80 mW/cm<sup>2</sup> light intensity from a tungsten halogen source. (5) Exposure to air (10 min). (6) After bias stress at a voltage of + 10 V during 30 s.

In the case of UV illumination, the metastable conductivity is likely to be induced by either photogenerated electrons or holes in the ZnO (persistent photoconductivity). In



order to distinguish between the two types of carriers, ZnO nanoparticles have been mixed with regioregular poly(3-hexylthiophene) polymer (P3HT, purchased from Rieke Metals Inc.). Also for this hybrid material, electronic memory effects can be observed after an initial forming. In this case illumination with visible light results in photoexcitation of the polymer and subsequently leads to charge generation at the ZnO:P3HT interface with the electrons residing on the ZnO nanoparticle.<sup>12</sup> Curiously, illumination with visible light ( $\lambda > 420$  nm) does not enhance the dark conduction level after prolonged irradiation while UV irradiation ( $\lambda < 420$  nm) of the same film indeed results in Ohmic conduction. Apparently the n-type doping is induced by the presence of photogenerated holes in the ZnO nanocrystal.

This behavior is completely in line with earlier studies on persistent photoconductivity in porous, bulk ZnO<sup>13-16</sup> and ZnO nanostructures<sup>17-22</sup> where it was shown that photogenerated holes induce desorption of oxygen adsorbed on the surface. Adsorbed oxygen acts as an electron trap and its release enhances the concentration of mobile electrons originating from the native doping and photoexcitation of the ZnO. Since UV illumination and voltage stress give rise to the same conduction levels, it is argued that the forming process observed under forward bias stress results from holes injected via the PEDOT:PSS contact (Figure 3.4c). In agreement with this, the forming process is only induced by applying a large positive bias voltage and does not occur under reverse bias conditions where the injection barrier for holes into ZnO is much larger (Figure 3.4a-b). After forming, the density of free electrons in ZnO is increased, explaining the significant increase in conductivity (Figure 3.4d). Near the PEDOT:PSS electrode diffusion of these free electrons will result in a narrow depletion zone, causing a strong band bending that facilitates electron injection from PEDOT:PSS into ZnO under reverse bias. Because the current under reverse bias is now controlled by a very thin interface region small changes near the contact such as a reversible electrochemical doping of the ZnO particle near the PEDOT:PSS interface may explain the memory effects observed. Possible electrochemical processes involve chemisorbed /physisorbed oxygen and small mobile ions ( $H^+$ ,  $Na^+$ ) originating from the PEDOT:PSS. Reversible switching is not observed for devices without the PEDOT:PSS layer.

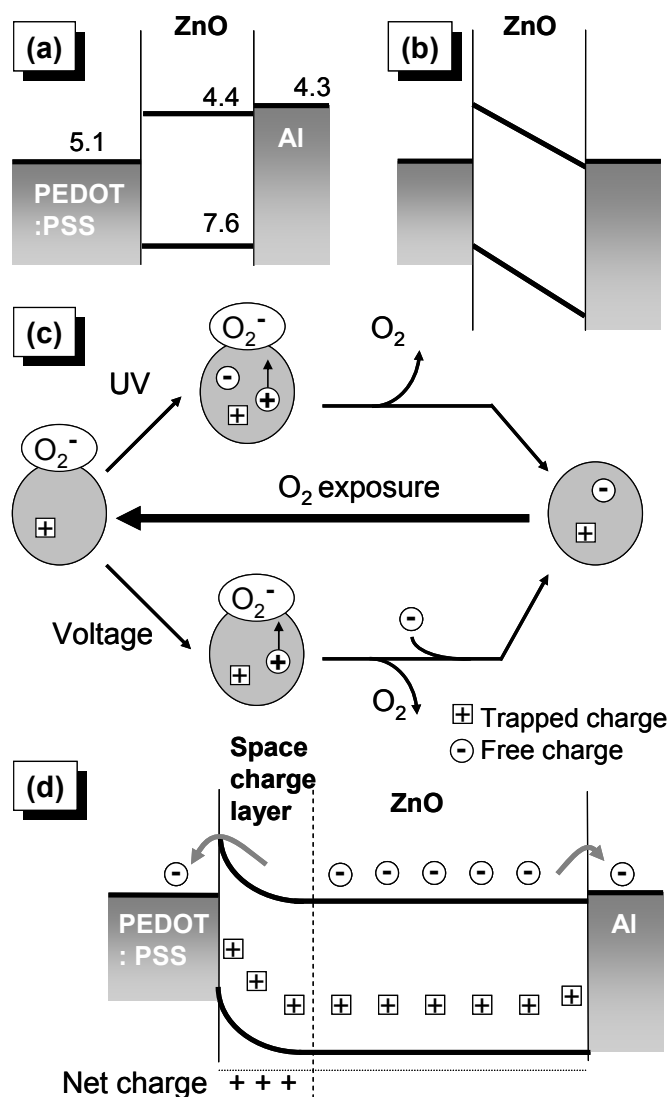


**Figure 3.4:** (a, b) Band level diagrams for pristine device illustrating the rectifying PEDOT:PSS/ZnO contact. (c) Schematic representation of the UV light and bias voltage induced changes in the ZnO particles. An injected or photogenerated hole induces desorption of oxygen. This results in a very thin space charge layer in the formed device (d) which lowers the barrier for electron injection via the PEDOT:PSS contact.

### 3.5. Conclusion

In conclusion, a reversible electronic memory effect has been observed in diode structures with a spincoated hybrid layer comprising ZnO nanoparticles. This memory effect is observed after a forming step. The forming process itself is interpreted in terms of desorption of oxygen from the ZnO nanoparticle surface induced by injection of holes via the PEDOT:PSS contact, leading to a higher n-type conductivity via interparticle ZnO

contacts. The electronic memory effects are attributed to a reversible electrochemical process at the ZnO/PEDOT:PSS interface.

### 3.6. Experimental

The diodes consist of a spin coated active layer between two electrodes (Figure 3.1). The bottom electrode is tin-doped indium oxide (ITO) with a spin coated film of poly(3,4-ethylene dioxythiophene): polystyrene sulfonate (PEDOT:PSS, H.C. Starck, Baytron P VP Al 4083) of  $0.7 \times 10^2$  nm thickness, which was added after cleaning as described in Chapter 2. The active layer is spin coated at 1500 rpm from a solution containing 20 mg PS ( $M_w = 250$  kg/mol, polydispersity index 2.2) and 10 mg of ZnO particles<sup>23</sup> (diameter  $\sim 5$  nm) per ml chloroform. This gives an active layer with a thickness of  $4 \times 10^2$  nm. The top electrode is made by evaporation of aluminum. The active device area is  $0.095$  cm<sup>2</sup>. After deposition of Al, the devices are stored and characterized in an inert atmosphere ( $O_2$ ,  $H_2O \leq 1$  ppm). ZnO nanoparticles were prepared using a procedure based on the work of W.J.E. Beek.<sup>24</sup> Zinc acetate dihydrate (Acros, >98%, 2.95 g, 13.4 mmol) was dissolved in methanol (125 mL) at 60 °C, a solution of KOH (Merck, 87%, 1.48 g, 23 mmol) in methanol (65 mL) was added in 10 min. to the zinc acetate dihydrate solution under vigorous stirring. Zinc-hydroxides precipitated but dissolved again. After 5 min. the solution became translucent and remained translucent, after 1.5 h the nanoparticles started to precipitate and the solution became turbid. After 2 h and 15 min., the heater and stirrer were removed and the nanoparticles were allowed to precipitate for an additional 2 h. Precipitate and mother-liquor were separated and the precipitate was washed with methanol (50 mL). Afterwards the suspension was left unstirred for a minimum of 1 h to reach full precipitation and again washed with methanol (50 mL). Further the suspension was centrifuged at 4300 rpm for 5 min, after which the nanoparticles were dissolved in chloroform (10 mL). This solution was only slightly translucent, almost transparent and was stable for more than two weeks.

IR (UATR):  $\nu$  (cm<sup>-1</sup>): 3402 (O-H stretch); 1570, 1445 (C=O stretch); 1025, 909, 677.

### 3.7. References

- 1 Y. Yang, L. Ma, and J. Wu, *MRS Bulletin* **29**, 833 (2004).
- 2 J. C. Scott, *Science* **304**, 62 (2004).
- 3 Y. Yang, J. Ouyang, L. Ma, R.J.-H. Tseng, and C.-W. Chu, *Adv. Func. Mater.* **16**, 1001 (2006).
- 4 L. D. Bozano, B.W. Kean, M. Beinhoff, K.R. Carter, P.M. Rice, and J.C. Scott, *Adv. Func. Mater.* **15** 1933 (2005).

- 5 W. Tang, H.Z. Shi, G. Xu, B.S. Ong, Z.D. Popovic, J.C. Deng, J. Zhao, and G.H. Rao, *Adv. Mater.* **17**, 2307 (2005).
- 6 T. Hada, K. Wasa, and S. Hayakawa, *Jpn. J. Appl. Phys.* **10**, 521 (1971).
- 7 O. Hunter Jr. and J.A. Schaefer, *US Patent* 4472296 (1984).
- 8 G. Dearnaley, A.M. Stoneham, and D.V. Morgan, *Rep. Prog. Phys.* **33**, 1129 (1970).
- 9 R.E. Thurstans and D.P. Oxley, *J. Phys. D.: Appl. Phys.* **35**, 802 (2002).
- 10 S.J. Pearton, D.P. Norton, K. Ip, Y.W. Heo, and T. Steiner, *J. Vac. Sci. Technol. B* **22**, 932 (2004).
- 11 Ü. Özgür, Ya. I. Alivov, C. Liu, A. Teke, M.A. Reshchikov, S. Doğan, V. Avrutin, S.-J. Cho, and H. Morkoç, *J. Appl. Phys.* **98**, 41301 (2005).
- 12 W.J.E. Beek, M.M. Wienk, and R.A.J. Janssen, *Adv. Func. Mater.* **16**, 1112 (2006).
- 13 D.A. Melnick, *J. Chem. Phys.* **26**, 1136 (1957).
- 14 R.J. Collins and D.G. Thomas, *Phys. Rev.* **112**, 388 (1958).
- 15 R. Ghosh, B. Mallik, and D. Basak, *Appl. Phys. A* **81**, 1281 (2005).
- 16 S.A. Studenikin, N. Golego, and M. Cocivera, *J. Appl. Phys.* **87**, 2413 (2000).
- 17 M. Haase, H. Weller, and A. Henglein, *J. Phys. Chem.* **92**, 482 (1988).
- 18 Q.H.Li, T.Gao, Y.G. Wang, and T.H. Wang, *Appl. Phys. Lett.* **86**, 123117 (2005).
- 19 K. Keem, H. Kim, G-T. Kim, J.S. Lee, B. Min, K. Cho, M.-Y. Sung, and S. Kim, *Appl. Phys. Lett.* **84**, 4376 (2004).
- 20 M.S. Arnold, Ph. Avouris, Z.W. Pan, and Z.L. Wang, *J. Phys. Chem. B* **107**, 659 (2003).
- 21 S.E. Ahn, J.S. Lee, H. Kim, S. Kim, B.H. Kang, K.H. Kim, and G.T. Kim, *Appl. Phys Lett.* **84**, 5022 (2004).
- 22 H. Kind, H. Yan, B. Messer, M. Law, and P. Yang, *Adv. Mater.* **14**, 158 (2002).
- 23 W.J.E. Beek, M.M. Wienk, M. Kemerink, X. Yang, and R.A.J. Janssen, *J. Phys. Chem. B* **109**, 9505 (2005).
- 24 W.J.E. Beek, *PhD. Thesis*, Eindhoven University of Technology (2005).  
<http://alexandria.tue.nl/repository/articles/621766.pdf>



# 4

## **Electronic memory effects in diodes of zinc oxide- nanoparticles in a matrix of polystyrene or poly(3-hexylthiophene)**

*Electronic memory effects in metal-insulator-metal devices with aluminum and poly(3,4-ethylenedioxythiophene):polystyrenesulfonate (PEDOT:PSS) as electrodes and a solution processed active layer consisting of zinc oxide (ZnO) nanoparticles embedded in a matrix of poly(3-hexylthiophene) or polystyrene are investigated. After an initial forming process, the devices show a reversible change in conductivity. The forming process itself is interpreted in terms of desorption of molecular oxygen from the ZnO nanoparticle surface, induced by injection of holes via the PEDOT:PSS contact, leading to a higher n-type conductivity via interparticle ZnO contacts. The forming can also be induced with ultraviolet light and the process is studied with electron paramagnetic resonance, photoinduced absorption spectroscopy, and field effect measurements. Also the composition of the active layer is varied and the memory effects can be influenced by changing the ZnO content and the polymer, allowing for data storage with lifetime >14 hours.*

This work has been published: F. Verbakel, S.C.J. Meskers, and R.A.J. Janssen, *J. Appl. Phys.* **102**, 083701 (2007) and F. Verbakel, S.C.J. Meskers, and R.A.J. Janssen, *Mater. Res. Soc. Symp. Proc.* **965**, 0965-S09-11 (2007).

### **4.1. Introduction**

Resistive switching in metal-insulator-metal (MIM) structures is an intriguing phenomenon in which the electrical resistance can be altered reversibly by the application of a voltage.<sup>1-3</sup> It is being investigated intensely, partly because of its potential application in data storage.<sup>4-8</sup> Switching in MIMs has been observed for a very wide variety of insulator materials. Well known are binary oxides (e.g. Nb<sub>2</sub>O<sub>5</sub>,<sup>9</sup> Al<sub>2</sub>O<sub>3</sub>,<sup>10</sup> Ta<sub>2</sub>O<sub>5</sub>,<sup>11</sup> TiO<sub>2</sub>,<sup>12-14</sup>, NiO,<sup>15</sup> Cu<sub>2</sub>O,<sup>16</sup> ZnO<sup>17</sup>), Perovskites,<sup>18,19</sup> polymers (e.g. polystyrene,<sup>20</sup> melanin<sup>21</sup>) and, more recently, complex molecular materials<sup>22-24</sup> and mixtures containing inorganic nanoparticles<sup>25-30</sup> and organic-inorganic interfaces.<sup>31</sup> Different mechanisms have been proposed to explain resistive switching phenomena,<sup>32-37</sup> but a large number of reports describe electronic transport via filaments that arise during a so-called forming step of the MIM.<sup>1,38-40</sup> This forming step occurs under application of a bias voltage and marks the transition from the pristine state of the MIM, which shows no resistive switching effect, to a state in which the resistance can be altered reversibly by application of a voltage.

In the previous chapters, memory effects in MIM diodes with a mixed insulating layer consisting of ZnO nanoparticles and polystyrene polymer (PS) were reported.<sup>41</sup> After a forming step, the resistance of these diodes can be switched by applying voltage pulses of different polarity and this switching effect resembles that reported for bulk ZnO.<sup>17,42</sup> The forming reaction in this material occurs upon illumination with ultraviolet (UV) light or upon application of a high forward bias voltage. The forming process has been ascribed to release of oxygen molecules from the surface of the nanoparticles induced by positive charge carriers in the particle. In this view, the surface bound oxygen acts as an electron trap, depleting the n-type ZnO particles of their mobile charge carriers. Introduction of holes, either via photogeneration<sup>43</sup> or injection through a contact, results in desorption of molecular oxygen (O<sub>2</sub>) from the surface of the nanoparticle, and the disappearance of the trap site associated with the oxygen allows for a higher concentration of *mobile*, negatively charged carriers<sup>44</sup> (Figure 4.1). Electrical conductivity through the material was postulated to occur via interparticle contacts and a percolating network. Consistent with this view, the forming process can be reversed by exposure to oxygen. At present, the origin of the reversible change in resistance that can be observed after the forming step is not known. It seems plausible that an electrochemical process at the interface of the ZnO:PS layer and one of the contacts is involved.

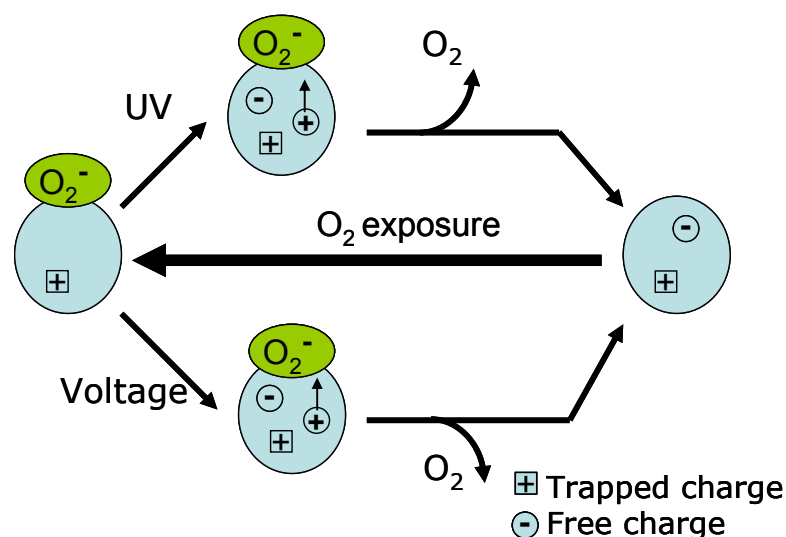


**Figure 4.1:** Schematic representation of the UV light and bias voltage induced changes in the ZnO particles. An injected or photogenerated hole induces desorption of oxygen by recombining with the electron trapped at the  $O_2$ . After elimination of the e-trap site formed by surface bound  $O_2$ , mobile photogenerated or injected electrons can contribute to a higher conductivity of the material comprising the ZnO particles.

In this chapter, the forming process in the ZnO:PS diodes is investigated in more detail by probing the mobile charge carriers after UV illumination directly, using electron paramagnetic resonance (EPR) and photoinduced absorption (PIA) spectroscopy. The action of electrically injected holes will be investigated using three electrodes in a field effect transistor geometry. MIM devices containing ZnO blended with polymer are then investigated, varying the loading of the ZnO particles in order to investigate the percolation behavior. In addition, a hybrid material consisting of ZnO nanoparticles blended with a polymer with semiconducting properties has been studied: poly(3-hexylthiophene) (P3HT). The results are consistent with electrical transport via the nanoparticles. The fact that the active layer is built up from nanoparticles and polymer allows one to influence the memory effects by changing the ZnO loading and the nature of the polymer. The minimum write time, ON/OFF ratio and retention time for rewritable data storage are evaluated for the ZnO:polymer MIM structures.

## 4.2. Mobile charge carriers in ZnO

In Figure 4.2a EPR spectra of the ZnO nanoparticles in vacuum are shown. Initially, no EPR signal is observed, but after illumination with ultraviolet (UV) light an intense EPR signal appears at  $g = 1.964$  which has been assigned to conduction electrons or weakly bound electrons originating from a shallow donor.<sup>45-47</sup> Upon exposure to air, this signal is reduced approximately 50 times and shifts to slightly higher field ( $g =$



1.962). This demonstrates that the concentration of mobile electrons can be raised with UV illumination and lowered by exposure to oxygen.

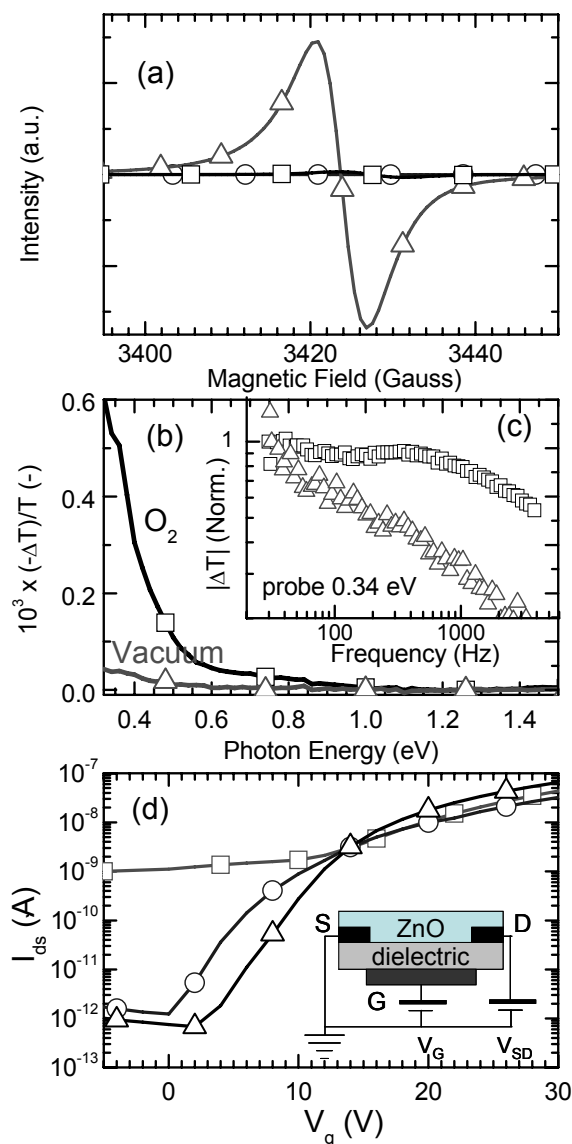


**Figure 4.2:** (a) Electron Paramagnetic Resonance (EPR) of pristine ZnO-nps in vacuum ( $\circ$ ), after UV illumination and in vacuum ( $\Delta$ ) and after subsequent exposed to air ( $\square$ ). (b) Near steady-state, photoinduced absorption (PIA) of ZnO-nps on quartz in air ( $\square$ ) and in vacuum ( $\Delta$ ). (c) Frequency dependence of the PIA signal at 0.34 eV in air ( $\square$ ) and in vacuum ( $\Delta$ ). (d) Transfer characteristics of a field effect transistor ( $V_{SD} = +40$  V) with channel length  $10 \mu\text{m}$  and width  $1000 \mu\text{m}$  in vacuum ( $\Delta$ ), after  $V_G = -40$  V during 5 s ( $\square$ ) and exposed to air ( $\circ$ ).

Mobile electrons in ZnO also give rise to absorption of infrared light.<sup>82,48</sup> This allows probing the charge carriers induced by UV illumination using photoinduced absorption (PIA) spectroscopy. In Figure 4.2b the results of a PIA experiment are shown, in which the intensity of the UV excitation beam (3.5 eV photon energy) is modulated and the amplitude of the periodic oscillation of the transmission of (white) light resulting

from the induced absorption, is recorded using phase-sensitive detection. As can be seen, UV illumination gives rise to a PIA signal in the infrared region of the spectrum (0.3 eV) which are ascribed to electrons in the conduction band. In oxygen atmosphere, the signal is much more intense, which can be explained by the fact that mobile electrons generated during the half period in which the ZnO is illuminated with UV light, can be trapped again by O<sub>2</sub> during the dark half period of the modulation cycle. In the absence of O<sub>2</sub>, the mobile electrons generated cannot be scavenged and this results in a much smaller *modulation* of the number of mobile electrons in the absence of O<sub>2</sub> and a reduced differential absorption signal in the modulation experiment. In addition, the mobile electrons may quench newly generated excitons by a fast Auger recombination limiting the photogeneration of additional carriers and suppressing the PIA response. The dependence of the PIA signal on the modulation frequency (Figure 4.2c) gives information on the lifetime of the charge carriers. In vacuum, the induced differential transmission ( $\Delta T$ ) decreases with increasing frequency approximately as  $|\Delta T(\omega)| \propto \omega^{-1/3}$ . Fourier transformation of the frequency dependent response gives an indication of the corresponding time dependence of the signal:<sup>49</sup>  $|\Delta T(t)| \propto t^{-2/3}$ . In air, the differential transmission shows a much flatter frequency dependence, implying a faster decay process. In particular, the flat response up to 1000 Hz, implies the presence of charge carriers with a lifetime shorter than 1 ms. This short lifetime is consistent with the proposed scavenging of mobile electrons by O<sub>2</sub>. This also gives some indication on how quickly the transition from the high to the low conductivity state through binding of oxygen may occur in the case where O<sub>2</sub> is present in close proximity to the ZnO particles (<1 ms).

In order to see which of the two types of photogenerated charge carriers induces the doping process, the ZnO particles have been applied as active layer in a field effect transistor (FET).<sup>50,51</sup> In Figure 4.2d the transfer characteristics of the device are illustrated. In vacuum, in the pristine state, the source drain current increases sharply for positive gate voltages, showing that the ZnO particles behave as an n-type semiconductor with an electron mobility on the order of 10<sup>-4</sup> cm<sup>2</sup>/Vs in the saturation regime. The device characteristics remain unaltered after application of positive gate voltages (+40 V) for short times, but upon application of negative gate voltages (-40 V, 5 s) the transfer characteristic change drastically, showing a much higher conductivity at zero gate voltage. This shows that the introduction of positive charge carriers by application of the negative gate voltage induces a transition in the material to a state with a much higher conductivity. After exposure to O<sub>2</sub>, the transfer characteristics of the ZnO transistor resemble again those for the pristine device.

In summary, the experiments illustrated in Figure 4.2, demonstrate that positive charge carriers in the ZnO, either photogenerated or injected via a contact, induce a change in the particles leading to a state with a higher concentration of mobile charge carriers (electrons) in the particles. In an interpretation that also takes into account the persistent photoconductivity and the release of O<sub>2</sub>, the holes recombine with the electron trapped at the surface of the ZnO by an O<sub>2</sub> molecule, inducing desorption of neutral O<sub>2</sub>.<sup>52,53</sup> After desorption, the O<sub>2</sub> can no longer act as an electron trap and this allows for an increase in the number of *mobile* electrons (see Figure 4.1), which themselves can be either photogenerated or supplied via an electrical contact. With this mechanistic information the forming reaction of the ZnO particles embedded in the diode structure can now be attended.

### **4.3. Diodes with ZnO:PS as active layer**

In this section the electrical properties of MIM devices with an insulating layer consisting of ZnO and polystyrene are described. The layout of the diodes used to study the memory effects is illustrated in Figure 4.3. The spin coated active layer is sandwiched between two different electrodes, PEDOT:PSS and aluminum. The corresponding band diagram is draw in Figure 4.3 (inset) using literature values of the conduction and valence bands of ZnO<sup>54,55</sup> and the work function of PEDOT:PSS<sup>56</sup> and Al.<sup>57</sup> By changing the weight ratio of ZnO and PS in the solution used for spin coating, the composition of the active layer can be varied in a systematic way.

In Figure 4.3 the current-voltage (*J-V*) characteristics of a device in various states is illustrated. The pristine device shows rectifying behavior and, considering the n-type nature of the ZnO and the Ohmic contact between ZnO and Al,<sup>58</sup> the high current densities under positive bias can be attributed to electrons injected through the Al electrode. More detailed analysis of the *J-V* characteristics shows that under forward bias, the current is dominated by an Ohmic (leakage) contribution for voltages below +0.5 V. For voltages higher than +0.5 V, a sharp rise of the current density with increasing voltage is observed, which eventually flattens and approaches a  $J \propto V^2$  behavior, which may be expected for space charge limited conduction. This shows that at low voltages ( $V \leq +0.5$  V) the active layer behaves as a semiconductor with a very low density of mobile carriers. The sharp increase in current density at +0.5 V, may arise from a built-in voltage resulting from the use of two different electrodes<sup>59</sup> but may also be influenced by trap filling effects.<sup>60</sup> Experiments with different metal to electrodes (Ca, Pd) yielded similar high current densities and also an onset of the current at +0.5 eV indicating that also with these metals an Ohmic contact is formed (Figure 4.4). In the case of Pd

formation of an Ohmic contact can only be expected if the ZnO at the interface with the metal is doped.

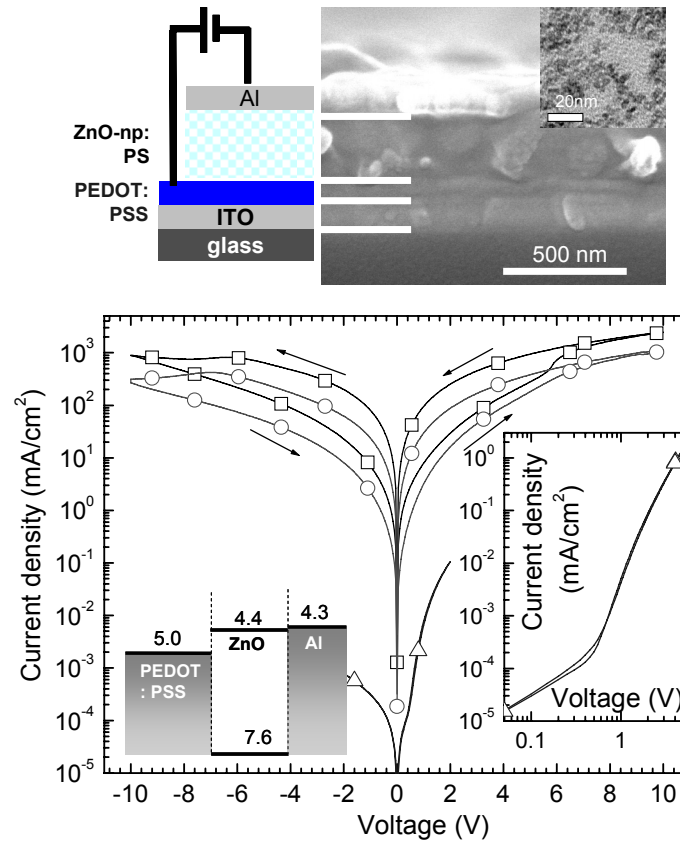


**Figure 4.3:** (top) Cross-sectional SEM image with a schematic representation of the device structure (ZnO:PS = 1:2 by weight) showing the bottom ITO/ PEDOT:PSS electrode, the active layer and the top Al electrode. (inset) TEM image of the ZnO-nps. (Bottom)  $J$ - $V$  characteristics of a device with ZnO:PS = 1:2 unformed ( $\Delta$ ) and formed in two manners with UV-illumination (10 s) ( $\circ$ ) or with an applied voltage (+17 V) ( $\square$ ). The arrows show the scan direction. ( $0\text{ V} \rightarrow +10\text{ V} \rightarrow -10\text{ V} \rightarrow 0\text{ V}$ ). A diagram, indicating the energetic position in eV of the conduction and valence bands with respect to the vacuum level is shown on the left. The values are obtained from literature.

After illumination of the diode with UV light through the transparent contact in a short time interval, the  $J$ - $V$  characteristic of the diode change drastically (Figure 4.3) The current densities are much higher, the rectifying behavior is strongly suppressed and a considerable hysteresis appears when performing a cyclic  $J$ - $V$  scan. Very similar characteristics can be obtained by applying forward bias stress to the device (+17 V, < 1 s) instead of illumination with UV light. This forming process is ascribed to the action of holes that are either photogenerated or injected electrically and which raise the density of mobile electrons in the ZnO particles as explained above. In this interpretation, the electrical conduction in the device is assumed to occur via interparticle contacts.

Therefore one expects a large variation of the electrical properties of the devices with the ZnO content of the active layer.

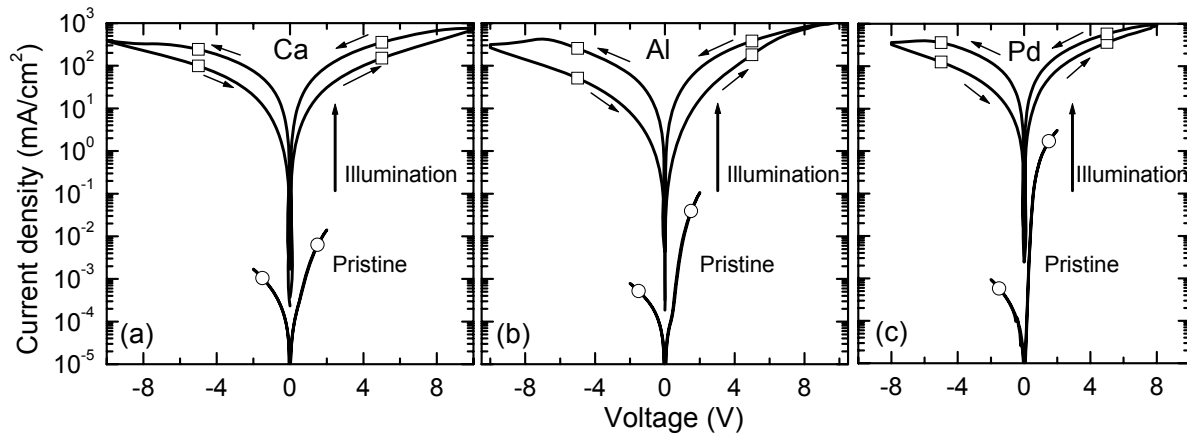


**Figure 4.4:** *J-V characteristics of a ZnO:PS = 1:2 (by weight) device with a Ca (a) an Al (b) and a Pd (c) top electrode in the pristine state (○) scanned between -2 and +2 V and after illumination (□) scanned from 0 V → +10 V → -10 V → 0 V.*

To test this idea, a series of devices with different ZnO-np content in the active layer has been characterized. *J-V* characteristics for this set of devices in their pristine state are shown in Figure 4.5a. Figure 4.5b shows the current densities when performing a cyclic *J-V* scan from 0, +10, -10 to 0 V while Figure 4.5c show the densities after illumination of pristine devices with UV light for 10 s. As expected, the device with neat polystyrene, shows only low current densities. UV illumination and application of bias voltage stress (+20 V for 30 sec) have only a negligible effect on the electrical properties of this device.

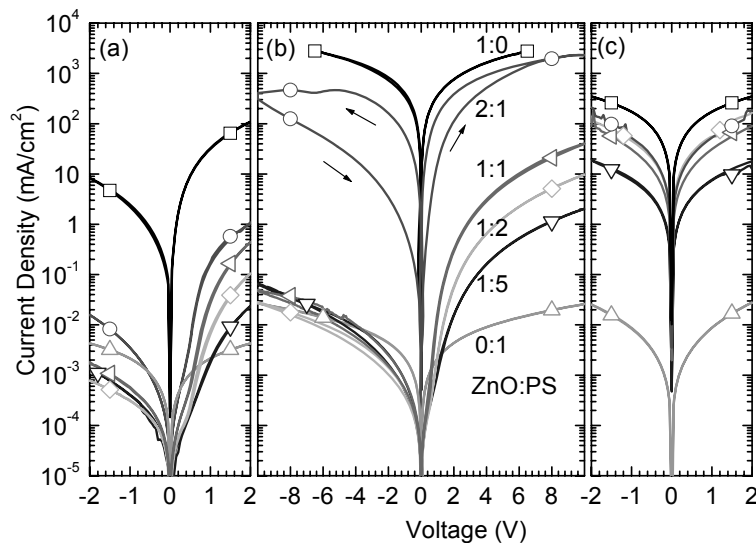


**Figure 4.5:** *Current density versus voltage of ZnO:PS devices with varying weight fractions of ZnO in the pristine state before forming (a) and after forming: by an applied voltage (b) or by UV-illumination (10 s) (c) ZnO:PS = 1:0 (□) 2:1 (○) 1:1 (◁) 1:2 (◇) 1:5 (▽) 0:1 (△) (by weight).*

For the devices containing ZnO particles, the electrical properties depend on the ZnO content of the film. The current density through the pristine devices measured at +2 V, increases with the volume fraction of ZnO in the active layer (Figure 4.6). Scanning the voltage over the +10/-10V range in the  $J$ - $V$  measurement, the device with a ZnO:PS ratio of 2:1 undergoes a forming reaction and the current density at +2 V is now markedly enhanced in comparison with the pristine devices scanned to bias voltages up to +2 V. Diodes with a lower ZnO content also undergo a forming reaction but at a much higher voltage (Figure 4.6).

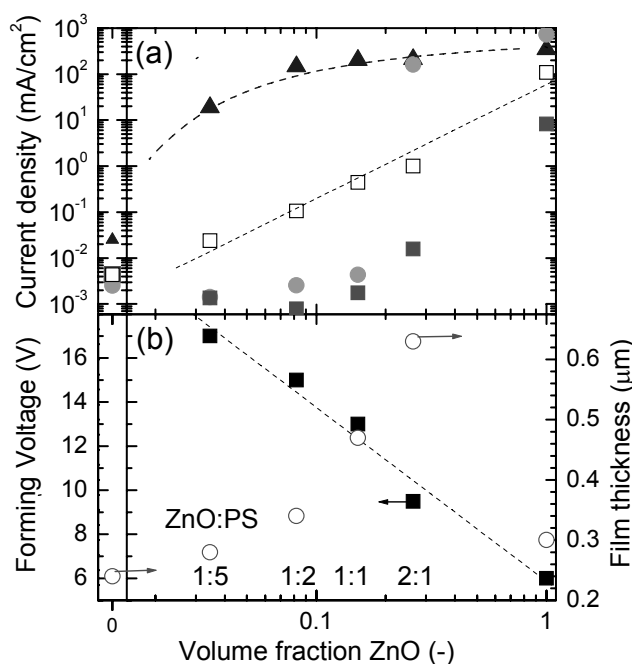


**Figure 4.6:** (a) Current density of ZnO:PS devices versus volume fraction ZnO. Current density,  $J$  at forward bias, +2 V (□) and at reverse bias, -2 V, of the pristine device (■).  $J$  at -2 V after voltage forming (●) and after UV illumination forming (15 s) forming (▲). (b) Forming voltage (■) and film thickness (○) versus volume fraction ZnO. For devices without ZnO no forming was observed.

All the diodes in the series containing ZnO, show a significant change in  $J$ - $V$  behavior upon illumination with UV light. The current densities probed at -2 V for devices with different ZnO content do not differ by more than an order of magnitude, which indicates that the ZnO volume fraction exceeds the threshold for percolation in all devices.<sup>61-64</sup> For randomly distributed spherical particles a percolation threshold of 16 vol-% is calculated. An oriented or aggregated distribution of the particles lowers the percolation threshold below 16 vol-%. For the unformed diodes no clear percolation threshold can be observed, which may be related to a large resistance associated with the interparticle contacts that changes gradually with the interparticle separation and contact area.<sup>65-67</sup>

In many metal oxides, hysteresis in the  $J$ - $V$  characteristic is associated with sudden jumps in the current density that occur in certain voltage ranges. In contrast, hysteresis in the ZnO:PS diodes studied here, is associated with a gradual change in the current density that occurs in the voltage range +6 to +9 V. This is illustrated in Figure 4.7a which shows the  $J$ - $V$  traces for a formed device that is subjected to a series of  $J$ - $V$  sweeps in which the maximal amplitude of the voltage sweep is increased in steps. As can be seen, cyclic  $J$ - $V$  scans with  $V$  in the range  $-5$  to  $+5$  V, do not show any significant hysteresis but upon extending the range of voltage sweep, the hysteresis gradually develops.

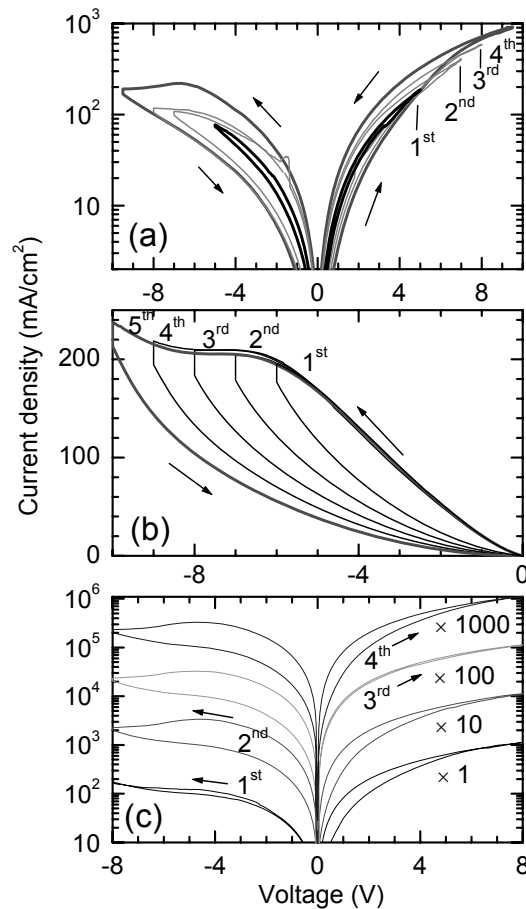


**Figure 4.7:**  $J$ - $V$  characteristics of a formed ZnO:PS diode (1:2 by wt). Sequential, cyclic  $J$ - $V$  scans with (a), incrementing the maximum amplitude  $X$  of the sweep in steps ( $0 \rightarrow +X \rightarrow -X \rightarrow 0$  V, with  $X = 5, 7, 8$  and  $9$  V). (b) Incrementing the maximum negative amplitude of the sweep ( $0, +8, -X, 0$  V with  $X = 5, 6, 7, 8$  and  $9$  V). (c) changing scan direction: preparation scan ( $0, +8, -8, 0$  V; not shown), 1<sup>st</sup> ( $0, -8, +8, 0$  V), 2<sup>nd</sup> ( $0, -8, +8, 0$  V), 3<sup>rd</sup> ( $0, +8, -8, 0$  V) and 4<sup>th</sup> ( $0, +8, -8, 0$  V). The arrow indicates the initial direction of the bias voltages sweep.

Application of negative bias voltages results in a decrease of the conductivity of the ZnO:PS devices. Also this "erase" process is a gradual transition and this is illustrated in Figure 4.7b where a series of cyclic  $J$ - $V$  scans is shown in which the voltage is scanned

from 0, +8, -X to 0 V, with X incremented in steps. As can be seen, the high conduction level, induced by application of +8 V bias, can be "erased" in a continuous manner. Models for the memory effect in oxide layers have been proposed in which a single (metallic) filament supports the high current density and where single events such as rupture can switch the conduction 'on' and 'off'.<sup>68,69</sup> Given the gradual change in conduction levels observed for the ZnO:PS, these models do not apply to the memory effects reported here.

It has also investigated whether reversible changes in the conductivity can be brought about by application of bias voltage pulses of *one* polarity, or whether application of voltage pulses of both polarities is needed to induce the switching effects. Switching of the resistance using voltage pulses of only one polarity but different voltage, is well known for metal oxide MIMs<sup>1</sup> and is associated with the occurrence of voltage controlled negative differential resistance (VCNR) as explained by *e.g.* Simmons and Verderber.<sup>34</sup> To test for unipolar switching, a formed ZnO:PS diode has been taken and prepared pre-conditional by sweeping the voltage in the direction 0, +8, -8, 0 V. After this preparation, the voltage was swept over 0, -8, +8, 0 V (Figure 4.7c, 1<sup>st</sup> J-V trace) and, as can be seen, no hysteresis occurs in negative leg of the J-V trace and the device is in its low conductivity state. This shows that the conductivity cannot be raised by application of negative bias voltage, but is raised only by application of positive bias voltages; see the positive limb of the 1<sup>st</sup> trace. From the 2<sup>nd</sup> scan (0, -8, +8, 0 V), it can be seen that the device does not return to its low conductivity state upon application of positive bias voltage. In a third consecutive scan (0, +8, -8, 0 V), no hysteresis is observed for the current densities under forward bias indicating that the high conducting level persists when zero or positive bias voltage is applied to the device. Finally, a fourth scan (0, +8, -8, 0 V) shows again hysteresis in the current density under both forward and reverse bias. It is concluded that the reversible changes in resistance are effected by periods of bias voltage stress of both polarities.



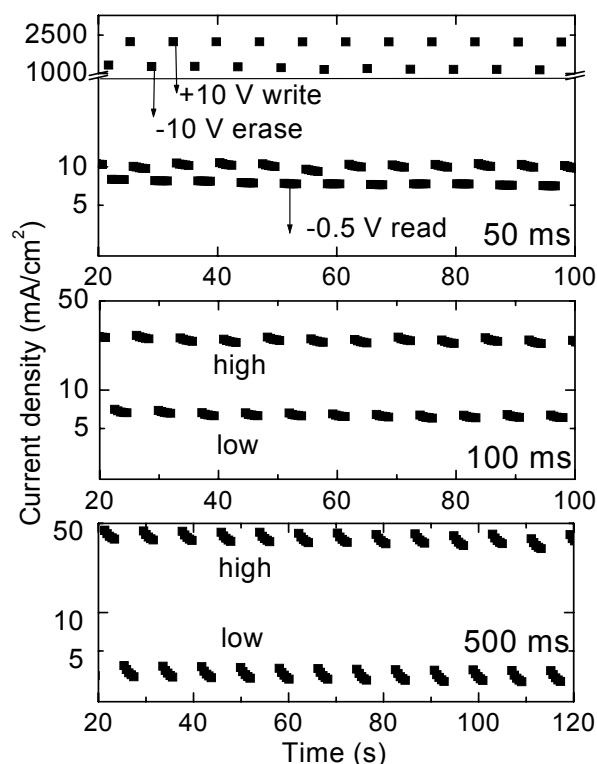


**Figure 4.8:** (a-c): Current density of the ZnO:PS (2:1 by weight) device upon application of a cycle of voltage pulses: a  $-10$  V (erase), five  $-0.5$  V (read) pulses, a  $+10$  V (write) and five  $-0.5$  V (read) pulses. Duration of the  $-0.5$  V pulses:  $0.1$  sec. Duration of the  $+10$  and  $-10$  V pulses is varied from  $50$  (a),  $100$  (b), to  $500$  ms (c). In between the pulses the device is kept at zero bias voltage.

The gradual and bipolar nature of the changes in resistivity are also evident from pulse measurements. Here, alternating voltage pulses of  $+10$  and  $-10$  V are applied to bring the diode to a state with high or low conductivity. In the experiment, the time duration of bias voltage pulses is varied, using the same interval for both the  $+10$  and  $-10$  V pulses. In between the  $+10/-10$  V pulses, the device is kept at zero bias and the conductivity is probed with short  $-0.5$  V pulse ( $100$  ms in duration). In figure 4.8, the current density of the high and low conductivity levels is shown as a function of the time duration of the  $+10/-10$  V pulses. It is found that the ratio of the current density in the high and low conductivity states (ON/OFF) depends on the pulse duration, consistent with a gradual change in resistivity upon application of a bias voltage stress exceeding  $5$  V in amplitude. The observation that the ON/OFF ratio changes with the weight content of ZnO of the active layer (Figure 4.9) support the view that the memory effects involve currents that flow via interparticle contacts between the ZnO nanocrystals. With a higher ZnO loading, a measurable ON/OFF ratio can be induced with shorter voltage pulses.

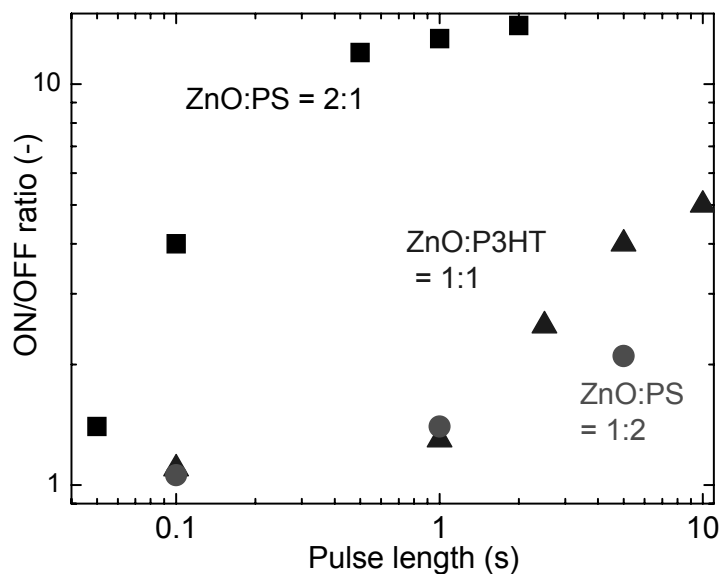


**Figure 4.9:** ON/OFF ratio versus temporal width of the write/erase pulses for devices with ZnO:PS = 1:2 (●) ZnO:PS = 2:1 (■) and ZnO:P3HT = 1:1 (▲) (by weight) Write/Erase voltages are  $\pm 10$  V (PS) and  $\pm 8$  V (P3HT). The ON/OFF ratio is calculated from the current density at  $-0.5$  V bias.

#### 4.4. Diodes with ZnO:P3HT as active layer

P3HT is a  $\pi$ -conjugated polymer with semiconducting properties, which can sustain a current of positive charge carriers. When applied as active layer in the device structure used here, rectification is observed (see Figure 4.10a) and this can be ascribed to injection of positive charge carriers through the PEDOT:PSS contact. Upon admixing of ZnO particles into the P3HT film, the current density through the diode at  $+2$  V bias goes up, which can be ascribed to a contribution of electrons moving via the ZnO to the total current density. This mixture of a p- and an n-type material, gives rise to a photovoltaic effect<sup>70</sup> (Figure 4.10a) resulting from efficient photoinduced charge generation at the ZnO:P3HT interface and the transport of holes towards the PEDOT:PSS electrode via the P3HT and transport of electrons via the ZnO towards the Al electrode. Interestingly, for a 1:1 mixture of ZnO:P3HT, illumination with visible light ( $\lambda > 400$  nm) does not modify the dark  $J$ - $V$  characteristics whereas illumination with UV light results in a large rise of the conductivity of the film, similar to the surge observed upon illumination of the ZnO:PS layers. These observations are consistent with the interpretation of the light induced changes in ZnO particles as the result of positive charge carriers in the ZnO.

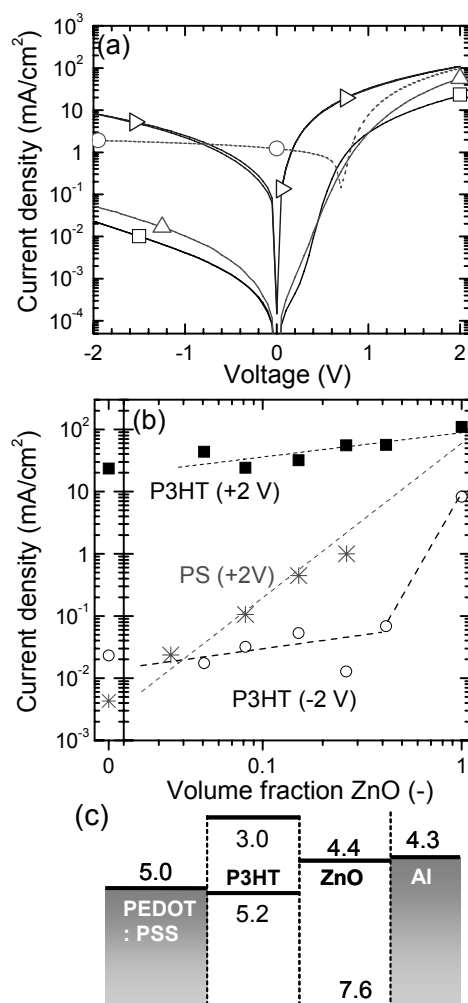


**Figure 4.10:** (a)  $J$ - $V$  characteristics with various ZnO-loading, ZnO:P3HT: = 0:1 (□), 1:1(Δ), 1:0 (▷) (by weight). The dotted line (---○---) shows the current density for ZnO: P3HT = 1:1 under illumination with filtered light ( $\lambda > 400$  nm) from a tungsten halogen source. (b) Current density for various ratios of ZnO:P3HT at +2V (■) and -2V (○) bias and for ZnO:PS at +2V (\*). The dotted lines serve as a guide to the eye. (c) Band diagram, illustrating the energetic position of the conduction and valence band of P3HT<sup>71</sup> and ZnO<sup>54,55</sup> and the work functions of PEDOT:PSS<sup>56</sup> and Al<sup>57</sup> with respect to the vacuum level in eV. The values are obtained from literature.

The ZnO:P3HT diodes also undergo a forming process upon application of positive bias voltage stress (Figure 4.11). Here a gradual transition has been seen to a much higher conductivity level and after the forming step also hysteresis in the  $J$ - $V$  characteristic is observed. The magnitude of the hysteresis effect depends on the scan speed used in the cyclic  $J$ - $V$  scan, which shows the memory effect is the result of changes inside the device that takes place a relatively slow rate (Figure 4.11c). Also here, hysteresis can only be observed when applying positive and negative bias voltage stress in an alternating way (Figure 4.11d) and that the conductivity changes in a gradual way rather than by sudden jumps (Figure 4.12).

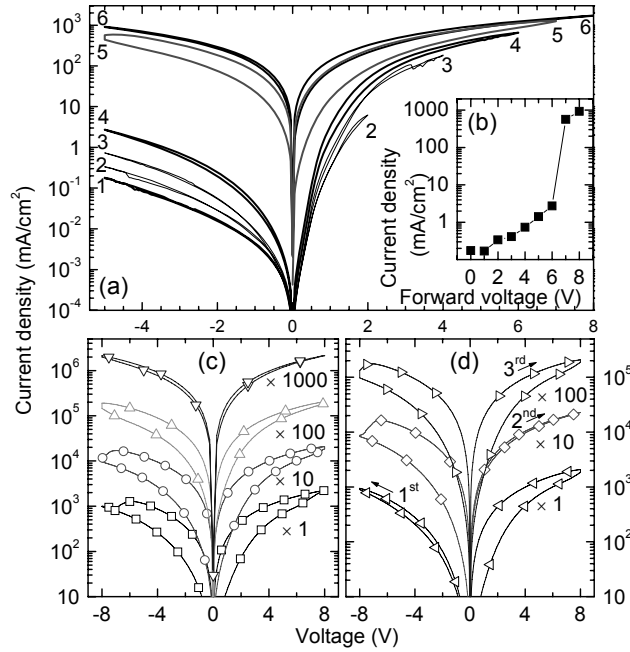


**Figure 4.11:** J-V characteristics of a ZnO: P3HT (1:1 by weight) device. (a) Sequential, cyclic J-V scans ( $0 \rightarrow +X \rightarrow -5 \rightarrow 0$  V) with  $X = 0, 2, 4, 6, 7$  and  $8$  V illustrating the forming reaction. (b) Corresponding current density at  $-5$  V as a function of amplitude  $X$  in the cyclic scan shown in (a). (c) Cyclic J-V scans ( $0, +8, -8, 0$  V) at various speeds:  $0.2$  V/s ( $\square$ ),  $0.3$  V/s ( $\circ$ ),  $0.5$  V/s ( $\triangle$ ) and  $1.3$  V/s ( $\nabla$ ) offset for clarity. Sequential, cyclic J-V Scan with different scan direction: ( $0, +8, -8, 0$  V, preparation, not shown), ( $0, -8, +8, 0$  V,  $\triangleleft$ ), ( $0, +8, -8, 0$  V,  $\diamond$ ) and ( $0, +8, -8, 0$  V,  $\triangleright$ ). Curves are offset for clarity and the arrow indicates the initial direction of the bias voltage sweep.

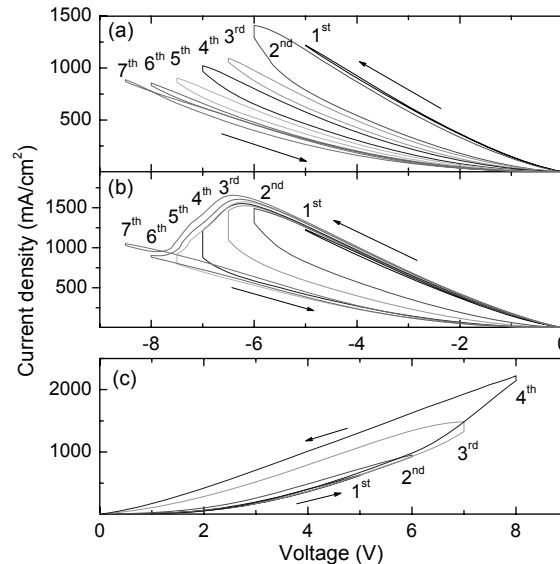


**Figure 4.12:** Sequential, cyclic J-V scans on a formed ZnO: P3HT (1:1 by weight) device (a) over the negative bias voltage range ( $0 \rightarrow -X \rightarrow 0$  V) with  $X = 5, 6, 6.5, 7, 7.5, 8, 8.5$  V after one initial forward scan to  $+8$  V; (b) over the positive and negative bias voltage range ( $0, +8, -X, 0$  V) with  $X = 5, 6, 6.5, 7, 7.5, 8, 8.5$  V; (c) over the range ( $0, +X, -8, 0$  V) with  $X = 5, 6, 7, 8$  V.

Finally, it is found that the polymer used has an influence on the 'lifetime' of the high and low conductivity states prepared by the positive and negative bias pulses. In Figure 4.13 the current densities for the two conductivity levels is shown, probed at  $-0.5$  V. Using PS as a matrix, a rapid initial decrease of the conductivity is observed in the first 10 seconds after the preparation pulses for both the high and the low conductivity state. This is followed by a second decay process occurring on the timescale of an hour. The latter drop can tentatively be assigned to oxygen rebinding. With P3HT as the matrix the rapid decay process is also observed but the slow decay is very much suppressed and the two current density levels can now be distinguished for times exceeding 14 hours. This difference between the two polymers may be related to a difference in the uptake of oxygen. The graph nicely illustrates that memory effect in these hybrid materials can be influenced by the choice of the host matrix.

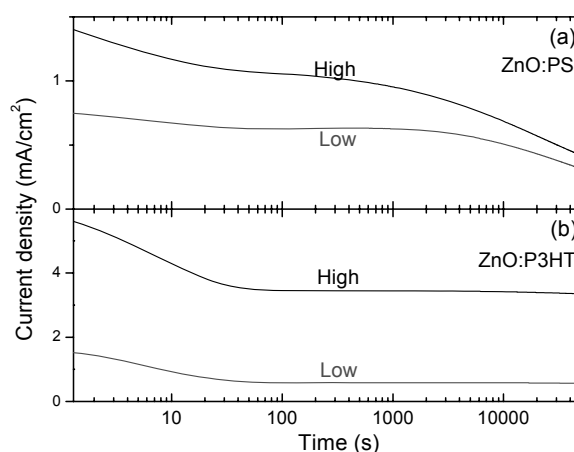


**Figure 4.13:** Stability of the high and low conductivity states in formed diodes with an active layer of (a) ZnO: PS= 1:2 and (b) ZnO:P3HT= 1:1 (by weight). Current densities are probed by application of short (100 ms)  $-0.5$  V pulses, in between these read pluses the device is kept at zero bias. The high and low conductivity states are prepared by application of  $\pm 10$  V, 10 s voltage pulses for ZnO:PS and  $\pm 8$  V pulses for ZnO:P3HT.

#### 4.5. Discussion

In the section above experimental evidence relating the forming reaction in the ZnO:polymer devices to an increase in the concentration of mobile electrons due to the desorption of surface bound oxygen from the ZnO nanoparticles induced by positive charge carriers has been presented. An active role for holes in dynamic effects in the resistivity of nanoparticulate materials containing ZnO is also known from research on ZnO varistors.<sup>72,73</sup> Also here molecular oxygen absorbed on the surface of ZnO particles is thought to play a role.<sup>74, 75</sup>

The reversible changes in the resistivity *after* the forming reaction requires application of bias voltage stress of both polarities. The changes themselves occur in a gradual manner and relatively slowly, which is consistent with an electrochemical process. Considering the band diagram (Figure 4.3 and 4.10), it seems likely that in the formed diode a depletion zone will arise in the ZnO:polymer layer near the PEDOT:PSS contact. Hence electrochemical processes occurring near this electrode are therefore expected to have a strong influence on the current density. A possible explanation may be the migration of dopants and native defects in the ZnO induced by the applied voltage or current. For instance, hydrogen, relatively mobile in ZnO,<sup>76,77</sup> may contribute to the n-type conductivity of ZnO<sup>78</sup> and is available from the PEDOT:PSS electrode. Migration of oxygen vacancies under the influence of an applied field, can contribute to memory effects in metal oxides.<sup>79</sup> Study of the degradation of the performance of varistors, has yielded experimental evidence for migration of Zn interstitials as a cause for electrically induced changes in the electrical properties of ZnO based materials.<sup>80,81</sup>

#### **4.6. Conclusions**

The resistivity of diode structures with an active layer of ZnO nanoparticles mixed with polymer can be altered by application of bias voltage stress. A forming step leading to much higher conductivity levels occurs under application of forward bias stress, and this process can be reversed by exposure to oxygen. After forming, the conductivity of the device can be reversibly changed by application of positive and negative bias voltage stress. These memory effects result from changes induced in the ZnO nanoparticles and their interparticle contacts which provide a percolation path for electrical conduction of electrons. The ZnO:polymer layers are solution processable and the memory effects can be influenced by modifying the (nanoscopic) chemical structure of the ZnO polymer film. This makes the MIM device amenable to chemical engineering, in contrast to the case of bulk metal oxides where one has little chemical control over the switching properties. Rewritable data storage could be demonstrated and minimum 'write'/'erase' times of 50 ms and retention times > 14 hours are possible.

#### **4.7. Experimental**

The devices studied consist of a spin coated active layer between two electrodes. The bottom electrode is tin-doped indium oxide (ITO) with a spin coated film of poly(3,4-ethylenedioxythiophene):polystyrenesulfonate (PEDOT:PSS, H.C. Starck, Baytron P VP Al 4083) of  $0.7 \times 10^2$  nm thickness, which was added after cleaning as described in Chapter 2. The active layer is spin coated at 1500 rpm from a solution containing ZnO particles and 20 mg PS ( $M_w = 250$  kg/mol, polydispersity index 2.2) or 10 mg regioregular poly(3-hexylthiophene) (P3HT, product code 4002, 98.5 % regioregularity, Rieke Metals Inc.) per mL chloroform. ZnO-nanoparticles (nps)

were synthesized by reacting zinc acetate with potassium hydroxide in methanol as described in Chapter 3.<sup>82</sup> The nanoparticle suspensions are used within a week after preparation to avoid clustering of the particles. Volume fractions of ZnO were calculated using a density of 5.6 g/cm<sup>3</sup>. The top electrode is made by evaporation of aluminum (100 nm). The active device area is 9.5 mm<sup>2</sup>. After deposition of Al, the devices are stored and characterized in an inert atmosphere (O<sub>2</sub>, H<sub>2</sub>O ≤ 1 ppm). A homemade Labview program with a computer controlled Keithley 2400 source-measure unit is used for electrical characterization, where positive (forward) bias voltage is defined by the PEDOT:PSS electrode being charged positive. In order to determine the forming voltage, the bias voltage applied is increased in steps of 1 V until the current through the diode reaches a compliance level (100 mA). The film thicknesses were measured with a Tencor P-10 Surface profiler. The effect of irradiation was studied with light from a tungsten-halogen source (total 80 mW/cm<sup>2</sup>). A cutoff filter, blocking light with wavelength <400 nm, was used to distinguish effects of UV and visible illumination. Electron paramagnetic resonance (EPR) at 9.43 GHz (X-band) was measured with a Bruker ESP 300E spectrometer using a cavity with a 50% transmission grid. In this setup, the sample can be illuminated with light from a 500 W Xe light source. The field effect transistor measurements are performed with a HP4155c semiconductor analyzer. A ring transistor with a channel length of 10 μm and a channel width of 1000 μm is used. Near steady-state photoinduced absorption (PIA) spectra for spin coated films of ZnO np deposited on quartz were recorded between 0.30 and 2.5 eV, exciting the film with 3.5 eV photons from mechanically modulated (73 Hz) cw argon ion laser beam. The sample was kept in a chamber, which could be evacuated or filled with air to test the influence of oxygen. During the spectroscopic experiment, the sample was then either continuously in air or in vacuum. The periodic change in the transmission of a tungsten-halogen probe beam through the sample ( $\Delta T$ ) is measured with a phase sensitive lock-in amplifier after dispersion through a monochromator and detection using Si, InGaAs, and cooled InSb detectors. The pump power was typically 50 mW with a beam diameter of 2 mm. The PIA signal ( $\Delta T/T$ ) was corrected for the photoluminescence, which was recorded in a separate experiment. The scanning electron microscopy (SEM) measurements were carried out at room temperature with a Philips XL30 FEG-ESEM. The devices were cut after cooling in liquid nitrogen to create a clean cut. The transmission electron microscopy (TEM) measurements were carried out on a FEI Tecnai 20, type Sphera TEM operating with 200kV LaB6 filament, equipped with a bottom mounted 1k x 1k Gatan CCD camera. The samples were created by drop coated a solution of the ZnO-np on a 200 mesh carbon-coated copper grids, purchased from Aurion.

### **4.8. References**

- 1 H. Pagnia and N. Sotnik, *Phys. Stat. Sol. A* **108**, 11 (1988).
- 2 G. Dearnaley, A.M. Stoneham, and D.V. Morgan, *Rep. Prog. Phys.* **33**, 1129. (1970).
- 3 R.E. Thurstans, and D.P. Oxley, *J. Phys. D-Appl. Phys.* **35**, 802 (2002).
- 4 A. Beck, J.G. Bednorz, C. Gerber, C. Rossel, and D. Widmer, *Appl. Phys. Lett.* **77**, 139 (2000).

- 5 A. Baikalov, Y.Q. Wang, B. Shen, B. Lorenz, S.Tsui, Y.Y. Sun, Y.Y. Xue, and C.W. Chu, *Appl. Phys. Lett.* **83**, 957 (2003).
- 6 K. Szot, W. Speier, G. Bihlmayer, and R. Waser, *Nature Mater.* **5**, 312 (2006).
- 7 K. Kinoshita, T. Tamura, M. Aoki, Y. Sugiyama, and H. Tanaka, *Appl. Phys. Lett.* **89**, 103509 (2006).
- 8 D.C. Kim, S. Seo, S.E. Ahn, D.-S. Suh, M.J. Lee, B.-H. Park, I. K. Yoo, I. G. Baek, H.-J. Kim, E. K. Yim, J.E. Lee, S.O. Park, H.S. Kim, U.-In Chung, J.T. Moon, and B.I. Ryu, *Appl. Phys. Lett.* **88**, 202102 (2006).
- 9 W.R. Hiatt and T.W. Hickmott, *Appl. Phys. Lett.* **6**, 106 (1965).
- 10 T.W. Hickmott, *J. Appl. Phys.* **88**, 2805 (2000).
- 11 K.L. Chopra, *J. Appl. Phys.* **36**, 184 (1965).
- 12 F. Argall, *Solid-State Electron.* **11**, 535 (1968).
- 13 K. Tsunoda, Y. Fukuzumi, J.R. Jameson, Z. Wang, P.B. Griffin, and Y. Nishi, *Appl. Phys. Lett.* **90**, 113501 (2007).
- 14 B.J. Choi, S. Choi, K.M. Kim, Y.C. Shin, C.S. Hwanga, S.-Y. Hwang, S. Cho, S. Park, and S.-K. Hong, *Appl. Phys. Lett.* **89**, 012906 (2006).
- 15 J.F. Gibbons, and W.E. Beadle, *Solid-State Electron.* **7**, 785 (1964).
- 16 J.H. Jung, J.H. Kim, T.W. Kim, M.S. Song, Y.H. Kim, and S. Jin, *Appl. Phys. Lett.* **89**, 122110 (2006).
- 17 T. Hada, K. Wasa, and S. Hayakawa, *Jpn. J. Appl. Phys.*, **10**, 521 (1971).
- 18 S.Q. Liu, N. J. Wu, and A. Ignatiev, *Appl. Phys. Lett.* **76**, 2749 (2000).
- 19 M. Hamaguchi, K. Aoyama, S. Asanuma, Y. Uesu, and T. Katsufuji, *Appl. Phys. Lett.* **88**, 142508 (2006).
- 20 H.K. Henisch and W.R. Smith, *Appl. Phys. Lett.* **24**, 589 (1974).
- 21 J. McGinness, P. Corry, and P. Proctor, *Science* **183**, 853 (1974).
- 22 R. Müller, S. De Jonge, K. Myny, D.J. Wouters, J. Genoe, and P. Heremans, *Appl. Phys. Lett.* **89**, 223501 (2006).
- 23 A. Bandyopadhyay and A.J. Pal, *Appl. Phys. Lett.* **82**, 1215 (2003).
- 24 D. Bloor, K. Donnelly, P.J. Hands, P. Laughlin, and D. Lussey, *J. Phys. D: Appl. Phys.* **38**, 2851 (2005).
- 25 Y. Yang, J. Ouyang, L. Ma, R.J.-H. Tseng, and C.-W. Chu, *Adv. Func. Mater.* **16**, 1001 (2006).
- 26 L.D. Bozano, B.W. Kean, M. Beinhoff, K.R. Carter, P.M. Rice, and J.C. Scott, *Adv. Func. Mater.* **15**, 1933 (2005).
- 27 W. Tang, H. Z. Shi, G. Xu, B.S. Ong, Z.D. Popovic, J.C. Deng, J. Zhao, and G.H. Rao, *Adv. Mater.* **17**, 2307 (2005).
- 28 K. Mohanta, S.K. Majee, S.K. Batabyal, and A.J. Pal, *J. Phys. Chem. B* **110**, 18231 (2006).
- 29 A. Prakash, J. Ouyang, J.-L. Lin, and Y. Yang, *J. Appl. Phys.* **100**, 54309 (2006).
- 30 Y. Yang, L. Ma, and J. Wu, *MRS Bulletin* **29**, 833 (2004).
- 31 J. Wu, K. Mobley, and R.L. McCreery, *J. Chem. Phys.* **126**, 024704 (2007).
- 32 J.E. Ralph and J.M.J. Woodcock, *Non-Cryst. Solids* **7**, 236 (1972).



- 33 D.S. Kim, Y.H. Kim, C.E. Lee, and Y.T. Kim, *Phys. Rev. B* **74**, 174430 (2006).
- 34 J.G. Simmons and R.R. Verderber, *Proc. R. Soc. Lond. Ser. A* **301**, 77 (1967).
- 35 S. Brauer, H. Pagnia, and N. Sotnik, *Int. J. Electronics* **76**, 707 (1994).
- 36 D.S. Jeong, B.J. Choi, and C.S. Hwang, *J. Appl. Phys.* **100**, 113724 (2006).
- 37 S. Tsui, Y.Q. Wang, X.Y. Yue, and C.W. Chu, *Appl. Phys. Lett.* **89**, 123502 (2006).
- 38 M. Cölle, M. Büchel, and D. M. de Leeuw, *Org. Electron.* **7**, 305 (2006).
- 39 W.-J. Joo, T.-L. Choi, J. Lee, S. K. Lee, M.-S. Jung, N. Kim, and J. M. Kim, *J. Phys. Chem. B* **110**, 23812 (2006).
- 40 S. Karthäuser, B. Lussem, M. Weides, M. Alba, A. Besmehn, R. Oligschlaeger, and R. Waser, *J. Appl. Phys.* **100** (9) 94504 (2006).
- 41 F. Verbakel, S.C.J. Meskers, and R.A.J. Janssen, *Appl. Phys. Lett.* **89**, 102103 (2006).
- 42 M. Villafuerte, S. P. Heluani, G. Juárez, G. Simonelli, G. Braunstein, and S. Duhalde, *Appl. Phys. Lett.* **90**, 052105 (2007).
- 43 W.K. Liu, K.M. Whitaker, K.R. Kittilstved, and D.R. Gamelin, *J. Am. Chem. Soc.* **128**, 3910 (2006).
- 44 Y. Takahashi, M. Kanamori, A. Kondoh, H. Minoura, and Y. Ohya, *Jpn. J. Appl. Phys I* **33**, 6611 (1994).
- 45 V. Ischenko, S. Polarz, D. Grote, V. Stavarache, K. Fink, and M. Driess, *Adv. Func. Mater* **15**, 1945 (2006).
- 46 S.B. Orlinskii, H. Blok, J. Schmidt, P.G. Baranov, C.D.M. Donega, and A. Meijerink, *Phys. Rev. B* **74**, 045204 (2006).
- 47 L.S. Vlasenko and G.D Watkins, *Phys. Rev. B* **72**, 035203 (2005).
- 48 M. Shim and P. Guyot-Sionnest, *J. Am. Chem. Soc.* **123**, 11651 (2001).
- 49 S.C.J. Meskers, J.K.J. van Duren, R.A.J. Janssen, F. Louwet, and L. Groenendaal, *Adv. Mater.* **15**, 613 (2003).
- 50 B. Sun and H. Sirringhaus, *J. Am. Chem. Soc.* **128**, 16231 (2006).
- 51 B.S. Ong, C. Li, Y. Li, Y. Wu, and R. Loutfy, *J. Am. Chem. Soc.* **129**, 2750 (2007).
- 52 S.A. Studenikin, N. Golego, and M. Cocivera, *J. Appl. Phys.* **87**, 2413 (2000).
- 53 P. Sharma, K. Sreenivas, and K. V. Rao, *J. Appl. Phys.* **93**, 3963 (2003).
- 54 A. Hagfeldt, M. Grätzel, *Chem. Rev.* **95**, 49 (1995).
- 55 S.J. Pearton, D.P. Norton, K. Ip, Y.W. Heo, and T. Steiner, *J. Vac. Sci. Technol. B* **22**, 932, (2004).
- 56 T.M. Brown, J.S. Kim, R.H. Friend, F. Caciallia, R. Daik, and W.J. Feast, *Appl. Phys. Lett.* **75**, 1679 (1999).
- 57 H.B. Michaelson, *J. Appl. Phys.* **48**, 4729 (1977).
- 58 L.J.A. Koster, *Ph.D. Thesis* Groningen University (2007) <http://dissertations.ub.rug.nl/faculties/science/2007/l.j.a.koster/?FullItemRecord=ON>
- 59 P.W.M. Blom and M.C.J.M. Vissenberg, *Mater. Sci. Eng.* **27**, 53 (2000).
- 60 V.R. Nikitenko, H. Heil, and H. von Seggern, *J. Appl. Phys.* **94**, 2480 (2003).
- 61 J. Vilčáková, P. Sába, V. Křesálek, and O. Quadrat, *Synth. Metals* **113**, 83 (2000).

- 62 F. El-Tantawy, K. Kamada, and H. Ohnabe, *Materials Letters* **56**, 112 (2002).
- 63 M. Xiao, L. Sun, J. Liu, Y. Li, and K. Gong, *Polymer* **43**, 2245 (2002).
- 64 W. Jia, R. Tchoudakov, E. Segal, R. Joseph, M. Narkis, and A. Siegmann, *Synth. Metals* **132**, 269 (2003).
- 65 A. Mikrajuddin, F.G. Shi, S. Chungpaiboonpatana, K. Okuyama, C. Davidson, and J.M. Adams, *Mater. Sci. Semicond. Proc.* **2**, 309 (1999).
- 66 Z. Rubin, S.A. Sunshine, M.B. Heaney, I. Bloom, and I. Balberg, *Phys. Rev. B* **59**, 12196 (1999).
- 67 V.A. Soloukhin, *PhD. Thesis*, Eindhoven University of Technology (2003) <http://alexandria.tue.nl/extra2/200312898.pdf>
- 68 Y. Sato, K. Kinoshita, M. Aoki, and Y. Sugiyama, *Appl. Phys. Lett.* **90**, 033503 (2007).
- 69 P.G. Lecomber, A.E. Owen, W.E. Spear, J. Hajto, A.J. Snell, W.K. Choi, M.J. Rose, and S. Reynolds, *J. Non-Cryst. Solids* **77-78**, 1373 (1985).
- 70 W.J.E. Beek, M. M. Wienk, and R.A.J. Janssen, *Adv. Func. Mater.* **16**, 1112 (2006).
- 71 M. Onoda, K. Tatda, A.A. Zakhidov, and K. Yoshino. *Thin Solid Films* **331**, 76 (1998).
- 72 T.K. Gupta, *J. Am. Cer. Soc.* **73**, 1817 (1990).
- 73 D.R. Clarke, *J. Am. Cer. Soc.* **82**, 485 (1999).
- 74 M.A. Ramirez, A.Z. Simoes, P.R. Bueno, M.A. Marquez, M.O. Orlandi, and J.A.Varela, *J. Mater. Sci.* **41**, 6221 (2006).
- 75 F. Stucki and F. Greuter, *Appl. Phys. Lett.* **57**, 446 (1990).
- 76 N.H. Nickel, *Phys. Rev.* **73**, 195204 (2006).
- 77 Y.L. Wang, F. Ren, H.S. Kim, S.J. Pearton, and D.P. Norton, *Appl. Phys. Lett.* **90**, 092116 (2007).
- 78 C.G. Van de Walle, *Phys. Rev. Lett.* **85**, 1012 (2000).
- 79 Y.B. Nian, J. Strozier, N.J. Wu, X. Chen, and A. Ignatiev, *Phys. Rev. Lett.* **98**, 146403 (2007).
- 80 P. Erhart and K. Albe, *Appl. Phys. Lett.* **88**, 201918 (2006).
- 81 T.K. Gupta and W.G. Carslon, *J. Mater. Res.* **20**, 745 (1985).
- 82 W.J.E. Beek, M.M. Wienk, M. Kemerink, X. Yang, and R.A.J. Janssen, *J. Phys. Chem. B* **109**, 9505 (2005).



# 5

## **Surface modification of zinc oxide nanoparticles induces electronic memory effects in ZnO - polystyrene diodes**

Resistive switching effects in diode structures with a spin-coated active layer containing zinc oxide (ZnO) nanoparticles in a polystyrene matrix are studied. The switching effect can be influenced by modification of the surface of the nanoparticles with coordinating ligands (amines and thiols). Using n-propylamine as a ligand, memory effects are observed without the diodes having undergone the forming step that is usually required before switching effects can be observed in bulk metal oxides. Memory effects are characterized by impedance spectroscopy and temperature dependent current-voltage measurements and involve a spontaneous, thermally activated gradual transition from a state with high, frequency independent conduction to a state with lower conductivity.

This work has been published: F. Verbakel, S.C.J. Meskers, and R.A.J. Janssen, *J. Phys. Chem. C* **111**, 10150 (2007).

## 5.1. Introduction

Resistive switching in metal oxides embedded in metal-insulator-metal (MIM) structures is well known<sup>1-4</sup> and is currently intensely investigated, partly because of its potential application in data storage.<sup>5-9</sup> Research has focused on switching in bulk oxide layers that are either amorphous, microcrystalline, porous, non-stoichiometric<sup>2,3</sup> or inhomogeneous.<sup>10</sup> Different mechanisms have been proposed to explain resistive switching phenomena.<sup>11-16</sup> A large number of reports describe electronic transport via filaments that arise during a forming step of the MIM diode.<sup>1,17</sup> Because of the structural disorder and spontaneous formation of filamentary conduction paths, the switching process is difficult to control, as it is influenced by random variations in the insulating layer.

In this chapter resistive switching effect in *nanostructured* oxide layers are shown, made by spin coating oxide nanoparticles from solution, which can be influenced via surface chemistry of the nanoparticles. This shows that knowledge from colloid and surface science of oxide nanoparticles may be used in the design of materials for the next generation memory technology.<sup>18-20</sup>

In Chapters 3 and 4, memory effects in MIM structures with an insulating layer consisting of ZnO nanoparticles mixed with polystyrene (PS) have been reported.<sup>21</sup> The use of different two electrodes (aluminum and poly(3,4-ethylenedioxy thiophene):polystyrene sulfonate (PEDOT:PSS)) results in diode-like current voltage characteristics for the pristine device. After a forming step induced by application of forward bias voltage, the resistance of these devices drops considerably and can be reversibly altered by applying voltage pulses of different polarity. These switching effects resemble those reported for bulk ZnO,<sup>22,23</sup> but the mechanism responsible for switching is not yet known for either the bulk or the nanostructured solid. The use of oxide nanoparticles offers the interesting possibility for chemical modification of the surface of the ZnO particle. Surface modification of ZnO nanoparticles is known and binding of thiols,<sup>24,25</sup> acids,<sup>26,27</sup> and amines<sup>28-30</sup> has been reported. The surface of the particles is expected to play an important role in determining the electrical properties of the blend because conduction of charge occurs through interparticle contacts.<sup>31-34</sup>

## 5.2. Diodes with various ligands

Figure 5.1a shows the current-voltage ( $J$ - $V$ ) characteristics of the ZnO-polymer MIM devices in their pristine, unformed state with as inset the device lay-out. Without any added ligands, the device shows diode characteristics when swept between  $-2$  and

+2 V, consistent with earlier reports. In forward bias the current density shows a sharp rise at a bias voltage of 0.5 V and scales as  $J \propto V^2$  for voltages exceed in 0.5 V (Figure 5.2b). This is consistent with the current being limited by space charge constraints in a layer in the device that is depleted of mobile charge carriers at zero bias. This can be interpreted in terms of the excess electrons of the n-type ZnO being trapped by oxygen bound to the surface of the nanoparticle.<sup>21</sup> UV illumination triggers the release of oxygen molecules, and this removal of trap sites results in a higher concentration of mobile electrons, allowing for much higher current densities with Ohmic behavior (Figure 5.1b).

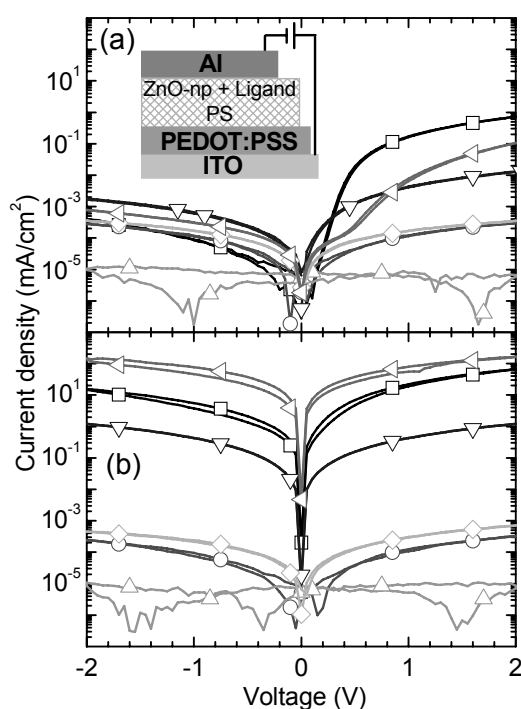


**Figure 5.1:** ZnO:PS device with different ligands added are characterized by J-V in the pristine state (a) and after UV illumination (b). Ligands added: none ( $\triangleleft$ ), *n*-propylamine ( $\square$ ), 1-octylaniline ( $\nabla$ ), 2-naphthalenethiol ( $\diamond$ ), 1-dodecanethiol ( $\circ$ ) and 1-hexadecylamine ( $\triangle$ ). Inset: Schematic layout of the device structure.

When adding *n*-propylamine (PA) or 1-octylaniline as additional coordinating ligand to the ZnO particles, the diode behavior and the persistent photodoping can still be observed, indicating that these ligands do not block the transport of electrical charges when bound to the particles. In contrast, with 2-naphthalenethiol, 1-dodecanethiol, and 1-hexadecylamine as ligands, the current densities are much lower both before and after illumination with UV light. This indicates that these ligands isolate the nanoparticles electrically from one another, blocking any charge transport through the MIM. This shows that the ZnO surface chemistry is indeed crucial in determining the electric properties of the blend. In the J-V scans for devices with 1-hexadecylamine and 1-octylaniline, a

depolarization current at  $V=0$  can be observed which is ascribed to ionic conductivity due to the presence of protonated ligand. For the other mixtures, the depolarization current is below the detection limit and therefore the contribution of ionic conductivity to the observed currents is expected to be very small.

When sweeping the voltage over a wider range ( $0\text{ V} \rightarrow +8\text{ V} \rightarrow -8\text{ V} \rightarrow 0\text{ V}$ , Figure 5.2), it is found that the diodes with ZnO:PA show a larger hysteresis in the  $J$ - $V$  characteristic than devices without additional ligand. For the latter devices, the  $J$ - $V$  trace recorded with increasing and decreasing bias voltage overlap. The hysteresis is larger under reverse bias voltages and is associated with negative differential resistance. Application of reverse bias voltages ( $V < -5$ ) reduces the conductivity at small bias voltages, while application of a forward bias voltage induces a higher conduction. As shown earlier, ZnO-MIM diodes without added ligand show a similar hysteresis, but only after a forming process induced by application of a forward bias voltage ( $\sim 15\text{ V}$ ) or by UV illumination. For bulk metal oxide layers, memory effects are observed only after a forming step.<sup>1-4</sup> In contrast, here it is shown that by using zinc oxide nanoparticles with appropriate surface modification, switching effects can be induced *without* the need of a forming process.

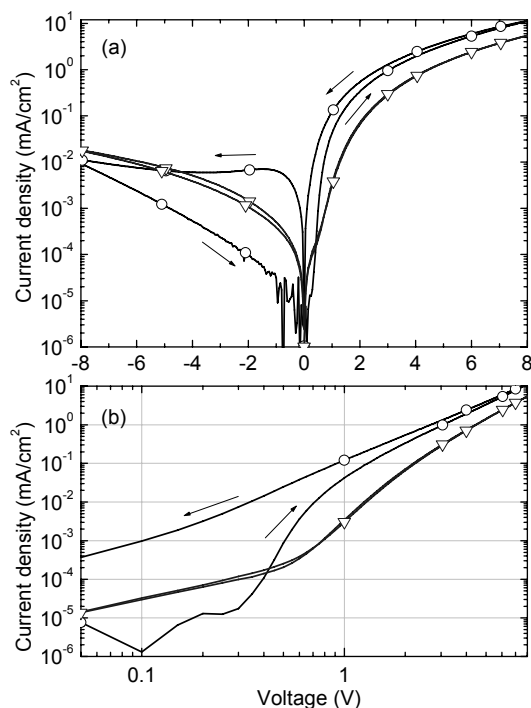


**Figure 5.2:** (a) Current-voltage characteristics ( $0\text{ V} \rightarrow +8\text{ V} \rightarrow -8\text{ V} \rightarrow 0\text{ V}$ ) of a device with *n*-propylamine capped ZnO-*np* (ZnO:PS:PA = 2:4:1 by weight) in the pristine state (O) and of a device with no ligands added to the ZnO-*np* in the pristine state ( $\nabla$ ) (ZnO:PS = 1:2 by weight). Scan speed 170 mV/s. (b) Same as (a) but in double logarithmic representation.

Of all ligands investigated, only n-propylamine is found to induce electronic memory effects in the ZnO diodes (Figure 5.3) and these effects have been characterized in more detail using impedance spectroscopy. Figure 5.4 shows the conductance and capacitance recorded at different probe frequencies (10 Hz - 1 kHz) using a voltage that is modulated around a quasi-constant bias voltage (AC amplitude 100 mV). The bias voltage is swept very slowly from 0 V  $\rightarrow$  +5 V  $\rightarrow$  -5 V  $\rightarrow$  0 V. The conductance, recorded while sweeping the bias (Figure 5.4b), shows a large hysteresis, which is the largest for reverse bias voltages. In this respect, this result resembles the static  $J$ - $V$  characteristics (Figure 5.3). Consistent with the  $J$ - $V$  characterization, application of a forward bias voltage enhances the conductance probed at small bias voltages. After forward bias stress, the conductance is almost symmetrical around zero bias voltage, indicating the ZnO layer behaves as a conductor. In contrast, application of reverse bias stress, strongly reduces the conductance and restores the asymmetry around zero bias illustrating that the devices behaves as a diode in this state.

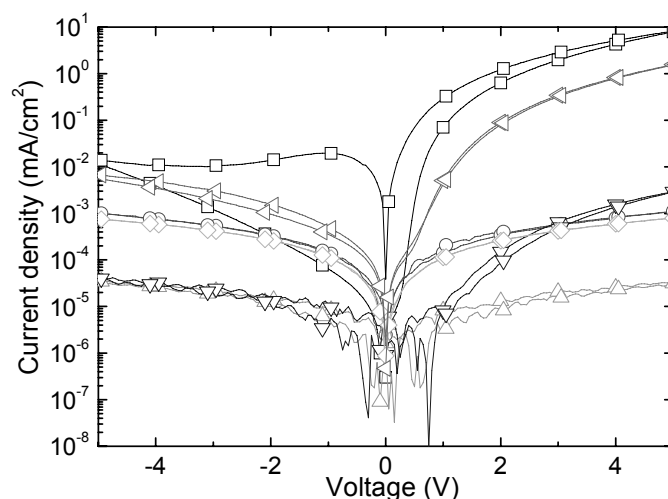


**Figure 5.3:** ZnO:PS device with different ligands added are characterized by  $J$ - $V$  (0 V  $\rightarrow$  +5 V  $\rightarrow$  - V  $\rightarrow$  0 V). Ligands added: none ( $\triangleleft$ ), n-propylamine ( $\square$ ), 1-octylaniline ( $\nabla$ ), 2-naphthalenethiol ( $\diamond$ ), 1-dodecanethiol ( $\circ$ ) and 1-hexadecylamine ( $\triangle$ ).

### 5.3. Frequency dependence

The frequency dependence of the conductance in the high and the low conductivity states (induced by resp. -5 V and +5 V bias) has also been measured, applying a constant bias voltage (-0.5 V, Figure 5.4b). Before each measurement point in the frequency scan, either a +5 V or -5 V bias voltage pulse of 1 s is applied to ensure that the device is prepared in the correct state. The high conductivity state is characterized by an admittance that is frequency independent up to 10 kHz. The low



conductivity state shows frequency dependent conductivity at high frequencies with  $Y \propto \omega$ , in agreement with the generally observed behavior in amorphous materials.<sup>35</sup> At frequencies below 100 Hz, the admittance shows a frequency dependence that is less steep.

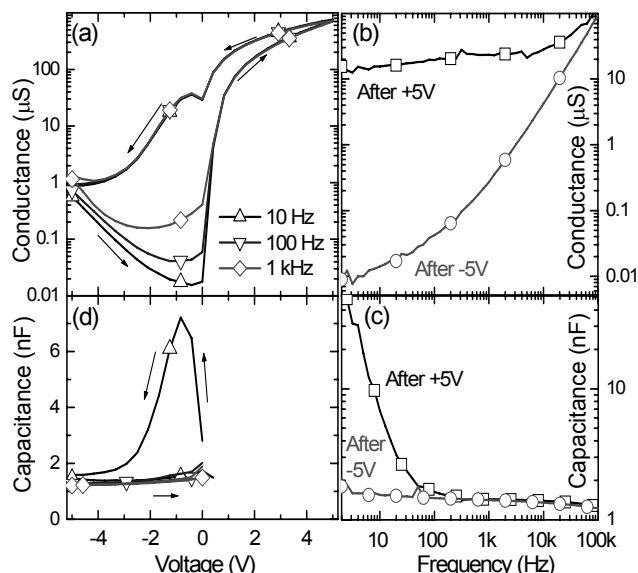


**Figure 5.4:** (a) Conductance of the ZnO: PS: PA device (2:4:1 by weight) as a function of bias voltage (scanned from 0 V  $\rightarrow$  +5 V  $\rightarrow$  -5 V  $\rightarrow$  0 V). The frequencies displayed are 10 Hz ( $\Delta$ ), 100 Hz ( $\nabla$ ) and 1 kHz ( $\diamond$ ). (b) Conductance and (c) capacitance versus frequency at -0.5 V bias. Each measurement point is taken after a +5 V ( $\square$ ) or a -5 V ( $\circ$ ) pulse with 1 s duration. (d) Capacitance versus bias voltage.

Together with the conductance also the capacitance can be monitored. In the low conductivity state, the capacitance probed at -0.5 V bias, is independent of frequency and approximately equal to the geometrical capacitance. In the high conductivity state, there is an additional contribution to the capacitance at low frequency. A scan of the bias voltage, indicates that this process takes place near bias voltages of  $\sim -1$  V (Figure 5.4d).

#### 5.4. Temperature dependence

The memory effect can also be characterized by its temperature dependence (Figure 5.5). Lowering the temperature down to 150 K, strongly reduces the hysteresis in the  $J$ - $V$  plots. This indicates that either the transition from the low to the high conductivity state and/or from the high to the low, involves a thermally activated step. In order to distinguish between these possibilities pulse measurements have been performed in which the stability of the conduction states is probed in time. The conduction level is probed by applying short (100 ms) -0.5 V bias pulses. In between

these probe pulses, the device is kept at zero bias. The conduction level in the low conductivity state, prepared by a 5 s,  $-5$  V bias voltage pulse, did not show any particular time dependence in the temperature range studied. Neither did the lower conductivity level reached, vary significantly with temperature. In contrast, the conduction level in the high conductivity state, prepared by a 5 s,  $+5$  V pulse, decreases with time. At 295 K, the ON/OFF ratio shows a decay with a characteristic time on the order of 10 s (Figure 5.5b). Upon lowering the temperature, the spontaneous relaxation for high to the low conductivity becomes much slower and therefore this step must be thermally activated. In addition, the conduction level reached after application of the  $+5$  V pulse is temperature dependent, so that also the bias voltage induced transition from the low to the high conductivity state is thermally activated. The ON/OFF ratio decreases at lower temperature when write and erase pulses of  $+5$  V and  $-5$  V are used. Presumably the devices can still be switched at lower temperature when using higher voltages. Field dependent activation energies are commonly observed in disordered systems. The role of PEDOT:PSS is not yet clear, however, devices without additional ligand show no reversible switching when the PEDOT:PSS layer is not included in the device structure.<sup>21</sup>

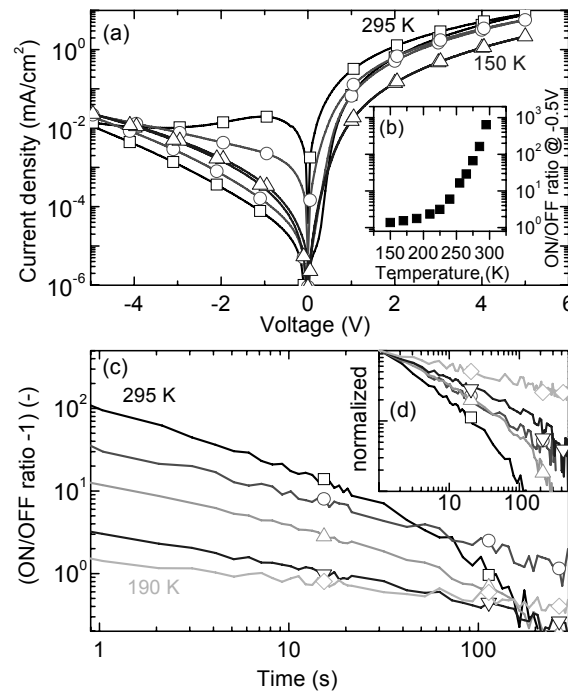


**Figure 5.5:** (a)  $J$ - $V$  characteristic with ( $0 \rightarrow +5 \rightarrow -5 \rightarrow 0$  V) bias voltage sweep of a ZnO:PS:PA device at 295 ( $\square$ ) 250 ( $\circ$ ) and 150 K ( $\Delta$ ); (b) The ratio of the current density at  $-0.5$  V after a  $0 \rightarrow +5$  V scan (ON) and after  $0 \rightarrow -5$  V scan (OFF) at varying temperature (150 to 295 K); (c) ON/OFF ratio minus 1 between the current densities probed at  $-0.5$  V after a  $+5$  V pulse, 5 s and after  $-5$  V, 5 s at 295 ( $\square$ ), 275 ( $\circ$ ), 255 K ( $\Delta$ ), 225 K ( $\nabla$ ) and 190 K ( $\diamond$ ); (d) Same as (c) but normalized to unit differential current density at  $t=0$ .

## 5.5. Conclusion

In conclusion, the electronic memory effect in a nanostructured metal oxide can be influenced by surface modification of the particles with coordinating ligands. The mechanism(s) responsible for the memory effects are not yet known, but here it is shown that chemical modification of ZnO nanoparticles with coordinating ligands opens new opportunities to study and control switching effects in organic-inorganic hybrid materials.

## 5.6. Experimental

The diodes consist of a spin-coated active layer between two electrodes (Figure 5.1). The bottom electrode is tin-doped indium oxide (ITO) is covered with a thin spin-coated film of poly(3,4-ethylenedioxythiophene): polystyrenesulfonate (PEDOT:PSS, H.C. Starck, Baytron P VP Al 4083) of  $0.6 \times 10^2$  nm after cleaning as described in chapter 2. The ZnO-nanoparticles were synthesized by reacting zinc acetate with potassium hydroxide in methanol as described in chapter 3.<sup>36</sup> The active layer is spin-coated at 1500 rpm from a solution containing 20 mg PS ( $M_w = 250$  kg/mol, PDI = 2.2), 10 mg of ZnO-np and ligand per mL chloroform. For *n*-propylamine (PA) the ratio is PS: ZnO: PA = 4: 2: 1 (by weight). The other ligands were added to the solution in such an amount that the molar concentration of the ligand was the same as for PA. The addition of ligand does not influence the film thickness ( $4 \times 10^2$  nm). The top electrode is made by evaporation of aluminum ( $1 \times 10^2$  nm). The active device area is  $9.5 \text{ mm}^2$ . After deposition of Al, the devices are stored and characterized in an inert atmosphere ( $\text{O}_2, \text{H}_2\text{O} \leq 1$  ppm) or in vacuum to prevent the transition back to the pristine state induced by oxygen.<sup>21</sup> A Keithley 2400 source-measure unit controlled by a Labview program is used for *J-V* characterization. A Solartron SI 1260 is used for impedance spectroscopy with the sample in vacuum. Because of the high admittance under forward bias voltages, capacitance could not be measured reliably under these conditions. Temperature dependent *J-V* measurements are performed in a vacuum cryostat. In all cases, positive bias voltage refers to the PEDOT:PSS electrode being charged positive with respect to the Al electrode.

## 5.7. References

- 1 R.E. Thurstans and D.P. Oxley, *J. Phys. D-Appl. Phys.* **35**, 802 (2002).
- 2 H. Pagnia and N. Sotnik, *Phys. Stat. Sol. A* **108**, 11 (1988).
- 3 G. Dearnaley, A.M. Stoneham, and D.V. Morgan, *Rep. Prog. Phys.* **33**, 1129 (1970).
- 4 T.W. Hickmott, *J. Appl. Phys.* **88**, 2805 (2000).
- 5 A. Beck, J.G. Bednorz, C. Gerber, C. Rossel, and D. Widmer, *Appl. Phys. Lett.* **77**, 139 (2000).

- 6 A. Baikalov, Y.Q. Wang, B. Shen, B. Lorenz, S. Tsui, Y.Y. Sun, Y.Y. Xue, and C.W. Chu, *Appl. Phys. Lett.* **83**, 957 (2003).
- 7 K. Szot, W. Speier, G. Bihlmayer, and R. Waser, *Nature Mater.* **5**, 312 (2006).
- 8 K. Kinoshita, T. Tamura, M. Aoki, Y. Sugiyama, and H. Tanaka, *Appl. Phys. Lett.* **89**, 103509 (2006).
- 9 D.C. Kim, S. Seo, ; S.E. Ahn, D.-S. Suh, M.J. Lee, B.-H. Park, I.K. Yoo, I.G. Baek, H.-J. Kim, E.K. Yim, J.E. Lee, S.O. Park, H.S. Kim, U-In Chung, J.T. Moon, and B.I. Ryu, *Appl. Phys. Lett.* **88**, 202102 (2006).
- 10 M.J. Rozenberg, I.H. Inoue, and M. Sánchez, *J. Phys. Rev. Lett.* **92**, 178302 (2004).
- 11 J.E. Ralph, and J.M. Woodcock, *J. Non-Cryst. Solids* **7**, 236 (1972).
- 12 D.S. Kim, Y.H. Kim, C.E. Lee, and Y.T. Kim, *Phys. Rev. B* **74**, 174430 (2006).
- 13 J.G. Simmons and R.R. Verderber, *Proc. R Soc. Lond. Ser. A* **301**, 77 (1967).
- 14 S. Brauer, H. Pagnia, and N. Sotnik, *Int. J. Electronics* **76**, 707 (1994).
- 15 D.S. Jeong, B.J. Choi, and C.S. Hwang, *J. Appl. Phys.* **100**, 113724 (2006).
- 16 S. Tsui, Y.Q. Wang, Y.Y. Xue, and C.W. Chu, *Appl. Phys. Lett.* **89**, 123502 (2006).
- 17 M. Cölle, M. Büchel, and D.M. de Leeuw, *Org. Electr.* **7**, 305 (2006).
- 18 J. C. Scott and L. D. Bozano, *Adv. Mater.* **19**, 1452 (2007).
- 19 K. Mohanta, S.K. Majee, S.K. Batabyal, and A.J. Pal, *J. Phys. Chem. B* **110**, 18231 (2006).
- 20 R.J. Tseng, C.O. Baker, B. Shedd, J.X. Huang, R.B. Kaner, J.Y. Ouyang, and Y. Yang, *Appl. Phys. Lett.* **90**, 053101 (2007).
- 21 F. Verbakel, S.C.J. Meskers, and R.A.J. Janssen, *Appl. Phys. Lett.* **89**, 102103 (2006).
- 22 T. Hada, K. Wasa, and S. Hayakawa, *Jpn. J. Appl. Phys.* **10**, 521 (1971).
- 23 O. Hunter Jr., and J.A. Schaefer, *US Patent* 4472296 (1984).
- 24 N.S. Pesika, Z. Hu, K.J. Stebe, and P.C. Searson, *J. Phys. Chem. B* **106**, 6985 (2002).
- 25 E.M. Wong, P.G. Hoertz, C.J. Liang, B.-M. Shi, G.J. Meyer, and P.C. Searson, *Langmuir* **17**, 8362 (2001).
- 26 S. Sakohara, M. Ishida, and M.A. Anderson, *J. Phys. Chem. B* **102**, 10169 (1998).
- 27 P.D. Cozzoli, A. Kornowski, and H. Weller, *J. Phys. Chem. B* **109**, 2638 (2005).
- 28 M.L. Kahn, M. Monge, V. Colliere, F. Senocq, A. Maisonnat, and B. Chaudret, *Adv. Funct. Mater.* **15**, 3 (2005).
- 29 M. Shim and P. Guyot-Sionnest, *J. Am. Chem. Soc.* **123**, 11651 (2001).
- 30 N.S. Norberg and D.R. Gamelin, *J. Phys. Chem. B* **109**, 20810 (2005).
- 31 V. Subramanian, J.M.J. Frechet, P.C. Chang, D.C. Huang, J.B. Lee, S.E. Molesa, A.R. Murphy, D.R. Redinger, and S.K. Volkman, *Proc. IEEE* **93**, 1330 (2005).
- 32 B. Sun and H. Sirringhaus, *J. Am. Chem. Soc.* **128**, 16231 (2006).
- 33 W.J.E. Beek Thesis, Eindhoven University of Technology (2005).
- 34 B.S. Ong, C. Li, Y. Li, Y. Wu, and R. Loutfy *J. Am. Chem. Soc.* **129**, 2750 (2007).
- 35 A.K. Jonscher, Dielectric relaxation in solids , *Chelsea Dielectrics Press* (1983).

- 36 W.J.E. Beek, M.M. Wienk, M. Kemerink, X. Yang, and R.A.J. Janssen *J. Phys. Chem. B* **109**, 9505 (2005).

# 6

## **Anomalous resistive switching at the percolation limit of ZnO nanoparticle – polymer diodes**

*Surface modification of zinc oxide (ZnO) nanoparticles with thiol ligands is investigated in solution with photoluminescence spectroscopy, electron paramagnetic resonance, and photoinduced absorption. Binding of the ligand to the ZnO controls the aggregation of ZnO particles in spin coated films with polystyrene as a matrix. The electrical properties of ligand bound ZnO nanoparticles are studied in diode structures of these materials. The device geometry consist of a poly(ethylenedioxythiophene): poly(styrenesulfonate) bottom electrode, an active layer consisting of ZnO nanoparticles with varying amount of octane thiol in a polystyrene matrix, and a top electrode of Al or Pd. With increasing surface coverage of octane thiol, the electrical resistance associated with electron transport via percolating networks of ZnO particles in the matrix, increases, due to deterioration of the ZnO interparticle contacts. Just before reaching the percolation limit, where the electrical current is supported by just a few percolation paths, the electrical characteristics change and noisy fluctuations between two levels in the current density are obtained. For unmodified ZnO particles, voltage pulses +10 V and -10 V bring the diode to respectively a low and a high resistive state. Using ZnO particles modified with octane thiol, the diodes can be switched between low and high resistive states with respectively -3.5 V and -7 V. This change is interpreted in terms of the conduction taking place via essentially a single, narrow channel of ZnO particles that can be blocked by trapping of a single charge carrier.*

## 6.1. Introduction

Zinc oxide is a material with interesting optical and electronic properties.<sup>1-4</sup> It behaves as an *n*-type semiconductor with a band gap of 3.2 eV and shows relatively high electron mobility. Under appropriate conditions, a large variety of nanostructures can be grown from ZnO such as dots, wires, rings, spirals or propellers.<sup>5</sup> This diversity of nanostructures, combined with easy synthetic accessibility, makes ZnO currently one of the most intensely investigated nano-structured materials.

The surface of ZnO nanoparticles can be modified by addition of coordinating ligands. Several different chemical functional groups are known to bind to the surface of the particles, e.g. phosphine oxides,<sup>6</sup> amines,<sup>7-9</sup> carboxylic acids,<sup>10,11</sup> and thiols.<sup>12,13</sup> Ligands carrying such a functionality can stabilize and solubilize ZnO nanoparticles in solution. A limited number of studies have sought a way to influence the electronic properties of a solid film built up from or containing ZnO nanoparticles, *via* modification of the ZnO particles with organic ligands.<sup>14-17</sup> A complication here is that the binding of the ligands to the nanoparticle often insulates the particles electronically from one another, especially when the ligands comprise bulky, saturated hydrocarbon chains. This insulation then inhibits the transport of charge carriers *via* interparticle contacts.<sup>18,19</sup>

Here, the possibilities offered by *partial* coverage of the ZnO particles with thiol ligands are explored. As will be shown, the surface modification influences the aggregation behavior of the particles, while at the same time, it still allows for direct electrical contact between unmodified surface parts of the semiconducting cores. In this way, charge transport is still possible but now via narrow electrical channels that are insulated from one another. At degrees of surface coverage close to the percolation threshold, the special nature of the conduction pathways gives rise to anomalous electronic memory effects.

Many (metal-)oxides,<sup>20-23</sup> including ZnO,<sup>24</sup> show resistive switching. This is an electronic memory effect where the resistance of a layer of oxide between two electrodes can be switched reversibly between a high and a low value by applying a voltage pulse between these electrodes.<sup>25</sup> The memory effects are usually only observed after the initially insulating or semiconducting oxide has undergone a "forming" step corresponding to 'soft' electrical breakdown of the oxide.<sup>26,27</sup> In this step, defects are introduced in the material by application of the high forming bias voltage. Currently the forming process and the memory effects are only partially understood. Still, arrays of memory cells with an active layer of metal oxide are currently being developed.<sup>28-32</sup> For active layers comprising ZnO nanoparticles, it could be shown that the forming process involves desorption of absorbed oxygen molecules from the surface of the ZnO particles. This

results in an increase in the density of mobile charge carriers and a drop in the resistance of the layer containing the ZnO particles. Here it is important to note that some oxides require voltage pulses of opposite polarity to switch between the low and high resistance state (bipolar switching) while other oxides can also be switched with voltage pulses of just one polarity (unipolar switching). The origin of this difference is presently not fully understood.<sup>20,33,34</sup>

Here it is shown that dispersion of ZnO nanoparticles with partial ligand coverage, as small clusters isolated from one another by a host polymer (polystyrene), in a film changes the nature of the resistive switching memory effect from bipolar to unipolar switching. Although we currently cannot provide a detailed mechanistic explanation for the changes in resistive switching, the results show that these electronic memory effects are amenable to molecular engineering at the nanoscale. This may open new possibilities for application of oxide nanoparticles in electronic devices.

In this work, the binding of the thiol functionalized ligands to ZnO nanoparticles is investigated using, photoluminescence spectroscopy, electron paramagnetic resonance and photoinduced absorption. This allows to choose ligand/particle ratios corresponding to partial coverage of the available surface of the semiconductor particles and to study the effect of partial surface coverage on the aggregation behavior of the hybrid particles in spin coated films with a matrix of polystyrene (PS). The electrical characteristics and memory effects of diode structures based on a thin layer of PS containing partially covered ZnO nanoparticles sandwiched between two electrodes are presented.

## **6.2. Monitoring ligand binding**

To study the binding of thiol containing ligand, ZnO nanoparticles were synthesized by hydrolysis and condensation of zinc acetate dihydrate by potassium hydroxide in methanol, using the method described by Pacholski *et al.*<sup>35</sup> Particles with an average size of 5 nm in diameter were obtained (Figure 6.1a). When octane thiol (**1**, Figure 6.1.b) is added to a solution of the ZnO nanoparticles in CHCl<sub>3</sub>, followed by evaporation of the solvent, binding of the thiol ligands to the nanoparticles is evidenced by thermogravimetric analysis (TGA). A substantial loss of weight is observed for temperatures up to 350 °C which we attribute to desorption of **1** from the nanoparticles. The boiling point of **1** is only 200 °C and, hence, there must be a considerable binding enthalpy between the ligand and the nanoparticles. Also changes in the infrared spectra of dried sample of the ZnO particles after ligand modification support the binding of the thiol groups to the particles (Loss of the 3500 cm<sup>-1</sup> OH stretch vibration, appearance of the 2900 cm<sup>-1</sup> CH stretch modes).



From literature, it is known that binding of thiol ligands decreases the photoluminescence (PL) efficiency of defects in ZnO nanoparticles.<sup>9,16,17</sup> Although the mechanism behind this quenching is still a matter of debate,<sup>36,37</sup> the effect may be used to monitor the binding of the ligands to the particles *in solution*. For untreated ZnO nanoparticles in CHCl<sub>3</sub> solution a broad, featureless PL band is observed with a maximum at ~560 nm (Figure 6.1c). Upon stepwise addition of **1**, this defect emission gradually decreases until only a rest emission is observed that is no longer affected by the ligands. Plotting the intensity versus the ratio of the concentration of **1** and the total concentration of Zn atoms in solution, a titration curve is obtained (Figure 6.1d). This curve does not show a sharp equivalence point, but this may be due to relatively weak binding of the ligand. To test this hypothesis we have also investigated divalent ligand **2**, which is expected to bind more strongly to the ZnO particles. This yields a titration curve with a steeper decay, indicating indeed a stronger binding. A titration point at ~0.08 mol **2** / mol Zn is obtained (Figure 6.1e). The titration experiment is also performed in solid state. Figure 6.1e shows the decay of the defect emission of ZnO films with different amounts of ligand. For the films a much steeper decay of the defect emission is observed.

Assuming a spherical particle with a 5 nm diameter, there are  $\sim 2.6 \times 10^3$  Zn atoms per particle. With a minimal surface area of 16 Å<sup>2</sup> for binding of a *single* thiol group to the surface,<sup>38</sup> this results in ~500 binding sites per particle, equivalent to ~250 molecules of dithiol **2**. Combining this with  $\sim 2.8 \times 10^3$  Zn atoms per particle, full ligand coverage of the ZnO nanoparticles is obtained at ~0.09 mol **2** / mol Zn and ~0.18 mol **1** / mol Zn. This corresponds nicely to the titration point observed.

Assuming furthermore that the luminescence quenching is linearly proportional to the degree of surface coverage and that the binding of a ligand is independent of the occupation of neighboring binding sites, we can then estimate the binding constant for a ligand to the surface from the titration curve (for details see experimental). This yields an association constant of 10<sup>5</sup> M<sup>-1</sup> for bidentate binding of **2** to a single binding site on the ZnO surface. For the monodentate binding of **1** we find an association constant of 10<sup>4</sup> M<sup>-1</sup>.

These experiments clearly show that in CHCl<sub>3</sub> solution, thiols coordinate to the ZnO particle. This surface modification also changes the aggregation properties of the particles. This leads for instance to gelation of a chloroform solution by aggregation of the hybrid oxide nanoparticles which can be observed at 0.9 M total Zn concentration and 2.5 molar ratio of **1** to Zn.

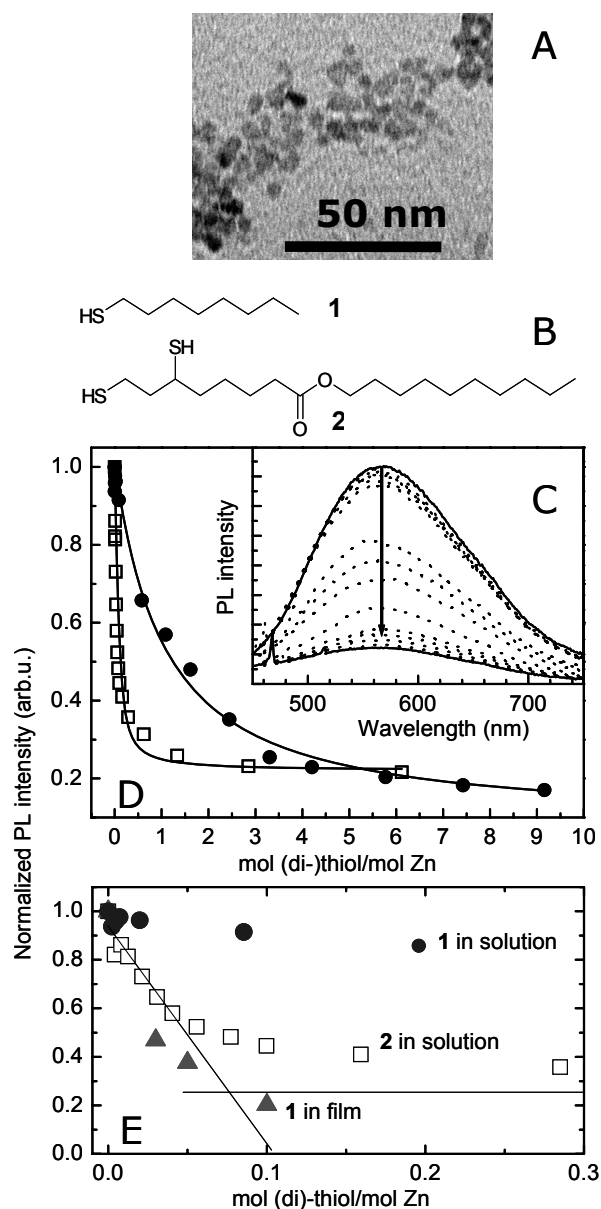


**Figure 6.1:** (a) TEM image of the ZnO nanoparticles. (b) Ligands (c) Photoluminescence (PL) spectra of ZnO nanoparticles in CHCl<sub>3</sub> upon stepwise addition of **1**. (d) (●): Normalized PL intensity versus the molar ratio of **1** and Zn. Total Zn concentration ( $15 \times 10^{-2}$  mM). Wavelength of excitation 333 nm; of PL detection: 557 nm. (□) *idem* for **2** except: total Zn concentration  $8.5 \times 10^{-2}$  mM, wavelength PL detection: 557 nm. The solid lines represent predictions of an association model with independent binding sites to the data (see experimental for details). (e) Zoom of (d) with additional PL data of films of ZnO nanoparticles containing **1** (▲).

### **6.3. Influence of surface modification on the morphology of ZnO nanoparticles / polystyrene blends**

In order to study the electronic properties of the ZnO nanoclusters in a device configuration, thin films have to be deposited on an electrode surface. This can be achieved by mixing the ZnO particles with polystyrene in chloroform solution followed by film deposition with spin coating.<sup>16</sup> In these mixed films, charge flows via interparticle contacts from one electrode to the other. Here we investigate the influence of the presence of ligands on the clustering of ZnO particles in the polymer matrix, which leads to the formation of the interparticle contacts. Transmission electron microscopy (TEM) and atomic force microscopy (AFM) are used to study the morphology.

In Figure 6.2, TEM (left) and AFM (right) images of spin coated films containing ZnO nanoparticles with different degree of surface coverage with **1** in a polystyrene (PS) matrix are shown. Solutions containing 20 mg PS, 10 mg ZnO nanoparticles, and 0, 0.05, 0.18 or 0.5 mol **1** / mol Zn in CHCl<sub>3</sub> were spin coated on top of a poly(3,4-ethylenedioxythiophene) :poly(styrenesulfonate) (PEDOT:PSS) layer. AFM was performed directly on these layers while for TEM the polystyrene layer was floated off the substrate.

Clusters of aggregated ZnO nanoparticles have been observed in films containing unmodified ZnO nanoparticles with a rough surface showing height differences of  $\sim 2 \times 10^2$  nm on a total layer thickness of  $\sim 3 \times 10^2$  nm. In TEM clustering of ZnO nanoparticles into larger domains forming an almost continuous network is observed (Figure 6.2a). This clustering in networks of ZnO nanoparticles can explain the surface roughness.

In case of partially capped nanoparticles (0.05 mol **1** / mol Zn), the film roughness is reduced to  $\sim 25$  nm and isolated clusters ( $\sim 7 \pm 1 \times 10^1$  nm) of ZnO nanoparticles can be observed in TEM. The high contrast of Figure 6.2b suggest that the main part of the nanoparticles are packed closely together (black dots), however some isolated nanoparticles (grey) are dissolved in the polymer matrix. Films of fully capped particles (0.18 mol **1** / mol Zn) look similar to films with 0.05 mol **1** (not shown). When adding even larger amounts of **1** (0.5 mol **1** / mol Zn), very smooth films were obtained with a roughness of only 2 nm (Figure 6.2c). Within these smooth films, large clusters ( $\sim 2.6 \pm 0.6 \times 10^2$  nm) which are organized in a hexagonal manner can be observed. The clusters are disk-shaped and considering the volume fraction of ZnO and the contrast in TEM, the inside of these clusters is made out of a material other than pure ZnO (inset Figure 6.2c). This may suggest the presence of shells consisting of ZnO nanoparticles filled with polymer and/or ligand, when large amounts of ligand are present.

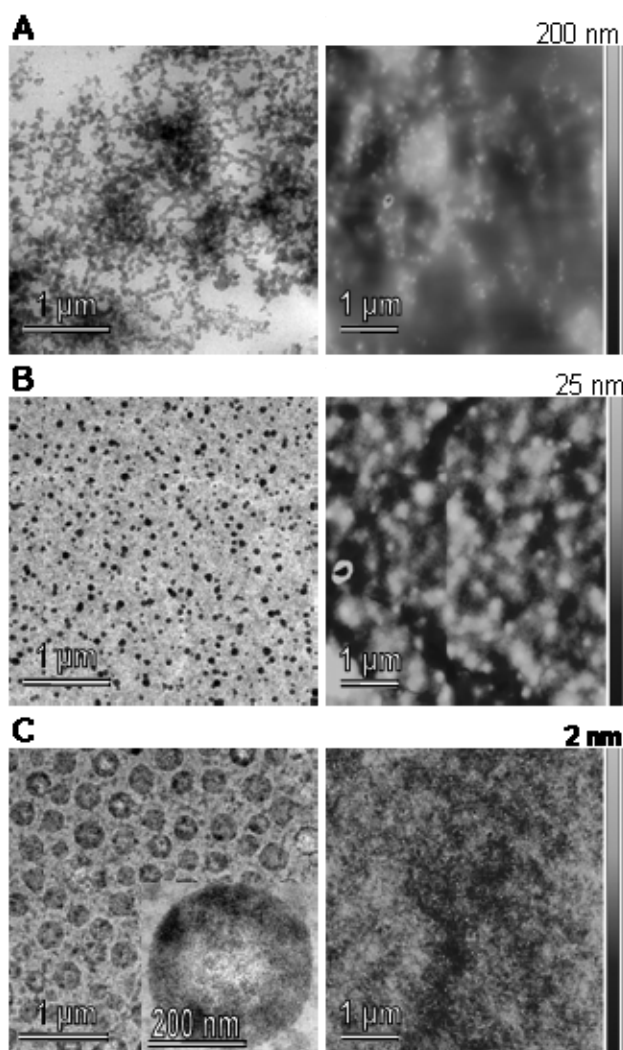


**Figure 6.2:** TEM images (left) and AFM height images (right) spin coated films of (a) ZnO-np, (b) ZnO-np + 0.05 mol **1** / mol Zn, and (c) 0.5 mol **1** / mol Zn in a PS matrix.

#### **6.4. Electronic properties of diodes with surface modified ZnO particles**

In the previous section we have seen that the distribution of ZnO particles in the polystyrene matrix and their interconnectivity can be affected by (partial) surface modification of the oxide particles by thiol ligands. An interesting question is now whether the morphological changes also lead to changes in the electrical behavior. To study this, diodes containing an active layer composed of ZnO nanoparticles with variable degree of surface modification with thiol ligand in polystyrene matrix were deposited on a bottom electrode of tin-doped indium oxide with a spin coated film of PEDOT:PSS and covered by a the top electrode of aluminum or palladium (Figure 6.3a).

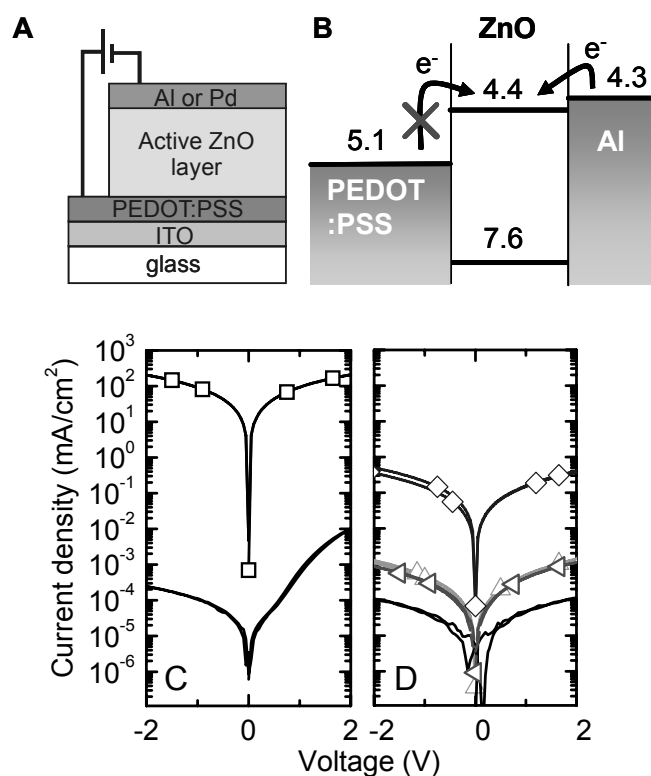


**Figure 6.3:** a,b) Schematic overview of the device layout with corresponding energy band diagram. c) J-V characteristics of a PEDOT:PSS/ZnO:PS/Al diode before (-) and after (-□-) UV illumination, d) same as c) with addition of ligand (0.5 mol **1** per mol Zn), before (-) and after (-◁-) illum., and 0.05 (◇), 0.18 (△) mol **1** per mol Zn after UV-illum.

Pristine diodes containing ZnO nanoparticles without ligand and with Al top electrode show current rectification (Figure 6.3c) which can be understood in terms of the n-type nature of the ZnO and formation of an Ohmic contact between ZnO and Al.<sup>39</sup> The high current density under positive bias is attributed to electrons injected through the Al electrode (Figure 6.3b). After UV-illumination, the conductivity increases drastically, and an Ohmic like behavior is observed.<sup>16</sup> This has been interpreted in terms of photodoping. This is obtained by photoexcitation, followed by desorption of molecular oxygen from the surface of the particles. Photoinduced holes in the valence band of the ZnO particles induce this process that can also be started by holes injected via an electrical contact.<sup>40</sup> After desorption, O<sub>2</sub> can no longer act as an electron trap and this allows for a quasi-permanent increase in the number of *mobile* electrons.<sup>40</sup> Surface modification of the particles with thiol ligands strongly reduces the current density before and after illumination (Figure 6.3d). This suggests that the nature of the interparticle contacts has changed. Systematic variation of the degree of surface coverage shows that this change occurs in a continuous manner. This is illustrated in Figure 6.4d which shows the current densities of PEDOT:PSS/ZnO:**1**:PS/Al diodes with various amounts of ligand

added and the ZnO:PS ratio is kept constant at 1:2 by weight. Results of the electrical characterization are summarized graphically in Figure 6.4a. Here it can be seen that the current densities under forward bias voltages before and after illumination decrease strongly with increasing amounts of ligand added up the point where, according to calculations and luminescence titrations (Figure 6.1e), full surface coverage can be reached (0.18 mol **1** / mol Zn, see above). Further increase of the ligand concentration results in only a marginal decrease of the current density. The current densities at  $-2$  V are similar for all devices, which can probably be ascribed to a leakage current through the diode not involving charge transport via the oxide particles.

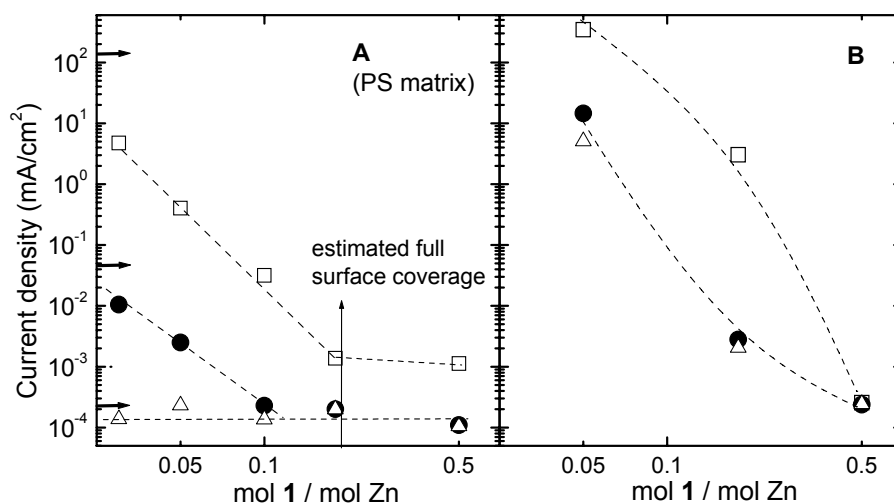


**Figure 6.4:** (a) Influence of the amount of **1** on the current density in PEDOT:PSS/ZnO:1:PS/Al diodes before UV illumination measured at bias voltage  $+2$  V ( $\bullet$ ) and  $-2$  V ( $\Delta$ ) and after UV-illumination at  $+2$  V ( $\square$ ). ZnO:PS = 1:2 by weight. b) Same as a) but now without PS matrix. The horizontal arrows indicate the current density of diodes with uncapped ZnO.

Electron paramagnetic resonance (EPR) can be used to characterize charge carriers in the ZnO that have been induced by UV illumination (Figure 6.5a).<sup>40</sup> The intense EPR signal that appears after illumination of ZnO nanoparticles may be assigned to conduction electrons or weakly bound electrons originating from a shallow donor.<sup>41-43</sup> Upon exposure to air, this signal is reduced  $\sim 50$  times (not shown) and this is consistent with  $O_2$  adsorbed to the surface of the particles acting as an electron trap that can be detached by action of UV light. Also for particles modified with **1**, mobile electrons can be induced by UV illumination and removed again by exposure to oxygen. In Figure 6.5a normalized EPR signals are shown for ZnO particles with different degree of surface coverage with **1**. The observed signal shifts slightly towards higher g-values upon addition of **1**, indicating a change in the environment of the unpaired electron.

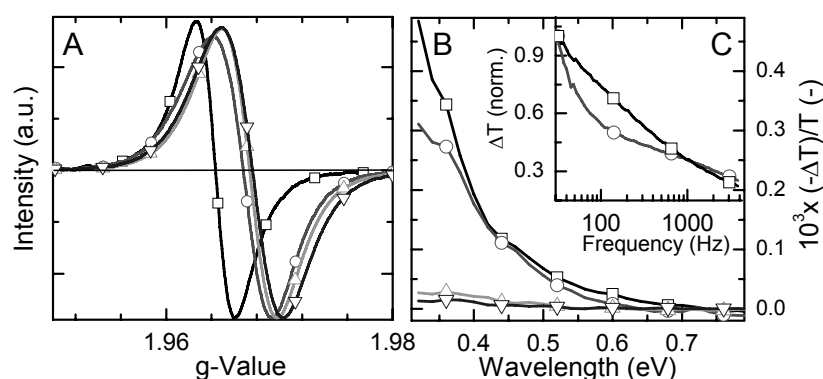


**Figure 6.5:** (a) EPR, (b) PIA of uncapped ZnO nanoparticles ( $\square$ ), ZnO-nanoparticles with 0.05 mol **1** / mol Zn ( $\circ$ ), with 0.2 mol C8SH / mol Zn ( $\triangle$ ), and with 0.5 mol **1** / mol Zn ( $\nabla$ ). c) Frequency dependency of the PIA signal at 0.34 eV.

Another method to characterize UV induced charge carriers is photoinduced absorption (PIA). Here the intensity of the UV excitation beam (3.5 eV) is modulated and the amplitude of the periodic oscillation of the transmission of (white) light is measured for the films of capped and uncapped ZnO nanoparticles held in open air (Figure 6.5b). For bare ZnO nanoparticles, a PIA signal at 0.3 eV can be observed which can be ascribed to electrons in the conduction band of the ZnO particles.<sup>40</sup> In the presence of oxygen from the air, this signal is much more intense than in vacuum. This can be explained by the fact that mobile electrons generated during the half period in which the ZnO is illuminated with UV light, can be trapped again by  $O_2$  during the dark half period of the modulation cycle. In the absence of  $O_2$ , the mobile electrons generated are not scavenged and this results in a much smaller *modulation* of the number of mobile electrons in the absence of  $O_2$  and a reduced differential absorption signal in the modulation experiment. In Figure 6.5b the PIA signal for ZnO nanoparticles with different amounts of ligand is shown. The intensity of this signal also decreases upon increasing the amount of **1**. The frequency dependence of the PIA signal at 0.34 eV for uncapped ZnO nanoparticles and with 0.05 mol **1** / mol Zn is shown in Figure 6.5c. Upon addition of the ligand the lifetime of the signal is increased. Combined with the results from the EPR measurements, which show that the electrons can still be generated, a possible explanation for the decrease of the PIA signal with increasing ligand coverage is the increased lifetime of the induced carriers with increasing degree of surface coverage with the ligand. If this lifetime increases beyond the modulation rate of the experiment, a decrease in the signal intensity is predicted due to the lower effective modulation of the carrier density between light on and off periods. The presence of the shell of ligand molecules may impede the capture of electrons in the conduction band by  $O_2$  molecules, because the approach of the scavenger towards the semiconductor surface is hindered by

the ligands, resulting in a prolonged lifetime of the carrier. In summary, EPR measurements indicate that mobile charge carriers in the ZnO nanoparticles can still be induced by UV illumination. The PIA experiments, however, indicate that the capture of electrons by O<sub>2</sub> is hindered by the ligand.

The observation of mobile carriers upon UV illumination of ZnO particles with a high surface loading of ligands indicates that the loss of electrical conduction via the ZnO particles in the polymer matrix upon increasing the amount of ligand, probably arises from deterioration of interparticle electrical contacts. This is consistent with the decrease in current density with increasing ligand loading in pristine diodes before UV illumination (Figure 6.4a). Deterioration of the interparticle contacts can, in principle, be caused by better mixing of the modified particles with the matrix so that the number of contacts is decreased or, alternatively, by a higher barrier for transport of charge carriers via the interparticle contact due to the presence of the insulating ligand shells around the particles. Experiments with an active layer of just the modified particles without the PS matrix (Figure 6.4b) also show a strong decrease in the conduction with increasing amounts of ligand. This indicates that for high loadings of surface of the ZnO particles with ligand, a barrier for transport of charge carriers develops at the interparticle contacts.

After UV forming, diodes containing ZnO particles and polystyrene show hysteresis in their  $J$ - $V$  characteristics (Figure 6.6a).<sup>40</sup> The hysteresis indicates the existence of at least two metastable conduction levels in the diode. These levels can indeed be observed when recording the current through the diode upon application of voltage pulses to switch the resistance (+10 V/-10 V) and to probe the resistance (-1 V) (Figure 6.6b). The conduction can be raised by a factor of  $\sim 2$  when applying +10 V ('write') before the -1 V probe voltage (ON-state), compared to the case where -10 V ('erase') is applied before the measurement (OFF-state). The hysteresis and switching can also be observed after application of a high voltage (electroforming) (Figure 6.6a) and is also observed for diodes with ZnO particles with low degree of surface coverage with **1** without the polymer matrix. Here the change in resistivity is induced by electrically injected holes in the valence band of the ZnO particles.

In the  $J$ - $V$  scans showing hysteresis, the absolute current density sometimes decreases with increasing (absolute) bias voltage (i.e. to more negative bias). For the ZnO nanoparticles, this negative differential resistance (NDR) usually occurs when scanning negative bias voltages in the onward direction after scanning positive bias voltages. The backwards part (i.e. the return scan to 0 V) of the negative bias voltage scan does normally not exhibit NDR. This shows that upon going from high negative bias voltage back to zero voltage, the high conduction state is not recovered spontaneously.



To reach the high conduction state, positive bias voltage needs to be used. Consistent with this no significant resistive switching is observed when applying only negative bias voltage pulses (Figure 6.6c). Curiously, such unipolar switching can be observed for a number of other oxides in diodes structures, with as most well-known example  $\text{Al}_2\text{O}_3$ .<sup>20</sup>

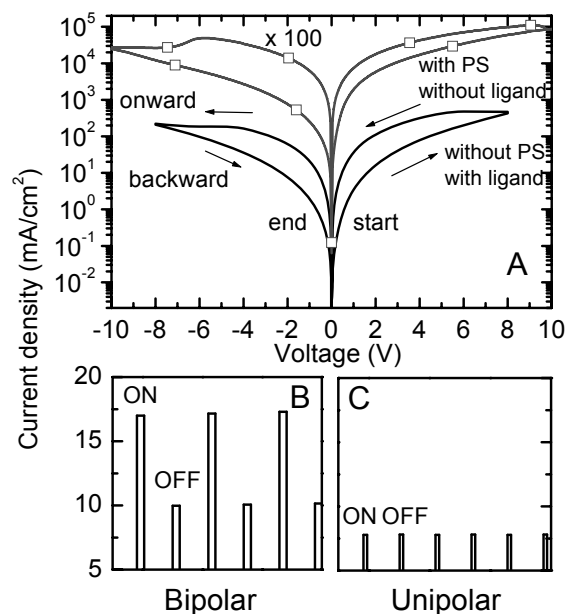


**Figure 6.6:** (a)  $J$ - $V$  characteristic of a PEDOT:PSS/ZnO:1/Al diode with 0.05 mol **1**/mol Zn (—) after electroforming and of a PEDOT:PSS/ZnO:PS/Al diode (-□-) after UV forming. (b) Current density at -1 V through the UV formed PEDOT:PSS/ZnO:PS/Al diode under bipolar voltage pulse cycle (Write +10 V, Erase -10 V). (c) Same as b but now with a unipolar pulse cycle (Write -3.5 V, Erase -7 V). The ZnO:PS ratio is 1:2 by weight.

Interestingly, when recording  $J$ - $V$  characteristics of pristine PEDOT:PSS/ZnO:1:PS/Al diodes with 0.03 - 0.05 mol **1** / mol Zn, scanning over a wider voltage range, changes in the characteristics of the diode occur because of the electroforming process. The  $J$ - $V$  trace changes to one showing pronounced NDR in both the onward and backward reverse bias part of the cyclic scan (-○-, Figure 6.7a).<sup>33,44</sup> Furthermore, the current measurement yields very noisy results, which on closer inspection may be interpreted in terms of rapid switching between two discrete resistance states. In about ~60 % of the tested diodes with 0.03 or 0.05 mol/mol **1** within a polystyrene matrix this type of NDR and the jumps in current density were observed (7 out of 11). At high ligand concentrations, the current densities decreases strongly and no jumps are observed. The appearance of the anomalous  $J$ - $V$  characteristics is accompanied by the possibility of unipolar resistive switching (Figure 6.8c). By applying a -3.5 V bias pulse the low resistive ON-state is induced. The state is read at -1 V, obtaining a high current density of ~0.1 mA/cm<sup>2</sup>. Application of a -7 V pulse results in the high resistive OFF-state with a

low current density of  $10^{-4}$  mA/cm<sup>2</sup> at  $-1$  V. Using 10 ms long pulses, reliable switching with an ON/OFF-ratio of  $\sim 10^3$  could be demonstrated over at least 20 write-erase cycles with good cycle endurance (Figure 6.7d). Furthermore, voltage pulses as short as 1 microsecond can switch ON the device, while for OFF-switching 0.5  $\mu$ s pulses suffice. This is much shorter than for diodes with ZnO particles without thiol ligands (Chapter 4). The high and low resistance states were found to be stable in time for at least 1hr.

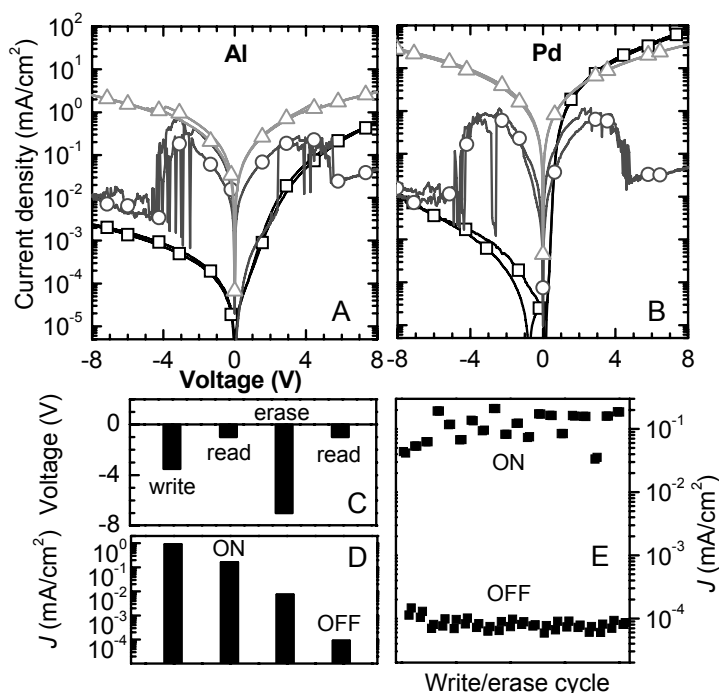


**Figure 6.7:** a – b)  $J$ - $V$  characteristics of ITO/PEDOT:PSS/ZnO- $np$  – PS/Al diodes (a) and ITO/PEDOT:PSS/ZnO- $np$  – PS/Pd diodes (b) without thiol ( $\square$ ), with 0.05 mol **1** / mol Zn ( $\circ$ ), and with 0.05 mol **1** / mol Zn after UV illumination ( $\triangle$ ). c – d) Unipolar switching of ZnO with 0.05 mol **1** / mol Zn in a PS matrix. Write pulse  $-3.5$  V, erase pulse  $-7$  V and read pulse  $-1$  V, with 10 ms duration of all pulses. c) The applied voltages and the obtained current densities. e) The low resistive (ON-state) and high resistive (OFF-state) state of the memory during 20 write and erase cycles, both read at  $-1$  V.

This switching behavior and NDR resemble those observed for diodes with semiconducting polymer and aluminum oxide as active layer.<sup>45,46</sup> To check whether the memory effects observed here do not originate from native oxide, formed at the aluminum electrode,<sup>22</sup> devices with a palladium top electrode were fabricated. These  $J$ - $V$  characteristics for these diodes are shown in Figure 6.7b. For the pristine device a diode behavior is observed. The formation of an Ohmic contact can only be expected if the ZnO at the interface with the Pd is doped. These diodes show similar behavior as observed for the diodes with the Al electrode. Therefore the switching can not be attributed to a native aluminum oxide layer in the diodes.

A time record of the current density of in these diodes at  $-3.5$  V bias is dominated by abrupt transitions between two distinct levels (Figure 6.8) Here, the change in resistance is close to three orders of magnitude, consistent with the results of the  $J$ - $V$  characterization in the same bias voltage range. In the time records we find that diodes with 0.03 to 0.05 mol octane thiol / mol Zn can give none, one or more than one of these low frequency, two level fluctuations. The changes in resistance observed at each step ranges from  $10^3$  times to very small fluctuations.

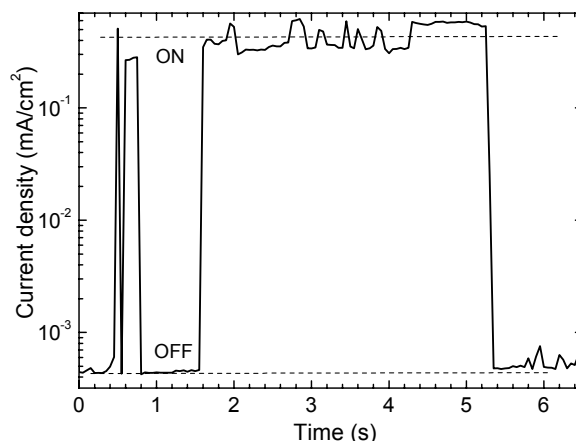


**Figure 6.8:** Fluctuations in current density through an ITO/PEDOT:PSS/ZnO-np – PS/Al diode with surface modified ZnO particles (0.05 mol octane thiol / mol Zn) Applied bias voltage:  $-3.5$  Volt.

The rapid, almost discrete nature of the switching between the states at intermediate bias voltages ( $\sim 4$ V) indicates that the current flows mainly via a single channel. In this case, trapping/release of a single electron at a defect or trap in the channel can block the conduction and induce switching between a low and a high resistance state.<sup>4748</sup>

By illuminating the diodes showing the anomalous  $J$ - $V$  characteristics with UV-light, the anomalous switching characteristics disappear ( $-\Delta-$ , Figure 6.7). After illumination, the pronounced NDR disappears and the resistance is slightly lower than in the ON state before illumination. This also indicates that the switching is related to the ZnO particles and not solely controlled by a native oxide layer at the electrodes.

Curiously, in the ON state of the electroformed diode containing 0.05 molar ratio the ligand, the resistance is lower than for the diodes without any ligand (see Figure 6.7a, b). For the latter diodes the electroforming is known to set in at voltages exceeding 8 V. As discussed above, the presence of thiol ligands does not inhibit the process in which  $O_2$  desorbs from the surface of the oxide particle under the influence of holes in the conduction band of the oxide. This process leads to an increase in the number of mobile charge carriers. In fact, the PIA measurements indicate that with ligand present

the lifetime of the mobile carriers, which is limited by rebinding of oxygen, is longer than in the absence of ligand. Rebinding of oxygen molecules, capturing the mobile carriers is slowed down by the presence of the ligand. This might increase the amount of mobile carriers. But also the local field at the percolation pathway might be higher when only a few pathways are present, resulting in lower forming voltages. Therefore to explain the lower resistivity in the ON state of the diodes containing ligand in comparison to the diodes without any ligand, it is argued that electroforming in the diodes with ligand sets in at lower voltage and may be more effective than in diodes without ligand.

### **6.5. Discussion**

An important question that remains unanswered is what causes the resistive switching in the diodes containing ZnO and ligand. As mentioned above, experimental evidence indicates the forming process, in which the density of mobile carriers in the oxide increases, still occurs when thiol ligand is bound to the particles. Microscopy shows that addition of ligand to the ZnO:PS mixture, induces morphological changes in the films. In the films that show the anomalous electrical characteristics, the interconnectivity of the oxide is reduced and they are grouped in small isolated cluster rather than in a pervading network. In Figure 6.9, we give a schematic interpretation of the morphological changes induced by the ligand. Spin coating uncapped nanoparticles results in large clusters of densely packed particles (Figure 6.9a). Due to poor solubility, the ZnO nanoparticles aggregate and form percolation pathways between the two electrodes, resulting in a good conduction in the diode. It is argued that without ligand, many conduction pathways exist between the electrodes. Partial capping the ZnO with ligand reduces the size of the cluster. Due to the presence of the aliphatic tail of the thiol ligand, the hybrid particles are more compatible with the solvent and the PS matrix. The number of conducting percolation pathways formed is significantly less than when uncapped ZnO nanoparticles are used (Figure 6.5b) and the resistivity is therefore higher.

In the films showing the anomalous behavior, essentially only one such a pathway may remain and all current passes through this path. For electrical conduction in nanoscopic systems it is well known that a single trapped charge carrier may block further conduction through the narrow channel by the Coulomb force that it exerts on the other charge carriers.<sup>49</sup> In this system, the assumption of a single active channel opens a way to explain the switching and the large noise in the current measurements: a blockade induced by a single charge carrier or defect may turn the channel on or off.

From research on electrical breakdown in SiO<sub>2</sub> it is known, that the high electric fields applied introduce charge defects which allow for mobile charge carriers with

electrical charge opposite to that of the defect to enter the insulator in significant numbers. When enough defects are induced at a close enough distance, a percolating path for the mobile charges carriers to go from one electrode to the other arises and current starts flowing. Close to this percolation threshold, creation or removal of a single defect can turn the conduction ON or OFF by completing or breaking the percolation path. This is evidenced in the  $J$ - $V$  characteristics of Figure 6.7a and Figure 6.8 by the observation of noise in the current density. In this noise fluctuations between two levels in the current density are obtained. This switching between a high and a low resistive state is characteristic for a so-called soft electrical breakdown.<sup>50</sup> Interestingly, after soft electrical breakdown, also  $\text{SiO}_2$  shows unipolar resistive switching and NDR.<sup>33</sup>

The large amplitude resistive switching observed in the diodes containing ZnO particles and ligands resemble those observed in electroformed  $\text{SiO}_2$  and  $\text{Al}_2\text{O}_3$ . In the interpretation sketched in Figure 6.9 it arises due to the presence of one or just a few conduction paths that can be blocked or opened by a single event, depending on the applied electric field. These nature of these events are not known in detail, but conceivably they may be trapping of a single charge carrier or ionization of a single defect.

When large amounts of ligands ( $> 0.18$  mol/mol) are added (Figure 6.9c), the particles are surrounded by an insulating shell of ligand and electrical transport *via* interparticle contacts is inhibited.

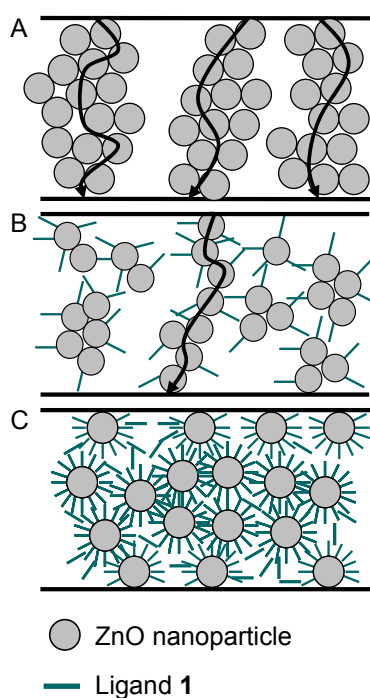


**Figure 6.9:** Schematic overview of the influence of **1** on the clustering of ZnO nanoparticles. a) No **1**. b) Low concentrations of **1** showing resistance switching. c) High concentrations of **1**.

## **6.6. Conclusion**

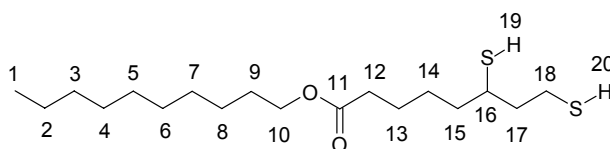
In conclusion, ZnO nanoparticles can be capped using ligands with a thiol functionality. The capping of the nanoparticles can be monitored using the defect emission of ZnO as a probe. The presence of the ligand strongly influences the clustering and aggregation of the ZnO particles in spin coated films with polystyrene as host matrix. The change in film morphology has a strong influence on the electrical characteristics of the film in a diode geometry. Capping the oxide particles with an insulating shell of aliphatic ligands strongly increases the resistance of the film. Interestingly, partial coverage of the surface of the particle with insulating ligands leads to more unexpected electrical behavior. Noise fluctuations between two levels in the current density are obtained. Under these conditions unipolar resistive switching is observed, an effect which is not observed for unmodified ZnO particles. The unusual characteristics are interpreted as arising from conduction through single, narrow channels of clustered oxide particles. This illustrates, that interactions between organic-inorganic hybrid particles can be used to influence electrical properties of materials. In particular processes leading to formation of narrow channels may lead to unexpected new electrical phenomena.

## **6.7. Experimental**

Infrared spectra were measured on a Perkin Elmer Spectrum One UATR FT-IR spectrophotometer. Thermogravimetric analysis (TGA) measurements were run on a Perkin Elmer Pyris 6 Thermogravimetric Analyzer. Method: Samples were heated under nitrogen purging at 20 ml/minute; 3 minutes at 30 °C, heat from 30 °C to 700 °C with 10 °C / minute and 3 minutes at 700 °C. UV/Vis Absorption spectra were recorded on a Perkin Elmer Lambda 40 UV/Vis Spectrometer or a Perkin Elmer Lambda 900 UV/Vis/NIR Spectrometer. Zinc oxide nanoparticles were synthesized as described in Chapter 3. Photoluminescence (PL) emission spectra were measured on an Edinburgh Instruments FS920 double monochromator luminescence spectrometer using a Peltier-cooled red-sensitive photomultiplier. All measured solutions had an optical density of 0.1 at the excitation wavelength. Near steady-state photoinduced absorption (PIA) spectra of spin coated films of capped and uncapped ZnO np deposited on quartz were recorded between 0.30 and 1 eV. A more detailed description is given in Chapter 4. Electron paramagnetic resonance (EPR) at 9.43 GHz (X-band) was measured with a Bruker ESP 300E spectrometer using a cavity with a 50% transmission grid. The sample was prepared by evaporating a solution of 0.5 mg ZnO per mL chloroform and the proper amount of **1** and kept in air or vacuum during the measurement. To investigate the influence of UV-light the sample can be illuminated with light from a 500 W Xe light source. Atomic Force Microscopy (AFM) was performed at room temperature with a Digital Instruments AFM, equipped with a Nanoscope IIIa controller in tapping mode. Transmission Electron Microscopy (TEM) are performed on a 200 mesh carbon-coated and 200 mesh copper only grids, purchased from Aurion. TEM grids were prepared by applying a droplet of sample solution

onto a 200 mesh carbon-coated copper grid. Excess solution was blotted away using a filter paper. The films were spin coated with first a poly(3,4-ethylene dioxythiophene): polystyrene sulfonate (PEDOT:PSS, H.C. Starck, Baytron P VP Al 4083) layer at 1500 rpm, resulting in a layer of  $0.7 \times 10^2$  nm and secondly with a solution containing 20 mg PS ( $M_w = 250$  kg/mol, polydispersity index 2.2) and 10 mg of ZnO particles per ml chloroform, bearing the right concentration **1** at 3000 rpm, resulting in a layer of  $2 \times 10^2$  nm. The films were cut and carefully brought into water. The PEDOT:PSS layer dissolved and the floating layer was brought onto 200 mesh copper only grids. Excess water was blotted away using a filter paper. The samples were analyzed at room temperature on a FEI Tecnai 20, type Sphera TEM operating with a 200 kV LaB<sub>6</sub> filament, equipped with a bottom mounted 1k × 1k Gatan CCD camera.

The ring opening of 5-[1,2]dithiolan-3-ylpentanoic acid decyl ester<sup>51</sup> was performed by dissolving 3.0 g (8.65 mmol) of this material in 20 mL THF (distilled). Subsequently, 1.87 g (49.4 mmol) NaBH<sub>4</sub> dissolved in 2 mL water was added, while cooling in ice. After stirring overnight at room temperature DCM was added and extraction with 0.1 M HCl and twice with water was performed. Purification by column chromatography on silica gel (chloroform) yielded pure 6,8-dimercapto-octanoic acid decyl ester (**2**) (2.1 g, 70%).



## 2

<sup>1</sup>H-NMR (400 MHz, CDCl<sub>3</sub>, 25 °C, TMS): δ 0.88 (t, 3 H, 1), 1.2 - 1.5 (m, 16 H, 2 - 8, 14), 1.55 - 1.75 (m, 6 H, 9, 13 and 15), 1.89 (m, 1 H, 17), 2.32 (t, 2 H, 12), 2.71 (m, 2 H, 18), 2.93 (m, 1 H, 16), 3.57 (m, 1 H, 16), 4.07 (t, 2 H, 10).

<sup>13</sup>C-NMR (100 MHz, CDCl<sub>3</sub>, 25 °C, TMS): δ 14.09 (1 C, 1), 22.24 (1 C, 2), 22.63 (1 C, 3), 24.59 (1 C, 13), 25.90 (1 C, 7), 26.49 (1 C, 14), {28.61, 29.21, 29.25, 29.48} (5 C, 4 -6, 8, 15), 31.85 (1 C, 9), 34.11 (1 C, 12), 38.70 (1 C, 18), 39.26 (1 C, 17), 42.74 (1 C, 16), 64.43 (1 C, 10), 173.48 (1 C, 11)

IR (UATR): ν (cm<sup>-1</sup>): 2924, 2854 (C-H stretch); 1730 (C=O stretch); 1459, 1390, 1247, 1172, 1088, 722.

GC-MS (FW = 348.60): one peak, m/z: 346 [M-2H]<sup>+</sup>, 206 [thioctic acid]<sup>+</sup>, 157 [decanol]<sup>+</sup>.

In the titration experiments, 100 mL of an  $8.5 \times 10^{-2}$  mM ( $M_w = 81.39$ ) ZnO solution was prepared by diluting 22 μL of a 31.4 g / L stock solution. A 2.8 mM solution of **2** was added in steps of 10 μL. After every step 3 mL was taken out of the solution to measure photoluminescence. This sample was thrown away after measurement to prevent influence of UV-illumination on the PL spectrum. The binding constant was fitted using:

$$PL = (1 - R) \left[ 1 - \frac{\frac{A_0}{2} + \frac{B_0}{2} + \frac{1}{2K} - \frac{\sqrt{A_0^2 K^2 - 2A_0 B_0 K^2 + 2A_0 K + B_0^2 K^2 + 2B_0 K + 1}}{2K}}{A_0} \right] + R$$

with:  $PL$  = relative photoluminescence

$R$  = rest emission

$K$  = binding constant, in  $M^{-1}$  binding places

$B_0$  = [ligand]

$A_0$  = [binding places]:

$$A_0 = \frac{[ZnO] S_{ZnO-np}}{N_{ZnO-np} S_{ligand}}$$

with:  $[ZnO]$  = concentration of molecular ZnO

$N_{ZnO-np}$  = number of ZnO units per np:  $2.6 \times 10^3$  for a diameter of 5 nm.

$S_{ZnO-np}$  = surface per ZnO np:  $7.85 \times 10^{-17} m^2$  for a diameter of 5 nm.

$S_{ligand}$  = surface needed per ligand:  $32 \times 10^{-20} m^2$  for **2** and  $16 \times 10^{-20} m^2$  for **1**.

The devices consists of a bottom electrode consists of tin-doped indium oxide with a spin coated film of PEDOT:PSS of approximately 70 nm thickness. The films without PS matrix were spin coated at 1000 rpm from a solution containing 50 mg of ZnO particles per milliliter chloroform and the specific amount of **1**. The obtained film thicknesses were  $2 \times 10^2$ ,  $2 \times 10^2$ ,  $3 \times 10^2$ , and  $8 \times 10^2$  nm for 0, 0.05, 0.18, and 0.5 mol **1** per mol ZnO nanoparticles, respectively. For the devices with PS matrix, the active layer was spin coated at 1500 rpm, from a solution containing 20 mg PS and 10 mg of ZnO particles per milliliter of chloroform, again with the different concentrations of **1**. For all films thicknesses of  $3 \times 10^2$  nm were obtained. Finally, the top electrode was made by evaporation of aluminum or palladium, at a base pressure of  $10^{-7}$  mbar. The active device area is  $9.5 mm^2$ . After deposition of Al, the devices are stored and characterized in an inert atmosphere ( $O_2$ ,  $H_2O \leq 1$  ppm). A homemade Labview program with a computer controlled Keithley 2400 (sweep) or 2600 (pulse) source-measure unit is used for electrical characterization, where positive (forward) bias voltage is defined by the PEDOT:PSS electrode being charged positive. The compliance level was 100 mA. The effect of UV-irradiation was studied with light from a tungsten-halogen source (total  $80 mW/cm^2$ ). The film thicknesses were measured with a Tencor P-10 Surface profiler.

## 6.8. References

- 1 S.J. Pearton, D.P. Norton, K. Ip, Y.W. Heo, and T. Steiner, *J. Vac. Sci. Technol. B* **22**, 932 (2004).
- 2 C. Klingshirn, *Phys. Stat. Sol. B* **244**, 3027 (2007).
- 3 U. Ozgur, Y.I. Alivov, C. Liu, A. Teke, M.A. Reshchikov, S. Dogan, V. Avrutin, S.J. Cho, and H. Morkoc, *J. Appl. Phys.* **98**, 041301 (2005).
- 4 L. Schmidt-Mende and J.L. MacManus-Driscoll, *Mater. Today* **10**, 40 (2007).
- 5 Z.L. Wang, *Mater. Today* **7**, 26 (2004).
- 6 N.S. Norberg and D.R. Gamelin, *J. Phys. Chem. B* **109**, 20810 (2005).



- 7 M.L. Kahn, M. Monge, V. Collière, F. Senocq, A. Maisonnat, and B. Chaudret, *Adv. Func. Mater.* **15**, 458 (2005).
- 8 M. Shim and P. Guyot-Sionnest, *J. Am. Chem. Soc.* **123**, 11651 (2001).
- 9 W.J.E. Beek, *PhD thesis: Hybrid Polymer Solar Cells*, Technische Universiteit Eindhoven, (2005).
- 10 P.D. Cozzoli, A. Kornowski, and H. Weller, *J. Phys. Chem. B* **109**, 2638 (2005).
- 11 S. Sakohara, M. Ishida, and M.A. Anderson, *J Phys. Chem. B* **102**, 10169 (1998).
- 12 N.S. Pesika, Z. Hu, K.J. Stebe, and P.C Searson, *J. Phys. Chem. B* **106**, 6985 (2002).
- 13 E.M. Wong, P.G. Hoertz, C.J. Liang, B.M. Shi, G.J. Meyer, and P.C. Searson, *Langmuir* **17**, 8362 (2001).
- 14 B. Sun, R.L. Peterson, H. Sirringhaus, and K. Mori, *J. Phys. Chem. C* **111**, 18831 (2007).
- 15 B.Q. Sun and H. Sirringhaus, *J. Am. Chem. Soc.* **28**, 16231 (2006).
- 16 F. Verbakel, S.C.J. Meskers, and R.A.J. Janssen, *J. Phys. Chem. C* **111**, 10150 (2007).
- 17 R. Munöz-Espí, G. Jeschke, I. Lieberwirth, C.M. Gómez, and G. Wegner, *J. Phys. Chem. B* **111**, 697 (2007).
- 18 N.C. Greenham, X. Peng, and A.P. Alivisatos, *Phys. Rev. B.* **54**, 17628 (1996).
- 19 B. Sun, E. Marx, and N.C. Greenham, *Nano Lett.* **3**, 961 (2003).
- 20 H. Pagnia and N. Sotnik, *Phys. Status Solidi A* **108**, 11 (1988).
- 21 S. Karthäuser, B. Lüssem, M. Weides, M. Alba, A. Besmehn, R. Oligschlaeger, and R. Waser, *J. Appl. Phys.* **100**, 94504-1 (2006).
- 22 M. Cölle, M. Büchel, and D.M. de Leeuw, *Org. Electron.* **7**, 305 (2006).
- 23 W.J. Joo, T.L. Choi, J. Lee, S.K. Lee, M.S. Jung, N. Kim, and J.M. Kim, *J. Phys. Chem. B* **110**, 23812 (2006).
- 24 T. Hada, K. Wasa, and S. Hayakawa, *Japan. J. Appl. Phys* **10**, 521 (1971).
- 25 J.C. Scott and L.D. Bozano, *Adv. Mater.* **19**, 1452 (2007).
- 26 W.-T. Li, D.R. McKenzie, W.D. McFall, Q.-C. Zhang, and W. Wiszniewski, *Solid-State Electronics* **44**, 1557 (2000).
- 27 J. Lee, S.S. Kim, and S. Im, *J. Vac. Sci. Technol. B* **21**, 953 (2003).
- 28 I.G. Baek, M.S. Lee, S. Seo, M.J. Lee, D.H. Seo, D.-S. Suh, J.C. Park, S.O. Park, H.S. Kim, I.K. Yoo, U.-In. Chung, and J.T. Moon, *IEDM Tech. Dig.-Int. Electron Devices Meet.* **04**, 587, (2004).
- 29 R. Waser and M. Aono, *Nature Mater.* **6**, 833 (2007).
- 30 A. Chen, S. Haddad, Y. C. Wu, T. N. Fang, Z. Lan, S. Avanzino, S. Pangrle, M. Buynoski, M. Rathor, W. Cai, N. Tripsas, C. Bill, M. Van Buskirk, and M. Taguchi, *IEDM Tech. Dig. - Int. Electron Devices Meet.* **05**, 765 (2005).
- 31 M.J. Lee, S. Seo, D.C. Kim, S.E. Ahn, D.H. Seo, I.K. Yoo, I.G. Baek, D.S. Kim, I.S. Byun, S.H. Kim, I.R. Hwang, J.S. Kim, S.H. Jeon, and B.H. Park, *Adv. Mater.* **19**, 73 (2007).
- 32 A. Chen, S. Haddad, Y. C. Wu, T. N. Fang, S. Kaza, and Z. Lan, *Appl. Phys. Lett.* **92**, 013503 (2008).
- 33 J.G. Simmons and R.R. Verderber, *Proc. R Soc. Lond. Ser. A* **301**, 77 (1967).

- 34 M. J. Rozenberg, I. H. Inoue, and M. J. Sánchez, *Phys. Rev. Lett.* **92**, 178302 (2004).
- 35 C. Pacholski, A. Kornowski, and H. Weller, *Angew. Chem.* **41**, 1188 (2002).
- 36 A. van Dijken, E. A. Meulen Kamp, D. Vanmaekelbergh, and A. Meijerink, *J. Phys. Chem B* **104**, 1715 (2000).
- 37 P. V. Kamat and B. Patrick, *J. Phys Chem.* **96**, 6829 (1992).
- 38 B.A. Korgel, S. Fullam, S. Connolly, and D. Fitzmaurice, *J. Phys. Chem. B* **102**, 8379 (1998).
- 39 L.J.A. Koster, *Ph.D. Thesis*, Groningen University (2007) <http://dissertations.ub.rug.nl/faculties/science/2007/l.j.a.koster/?FullItemRecord=ON>
- 40 F. Verbakel, S.C.J. Meskers, and R.A.J. Janssen, *J. Appl. Phys.* **102**, 083701-1 (2007).
- 41 V. Ischenko, S. Polarz, D. Grote, V. Stavarache, K. Fink, and M. Driess, *Adv. Func. Mater* **15**, 1945 (2006).
- 42 S.B. Orlinskii, H. Blok, J. Schmidt, P.G. Baranov, C.D.M. Donega, and A. Meijerink, *Phys. Rev. B* **74**, 045204 (2006).
- 43 L.S. Vlasenko and G.D Watkins, *Phys. Rev. B* **72**, 035203 (2005).
- 44 L.D. Bozano, B.W. Kean, V.R. Deline, J.R. Salem, and J.C. Scott, *Appl. Phys. Lett.* **84**, 607 (2004).
- 45 L.D. Bozano, B.W. Kean, M. Beinhoff, K.R. Carter, P.M. Rice, and J.C. Scott, *Adv. Func. Mater.* **15**, 1933 (2005).
- 46 F. Verbakel, S. C. J. Meskers, M. Cölle, M. Büchel, H. L. Gomes, R. A. J. Janssen, and D. M. de Leeuw, *Appl. Phys. Lett.* **91**, 192103 (2007).
- 47 K.R. Farmer, R. Saletti, and R.A. Buhrman, *Appl. Phys. Lett.* **52**, 1749 (1988).
- 48 F. Crupi, R. Degraeve, G. Groeseneken, T. Nigam, and H.E. Maes, *IEEE Trans. Electron Dev.* **45**, 2329 (1998).
- 49 W. Tang, H. Shi, G. Xu, B.S. Ong, Z.D. Popovic, J. Deng, J. Zhao, and G. Rao, *Adv. Mater.* **17**, 2307 (2005).
- 50 J. Suñe, D. Jimenez, and E. Mirand, In: *Oxide reliability. A summary of silicon oxide wearout, breakdown and reliability*. D.J. Dumin ed. World Scientific, Singapore, 173 (2002).
- 51 J. van Herrikhuyzen, *Ph.D. Thesis*, Technische Universiteit Eindhoven (2007).



# 7

## **Reproducible resistive switching in non-volatile organic memories**

*Resistive switching in non-volatile, two terminal organic memories can be due to the presence of a native oxide layer at one of the aluminum electrodes. Reproducible solid state-memories can be realized by deliberately adding a thin sputtered  $\text{Al}_2\text{O}_3$  layer to nominal electron-only, hole-only, and bipolar organic diodes. Before memory operation, the devices have to be formed at an electric field of  $10^9$  V/m, corresponding to soft-breakdown of  $\text{Al}_2\text{O}_3$ . After forming, the structures show pronounced negative differential resistance and the local maximum in the current scales with the thickness of the oxide layer. The polymer acts as a current limiting series resistance.*

This work has been published: F. Verbakel, S.C.J. Meskers, M. Cölle, M. Büchel, H.L. Gomes, R.A.J. Janssen, and D.M. de Leeuw, *Appl. Phys. Lett.* **91**, 192103 (2007).

## 7.1. Introduction

Non-volatile organic memories consist of *any* organic semiconductor sandwiched between two electrodes, one of which typically is aluminum.<sup>1-6</sup> First, by applying a high bias, the rectifying diode with an aluminum electrode is transformed into a nonlinear resistor that, moreover, often shows a negative differential resistance (NDR).<sup>7</sup> This forming process, however, is not always observed for the devices with a native oxide. The formed memory can be switched between high and low resistance states by applying voltage pulses of different biases but of the same polarity. It has recently been shown that the conduction is through filaments and that the switching occurs in the native aluminum oxide.<sup>8</sup> Studies using an Al<sub>2</sub>O<sub>3</sub> layer obtained via deliberate oxidation of an aluminum layer, support the view of the oxide being the active layer.<sup>9,10</sup>

Note, that the yield of working devices is often low and that the forming and switching bias voltages are irreproducible.<sup>11</sup> To improve the reliability, an Al<sub>2</sub>O<sub>3</sub> layer with controlled thickness has deliberately been added. The data shows that reproducible memories can then be obtained not only for *electron*-only, but also for nominal *hole*-only, and nominal bipolar diodes. Furthermore the forming and switching biases systematically vary with the thickness of the Al<sub>2</sub>O<sub>3</sub> layer.

## 7.2. Forming process

As a typical example the electrical transport of a pristine e-only diode with a 20 nm Al<sub>2</sub>O<sub>3</sub> layer is presented in Figure 7.1. Figure 7.1a shows cyclic current-voltage (*J-V*) scans indicated by arrows where the maximum bias is increased stepwise. In the first scan, the current density increases with bias up to 10<sup>-4</sup> mA/cm<sup>2</sup> at 2 V. Strong hysteresis is observed; the current density scanning back is negligibly low. In the subsequent scans the current density sharply increases at about the maximum bias of the previous scan. This *J-V* behavior is typical for charge trapping. It seems still reversible, albeit on a time scale of hours.

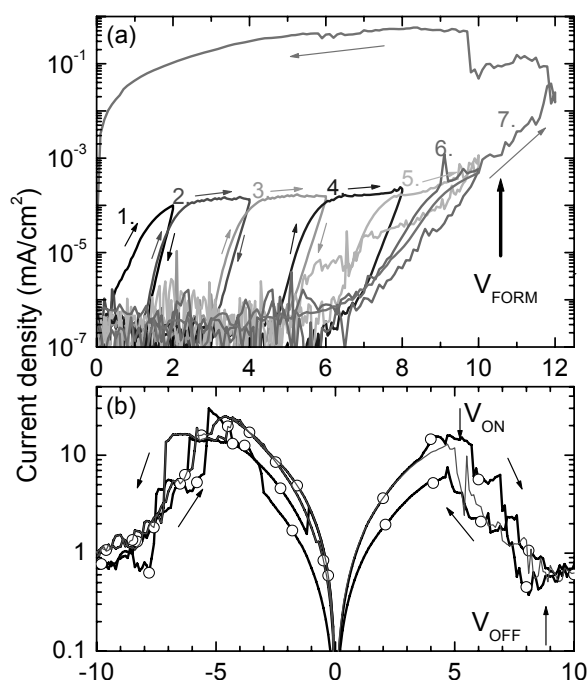


**Figure 7.1:** (a) Sequential  $J$ - $V$  characteristic of a pristine  $e$ -only diode ( $\text{Al}/\text{Al}_2\text{O}_3/\text{Polymer}/\text{Ba,Al}$ ) with a 20 nm  $\text{Al}_2\text{O}_3$  layer. The maximum applied bias voltage is increased in steps.  $V_{\text{FORM}}$  is the voltage required for the forming process (b) The device after forming, first scan ( $-O-$ ), second scan ( $---$ ), showing the NDR, with  $V_{\text{ON}}$  and  $V_{\text{OFF}}$  as the voltage used for switching. The scan speed of the  $J$ - $V$  characterization is 1 V/s.

At about 10 V, the forming voltage, a sudden increase in current density is observed. Figure 7.1b shows that the  $J$ - $V$  characteristics have irreversibly changed into that of a symmetric but nonlinear resistor with a pronounced NDR. Typically, at biases above the maximum of the NDR, the  $J$ - $V$  traces show large current fluctuations.

After forming, the devices can be switched reversibly between a high and low resistance state. Figure 7.2 shows the current density of the read voltage pulse upon applying 100 sequential write/read/erase/read voltage pulses. Reliable switching is obtained when the biases correspond to the NDR.<sup>12,13</sup> At the onset of the NDR, the maximum observed current, here +5 V (or -5 V) the memory switches to the high resistance state, while at the minimum current, at the end of the NDR, here +10 V (or -10 V), the low resistance state is obtained. The ON/OFF ratio is typically one order of magnitude. In this experiment, a minimum pulse width of 10 ms is necessary to induce resistive switching. The higher the pulse width, the better is the switching reliability, usually a pulse width of 100 ms gives a switching reproducibility of almost 100%.

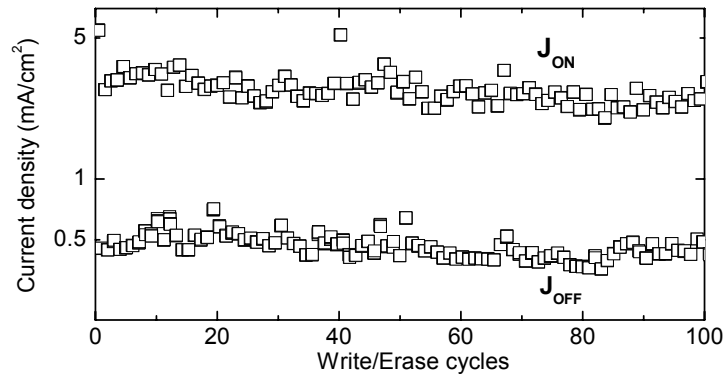


**Figure 7.2:** The current density under application of the +0.5 V read pulses after a +5 V write pulse ( $J_{ON}$ ) or a +10 V erase pulse ( $J_{OFF}$ ), both with a length of 100 ms.

### 7.3. $Al_2O_3$ layer thickness

The thickness of the  $Al_2O_3$  layer is systematically varied. The polymer layer was fixed at 80 nm. Figure 7.3a shows that the forming voltage for e-only diodes ( $\blacktriangledown$ ) increases linearly with  $Al_2O_3$  thickness. For comparison the breakdown voltages reported for Ti/ $Al_2O_3$ /Al diodes ( $\bullet$ ) are included. The good agreement indicates that the forming field of the organic memories is similar to the reported soft breakdown field of  $Al_2O_3$ , viz. about  $10^9$  V/m.<sup>14,15</sup> For a fixed thickness of the  $Al_2O_3$  layer of 20 nm, the thickness of the polymer film is varied. Figure 7.3b shows the forming voltage as function of the layer thickness. Up to about 200 nm a linear dependence is observed indicating that the equivalent circuit is a simple series resistance of a polymer and  $Al_2O_3$  layer. The deviation for thicker polymer layers is not yet understood.

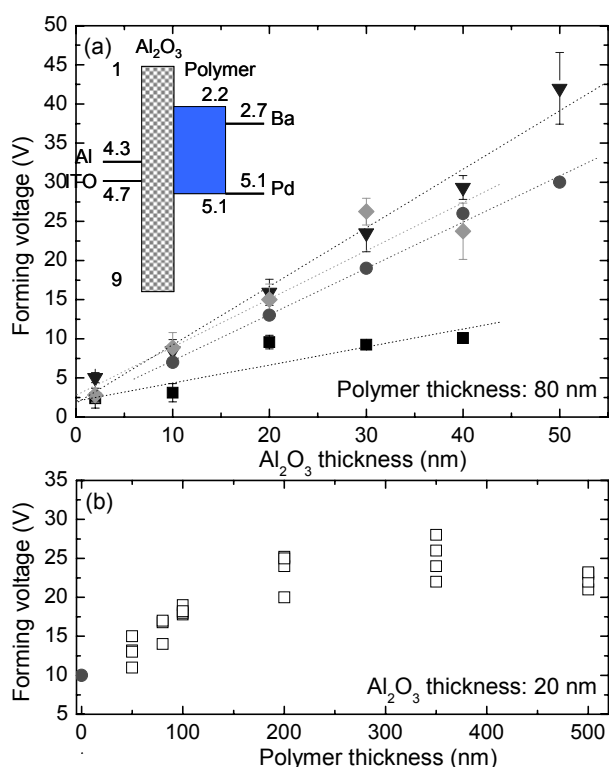


**Figure 7.3:** (Inset) Flat band diagram for the investigated diodes (eV). (a) Forming voltage versus the layer thickness of Al<sub>2</sub>O<sub>3</sub> (Polymer thickness: 80 nm). (Al/ Al<sub>2</sub>O<sub>3</sub>/ Polymer/ Ba,Al) (▼), (ITO/ Al<sub>2</sub>O<sub>3</sub>/ Polymer/Pd) (■), (ITO/ Al<sub>2</sub>O<sub>3</sub>/ Polymer/ Ba,Al) (◆) and (Ti/ Al<sub>2</sub>O<sub>3</sub>/ Al) (●) device structures. (b) Forming voltage versus the polymer layer thickness (Al<sub>2</sub>O<sub>3</sub> thickness: 20 nm) (Al/ Al<sub>2</sub>O<sub>3</sub>/ Polymer/ Ba,Al) (□) and without polymer (Ti/ Al<sub>2</sub>O<sub>3</sub>/ Al) (●).

Switching is not limited to *e*-only diodes. By adding Al<sub>2</sub>O<sub>3</sub> layers to the stack, memories have been realized from *h*-only and bipolar diodes as well. The forming voltages as a function of Al<sub>2</sub>O<sub>3</sub> thickness are presented in Figure 7.3a. Similar as for the *e*-only diodes a linear dependence is obtained. The forming field for the bipolar diodes is similar to that of the *e*-only diodes. For the *h*-only diodes the field is smaller by about a factor of 2. Although the difference might be related to limited injection by the Pd electrode, it is not yet fully understood. For all memories investigated, the optimal switching biases,  $V_{ON}$  and  $V_{OFF}$ , correspond to the maxima and minima in the NDR. The switching biases, presented in Table 7.1, systematically increase with Al<sub>2</sub>O<sub>3</sub> layer thickness, for  $V_{ON}$  to 10 V and for  $V_{OFF}$  to 20 V. For all memories the current density was measured in the ON- and OFF-state. The current ratios using switching pulses of 100 ms are presented in Table 1. The modulation decreases with increasing Al<sub>2</sub>O<sub>3</sub> layer thickness. This dependence is counterintuitive and requires further investigation as a function of *e.g.* pulse length. The maximum currents observed in the *J-V* characteristics show no correlation with the thickness of the Al<sub>2</sub>O<sub>3</sub> or the polymer layer, or with the electrodes,



*i.e.* *e*-only, *h*-only or bipolar. This can be expected for a filamentary conduction mechanism. However, the reliability of the switching generally decreases for thicker Al<sub>2</sub>O<sub>3</sub> layers.

**Table 7.1:** Switching biases,  $V_{ON}$  and  $V_{OFF}$ , resistance modulation  $R_{ON}/R_{OFF}$ , and yield of switching in the memory devices for *e*-only, *h*-only and bipolar pristine diodes as a function of Al<sub>2</sub>O<sub>3</sub> layer thickness, with in brackets, the number of switching events in the total number of write/erase cycles performed.

Al <sub>2</sub> O <sub>3</sub>	$V_{ON}$	$V_{OFF}$	$R_{ON}/R_{OFF}$	YIELD	
<b>e-only: Al/Al<sub>2</sub>O<sub>3</sub>/Polymer/Ba,Al</b>					
2 nm	-	-	-	~0 %	(0/7)
10 nm	4	8	~100	~90 %	(24/27)
20 nm	5	10	~10	~100 %	(15/15)
30 nm	10	20	~5	~100 %	(30/30)
40 nm	10	20	~5	~100 %	(30/30)
50 nm	10	20	~4	~100 %	(30/30)
<b>h-only: ITO/Al<sub>2</sub>O<sub>3</sub>/Polymer/Pd</b>					
0 nm	-	-	-	~0 %	(0/9)
2 nm	2.5	5	~100	~50 %	(9/17)
10 nm	3	6	~50	~90 %	(23/25)
20 nm	5	10	~2	~100 %	(11/11)
30 nm	5	10	~2	~100 %	(10/10)
40 nm	5	10	~5	~90 %	(8/9)
<b>Bipolar: ITO/Al<sub>2</sub>O<sub>3</sub>/Polymer/Ba,Al</b>					
0 nm	2.5	5	~10	~15 %	(3/19)
2 nm	2	5	~4	~80 %	(14/18)
10 nm	4	8	~2	~90 %	(32/35)
20 nm	6	12	~50	~85 %	(21/25)
30 nm	6	12	~2	~100 %	(25/25)
40 nm	8	16	~2	~90 %	(18/20)

In order to determine the reproducibility for *e*-only, *h*-only and bipolar pristine diodes with six different Al<sub>2</sub>O<sub>3</sub> layer thickness ranging from 2 nm up to 50 nm have been fabricated. All together, the forming process was found to occur in 100 out of 100 devices with Al<sub>2</sub>O<sub>3</sub>. Switching in 50 devices with Al<sub>2</sub>O<sub>3</sub> has been investigated and 50 of these show switching, while with only a native oxide layer, the yield is low, a few % at most. The yield of switching in these memories is presented in Table 7.1 and Figure 7.4.

The reproducibility increases to about unity when an Al<sub>2</sub>O<sub>3</sub> layer is inserted in the stack. It clearly demonstrates that a native aluminum oxide layer, which can be present when using Al electrodes, can cause resistive switching effects. The organic semiconductor only acts as a current limiting series resistance.

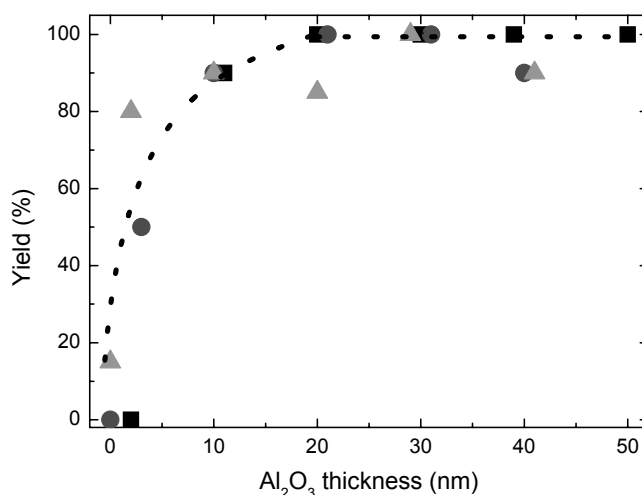


**Figure 7.4:** Switching yield versus the Al<sub>2</sub>O<sub>3</sub> layer thickness for the e-only (■), h-only (●) and bipolar devices (▲).

#### 7.4. Conclusions

Reproducible solid state-memories can be realized by deliberately adding a thin sputtered Al<sub>2</sub>O<sub>3</sub> layer to nominal electron-only, hole-only, and bipolar organic diodes. Before memory operation, the devices have to be formed at an electric field of 10<sup>9</sup> V/m, corresponding to soft-breakdown of Al<sub>2</sub>O<sub>3</sub>. After forming, the structures show pronounced negative differential resistance and the local maximum in the current scales with the thickness of the oxide layer. It clearly demonstrates that a native aluminum oxide layer, which can be present when using Al electrodes, can cause resistive switching effects. The organic semiconductor only acts as a current limiting series resistance.

#### 7.5. Experimental

The e-only diodes consisted of an Al bottom electrode, a sputtered Al<sub>2</sub>O<sub>3</sub> layer, a spirofluorene polymer and a Ba/Al top electrode. For h-only diodes the spirofluorene derivate was sandwiched between an ITO/ Al<sub>2</sub>O<sub>3</sub> bottom electrode and a Pd top electrode. Bipolar diodes were made using an ITO/ Al<sub>2</sub>O<sub>3</sub> bottom electrode and a Ba/Al electrode. The sputtering of the Al<sub>2</sub>O<sub>3</sub> was performed on a Balzers Vanguard with an Al<sub>2</sub>O<sub>3</sub> target at an RF sputterpower of 2 kW. A gasflow of 100 sccm Ar and 10 sccm Ar/ 10% O<sub>2</sub> was used. The sputtering was performed at 2.5 nm/min with a base pressure of 8x10<sup>-7</sup> mbar. The lay-out and schematic flat band diagram are presented in the inset of Fig. 3. The devices with an active area of 9 mm<sup>2</sup>, were encapsulated to exclude O<sub>2</sub> and H<sub>2</sub>O. The J-V characterization was performed using a HP4155c semiconductor analyzer. The pulse measurement were performed with a homemade Labview program using a computer controlled Keithley 2610. In all cases, positive bias voltage refers to the bottom electrode being charged positive with respect to the top electrode.

## 7.6. References

- 1 J.C. Scott and L.D. Bozano, *Adv. Mater.* **19**, 1452 (2007).
- 2 L. Ma, S. Pyo, J. Ouyang, Q. Xu, and Y. Yang, *Appl. Phys. Lett.* **82**, 1419 (2003).
- 3 L.D. Bozano, B.W. Kean, M. Beinhoff, K.R. Carter, P.M. Rice, and J.C. Scott, *Adv. Funct. Mater.* **15**, 1933 (2005).
- 4 P.D. Hooper, G. McHale, and M.I. Newton, *Int. J. Electronics* **81**, 435 (1996).
- 5 V.A. Kolesnikov, V.I. Zolotarevsky, and A.V. Vannikov, *Phys. Stat. Sol. A* **200**, 388 (2003).
- 6 S. Berleb, W. Brütting, and M. Schwoerer, *Synth. Met.* **102**, 1034 (1999).
- 7 G. Dearnaley, A.M. Stoneham, and D. V. Morgan, *Rep. Prog. Phys.* **33**, 1129 (1970).
- 8 M. Cölle, M. Büchel, and D.M. de Leeuw, *Org. Electron.* **7**, 305 (2006).
- 9 A. Prakash, J. Ouyang, J.-L. Lin, and Y. Yang, *J. Appl. Phys.* **100**, 054309 (2006).
- 10 C. W. Chu, J. Ouyang, J.-L. Lin, and Y. Yang, *Adv. Mater.* **17**, 1440 (2005).
- 11 W.-J. Joo, T.-L. Choi, J. Lee, S. K. Lee, M.-S. Jung, N. Kim, and J.M. Kim, *J. Phys. Chem. B* **110**, 23812 (2006).
- 12 L.D. Bozano, B.W. Kean, V.R. Deline, J.R. Salem, and J.C. Scott, *Appl. Phys. Lett.* **84**, 607 (2004).
- 13 J.G. Simmons and R.R. Verderber, *Proc. R Soc. Lond. Ser. A* **301**, 77. (1967).
- 14 W.-T. Li, D.R. McKenzie, W.D. McFall, Q.-C. Zhang, and W. Wisniewski, *Solid-State Electronics* **44**, 1557 (2000).
- 15 J. Lee, S.S. Kim, and S. Im, *J. Vac. Sci. Technol. B* **21**, 953 (2003).

# 8

## **Switching dynamics in non-volatile polymer memories**

*The time dependence of resistive switching in metal-organic semiconductor-metal diodes is investigated. A 10 nm thin Al<sub>2</sub>O<sub>3</sub> layer was added to obtain reproducible memories with a yield of unity. After forming with a high voltage pulse, the memories can reversibly be switched between a high and low resistance state. Single pulse measurements show that the switching is extremely fast, less than 400 ns. Repeated pulse sequence measurements show the occurrence of a 'dead time', that is the time after programming in which a next switch is inhibited, of about 3 ms. The dead time is a key ingredient to observe non-volatile switching because it prevents changing the resistance state when ramping down the bias. Furthermore, the dead time explains the huge variation in the reported switching times.*

## **8.1. Introduction**

Resistive switching in organic and polymer metal-semiconductor-metal (MIM) diodes currently attracts attention for application in future non-volatile memories.<sup>1</sup> A variety of semiconductor layers, ranging from small molecules to polymers, sometimes blended with inorganic semiconductor or metal nanoparticles have been investigated. Despite significant progress, many details of the switching mechanism and charge transport in the ON and OFF states have not clearly been identified. These organic memories show excellent programming cycle endurance<sup>2,3</sup> and data retention.<sup>4,5</sup> There is no consensus however on the write and erase times. Reported switching times vary by orders of magnitude.<sup>5-13</sup> The values range from nanoseconds to milliseconds. The discrepancies might be due to different semiconductors, device geometries, or measurement procedures. A prerequisite to study the switching dynamics is the availability of reproducible memories. We have recently shown that in fabrication, the yield of functioning memory diodes can be increased up to unity by insertion of a thin oxide layer.<sup>14</sup> Switching is a generic property of metal oxides in the presence of intrinsic defects,<sup>15</sup> the polymer acts as a current limiting series resistance.<sup>4,16</sup> The memory is formed by applying a high bias pulse to the pristine diode. After this forming process the memory can be switched reversibly between high and low resistance states. In this letter we show that the switching is very fast, less than 400 ns. From pulse sequence measurements we show that the scatter in the reported data is due to the occurrence of a 'dead time', that is the time after programming in which a next switch is inhibited.

## **8.2. Negative differential resistance**

Pristine MIM diodes (Figure 8.1) consisted of an Al bottom electrode, a sputtered layer of Al<sub>2</sub>O<sub>3</sub> (10 nm), a spirofluorene polymer (80 nm), and a Ba/Al (5 nm / 100 nm) top electrode that forms an Ohmic contact with the polymer. The devices with an active area of 9 mm<sup>2</sup> were encapsulated to exclude O<sub>2</sub> and H<sub>2</sub>O. In all cases, positive bias voltage refers to the bottom electrode being poled positive with respect to the top electrode. The memories were 'formed' by applying a 15 V pulse, which was terminated immediately after the current through the device reaches a compliance level of 10 mA. The *J-V* characteristics after forming are presented in Figure 8.1. They show a symmetric, voltage controlled negative differential resistance (NDR). Reliable switching is obtained at the top and bottom of the NDR.<sup>17,18</sup> Using a pulse at about 4-6 V the memory switches to the low resistance ON state and at the minimum of the NDR at about 8-10 V the memory switches to the high resistance OFF state.

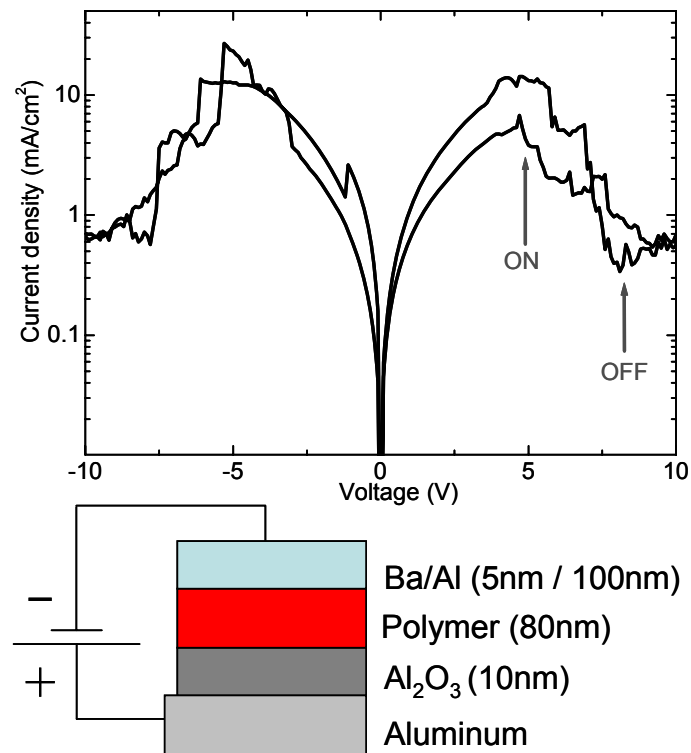


**Figure 8.1:** (top)  $J$ - $V$  characteristics of a device scanned from  $0\text{ V} \rightarrow +10\text{ V} \rightarrow -10\text{ V} \rightarrow 0\text{ V}$ . Arrows indicate the voltages levels applied to switch the device to the low resistance ON and high resistance OFF state in pulse experiments. (bottom) Lay-out of the memory diode.

Already in 1967 Simmons and Verderber studied the switching dynamics of  $\text{SiO}_x$  memories. The  $J$ - $V$  characteristics were measured using a saw tooth bias profile. At low repetition frequencies a clear NDR was observed. With increasing frequency the magnitude of the NDR gradually decreases, and vanishes at about 1 kHz. They concluded that a dead time was responsible for the disappearance of the NDR.<sup>18,19</sup> After programming, a waiting time of at least 1 ms is needed to switch the resistance again. The  $J$ - $V$  characteristics of similar saw tooth measurements on our memories are presented in Figure 8.2. In perfect agreement with Simmons and Verderber the NDR disappears at a repetition rate of about 1 kHz.

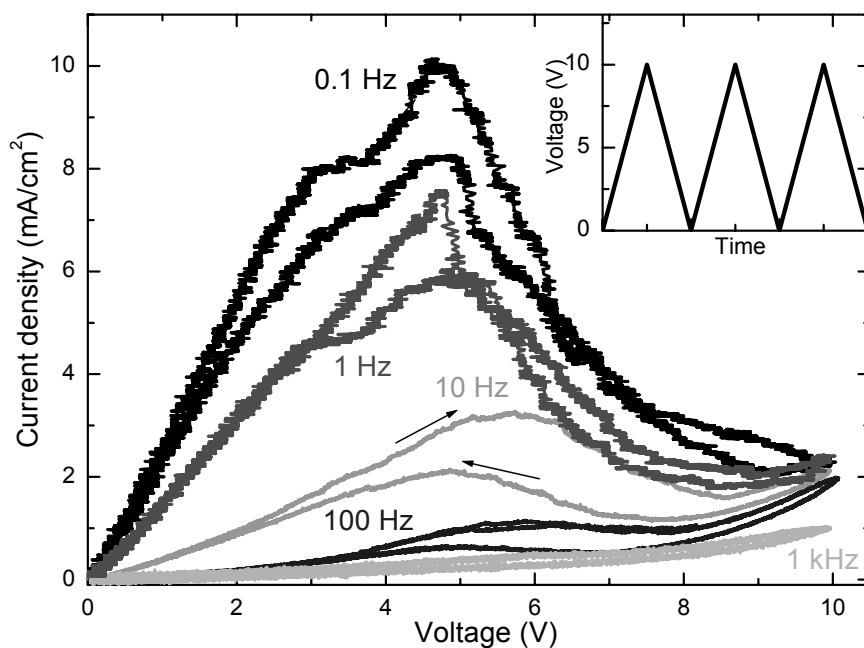


**Figure 8.2:** *J-V characteristics measured using a time modulated voltage with a saw tooth waveform (see inset) with modulation frequency from 0.1 Hz to 1 kHz, averaged over more than 5 cycles.*

### 8.3. Switching dynamics

Before investigating the dead time, we measured single switching events using a waiting time of 10 s. The current density was measured before and after switching using a low reading bias of 1 V. The current density as a function of pulse length for switching from the high resistance OFF state to the low resistance ON state is shown in Figure 8.3a, and from the ON to the OFF state in Figure 8.3b. Figure 8.3a shows that a minimum pulse length of 200 ns is needed to induce a change in resistance. Figure 8.3b shows that the switching time from the ON to the OFF state is 400 ns. These times are one order of magnitude longer than the fastest switching times reported for organic memories in the literature<sup>5</sup> and might be limited by the RC-time of the device due to the measurement set-up.

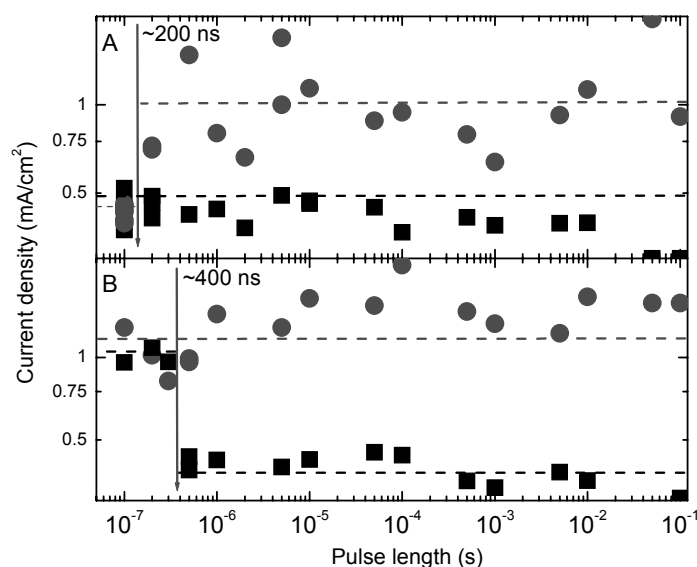


**Figure 8.3:** The current density measured using a low reading bias of 1 V before and after switching after a ON or OFF voltage pulse with varying length.: A) OFF (■) to ON (●) switching with a +4 V pulse; B) ON (●) to OFF (■) switching with a +8 V pulse. The initial states were prepared  $\sim 10$  s before the programming pulse.

Subsequently the switching dynamics was investigated using a fixed programming pulse length of 0.5 ms and varying the delay time between the programming cycles. The voltage sequence is shown in Figure 8.4. Using a high bias of 8 V the memory is switched OFF. After 1 ms the memory is switched back to the ON state. This pulse sequence is repeated after a variable delay time. The current density is measured after each pulse using a low reading voltage of 1 V. Figure 8.4 shows the current density in the first cycle (open symbols) and the second cycle (closed symbols) as a function of delay time between the cycles. Repeated OFF-ON switching is presented in Figure 8.4c. For times longer than 3 ms the current densities in the first and second cycle are identical; the closed symbols overlap the open symbols. For shorter delay times the memory can be switched in the first cycle (open symbols) but not anymore in the second programming cycle (closed symbols). This demonstrates the presence of a dead time of about 3 ms for OFF-ON switching. Similarly Figure 8.4d shows a dead time of about 1.5 ms for repeated ON-OFF switching. These times are orders of magnitude larger than the RC-time of the system ( $\sim 10^{-5}$  s) and therefore no relation between the RC-time and the dead time is expected. The difference between repeated OFF-ON and repeated ON-OFF switching is not yet understood. Note, that the dead times obtained from the pulse measurements agree very well with the dead time obtained using a saw tooth bias profile.



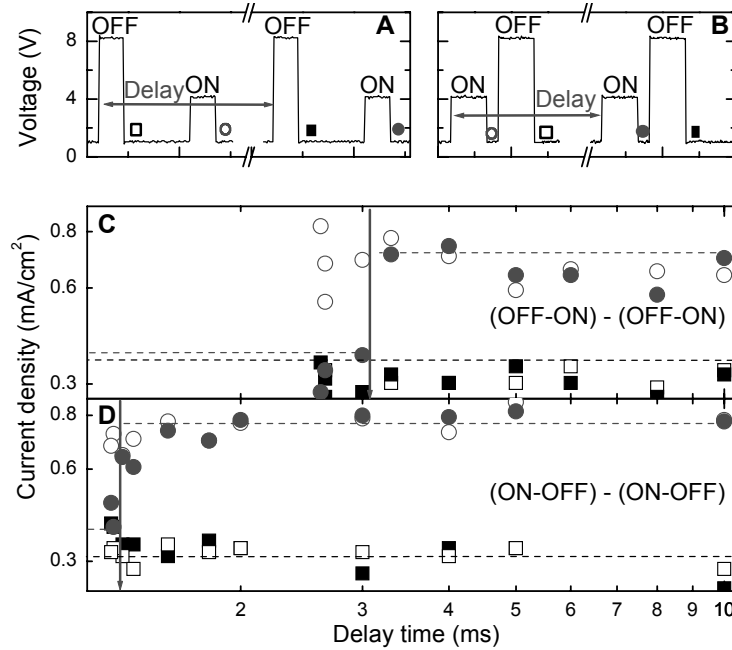


**Figure 8.4:** (a, b) Pulse sequence for (OFF-ON)-(OFF-ON) and (ON-OFF)-(ON-OFF) switching, and (c, d) Current density under application of +1 V bias voltage monitoring the conductivity state after :  $\square$  first +8 V off pulse ;  $\circ$  first +4 V ON pulse ;  $\blacksquare$  second +8 V OFF ;  $\bullet$  second +4 V, ON pulse.

In systems exhibiting voltage controlled NDR, domains with high and low resistivity form spontaneously, leading to an inhomogeneous distribution of charge density inside the material.<sup>20</sup> The domain boundaries relocate when changing the applied voltage<sup>21</sup> and the “dead time” can now be interpreted in terms of a time needed for domain boundary relocation and redistribution of charge density, in such a way that a next switching event can occur. The huge variation in reported switching times can be explained by the different measuring protocols. Measurements of single switching events yield microsecond switching times. The use of repeated switching cycles invariably leads to millisecond switching times dominated by the dead time.

We note that the occurrence of a dead time is a key ingredient to observe non-volatile switching. At high bias the memory is programmed in the high resistance OFF-state. When the bias voltage is ramped down on a time scale smaller than the dead time, the memory cannot switch back to the ON-state. The OFF-state is preserved. A dead time is a prerequisite for a non-volatile memory.

#### 8.4. Conclusion

Resistive switching in metal-semiconductor-metal diodes is investigated. A thin  $\text{Al}_2\text{O}_3$  layer was added to obtain reproducible memories. The huge variation in reported

switching times can be explained by the different measuring protocols. Single pulse measurements show that the switching is extremely fast, less than 400 ns. Repeated pulse sequence measurements show the occurrence of a "dead time", that is the time after programming in which a next switch is inhibited, of about 3 ms. The occurrence of a dead time is a key ingredient to observe non-volatile switching.

## 8.5. Experimental

Pristine MIM diodes consisted of an Al bottom electrode, a sputtered layer of Al<sub>2</sub>O<sub>3</sub> (10 nm), a spirofluorene polymer (80 nm), and a Ba/Al (5 nm / 100 nm) top electrode (Figure 1). The sputtering details are described in Chapter 7. The devices with an active area of 9 mm<sup>2</sup> were encapsulated to exclude O<sub>2</sub> and H<sub>2</sub>O. In all cases, positive bias voltage refers to the bottom electrode being poled positive with respect to the top electrode.

## 8.6. References

- 1 J. C. Scott and L. D. Bozano, *Adv. Mater.* **19**, 1452 (2007).
- 2 A. Prakash, J. Ouyang, J.-L. Lin, and Y. Yang, *J. Appl. Phys.* **100**, 054309 (2006).
- 3 R. Müller, R. Naulaerts, J. Billen, J. Genoe, and P. Heremans, *Appl. Phys. Lett.* **90**, 063503 (2007).
- 4 M. Cölle, M. Büchel, and D. M. de Leeuw, *Org. Electron.* **7**, 305 (2006).
- 5 L. P. Ma, J. Liu, and Y. Yang, *Appl. Phys. Lett.* **80**, 2997 (2002).
- 6 L. Ma, S. Pyo, J. Ouyang, Q. Xu, and Y. Yang, *Appl. Phys. Lett.* **82**, 1419 (2003).
- 7 L. Ma, Q. Xu, and Y. Yang, *Appl. Phys. Lett.* **84**, 4908 (2004).
- 8 S. Smith and S. R. Forrest, *Appl. Phys. Lett.* **84**, 5019 (2004).
- 9 D. Ma, M. Aguiar, J. A. Freire, and I. A. Hümmelgen, *Adv. Mater.* **12**, 1063 (2000).
- 10 H. K. Henisch and W. R. Smith, *Appl. Phys. Lett.* **24**, 589 (1974).
- 11 F. L. E. Jakobsson, X. Crispin, M. Cölle, M. Büchel, D. M. de Leeuw, and M. Berggren, *Org. Electron.* **8**, 559 (2007).
- 12 J. Chen and D. Ma, *Appl. Phys. Lett.* **87**, 23505 (2005).
- 13 H. X. He, X. L. Li, N. J. Tao, L.A. Nagahara, I. Amlani, and R. Tsui, *Phys. Rev. B* **68**, 45302 (2003).
- 14 F. Verbakel, S.C.J. Meskers, M. Cölle, M. Büchel, H. L. Gomes, R. A. J. Janssen, and D. M. de Leeuw, *Appl. Phys. Lett.* **91**, 192103 (2007).
- 15 A. Beck, J.G. Bednorz, C. Gerber, C. Rossel, and D. Widmer, *Appl. Phys. Lett.* **77**, 139 (2000).
- 16 H. L. Gomes, A. R. Benvenho, D. M. de Leeuw, M. Cölle, P. Stallinga, F. Verbakel, and D. M. Taylor, *Org. Electron.* **9**, 119 (2008).
- 17 L. D. Bozano, B. W. Kean, V. R. Deline, J. R. Salem, and J. C. Scott, *Appl. Phys. Lett.* **84**, 607 (2004).

- 18 J. G. Simmons and R. R. Verderber, *Proc. R. Soc. Lond. Ser. A* **301**, 77. (1967).
- 19 R.D. Gould and C.A. Hogarth, *Phys. Stat. Sol. (a)* **23**, 531 (1974).
- 20 B. K. Ridley, *Proc. Phys. Soc.* **82**, 954 (1963).
- 21 K. J. Lou, H. T. Grahn, and K. H. Ploog, *Phys. Rev. B* **57**, R6838 (1998).

# 9

## **Resistive switching in organic memories with a spin coated metal oxide nanoparticle layer**

*Resistive switching is demonstrated in diodes based on spin coated layers of nanoparticles of  $Al_2O_3$ ,  $CeO_2$ ,  $TiO_2$ ,  $ZrO_2$ ,  $Y_2O_3$  or  $ZnO$  and a semiconducting polymer, sandwiched between two electrodes. Inclusion of the metal oxide nanoparticles results in non-volatile electronic memory characteristics that are similar to those observed for the corresponding 'bulk' oxide. The major difference is that the nanoparticulate layers do not require a forming step.  $ZnO$  and  $TiO_2$  can be switched between a high and low resistance state using voltages pulses of opposite polarity, while  $Al_2O_3$ ,  $CeO_2$ ,  $ZrO_2$ ,  $Y_2O_3$  can be switched with both bipolar and unipolar voltage pulses.*

## 9.1. Introduction

Resistive switching in metal-organic semiconductor-metal diodes is being investigated for application as non-volatile memory elements in organic integrated circuits.<sup>1-4</sup> Upon applying a voltage bias pulse, the resistance of these diodes switches between a low resistive ON-state and a high resistive OFF-state. Typically aluminum is used as one of the electrodes. The switching is then due to the presence of native  $\text{Al}_2\text{O}_3$ .<sup>4,5</sup> Accordingly, it is recently reported that the yield for working memories can be improved to about unity by deliberately inserting a thin sputtered  $\text{Al}_2\text{O}_3$  layer<sup>6</sup> and the switching mechanism is investigated with impedance spectroscopy.<sup>7</sup> The reproducibility does not depend on the type of electrode or on the type of semiconductor. The memory elements, however, must first be "formed" by applying a high bias voltage. The forming mechanism is associated with a soft breakdown of the  $\text{Al}_2\text{O}_3$  layer.<sup>8</sup> The organic semiconductor only acts as a current limiting series resistance.

At present it is unclear, if the switching depends on the type of metal oxide or on the morphology of the layer. Application of metal oxide nanoparticles is of interest in this respect because their composition, stoichiometry, and surface area can easily be modified by synthetic methods. Here metal oxide nanoparticles are applied as switching layer in non-volatile memories and compare their switching to layers of the corresponding bulk oxides.

## 9.2. Spin coated $\text{Al}_2\text{O}_3$ nanoparticles

Figure 9.1a shows the  $J$ - $V$  characteristics of a diode containing a layer of spin coated  $\text{Al}_2\text{O}_3$  nanoparticles. When scanning the voltage in both forward and reverse bias, the  $J$ - $V$  trace shows a negative differential resistance (NDR) regime. At this voltage, the current decreases with increasing bias (e.g. 3 to 5 V). At bias voltages higher than the onset of the NDR, the  $J$ - $V$  traces typically exhibit large current fluctuations. The  $J$ - $V$  traces reveal rectification at  $\pm 6$  V and hysteresis in the current density between the onwards (from 0 V to maximum bias) and backwards (towards 0 V) scans in both forward as reverse bias regime. The NDR observed for these memories with spin coated  $\text{Al}_2\text{O}_3$  layers resembles the NDR for similar memories with sputtered  $\text{Al}_2\text{O}_3$  layers.<sup>6</sup> An important difference, however, is that the memories based on sputtered  $\text{Al}_2\text{O}_3$  only show NDR after a forming step. In this forming step a high voltage ( $\sim 15$  V for a layer of 20 nm  $\text{Al}_2\text{O}_3$ ) is applied to the devices,<sup>6</sup> resulting in a surge of the current. The forming voltage is terminated immediately when the current reaches a predetermined compliance level. The memories with spin coated  $\text{Al}_2\text{O}_3$  layers do not require this forming to observe NDR.

The origin of the NDR is not yet known, but might be explained by filamentary conduction.

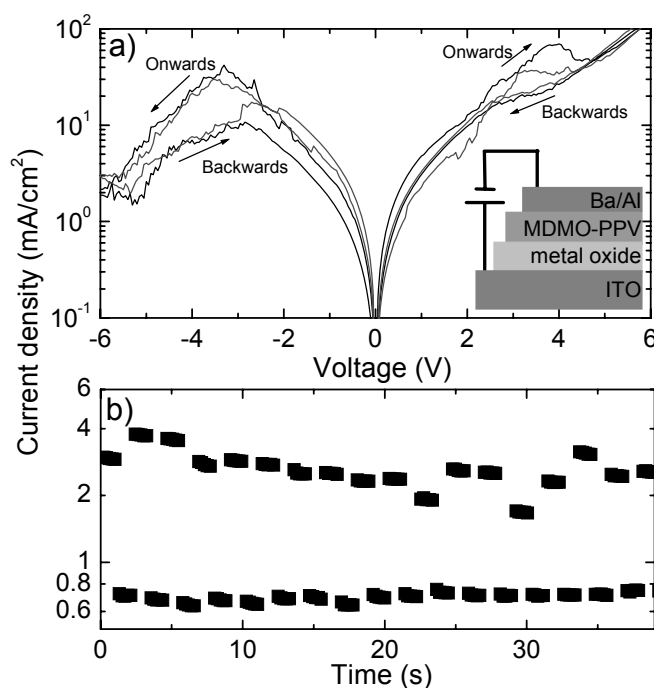


**Figure 9.1:** (a) Current-voltage ( $J$ - $V$ ) characteristics of the ITO/ $\text{Al}_2\text{O}_3$  nanoparticles/ MDMO-PPV/Ba/Al memories scanned  $0\text{ V} \rightarrow +6\text{ V} \rightarrow 0\text{ V} \rightarrow -6\text{ V} \rightarrow 0\text{ V}$ , showing two sequential scans. The inset shows the layout of the devices (see text for description of layers). (b) Current density of the device upon application of a cycle of voltage pulses: one  $-5\text{ V}$  erase pulse, five  $+1\text{ V}$  read pulses, one  $+3\text{ V}$  write pulse, and five  $+1\text{ V}$  read pulses. Duration of the  $+1\text{ V}$  pulses is  $100\text{ ms}$ . Duration of the  $+3$  and  $-5\text{ V}$  pulses is  $10\text{ ms}$ .

For devices with a sputtered  $\text{Al}_2\text{O}_3$  layer, the emergence of the NDR after forming coincides with the appearance of resistive switching upon application of *unipolar* voltage bias pulses.<sup>9</sup> The cycle endurance of memories with spin coated  $\text{Al}_2\text{O}_3$  layers is shown in Figure 9.1b. Voltage pulses of different magnitude are applied to the memory to induce resistive switching. The amplitude of voltage pulses required to switch the memory from its low resistive ON-state to the high resistive OFF-state ("erase") and vice versa ("write") can be determined from the  $J$ - $V$  characteristics.<sup>10,11</sup> For "writing", the bias corresponds to the local maximum current density ( $3\text{ V}$ ) where the NDR sets in. For erasing the bias corresponding to the local minimum in current density ( $5\text{ V}$ ) at the end of the NDR regime has to be applied. The obtained resistance states are read by application of a  $+1\text{ V}$  voltage pulse. The switching can be performed both with bipolar and unipolar voltage pulses, but switching is slightly more reproducible when bipolar pulses are used (write:  $+3\text{ V}$ , erase:  $-5\text{ V}$ , Figure 9.1b). In this case, the ratio between

the high and low resistive states is  $\sim 3$  and reliable switching is obtained with voltage pulse widths of 10 ms.

### 9.3. Various metal oxides nanoparticles

The  $J$ - $V$  characteristics of diodes with various metal oxide nanoparticle ( $\text{Al}_2\text{O}_3$ ,  $\text{CeO}_2$ ,  $\text{TiO}_2$ ,  $\text{ZrO}_2$ ,  $\text{Y}_2\text{O}_3$ , and  $\text{ZnO}$ ) layers are shown in Figure 9.2. In Table 9.1 the  $J$ - $V$  characteristics of these metal oxides are summarized and distinguished between NDR in the onward scan (from 0 V to maximum bias) and in the backward scan (towards 0 V). Most metal oxides show NDR in both scan directions and for positive as well as negative bias, exceptions are  $\text{ZnO}^{12,13}$  (NDR only in onward scan under negative bias), and  $\text{TiO}_2$  (no NDR at all). For all metal oxides a hysteresis in the current between onward and backward scans is observed, which is most pronounced for  $\text{Al}_2\text{O}_3$ ,  $\text{Y}_2\text{O}_3$ ,  $\text{TiO}_2$  and  $\text{ZnO}$ . No hysteresis or NDR is observed for the reference device with ITO/PEDOT:PSS/MDMO-PPV/Ba/Al (not shown). Therefore it is unlikely that the NDR observed for the memories with the oxide layers is due to the native oxide formed at the top electrode.<sup>5</sup>

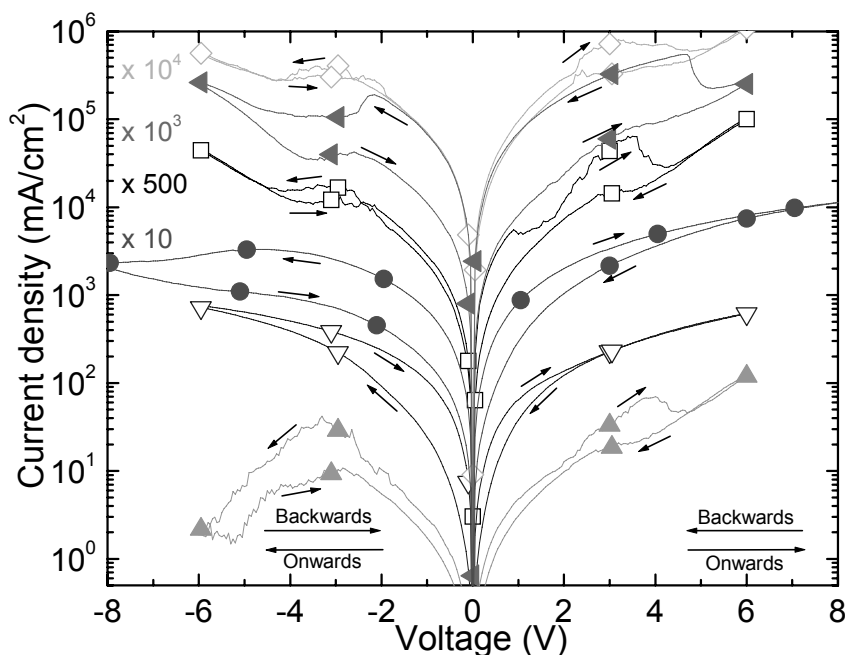


**Figure 9.2:** Current-voltage ( $J$ - $V$ ) characteristics of diodes with  $\text{Al}_2\text{O}_3$  ( $\blacktriangle$ ),  $\text{TiO}_2$  ( $\nabla$ ),  $\text{ZnO}$  ( $\bullet$ ),  $\text{CeO}_2$  ( $\square$ ),  $\text{Y}_2\text{O}_3$  ( $\blacktriangleleft$ ), and  $\text{ZrO}_2$  ( $\blacklozenge$ ) nanoparticles scanned  $0\text{ V} \rightarrow +6\text{ V} \rightarrow 0\text{ V} \rightarrow -6\text{ V} \rightarrow 0\text{ V}$ , in case of  $\text{ZnO}$  nanoparticles scanned  $0\text{ V} \rightarrow +8\text{ V} \rightarrow 0\text{ V} \rightarrow -8\text{ V} \rightarrow 0\text{ V}$ .

The cycle endurance of the nanoparticle metal oxides memories is shown in Figure 9.3. The current density at the “read” voltage pulse after either a “write” or an “erase” pulse is shown. Unipolar switching is observed for  $\text{Al}_2\text{O}_3$ ,  $\text{CeO}_2$ ,  $\text{ZrO}_2$ , and  $\text{Y}_2\text{O}_3$ . All measured metal oxides can be switched by bipolar voltage pulses. For  $\text{ZnO}$  and  $\text{TiO}_2$

bipolar voltage pulses of the same amplitude need to be applied. The voltage pulses for the other oxides should correspond with the local maximum and local minimum in current density at the NDR, as described above.

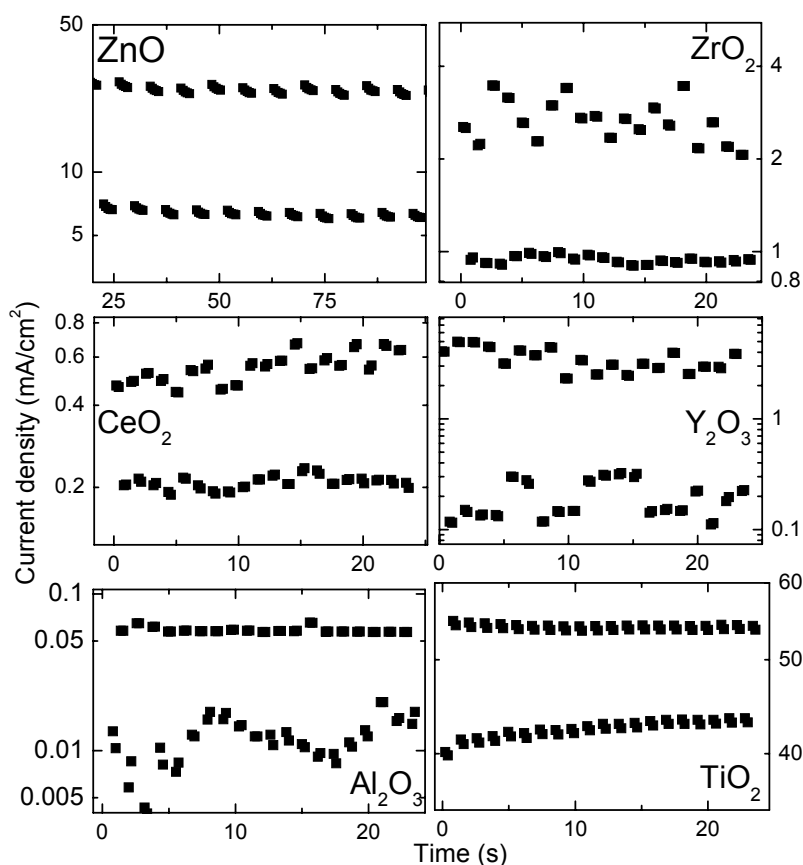


**Figure 9.3:** Current density of the memories with the different metal oxide nanoparticle layers upon application of a cycle of voltage pulses: an erase (E) pulse, two read (R) pulses (5 for ZnO), a write (W) pulse, and again two read pulses (5 for ZnO). Duration of the all pulses is 100 ms. Voltage pulses (in V) used: TiO<sub>2</sub>: E = +5, W = -5, R = -1; Al<sub>2</sub>O<sub>3</sub>: E = -6, W = -3, R = -1; CeO<sub>2</sub>: E = +6, W = +5, R = +1; Y<sub>2</sub>O<sub>3</sub>: E = +6, W = +3, R = +1, ZrO<sub>2</sub>: E = +6, W = +3.5, R = +1; ZnO: E = -10, W = +10, R = -0.5.

The memory properties of the nanoparticles diodes can be compared to literature data for their corresponding diodes containing the bulk metal oxides<sup>14</sup> (e.g. TiO<sub>2</sub>,<sup>15-17</sup> ZnO,<sup>18</sup> ZrO<sub>2</sub>,<sup>19</sup> CeO<sub>2</sub>,<sup>20</sup> and Y<sub>2</sub>O<sub>3</sub>,<sup>21</sup> see Table 9.1). For the metal oxides nanoparticle layers that give rise to a NDR region, NDR has also been reported for the bulk oxide layers. For some metal oxides hysteresis is observed in both bulk and nanoparticulate layers (TiO<sub>2</sub> and ZnO), while for other metal oxides a pronounced hysteresis is only seen in the bulk (ZrO<sub>2</sub> and CeO<sub>2</sub>). For diodes with Al<sub>2</sub>O<sub>3</sub> nanoparticles, some hysteresis is seen, while for bulk Al<sub>2</sub>O<sub>3</sub> virtually no hysteresis is observed provided that slow scan speeds are used. Here there may be a possible relation with the 'dead time' that has been demonstrated



for memories consisting bulk  $\text{Al}_2\text{O}_3$  layers.<sup>9</sup> This 'dead time' is the time after programming in which a next switch is inhibited. Naturally, hysteresis will be observed if the backward scan differs from the onwads scan. In the backward scan the ON-state has to be programmed for a second time. However when executed within the "dead time" after the onward scan, this programming of the ON-state will be inhibited. In this case, the resistive state in this onwads scan at which the ON-state was first prepared, will differ for the resistance observed in the backward scan and therefore result in a hysteresis in current density.

**Table 9.1:** A summary of  $J$ - $V$  characteristics and switching properties of the different metal oxide nanoparticle (including the particle size) and the bulk metal oxide (literature) memories. The properties of the metal oxides regarding to NDR (Yes/No/Some), hysteresis in  $J$ - $V$  characteristics (Yes/No) and the switching type (Unipolar and/or Bipolar) are specified. \* Not specified.

Metal oxide	Nanoparticles				Bulk (Literature)			
	Particle size	NDR in reverse bias		Hyst.	Switch type	NDR	Hyst.	Switch type
		Onward	Backward					
$\text{Al}_2\text{O}_3$	< 50 nm	Y	Y	Y	U+B	Y	N	Unipolar <sup>6</sup>
$\text{CeO}_2$	< 25 nm	Y	Y	N	U+B	Y	Y	Bipolar <sup>20</sup>
$\text{ZrO}_2$	< 50 nm	Y	Y	N	U+B	Y	Y	* <sup>19</sup>
$\text{Y}_2\text{O}_3$	< 50 nm	Y	S	Y	U+B	Y	*	* <sup>21</sup>
$\text{TiO}_2$	< 50 nm	N	N	Y	B	N	Y	Bipolar <sup>15</sup> Unipolar <sup>22</sup>
$\text{ZnO}$ <sup>12,13</sup>	~ 5 nm	Y	N	Y	B	*	Y	Bipolar <sup>18</sup>

The presence of NDR in the backward  $J$ - $V$  scan (*i.e* from high bias amplitude to zero) coincides with the possibility of unipolar switching for all metal oxide nanoparticles devices. This correlation is expected because NDR in the backward scan points out that the device can be switched to a state with lower resistance with just one bias voltage polarity. Furthermore, experimentally, unipolar switching implies bipolar switching, but not vice versa.

The combined characteristics of bipolar switching and backward sweep NDR may then be used to classify metal oxide nanoparticles into two categories: those that show only bipolar switching ( $\text{ZnO}$  and  $\text{TiO}_2$ ) and those that show both unipolar as well as bipolar behavior ( $\text{Al}_2\text{O}_3$ ,  $\text{CeO}_2$ ,  $\text{ZrO}_2$ , and  $\text{Y}_2\text{O}_3$ ).

#### 9.4. Conclusion

In conclusion, non-volatile resistive switching in diodes of metal oxide nanoparticles of  $\text{Al}_2\text{O}_3$ ,  $\text{CeO}_2$ ,  $\text{TiO}_2$ ,  $\text{ZrO}_2$ ,  $\text{Y}_2\text{O}_3$  or  $\text{ZnO}$  and a semiconducting polymer, processed from solution has been demonstrated. The observed NDR and required voltage to switch the memories are similar to those for memories based on bulk metal oxide layers. A major

difference, however, is that memories based on nanoparticle metal oxide layers do not require a forming step. The type of voltage pulses, unipolar or bipolar, needed for the switching depends on the metal oxide. These variations indicate that the memory effects are related to the electronic structure of the metal oxide.

## 9.5. Experimental

The device structure (inset of Figure 9.1) consists of a  $\sim 100$  nm layer of metal oxide nanoparticles spin coated on an indium tin oxide (ITO) electrode from an aqueous dispersion (1% by weight, Aldrich). Nanoparticles of the following metal oxides have been explored:  $\text{Al}_2\text{O}_3$ ,  $\text{CeO}_2$ ,  $\text{TiO}_2$ ,  $\text{ZrO}_2$ , and  $\text{Y}_2\text{O}_3$ . On top of these nanoparticles, poly[2-(3',8'-dimethyloctyloxy)-5-methoxy-*p*-phenylenevinylene] (MDMO-PPV) is spin coated from chlorobenzene. Finally the top electrode (Ba (5 nm) /Al (100 nm)) is evaporated at a base pressure of  $10^{-7}$  mbar.

ZnO nanoparticles are not commercially available and, therefore, have been prepared separately. The ZnO nanoparticles have been synthesized by hydrolysis and condensation of zinc acetate dehydrate by potassium hydroxide in methanol, using the method described by Pacholski *et al.*<sup>23</sup> These particles are not soluble in water and therefore a different device layout had to be used. The ZnO nanoparticles are mixed with polystyrene (1:2 by wt) in chloroform and spin coated on an ITO/PEDOT:PSS electrode. On top of this ZnO layer an aluminum electrode was evaporated. Devices with an active area of  $9.5 \text{ mm}^2$  were measured in inert atmosphere to exclude  $\text{O}_2$  and  $\text{H}_2\text{O}$ . Current density – voltage (*J-V*) characteristics were measured with a Keithley 2400. The cycle endurance were performed with a homemade Labview program using a computer controlled Keithley 2600. A positive bias voltage refers to the ITO being poled positive with respect the Ba/Al electrode.

## 9.6. References

- 1 J.C. Scott and L.D. Bozano, *Adv. Mater.* **19**, 1452 (2007).
- 2 Y. Yang, J. Ouyang, L. Ma, R.J.-H. Tseng, and C.-W. Chu, *Adv. Func. Mater.* **16**, 1001 (2006).
- 3 L.D. Bozano, B.W. Kean, M. Beinhoff, K.R. Carter, P.M. Rice, and J.C. Scott, *Adv. Func. Mater.* **15**, 1933 (2005).
- 4 W. Tang, H.Z. Shi, G. Xu, B.S. Ong, Z.D. Popovic, J.C. Deng, J. Zhao, and G.H. Rao, *Adv. Mater.* **17**, 2307 (2005).
- 5 M. Cölle, M. Büchel, and D.M. de Leeuw, *Org. Electron.* **7**, 305 (2006).
- 6 F. Verbakel, S.C.J. Meskers, M. Cölle, M. Büchel, H.L. Gomes, R.A.J. Janssen, and D.M. de Leeuw, *Appl. Phys. Lett.* **91**, 192103 (2007).
- 7 H.L. Gomes, A.R. Benvenho, D.M. de Leeuw, M. Cölle, P. Stallinga, F. Verbakel and D.M. Taylor, *Org. Electron.* **9**, 119 (2008).
- 8 T. W. Hickmott, *J. Appl. Phys.* **88**, 2805 (2000).

- 9 F. Verbakel, S.C.J. Meskers, A.J.M. van den Biggelaar, H. L. Gomes, R.A.J. Janssen, and D.M. de Leeuw, Submitted.
- 10 J.G. Simmons and R.R. Verderber, *Proc. R Soc. Lond. Ser. A* **301**, 77. (1967).
- 11 L.D. Bozano, B.W. Kean, V.R. Deline, J.R. Salem, and J.C. Scott, *Appl. Phys. Lett.* **84**, 607 (2004).
- 12 F. Verbakel, S.C.J. Meskers, and R.A.J. Janssen, *J. Appl. Phys.* **102**, 083701 (2007).
- 13 F. Verbakel, S.C.J. Meskers, and R.A.J. Janssen, *Appl. Phys Lett.* **89**, 102103 (2006).
- 14 T.W. Hickmott, *J. Appl. Phys.* **88**, 2805 (2000).
- 15 F. Argall, *Solid-State Electron.* **11**, 535 (1968).
- 16 K. Tsunoda, Y. Fukuzumi, J.R. Jameson, Z. Wang, P.B. Griffin, and Y. Nishi, *Appl. Phys. Lett.* **90**, 113501 (2007).
- 17 B.J. Choi, S. Choi, K.M. Kim, Y.C. Shin, C.S. Hwanga, S.-Y. Hwang, S. Cho, S. Park, and S.-K. Hong, *Appl. Phys. Lett.* **89**, 012906 (2006).
- 18 T. Hada, K. Wasa, and S. Hayakawa, *Jpn. J. Appl. Phys.* **10**, 521 (1971).
- 19 K.C. Park and S. Basavaiah, *J. Non-Cryst. Solids* **2**, 284 (1970).
- 20 R. Fors, S.I. Khartsev, and A.M. Grishin, *Phys. Rev. B* **71**, 045305 (2005).
- 21 A.L. Pergament, V.P. Malinenko, O.I. Tulubaeva, and L.A. Aleshina, *Phys. Stat. Solidi A* **201**, 1543 (2004).
- 22 C. Yoshida, K. Tsunoda, H. Noshiro, and Y. Sugiyama, *Appl. Phys. Lett.* **91**, 223510 (2007).
- 23 C. Pacholski, A. Kornowski, and H. Weller, *Angew. Chem. Int. Ed.* **41**, 1188 (2002).

# 10

## **Mechanism for resistive switching and negative differential resistance in organic non-volatile memories**

*Negative differential resistance (NDR) in polymer-Al<sub>2</sub>O<sub>3</sub> diodes is investigated using time domain current voltage measurement, impedance spectroscopy and thermal imaging. After a forming step, the diodes show a time dependent NDR. In the bias voltage range where NDR is observed, the capacitance at low frequency is significantly larger than for the unformed diode. Conduction in the formed diodes is filamentary in nature. Upon forming oxygen vacancies are created. We assume that the vacancy is metastable. Hence the degree of ionization depends on the electric field. This single assumption is enough to perfectly explain in first approximation all experimental data.*

### **10.1. Introduction**

Metal-insulator-metal (MIM) diodes containing a layer of conjugated polymer (polyspirofluorene) combined with a layer of aluminum oxide show remarkable electrical properties after the diodes have undergone a forming step.<sup>1</sup>

In this forming step, a high voltage is applied to the diode, resulting in a soft electrical breakdown. After this forming process, the diodes show negative differential resistance (NDR) as well as resistive switching. For the formed diodes, a jump between the high and low resistive states can be induced by a voltage pulses as short as  $\sim 400$  ns, as shown in Chapter 8. These diodes have characteristics in common with MIM diodes containing only a single layer of aluminum oxide.<sup>2</sup> Furthermore the resistance switching is not only observed for  $\text{Al}_2\text{O}_3$ , but also occurs in many other oxides<sup>3</sup> (e.g.  $\text{SiO}_2$ ,<sup>4</sup>  $\text{TiO}_2$ ,<sup>5-7</sup>  $\text{ZnO}$ ,<sup>8</sup>  $\text{ZrO}_2$ ,<sup>9</sup>  $\text{CeO}_2$ ,<sup>10</sup> and  $\text{Y}_2\text{O}_3$ <sup>11</sup>). Therefore an explanation of the memory effects and the differential resistance in terms of properties of the oxide layer is indicated.<sup>12</sup>

The influence of the polymer layer on the memory effect and switching processes is not yet fully understood. Incorporation of a polymer in combination with the oxide gives the opportunity to control the forming voltage.<sup>13</sup> Forming and switching effects are remarkably reproducible (Chapter 7), but at this moment it is not clear whether the polymer contributes to this reproducibility. Studies on this issue for memories without polymer layer have hardly been reported.<sup>14,15</sup> The polymer layer acts as a current limiter. The layer is only needed to prevent the occurrence of a 'hard', irreversible and destructive breakdown.<sup>16</sup>

In this chapter, the NDR and switching will be characterized in detail. Switching is investigated in the time and frequency domain. A convincing mechanism to explain the switching dynamics has not yet been reported. In this chapter a mechanism is introduced based on metastable oxygen vacancies, *i.e.* defects of which the degree of ionization depends on the electric field. This single assumption is enough to perfectly explain in first approximation all experimental data.

### **10.2. Voltage-current and current-voltage characteristics**

A schematic layout of the diodes investigated is given Figure 10.1. They consist of a layer of  $\text{Al}_2\text{O}_3$  (thickness 10 nm) sputtered on top of glass substrate covered with an Al electrode. A layer of polyspirofluorene is spin coated on the oxide (thickness 80 nm) and covered with a metal electrode (Ba / Al).

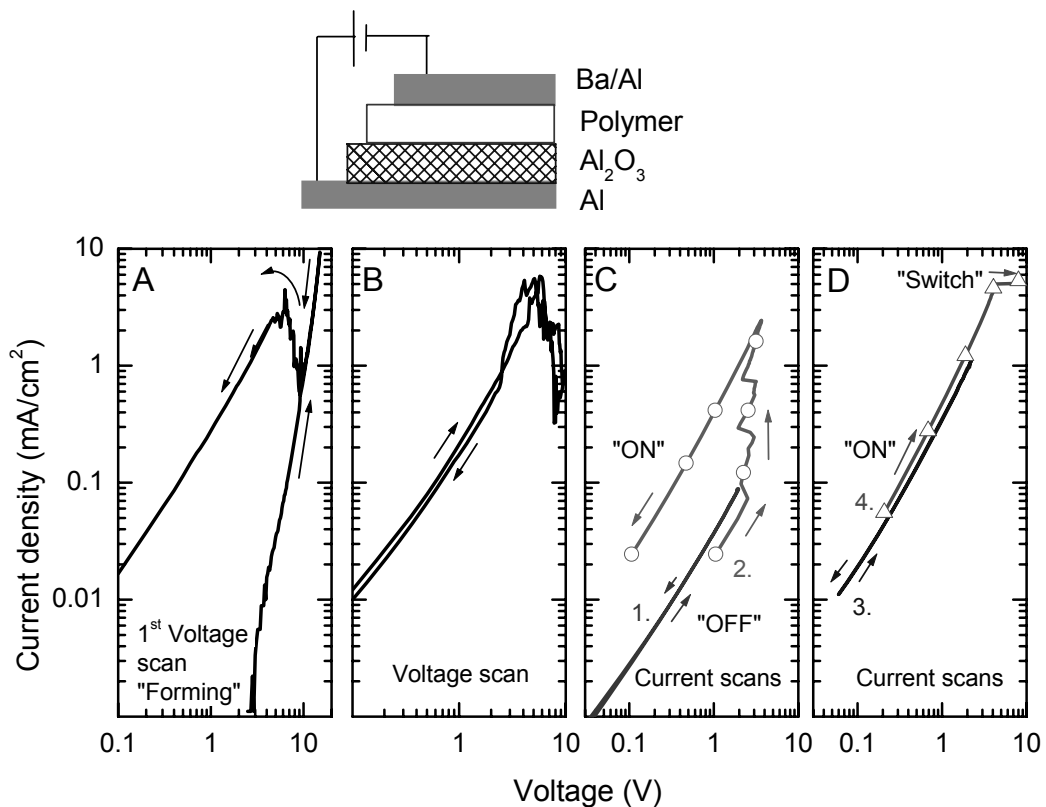


**Figure 10.1:** (top) A schematic layout of the diodes (bottom) J-V characteristics of (a) the forming, (b) a voltage scan showing NDR and (c) V-J characteristics where the current is scanned and the voltage recorded. The diode is prepared by applying a +8 V pulse after which scan 1 and 2 are performed (d) V-J scans subsequent to 2.

Initially, the current densities that go through the MIM diode are very low, but when applying higher voltages ( $\sim 15$  V), the forming process sets in (Figure 10.1a). After this step, the resistance at a bias of  $< \sim 9$  V has dropped drastically. The J-V characteristic of the formed diode shows a local maximum in the current density at 4 V (Figure 10.1b). At voltages exceeding +4 V, the current decreases with increasing bias voltage. This negative differential resistance (NDR) regime extends to bias voltages of about +9 V. For higher voltages the currents increase again with increasing bias voltage.

Figure 10.1c shows the characteristics of the formed diode when the current is scanned and where the voltage needed to sustain this current is recorded as the observable. Before the scan, the already formed diode was prepared by applying a +8 V voltage pulse. When the current scanned up to  $0.1 \text{ mA/cm}^2$ , reversible, Ohmic like behavior is obtained (scan 1). When the current is scanned up to  $2 \text{ mA/cm}^2$  (scan 2) the voltage required approaches 3 V, and the diode is brought from a high resistance (OFF) state to a state with lower resistance (ON). Once the diode is in the ON state, voltage current characteristics are again reversible and almost Ohmic, provided that the voltage stays below 3 V (Figure 10.1 d, scan 3). When attempting to scan to higher current

densities, the diode makes another switch at very high bias to a state with much higher resistance (Figure 10.1d, scan 4). Experimentally, this transition is difficult to characterize completely because the diodes undergo irreversible changes at very high voltage ( $>10$  V).

These results illustrate the voltage controlled NDR and bistable switching in formed diodes. For this diode with a 10 nm thick oxide layer, +4 V is a characteristic voltage corresponding to the local maximum in the current density. Furthermore switching to the ON state occurs at voltages slightly below this characteristic + 4 V, while voltages exceeding + 4V can result in the OFF state. A second characteristic voltage is +8V, where the current density reaches a local minimum.

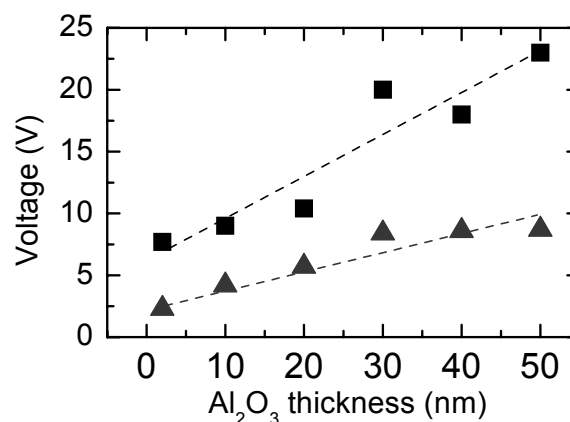


**Figure 10.2:** Characteristic NDR voltages from the  $J$ - $V$  characteristics of formed polymer-aluminum oxide diodes corresponding to the local maximum in current density (▲) and the local minimum (■) for diodes with different thickness of the oxide layer. Thickness of the polymer layer: 80 nm.

The location of the observed NDR is plotted for different thickness of the oxide layer (Figure 10.2). At increasing thickness both the onset of the NDR, with a local maximum in current density (▲) as the local minimum in current density (■) is shifted to higher bias. The position of the local minimum in current density has a stronger dependence on the oxide thickness than the position of the onset of the observed NDR. The thickness of the polymer layer is constant. Figure 10.2 indicates that the origin of the NDR is the oxide layer.

By recording  $J$ - $V$  characteristic at different temperatures (Figure 10.3), it becomes clear that the processes leading to the formation of the low resistance ON state are not only field dependent but also temperature dependent, indicating a thermally activated process. At  $T = 300$  K the  $J$ - $V$  plot shows a clear NDR regime at voltages between +4 V and +8 V where the current density  $J$  is reduced by a factor of five at the second characteristic voltage near +8 V in comparison with  $J$  at +4 V. At 250 K the difference is less than a factor of two, while at 200 K the NDR has almost disappeared.

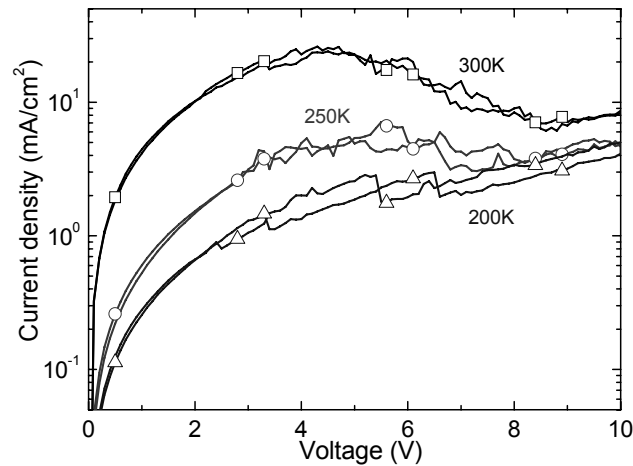


**Figure 10.3:** Temperature dependence of the  $J$ - $V$  characteristics at 300 K ( $\square$ ), 250 K ( $\circ$ ) and 200 K ( $\triangle$ ).

### 10.3. Time domain measurements

The results illustrated in the section above, point toward a special nature of the ON state and indicate that this state can only be reached under certain conditions with regards to the strength of the electric field and the temperature. This section analyzes dynamic aspects of the NDR and explores the formation of the ON state using time domain current-voltage measurements.

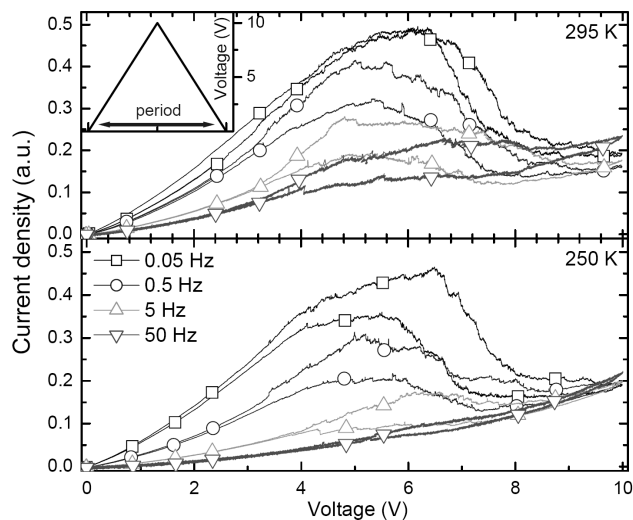


**Figure 10.4:** Frequency dependent current-voltage characteristics at 295 K (top) and 250 K (bottom) recorded by applying a time modulated voltage with a saw tooth waveform (see inset) with a period of 0.05 Hz ( $-\square-$ ), 0.5 Hz ( $-\circ-$ ), 5 Hz ( $-\triangle-$ ), and 50 Hz ( $-\nabla-$ ). The results are averaged over 10 measurements.

The  $J$ - $V$  characteristics were measured using a time modulated saw tooth bias profile (Figure 10.4). Here the period of the repeating waveform is varied from 20 s / period (0.05 Hz) down to 20 ms / period (50 Hz) and the current is monitored using an



oscilloscope and a probe resistor. At low repetition frequencies and 295 K a clear NDR was observed, which is in agreement with results in Figure 10.1b. With increasing frequency the magnitude of the NDR gradually decreases and hysteresis becomes apparent. At high scan rates the NDR is strongly suppressed. This shows that the NDR in these diodes is also characterized by a specific time-dependence. At a lower temperature (250 K) similar effects are observed. Here the hysteresis is already apparent at 0.05 Hz, and the NDR suppressed even more strongly in comparison to room temperature data.

Apart from the scan rate, the amplitude of the voltage scan may also be varied. In Figure 10.5, an  $J$ - $V$  measurement is illustrated where the voltage is scanned slowly over the 0-10 V bias voltage range, showing the NDR. Here also saw tooth waveform is used for the modulation of the applied voltage in time. In addition,  $J$ - $V$  measurements recorded at high scan rate and sweeping the bias voltage over the ranges from 0 to 2, 4, 6, 8, and 10 V are shown. At high scan rate, the current does not trace the same curve as at low frequency: the NDR behavior disappears. The current densities reached at the maximum amplitude of the voltage sweep, however, still follow the  $J$ - $V$  trace recorded at slow scan rate.

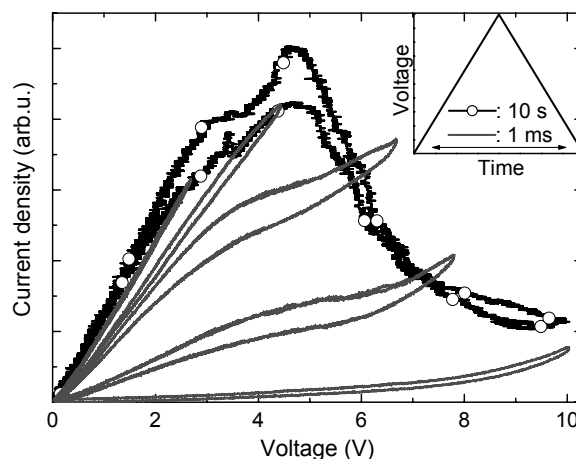


**Figure 10.5:**  $I$ - $V$  characteristics measured using a time modulated voltage with a saw tooth waveform (see inset) scanning over the bias voltage ranges from 0 to 2, 4, 6, 8, and 10 V with a repetition rate of 1 kHz (—, 1 ms). The scan over the 0-10 V range is also performed at a repetition rate of 0.1 Hz (-○-, 10s) Results are averaged over >5 cycles.

The experiments illustrated in Figure 10.5 indicate that when scanning with high speed *through* the bias voltage range around +4 V, the low resistance state cannot be induced in the short time available during the passage of the bias voltage through the region near 4 V. To investigate the time dependence in the formation of the low resistance state in more detail, we have monitored the rise of the conduction level during the application of a bias voltage pulse of around +4 V in order to monitor the built up of the ON state directly.

In Figure 10.6 an experiment is illustrated in which a train of voltage pulse is applied to the diode. First a 'write' voltage pulse of  $\sim 4$  V ( $V_{write}(1)$ ) is applied for 20 ms then, +1 V is applied for 20 ms followed by an "erase" voltage pulse ( $V_{erase}$ ) of  $\sim 8$  V, 20 ms. After another 20 ms interval applying +1 V, the +4 V is applied a second time ( $V_{write}(2)$ ) together with a +8 V erase pulse. During the experiment the current density is monitored continuously, and the current density during the first and second write pulses are labeled  $J_{write}(1)$  and  $J_{write}(2)$ .

When plotting the current density as a function of time after the start of the write pulse on a semi-logarithmic time scale, it becomes apparent that the current density increases steadily with time during the application of the bias following a  $J(t) \propto \ln(t)$ . Interestingly, also during the second write pulse, the proportionality  $J(t) \propto \ln(t)$  seems to hold but at early times during the second the rise of the current density occurs at a slower rate. This seems to be related to the 'dead time' discussed in Chapter 7.

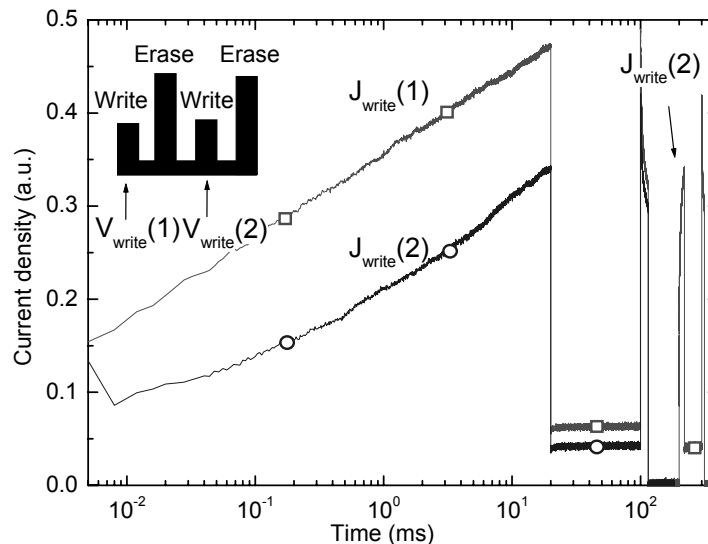


**Figure 10.6:** Current density through the formed polymer- $\text{Al}_2\text{O}_3$  diode under application of the voltage pulse pattern illustrated in the insert. The trace ( $-\square-$ ) shows the current density plotted on a logarithmic time axis with  $t=0$  defined as start of the first +4V pulse. The second trace ( $-\circ-$ ) shows the same current density but now the start of the second write pulse is set as  $t=0$  in time. The results are averaged over 10 measurements with an interval between the measurements of 10 s.

The existence of a "dead time", a time in which an attempt to induce switching is inhibited, is required for a unipolar switching memory.<sup>4,17</sup> Without this time the high resistance state can never be obtained, due to the simple reason that when removing the high applied voltage, the "write" voltage will always be applied for a small amount of time. When this time is larger than the dead time the ON-state will be re-obtained.

### 10.4. Frequency domain methods

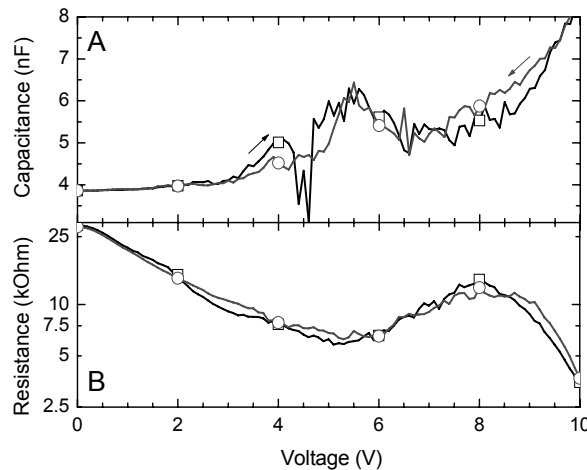
This section describes the use of impedance spectroscopy to characterize the resistance and capacitance of *formed* memories. The relation between the time-based measurements presented in the section above and the frequency domain measurements shown here will be discussed at the end of this section.

Figure 10.7 shows the capacitance and resistance of a formed polymer  $\text{Al}_2\text{O}_3$  diode as a function of the bias voltage, as measured using a modulation of 0.5 V at 400 Hz at 295 K. At low bias voltage, the measured capacitance is close to the geometrical capacitance. This can be calculated according to

$$C_{geo} = \epsilon_0 \cdot \frac{(\epsilon_{\text{Al}_2\text{O}_3} \cdot d_{\text{Al}_2\text{O}_3} + \epsilon_{\text{pol}} \cdot d_{\text{pol}})}{(d_{\text{Al}_2\text{O}_3} + d_{\text{pol}})^2} \cdot A \quad (10.1)$$

Using  $\epsilon_{\text{Al}_2\text{O}_3} = 10$ ,  $d_{\text{Al}_2\text{O}_3} = 10$  nm,  $\epsilon_{\text{pol}} = 3$ ,  $d_{\text{pol}} = 80$  nm and  $A = 0.09$  cm<sup>2</sup>, it follows that  $C_{geo} = 3.3$  nF.

Around a bias voltage of +3 V there is an increase in the capacitance. A NDR between 5 V and 8 V is observed in the resistance plot (Figure 10.7b). At the onset of the NDR there is an increase in capacitance which reaches a local maximum at +5.5 bias voltage. This onset of the excess capacitance coincides with the voltage at which switching from the OFF to the ON state is possible (see Figure 10.1). The capacitance measurement show excessive noise from bias voltages exceeding +3 V and in this respect they resemble the static current-voltage measurements. The capacitance does not show any major hysteresis.



**Figure 10.7:** Impedance spectroscopy (a) capacitance, (b) resistance measured at 400 Hz ( $T = 295$  K). The results are averaged over 10 measurements and an AC amplitude of 0.5 V is used. Showing the onward scan ( $-\square-$ ), and the backward scan ( $-\circ-$ ). Thickness of the polymer layer is 80 nm and of the oxide layer 10 nm.

The impedance measurements also yield a differential resistance for the formed diode, which is plotted as a function of the bias voltage in Figure 10.7b. Curiously, the differential resistance does not become negative in the bias voltage range from 4 to 8 V where the quasi-static  $J$ - $V$  characterization shows the NDR. The results from the impedance measurements are however in agreement with the  $J$ - $V$  characterization at high scan speeds where also no NDR is observed (Figures 10.4 and 10.5) and consistent with the notion that the NDR is a time dependent phenomenon. The differential resistance at 400 Hz shows a local minimum at 5.5 V that most likely corresponds to the NDR observed in the quasi-static measurements

The excess capacitance observed for bias voltages exceeding +3 V proves to be frequency dependent. At higher modulation frequencies the excess capacitance diminishes and at 2.5 kHz only the 'geometrical' capacitance ( $C_{geo}$ ) is observed showing no particular bias voltage dependence and no excessive noise.

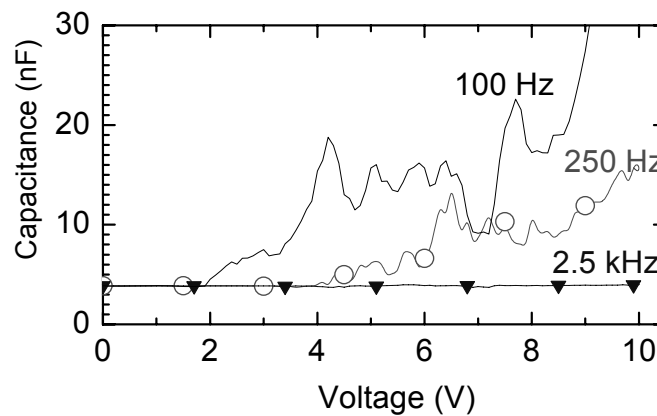


**Figure 10.8:** Capacitance (a) and resistance (b) versus voltage at AC- frequencies of 100 Hz (---), 250 Hz (-○-) and 2.5 kHz (-▼-), an AC bias of 0.5 V is used. Scanned from 0 V to 10 V at 295 K.

The frequency dependence has been studied in more detail for a bias voltage of +5 V (Figure 10.9). In these measurements the amplitudes of the AC modulation has been varied systematically and the capacitance does not significantly depend of the magnitude of this amplitude. At high frequency the geometrical capacitance is obtained and when scanning towards lower frequencies the capacitance rises steeply for frequencies below  $\sim 1$  kHz. This characteristic frequency (1 kHz) was also found in the time domain measurements of the current-voltage characteristics as the frequency below which NDR can be observed.

The fast rise in capacitance upon decreasing the frequency can be due to a high level of injection of carriers. When the mobility of these charge carriers is low, they will accumulate in the device and contribute to a rise in capacitance. This contribution to the

device capacitance increases with the applied bias in a similar way to the diffusion capacitance increase in a  $pn$  junction after the collapse of the depletion layer.<sup>18</sup>

Also the differential resistance as recorded with impedance spectroscopy shows a frequency dependence (Figure 10.9b). At high frequencies, the resistance decreases with increasing frequency. This type of behavior is shown by many materials<sup>19</sup> and will not be discussed further here. For frequencies lower than 4 kHz, the resistance decreases slightly with decreasing frequency. This is consistent with the time domain measurements in Figure 10.5. From the time domain measurements we concluded that the NDR is a time-dependent phenomenon. In the section below it will be argued that a time dependent negative differential resistance may contribute to the capacitance of the diode.

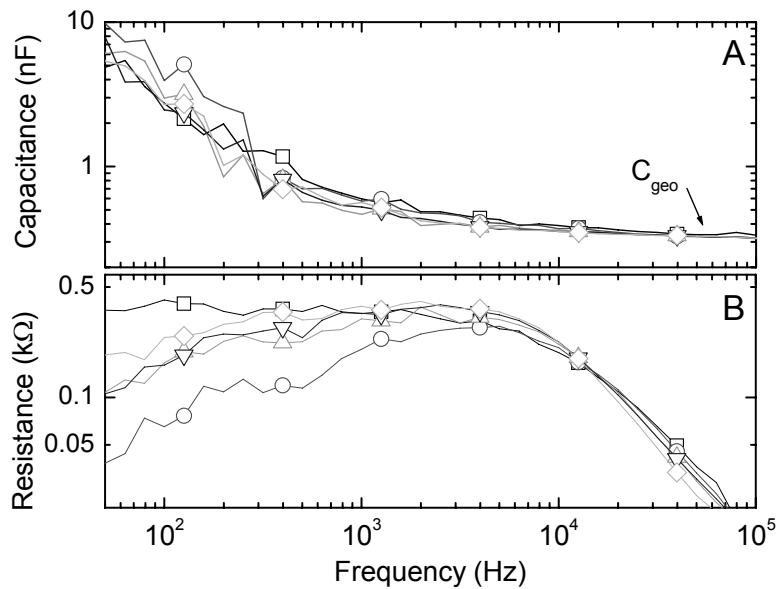


**Figure 10.9:** Capacitance (a) and resistance (b) at different AC amplitude voltages; 0.1 V ( $-\square-$ ), 0.3 V ( $-O-$ ), 0.5 V ( $-\triangle-$ ), 0.7 V ( $-\nabla-$ ), and 1 V ( $-\diamond-$ ). Measured at a frequency of 250 Hz at +5 V DC bias at 295 K.

Upon applying an oscillating voltage to the diode with a bias voltage offset corresponding to the NDR regime of the formed diode, the resulting AC current may be decomposed in two components. The first contribution is a normal Ohmic like component ( $I_{Ohm}$ ) proportional to the applied bias voltage. The second component represents the NDR behavior and is at first instance given  $I_{NDR}(t) \propto -V(t-\delta)$ . Here the negative sign symbolizes the decrease in the current when the *total* bias voltage applied to the diode increases in the NDR regime. From the time domain measurements we know, however, that the NDR is a time dependent phenomenon where the high and low conductivity states need time to develop fully. This may be represented by a phase shift of the  $I_{NDR}$  component so that the maximum current is reached shortly after the minimum voltage

has been applied to the diode. Combining the two components, one obtains a total current that precedes the applied voltage (Figure 10.10a) and therefore seems to have a capacitive component. In Figure 10.10b the voltage and corresponding current density are shown. The current density shows a NDR, at which the phase shift occurs. The voltage scan towards zero bias shows a decreased current density compared to the onwards scan. This is probably caused by the "dead time" in which this scan takes place.

At this point we cannot exclude other contributions to the capacitive component, and the simple, intuitive analysis presented here is not meant to give an exclusive, quantitative explanation of the impedance of the formed diodes. Interestingly, however, the consideration of the time dependent NDR provides an intuitive explanation for the observation that the excess capacitance and the NDR have an onset at almost similar bias voltages.

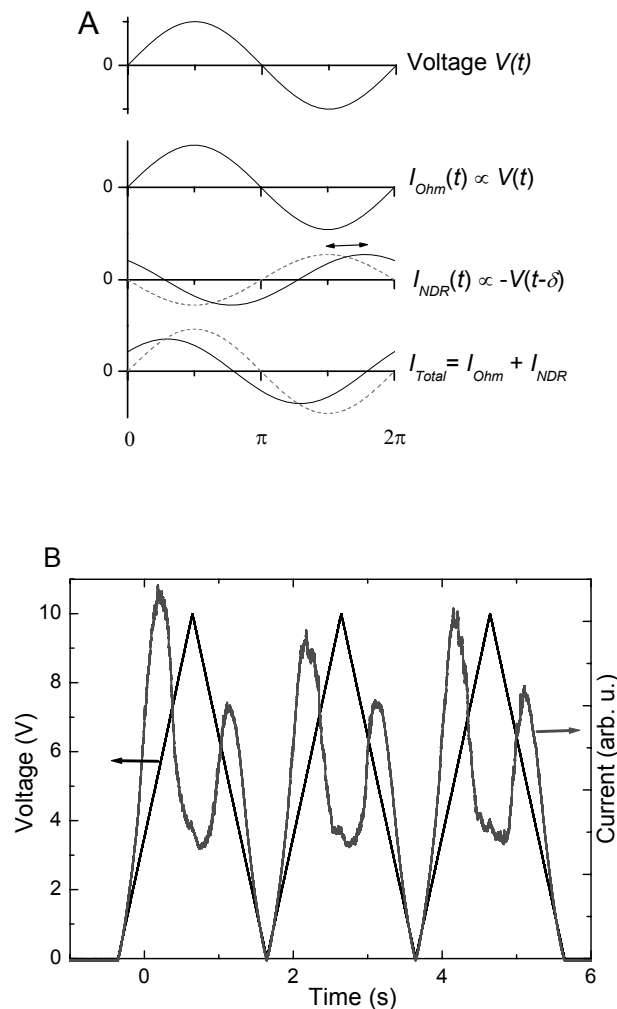


**Figure 10.10:** (a) Schematic illustration of the decomposition of the AC current through the diode upon application of an alternating voltage in an Ohmic like component and a component representing a time dependent negative differential resistance. (b) Time domain measurement of the current density, illustrating phase difference between current and voltage.

### 10.5. Filaments

In this last section devoted to experimental results, we investigate the lateral distribution of current density in the planar polymer- $\text{Al}_2\text{O}_3$  diodes in the formed state using thermal imaging techniques. Here an infrared camera is used to image the thermal radiation emitted as the result of Joule heating in the diode due to the current flowing under application of the bias voltage. The diode is repeatedly switched between the ON and OFF-state by a +5 V and +10 V voltage pulse, respectively. After preparing the diode in a particular state, a +1 V bias voltage is applied and the thermal radiation produced is imaged spatially. The thermograms (Figure 10.11) show very inhomogeneous temperature distributions in the diodes in both the ON and the OFF state. This is interpreted in terms of strongly localized current densities in the diodes flowing via a limited number of conduction pathways or filaments. The relative temperature differences between the “filaments” and the remaining parts of the device are larger in the ON-state than in the OFF-state, which is consistent with a lower local resistance in the ON state. Comparing images of ON states with those of OFF states, it seems that certain filaments are active in both states while others are only active in the On state. For the latter type of filaments we conclude that the conduction via the particular channel must have been blocked by application of the erase pulse. Comparing images of the ON or OFF states among each other it appears that not always the same filaments are active.

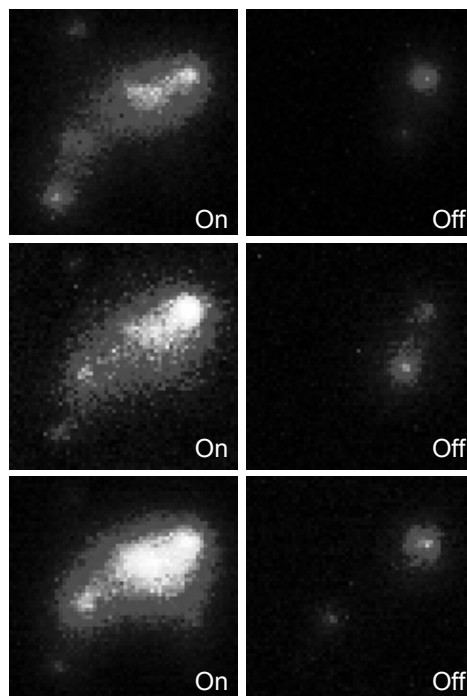


**Figure 10.11:** A memory with an  $\text{Al}_2\text{O}_3$  layer of 20 nm is switched between the ON and OFF state by a +5 V and +10 V voltage pulse, respectively. The spatial resolved current density recorded at +1 V is visualized with an infrared camera, between the switching events.

## 10.6. Discussion

In the preceding sections the negative differential resistance in non-volatile memories has been characterized. The diodes show special characteristics: disappearance of the NDR at high scan rates, the occurrence of a dead time, and the filamentary conduction. The causes of the switching and the NDR to processes are related to the oxide layer. The influence of the polymer layer is still an open question.<sup>20</sup> Many oxides show resistive switching, with often very similar characteristics.<sup>2,21</sup> This leads one to surmise that there might be a common mechanism for the switching which is operative in a number of different oxides.

A number of tentative explanations for the resistive switching and negative differential resistance in oxides have been given.<sup>2,21</sup> Recent studies on the scaling of the memory effects with the size of the electrode area of MIM diodes<sup>15</sup> and the measurement local conduction properties using scanning probe techniques<sup>22</sup> suggest that the switching effects are not dependent on macroscopic defects or edge effects in the oxide layers, but rather are intrinsic to the microstructure of the material.

In a number of studies, the role of oxygen vacancies in the crystal lattice of the oxide in the switching process has been implied.<sup>21,23,24</sup> This type of defect is supposed to be created during the electroforming. The presence of this defect may lower the barrier for charge injection and allow for higher conductivity in the bulk of the oxide especially when the defects are grouped close together forming a filament in which mobile carriers can migrate between the gap states associated with the defects.

Recently it was hypothesized that the resistance-switching process involves a drift of the charged oxygen vacancies along the applied bias field.<sup>24</sup> Although this may provide an explanation for bipolar switching in which pulses of opposite polarity are used to induce switching between the ON and OFF state, it is difficult to see how a field induced drift of the charged defect can explain the *unipolar* switching observed here. A second issue is the speed of switching. The drift of oxygen vacancies is associated with transfer of mass and therefore one may expect the mobility of the vacancies to be rather low. Switching events can occur on the nanosecond time scale, and in this short time interval the defects can only migrate over short distances. This seems at odds with the sometimes very large changes in resistance associated with the switching. The mechanism of field induced drift of charged defects resembles the resistive switching in conjugated polymers induced by migration of inorganic ions (Chapter 2). Here only slow switching speeds are observed and retention times are often limited by *diffusion* of the ions.



For oxygen vacancies in ZnO it was recently proposed that a defect may exist in two different, metastable, configurations.<sup>25</sup> The two configurations differ in the atomic positions of the metal ions surrounding the vacancy. In the so-called  $\alpha$  configuration of the defect, the defect localized electronic states lie in the band gap of the material, whilst in the  $\beta$  configuration, the defect localized states are above the conduction band minimum. When in the  $\beta$  configuration, the oxygen vacancies would constitute a shallow trap for electrons and contribute to the free carrier concentration. The ionized states of the defect ( $V_O^+$  and  $V_O^{2+}$  in the Kröger Vink notation) do not recombine spontaneously with an electron to form the neutral state of the vacancy ( $V_O$ ). In this way, the persistent photocurrent in this material may be explained.

In this section we explore the possibility offered by this suggestion in rationalizing the switching in the oxide layers. The polymer layer in the diodes has not been considered. We assume that a defect is present in the material and that it can be in two meta-stable states: a neutral one and an ionized one.

Furthermore mobile charge carriers are assumed to exist in the oxide carrying a negative charge, while the defects are assumed to carry a positive charge in the ionized state and do not recombine spontaneously with a mobile electron. The defects themselves are assumed to have negligible mobility in an applied electric field.

The key assumption required for modeling the switching, is that the ionization state of the defect depends on the local electric field. We assume a total defect concentration in the material  $p_{max}$ , which is constant throughout the material. The density of *ionized* defects is given by  $p(E)$ . At high values of the electric field strength ( $E > E_{crit}$ ) the degree of ionization is given by Figure 10.12a. With increasing  $E$ , the fraction of ionized defects,  $p(E)$  is assumed to decrease from  $p(E_{crit}) = p_{max}$  and approach zero for very high values of  $E$ . While at lower field strengths ( $E < E_{crit}$ ), the ionization state should be independent of the applied field, but dependent on the history of the device. As example, a field strength of  $E_{set}$  is applied to the device in Figure 10.12b. Upon decreasing the field within the dead time below  $E_{crit}$  the number of ionized defects at low fields will be equal to the number of defects at  $E_{set}$  and does not change unless the strength of the electric field is raised again above  $E_{crit}$ . This assumption is needed in order to account for the non-volatility of the memory effect.

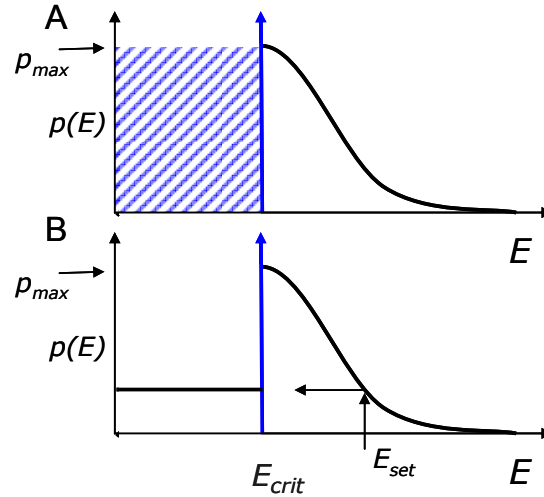


**Figure 10.12:** (a) Field dependence of the ionization of the defects. Only above  $E_{crit}$  the charge state of the defects depends on the field strength. (b) The number of ionized defects after application and fast removal of the field strength,  $E_{set}$ .

The density of charged defects is described by the following mathematical approximation:

$$\rho(E(x)) = \rho_{max} \frac{(E(x)/E_{crit})^2}{1 + (E(x)/E_{crit})^4} \quad \text{if } E > E_{crit} \quad (10.2)$$

Where  $x$  is the coordinate in the direction normal to the surface of the layers.

The derivative electric field strength ( $dE$ ) inside the oxide can be described by the Poisson equation:

$$\frac{dE}{dx} = \frac{|q_e|}{\epsilon_0 \epsilon_r} (\rho(x) - n(x)) \quad (10.3)$$

Where  $n(x)$  is the number density of mobile majority carriers (assigned negative charge) and  $\rho(x)$  is the number density of stationary ionized defects (assigned positive charge). The relative dielectric constant ( $\epsilon_r$ ) of  $\text{Al}_2\text{O}_3$  is taken to be isotropic  $\sim 10$  (literature:  $\epsilon_{r,11} = \epsilon_{r,22} = 9.34$ ,  $\epsilon_{r,33} = 11.54$  (25 °C)).

### Space charge limited drift currents

When applying a voltage the diode reaches a *steady state*. This implies that the current density ( $J$ ) is constant through the diode. From non-equilibrium thermodynamics it is known that steady states are characterized by minimal entropy production.<sup>26</sup> Thus in experiments in which the voltage is controlled to a certain value and the resulting current is recorded as observable, the principle of least entropy production implies that the current is as low as possible in the steady state. In experiments where the current is

controlled and the voltage needed to sustain this current is the observable, the steady state correspond to a minimal potential difference over the diode (minimal  $V$ ).

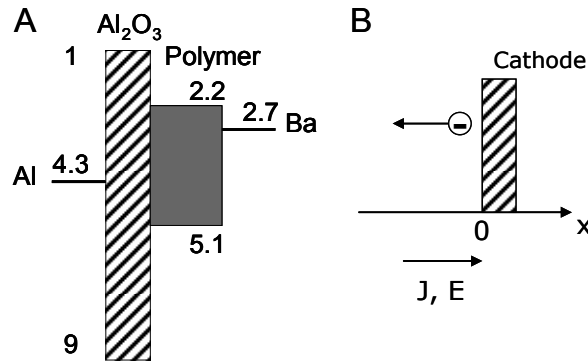


**Figure 10.13:** (a) Flat Band diagram of the investigated diode (eV). (b) Geometry around the electron injecting contact.

Experiments on the formed polymer-Al<sub>2</sub>O<sub>3</sub> diodes at low applied bias show almost Ohmic behavior at both bias directions. In the band diagram (Figure 10.13a) in forward bias a barrier for electron is expected at the polymer-Al<sub>2</sub>O<sub>3</sub> interface and in reverse bias at the Al-Al<sub>2</sub>O<sub>3</sub> interface. However, given this experimental fact one is led to assume the existence of Ohmic contacts between Ba-polymer, polymer-Al<sub>2</sub>O<sub>3</sub>, and Al<sub>2</sub>O<sub>3</sub>-Al interface.<sup>27</sup> In qualitative terms the existence of such a contact may be explained by the presence of charged defects near the polymer-Al<sub>2</sub>O<sub>3</sub>, and Al<sub>2</sub>O<sub>3</sub>-Al interface, which aid the injection of mobile carrier with charge opposite to that of the defect. With the assumption of an Ohmic contact, the conduction through the diodes must then be limited by the space charge that can accumulate in the metal oxide at a given applied potential and is not limited by the contacts and the polymer.

Here we assume that there is only one type of mobile charge carriers, which are assigned a negative charge in the metal oxide. We take into account only drift transport although for a fully consistent description of the Ohmic contact also diffusion needs to be taken into account. In space charge limited conduction, the number density of these mobile electrons is related to the current density and the electric field. In the steady state, the current density ( $J$ ) is independent of the position in the layer ( $x$ ).

$$J = \mu_n n(x) E(x) \Rightarrow n(x) = \frac{J}{\mu_n E(x)} \quad (10.4)$$

The geometry of the electrode in this analysis is defined such that the electron injected by the cathode contact at  $x=0$ , travels through the oxide in the  $-x$  direction towards anode at  $x = -d$  (Figure 10.13b).

The expressions for the field dependent charge densities  $p$  and  $n$  can now be inserted in the Poisson equation (Equation 10.3) yielding a first order non-linear differential equation that can be solved by standard methods. Before investigating its

solutions, we first express the electric field strength ( $E$ ), the current density ( $J$ ) and the distance ( $x$ ) in dimensionless units ( $J$ ,  $E$ , and  $x$ ):

$$J = \frac{J}{J_0} \quad E(x) = \frac{E(x)}{E_{crit}} \quad x = \frac{x}{x_0} \quad (10.5, 10.6, 10.7)$$

$$J_0 = |q_e| \mu_n E_{crit} p^{max} \quad x_0 = \frac{\epsilon_0 \epsilon_r E_{crit}}{|q_e| p^{max}} \quad (10.8, 10.9)$$

Here we take  $\epsilon_r = 10$ ,  $p^{max} = 10^{20} \text{ cm}^{-3}$ , and  $\mu_n = 10^{-10} \text{ cm}^2/\text{Vs}$ . The critical electric field,  $E_{crit}$  is set at  $2 \times 10^6 \text{ V/cm}$ , corresponding to 2 V potential difference over 10 nm. For comparison,  $10^{19}$  oxygen defects per  $\text{cm}^3$  have been reported for  $\text{Ba}_{0.3}\text{Sr}_{0.7}\text{TiO}_3$ .<sup>28</sup> This yields  $J_0 = 3.2 \text{ mA/cm}^2$ , and  $x_0 = 1.1 \times 10^{-7} \text{ cm}$ . The latter distance can be interpreted as a characteristic length scale for band bending effects and is smaller than the typical thicknesses of the oxide layer used in the experiment.

Combining Equations 10.2, 10.3, and 10.4 the following differential equation can be derived for the electric field strength. Here the dimensionless units described above are used:

$$\frac{dE}{dx} = f(E(x)) = \frac{E(x)^2}{1+E(x)^4} - \frac{J}{E(x)} \quad (10.10)$$

This describes the derivative of  $E(x)$  with respect to  $x$ . Note that  $f(E)$  is independent of  $x$ , but dependent of  $E$ . This equation is valid only for  $E > E_{crit}$ . The case of  $E < E_{crit}$  will be dealt with in more detail below.

In the search for appropriate possible solutions of 10.10, we first investigate for which values of  $E$ , the flow field  $f(E(x))$  is zero. For this we need to solve:

$$J(1+E(x)^4) - E(x)^3 = 0 \quad (10.11)$$

When  $J < 0.57$  there are two positive values for  $E$  for which  $f(E) = 0$ . The solutions with  $E$  negative are not considered because we are interested in unipolar switching. The two solutions are labeled  $E_{z1}$  and  $E_{z2}$  and can even be expressed analytically as a function of  $J$  (Figure 10.14). For  $J = J_{crit} = 0.57$ , it holds that  $E_{z1} = E_{z2} = E_z = 1.32$ . For  $J > 0.57$  there are no solutions to Equation 10.11. The importance of the fields  $E_{z1}$  and  $E_{z2}$  is that they act as "attractors" and mark the asymptotic values to which  $E(x)$  can converge to at the ends of the layer in the thickness direction.

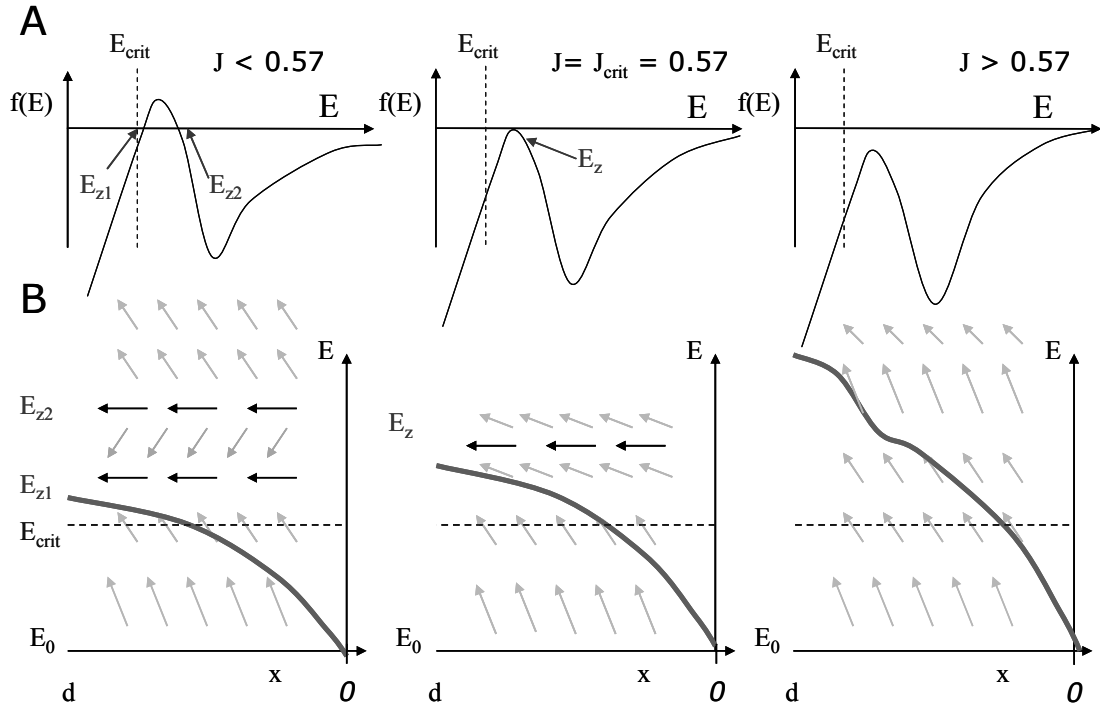


**Figure 10.14:** (a) Derivative of the electric field strength  $E$  plotted vs  $E$  as calculated from Eq. 10.9 for different values of current density  $J$ : low current ( $J < 0.57$ ), critical current ( $J = 0.57$ ) and high current ( $J > 0.57$ ). (b) Electric field plotted vs position  $x$  corresponding to the three different values for  $J$ . The arrows correspond to the derivative of the electric field  $f(E)$ . The solid lines indicate possible solutions to Equation 10.9.

For a set value of  $J$ , we now investigate solutions of Equation 10.10 that are compatible with the assumed presence of an Ohmic contact and with a minimal potential drop over the diode, so as to mimic experiments in which the current is controlled. At a quasi-Ohmic contact only small values for the electric field are allowed because the many free charge carriers available will tend to reduce any electric field. Considering that the density of states is limited, small values of the electric field at the contact are justifiable.<sup>29</sup> Here we set the electric field at the interface  $x = 0$  to  $E = 0.01$ . It should be pointed out that a consistent description of the contact also requires diffusion of charge carriers to be taken into account. The low electric field at the interface is compatible with the requirement of minimal potential drop over the diode. In a qualitative manner, these solutions to Equation 10.9 can now be illustrated in the  $E(x)$  vs  $x$  diagrams in Figure 10.14b. We first investigate the steady states for which  $J \leq 0.57$ . Here  $E_{z1}$  serves as an attractor. Solutions with minimal  $V$  should start with  $E$  as low as possible at  $x = 0$  followed by  $E(x)$  approaching  $E_{z1}$  at larger values of  $x$ . For higher values of  $J$  ( $J > 0.57$ ) no attractor exists and therefore the field increases continuously with increasing  $x$ . In sketching the solutions to Equation 10.10 in Figure 10.14, we have tacitly applied

Equation 10.11 also for  $E < E_{crit}$ . This analysis does not yet include all the details of the model assumed for the ionization state of the defects. In the section below we give a more complete account which also allows for switching effects.

### **High and low resistance states**

For  $E < 1$  (remember in the dimensionless units introduced:  $E_{crit} = 1$ ) an ambiguity in our description is encountered: the defects may be in the charged or in the neutral state depending on the history of the device. Here we consider two limiting cases. The first is the case in which all the defects are in the charged state at the start of the experiment and where defects at position  $x$  can only neutralize when  $E(x) > 1$ . To describe this we introduce a modified flow field  $f_{max}(E)$ :

$$f_{max}(E(x)) = \begin{cases} 0.5 - \frac{J}{E(x)} & \text{if } E < 1 \\ \frac{E(x)^2}{1+E(x)^4} - \frac{J}{E(x)} & \text{if } E > 1 \end{cases} \quad (10.12)$$

An initial state in which all defects are ionized may be realized experimentally by applying a very high bias voltage to the diode and reducing this bias voltage again rapidly within a time interval shorter than the dead time.

The other limiting case is where all the defects are initially neutral and ionize as soon as  $E > 1$ :

$$f_{min}(E(x)) = \begin{cases} -\frac{J}{E(x)} & \text{if } E < 1 \\ \frac{E(x)^2}{1+E(x)^4} - \frac{J}{E(x)} & \text{if } E > 1 \end{cases} \quad (10.13)$$

The initial states implied by equation 10.13, may be prepared experimentally by applying a moderate potential difference over the diode so that the electric field inside the device is as close to  $E_{crit}$  as possible.

Standard numerical procedures can now be used to solve the differential equation (Equation 10.10) using the modified flow fields (Equation 10.12 and 10.13). Here the value of  $E$  at the contact at  $x = 0$ ,  $E_0$  is taken equal to  $E_0 = 0.01 \times E_{crit}$ . This yields *calculated* voltage-current characteristics shown in Figure 10.15. Starting from a state in which all defects are ionized using  $f_{max}(E)$  the calculated electrical characteristics seem to describe a low resistance ON-state for low bias voltages. For bias voltages exceeding the critical voltage  $V_{crit} = E_{crit} \times d$ , with  $d$  the thickness of the oxide layer, a different voltage-current behavior is predicted corresponding to a much higher resistance. The calculations for the starting state with neutral defects using  $f_{min}(E)$  predict a high resistance "OFF"

state at low voltages. This state converts to a state with higher resistance when applying voltages  $V > V_{crit}$ . At these voltages the predictions starting from the two different initial state coalesce.

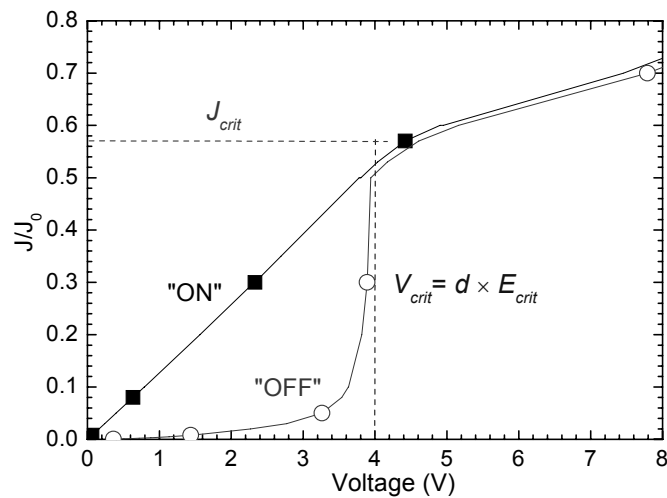


**Figure 10.15:** Theoretical Voltage-current characteristics calculated using Eq. 10.10 in combination with flow field  $f_{min}(E)$ , Equation 10.13 ( $-O-$ ) or in combination with flow field  $f_{min}(E)$ , Eq. 10.12 ( $-■-$ ) Thickness of the oxide layer : 20 nm.

These predictions can now be compared in detail to the experimental results (Figure 10.16). In the calculations, the polymer layer in the diodes has not been considered. As can be seen, the calculations are able to account qualitatively for the observed bistability and the switching between the regimes with high and low resistance.

For bias voltages around +4 V, the calculations predict current densities on the order of  $J_0$ , amounting to 3 mA/cm<sup>2</sup> when assuming a mobility of 10<sup>-10</sup> cm<sup>2</sup>/Vs so as to obtain agreement with the experiment, however the mobility might be higher if the current in the device is not homogeneous as shown in Figure 10.11. Here it should be pointed out that in the calculation, the whole area of the diode is assumed to be active, while the experiments indicate that only part of the electrode area contributes significantly to the current density. For bias voltages close to 1 V the calculations predict a difference in the current density in the ON and OFF state of an order of magnitude which matches quite well with the experimental observations.

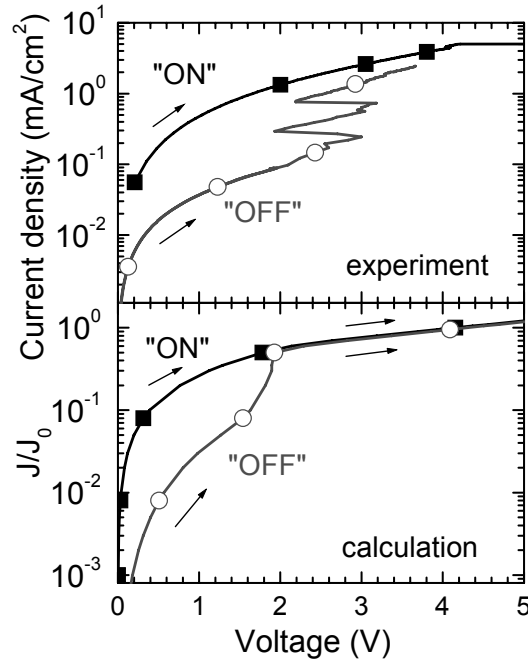


**Figure 10.16:** Experimental voltage-current characteristics of a formed polymer- $\text{Al}_2\text{O}_3$  diode. The current is scanned after preparation by applying a +8 V pulse (—■—) of a +4 V pulse to the diode. Thickness of the oxide layer: 10 nm of the polymer layer 80 nm. Theoretical voltage-current characteristics calculated using Equation 10.10 in combination with flow field  $f_{\min}(E)$ , Eq. 10.13 (—○—) or in combination with flow field  $f_{\min}(E)$ , Equation 10.12 (—■—) Thickness of the oxide layer : 10 nm.

In summary, the model including the defects with two metastable ionization states can account for bistability and switching between the OFF and ON state in experiments in which the current is scanned.

Accounting for the NDR observed in current-voltage scan is more difficult. When controlling the voltage, then according to thermodynamics, the system strives towards minimalization of the current density. Spontaneous degradation of the Ohmic contact due to neutralization of the ionized defects is a possible way to reduce the current density. Another possibility is the spontaneous formation of domains inside the insulator with different field strengths.<sup>30</sup> If the potential drop across the diode can be distributed in such a way that domains in which the electric field strength is close to zero arise, then the presence of these domains blocks the current density in the diode because drift currents in these domain are very small.

We expect that when applying a voltage exceeding the critical voltage to the diode, the relatively high electric field inside the device will also cause neutralization of defects close to the metal electrode. This may lead to gradual degradation of the Ohmic contact and a lowering of the current densities with increasing applied electric field. However, at even higher electric fields, the current density will increase again.



In the model discussed above it was assumed that the defects are distributed homogeneously throughout the insulator. It seems likely that the majority of the defects are in fact induced during the forming step and here it is possible that generation of defects does not occur uniformly. Regions with relatively high defect density close to the metal contact may then give rise to high local injection currents and thus to current filaments.

Based on the suggestion of Lany and Zunger<sup>25</sup> for ZnO we have assumed that the actual active defects are oxygen vacancies. Furthermore it was assumed that the ionized states of the defect ( $V_O^{\bullet}$  and  $V_O^{\bullet\bullet}$  in the Kröger Vink notation) do not recombine spontaneously with an electron to form the neutral state of the vacancy ( $V_O$ ). This implies that an electron compensating the electrical charge of the defect must remain in the conduction band of the oxide. For  $Al_2O_3$ , the conduction band minimum is estimated to lie relatively close below the vacuum level ( $\sim 1$  eV)<sup>31</sup> so that electrons in the oxide can be emitted relatively easily into the vacuum. In accordance with this, electron emission from formed planar diodes with  $Al_2O_3$  is commonly observed in vacuum.<sup>2</sup> In presence of air, the electrons in the conduction band of the oxide are likely to be captured by  $O_2$  molecules so that the high conduction state cannot be formed (See also chapter 4).

The conduction band of  $Al_2O_3$  ( $\sim 1$  eV below the vacuum level) lies well above the LUMO levels of the conjugated polymer ( $\sim 2.2$  eV below the vacuum level<sup>32</sup>). In forward bias charged defects at the interface between the oxide and polymer can dope this layer, resulting in an Ohmic contact. In reverse bias electron injection from the *formed*  $Al_2O_3$  into the polymer is expected to be possible. This may provide a first step in explaining why addition of a polyfluorene layer on top of the oxide has such remarkably little influence on the current-voltage characteristics of the formed diodes.

### **10.7. Conclusion**

In conclusion, polymer- $Al_2O_3$  diodes show time dependent negative differential resistance after forming and behave in many aspects similar to diodes with only an oxide layer. Currently no comprehensive mechanistic explanation for all the peculiar electrical characteristics of the oxide is available, but many studies point towards the involvement of defects in the oxide that are probably introduced during the forming step. Here we have shown that the assumption of different metastable ionization states of a defect in the oxide can explain some rudimentary aspects of the complicated electrical characteristics. Further theoretical development is required in order to describe the more intricate features of the electrical behavior.

## 10.8. Experimental

The memory diodes consisted of an Al bottom electrode, a sputtered Al<sub>2</sub>O<sub>3</sub> layer, a spirofluorene polymer and a Ba/Al top electrode. The devices with an active area of 9 mm<sup>2</sup>, were encapsulated to exclude O<sub>2</sub> and H<sub>2</sub>O. In all cases, positive bias voltage refers to the bottom electrode being charged positive with respect to the top electrode. A Schlumberger SI 1260 impedance analyzer was used for the C–V measurements. A Semicaps SOM 3000 was used for spatially resolved IR measurements. The InGaAs camera has a spectral response from 950 to 1700 nm and a spatial resolution of 10 μm. The voltage saw tooth waveform used in the experiments is applied by an Agilent 33250A function generator in combination with a Krohn-Hite model 7600 wideband amplifier and read out with a Tektronix TDS5052B oscilloscope.

## 10.9. References

- 1 F. Verbakel, S.C.J. Meskers, M. Cölle, M. Büchel, H.L. Gomes, R.A.J. Janssen, and D.M. de Leeuw, *Appl. Phys. Lett.* **91**, 192103 (2007).
- 2 H. Pagnia and N. Sotnik, *Physica Stat. Sol. A* **108**: 11 (1988).
- 3 T.W. Hickmott, *J. Appl. Phys.* **88**, 2805 (2000).
- 4 J.G. Simmons and R.R. Verderber, *Proc. R Soc. Lond. Ser. A* **301**, 77 (1967).
- 5 F. Argall, *Solid-State Electron.* **11**, 535 (1968).
- 6 K. Tsunoda, Y. Fukuzumi, J.R. Jameson, Z. Wang, P.B. Griffin, and Y. Nishi, *Appl. Phys. Lett.* **90**, 113501 (2007).
- 7 B.J. Choi, S. Choi, K.M. Kim, Y.C. Shin, C.S. Hwanga, S.-Y. Hwang, S. Cho, S. Park, and S.-K. Hong, *Appl. Phys. Lett.* **89**, 012906 (2006).
- 8 T. Hada, K. Wasa, and S. Hayakawa, *Jpn. J. Appl. Phys.* **10**, 521 (1971).
- 9 K.C. Park and S. Basavaiah, *J. Non-Cryst. Solids* **2**, 284 (1970).
- 10 R. Fors, S.I. Khartsev, and A.M. Grishin, *Phys. Rev. B* **71**, 045305 (2005).
- 11 A.L. Pergament, V.P. Malinenko, O.I. Tulubaeva, and L.A. Aleshina, *Phys. Stat. Solidi A* **201**, 1543 (2004).
- 12 M. Cölle, M. Büchel, and D.M. de Leeuw, *Org. Electron.* **7**, 305 (2006).
- 13 See Chapter 7
- 14 A. Chen, S. Haddad, Y. C. Wu, T. N. Fang, S. Kaza, and Z. Lan, *Appl. Phys. Lett.* **92**, 013503 (2008).
- 15 I.G. Baek, M.S. Lee, S. Seo, M.J. Lee, D.H. Seo, D.-S. Suh, J.C. Park, S.O. Park, H.S. Kim, I.K. Yoo, U.-In. Chung, and J.T. Moon, *IEDM Tech. Dig.-Int. Electron Devices Meet.* **04**, 587, (2004).
- 16 D.J. Dumin, Oxide reliability. A summary of silicon oxide wearout, breakdown and reliability. *World Scientific Publishing Co. Pte. Ltd. Singapore* (2002).
- 17 R.D. Gould and C.A. Hogarth, *Phys. Stat. Sol. (a)* **23**, 531 (1974).
- 18 S. M. Sze, Physics of semiconductor devices, 2nd ed. *Wiley*, New York (1981).

- 19 Jonscher, A.K. *Dielectric relaxation in solids*, Chelsea Dielectrics Press (1983).
- 20 J.C. Scott and L.D. Bozano, *Adv. Mater.* **19**, 1452 (2007).
- 21 R. Waser and M. Aono *Nature Mater.* **6**, 833 (2007).
- 22 K. Szot, R. Dittmann, W. Speier, and R. Waser, *Phys. Status Solidi* **1**, R86 (2007).
- 23 I. Emmer *Thin Solid Films* **20**, 43 (1974).
- 24 M. Janousch, G. I. Meijer, U. Staub, B. Delley, S. F. Karg, and B. P. Andreasson, *Adv. Mater.* **19**, 2232 (2007).
- 25 S. Lany and A. Zunger, *Phys. Rev. Lett.* **98**, 045501 (2007).
- 26 S.R. de Groot, and P. Mazur, *Non-equilibrium thermodynamics*, Dover New York (1984).
- 27 T.W. Hickmott, *J. Appl. Phys.* **100**, 083712 (2006).
- 28 R. Meyer, R. Liedtke, and R. Waser, *Appl. Phys. Lett.* **86**, 112904 (2005).
- 29 V.D. Mihalevich, J.K.J. van Duren, P.W.M. Blom, J.C. Hummelen, R.A.J. Janssen, J.M. Kroon, M.T. Rispens, W.J.H. Verhees, and M.M. Wienk, *Adv. Func. Mater.* **13**, 43 (2003).
- 30 B.K. Ridley, *Proc. Phys. Soc.* **82**, 954 (1963).
- 31 E.A. Colbourn and W.C. Mackrodt, *Solid State Comm.* **40**, 265 (1981).
- 32 H.L. Gomes, A.R. Benvenho, D.M. de Leeuw, M. Cöelle, P. Stallinga, F. Verbakel and D.M. Taylor, *Org. Electron.* **9**, 119 (2007).

# Summary

Resistive switching in metal-insulator-metal (MIM) structures is an intriguing phenomenon in which the electrical resistance can be altered reversibly, and permanent in case of a non-volatile memory, by applying a voltage. It is being investigated intensely, partly because of its potential application in data storage. The mechanism of this switching is largely unknown. This thesis describes the design, construction and electrical characterization of diodes with an active layer consisting of organic-inorganic hybrid materials that show resistive switching.

In the realization of the memory diodes, two different approaches were followed. Chapter 2 describes the first approach in which the active layer is made of a block copolymer consisting of a semiconducting part (sexithiophene) and a part facilitating migration of added inorganic ions (ethylene oxide). Inorganic salt is added as a dopant. From an analysis of the electro-optical behavior of these diodes, it is concluded that the resistive switching and the associated memory effect is due to electric field induced migration of the inorganic ions in the active layer. The switching allows for storage of information and rewritable memory operation is demonstrated for the diodes although the retention time of the information is still very short ( $\sim 10$  s). In this system, the energetic barrier for injection of a mobile carrier into the semiconducting block can be lowered by the presence of an inorganic ion of opposite sign in a neighboring ion transporting block. Hence, the resistivity of the diode can be modulated by changing the concentration of ions at the electrode.

The second approach involves metal oxides in combination with polymers as active layer. In Chapter 3 to 6, zinc oxide nanoparticles have been used as one of the active components. After a forming reaction, resistive switching could be established within 50 ms and retention of the memory was increased to hours. The forming process itself is interpreted in terms of desorption of molecular oxygen from the ZnO nanoparticle surface, induced by injection of holes via the PEDOT:PSS contact, leading to a higher n-type conductivity via interparticle ZnO contacts. The forming can also be induced by ultraviolet light and the process is studied with electron paramagnetic resonance, photoinduced absorption spectroscopy, and field-effect measurements. By varying the content of ZnO and the type of polymer in the active layer the memory effects can be influenced and a data storage with lifetime  $>14$  hours has been achieved.

Chapter 5 shows that the electronic properties can be altered by capping the ZnO nanoparticles with various ligands. Capping with propylamine gives hysteresis and resistive switching after application of  $-5$  V and  $+5$  V bias pulses, while retaining the rectifying behavior of the device. This is a crucial requirement when these devices are

used in passive matrix arrays. In Chapter 6 it is shown that with increasing surface coverage of the ZnO nanoparticles with a thiol ligand, the electrical resistance, associated with electron transport via percolating networks of ZnO particles in the matrix, increases, due to deterioration of the ZnO interparticle contacts. Just before reaching the percolation limit obtained by adding  $\sim 0.05$  mol thiol per mol Zn to the ZnO nanoparticles, where the electrical current is supported by just a few percolation paths, the electrical characteristics change. For unmodified ZnO particles, voltage pulses of opposite polarity (bipolar) bring the diode to a low and a high resistive state. With the ZnO particles modified with octane thiol, the diodes can be switched between low and high resistance with unipolar voltage pulses of 1  $\mu$ s. Using write and erase pulses of 10 ms, an ON/OFF ratio of  $10^3$  can be achieved with good cycle endurance. This change is observed with Al or Pd top electrodes, and is interpreted in terms of the conduction taking place via essentially a single, narrow channel of ZnO particles that can be blocked by trapping of a single charged species.

In Chapter 7, it is concluded that the switching function of the polymer–aluminum oxide diodes mainly reflects a property of the aluminum oxide. The yield in switching of solid state-memories can be increased to about unity by deliberately adding a thin sputtered  $\text{Al}_2\text{O}_3$  layer to organic diodes. Before memory operation, the devices have to be formed at an electric field of  $10^9$  V/m, corresponding to soft-breakdown of  $\text{Al}_2\text{O}_3$ . After forming, the structures show pronounced negative differential resistance and the local maximum in the current scales with the thickness of the oxide layer. After the forming, switching in hundreds of nanoseconds can be achieved. Repeated pulse sequence measurements of Chapter 8, show the occurrence of a 'dead time', that is the time after programming in which a next switch is inhibited, of about 3 ms. The dead time, which is known for bulk oxides, explains the huge variation in the reported switching times.

Resistive switching is demonstrated in diodes based on spin coated layers of various metal oxide nanoparticles and a semiconducting polymer, sandwiched between two electrodes in Chapter 9. Inclusion of the oxide nanoparticles results in non-volatile electronic memory characteristics that are similar to those observed for the corresponding 'bulk' oxide. A major difference is that the nanoparticulate layers do not require a forming step. In the absence of oxygen, resistive switching is observed in many metal oxides. Among the various oxides, there are differences in switching behavior (unipolar/bipolar) that may be related to the different electronic structure of the materials. In the case of ZnO particles modification of the layer morphology, leads to change in the memory properties (Chapter 7). This indicates that besides electronic structure, also the geometry and number of the filaments formed is important in determining the type of resistive switching of the memory.

In Chapter 10, negative differential resistance (NDR) in polymer- $\text{Al}_2\text{O}_3$  diodes is investigated using time and frequency domain electrical measurements and thermal imaging. After a forming step, the diodes show a time dependent NDR. In the bias voltage range where NDR is observed, the capacitance at low frequency is significantly larger than for the unformed diode. Conduction in the formed diodes is filamentary in nature. Assuming different metastable ionization states of defects in the oxide and space charge limited conduction, some fundamental aspects of the switching can be accounted for.

In conclusion, this thesis shows resistive switching for diodes containing various materials. The combination of metal oxides and polymers emerges as appealing because it exhibits a range of intriguing resistive switching effects that are potentially of interest for future nonvolatile memory element applications. A first step is made to rationalize the origin, mechanism, and magnitude of the resistive switching in terms of a quantitative model.



# Samenvatting

Het omkeerbaar schakelen van het elektrische weerstandniveau in metaal-isolator-metaal (MIM) structuren door het aanbrengen van een voltage is een intrigerend fenomeen dat intensief bestudeerd wordt, onder andere, vanwege de potentiële toepassing in elektrische dataopslag. Het mechanisme dat ten grondslag ligt aan het schakelen en de geheugenwerking is grotendeels onbekend. Dit proefschrift beschrijft het ontwerp, de fabricage en de elektrische karakterisatie van diodes waarin de actieve laag bestaat uit een hybride organisch-anorganisch materiaal dat deze schakeling in weerstand vertoont.

Bij de verwezenlijking van de geheugens zijn er twee benaderingen gevolgd. Hoofdstuk 2 beschrijft de eerste benadering waarin de actieve laag is gemaakt van een blokcopolymeer dat bestaat uit een halfgeleidend deel (sexithiofeen) en een deel dat de migratie van toegevoegde anorganische ionen vergemakkelijkt (ethyleenoxide). Het anorganische zout is toegevoegd als doping. Uit de analyse van het elektro-optisch gedrag van deze diodes, concluderen we dat het schakelen van de weerstand en het bijbehorend geheugeneffect is geïnduceerd door migratie van ionen in de actieve laag onder invloed van het elektrisch veld. Het schakelen staat de opslag en het wissen van informatie toe, al blijkt voor deze diodes de retentietijd van de opslag van informatie nog erg kort ( $\sim 10$  s) te zijn. In dit systeem kan de energetische barrière voor injectie van een mobiele ladingsdrager in een halfgeleidende blok verlaagd worden door de aanwezigheid van anorganische ionen van tegengestelde lading in een nabij ion-transporterend blok. Hiermee wordt de weerstand van de diode gemoduleerd door de ionenconcentratie aan de elektrode te veranderen.

De tweede benadering gebruikt metaal oxides in combinatie met een polymeer als actieve laag. In Hoofdstuk 3 tot 6 zijn zink oxide nanodeeltjes gebruikt als actieve component. Na een vormingsreactie kan de weerstand binnen 50 ms geschakeld worden tussen een hoog en laag weerstandsniveau. De retentietijd van dit geheugen is toegenomen tot uren. Het vormingsproces zelf, wordt geïnterpreteerd in termen van desorptie van moleculaire zuurstof aan het oppervlak van de ZnO nanodeeltjes. Dit wordt geïnduceerd door injectie van gaten via het positieve contact en leidt tot een hogere n-type geleiding door de contacten tussen de ZnO deeltjes. De vorming kan ook bereikt worden door belichting met ultraviolet licht en het proces is bestudeerd met elektronische paramagnetische resonantie (EPR), fotogeïnduceerde absorptie (PIA) en veld-effect metingen. Ook is de samenstelling van de actieve laag gevarieerd. Het geheugeneffect kan beïnvloed worden door veranderingen in de ZnO hoeveelheid en het type polymeer, waarmee een levensduur voor opslag van gegevens van meer dan 14 uur mogelijk is.



Hoofdstuk 5 laat zien dat de elektrische eigenschappen veranderen door het bedekken van ZnO nanodeeltjes met verschillende liganden. Bedekken met propylamine geeft hysteresis en schakeling in de weerstand, terwijl het diodegedrag behouden blijft. Dit is een cruciaal vereiste om deze cellen toe te passen in een passieve matrix. In Hoofdstuk 6, wordt aangetoond dat met toenemende oppervlaktebedekking van de ZnO nanodeeltjes met octaanthiolliganden, de elektrische weerstand die geassocieerd wordt met elektronentransport via percolerende netwerken van ZnO deeltjes in de matrix, toeneemt door een verslechterend contact tussen de ZnO deeltjes. Net voordat de percolatiegrens wordt bereikt, waar de elektrische stroom wordt gedragen door slechts enkele percolatiepaden, veranderen de elektrische eigenschappen drastisch. Voor ongemodificeerde ZnO deeltjes, brengen voltage pulsen van tegengestelde polariteit (bipolair) de diode naar een hoog en laag weerstandsniveau. Diodes op basis van ZnO deeltjes die gemodificeerd zijn met octaanthiol kunnen geschakeld worden met unipolaire pulsen van 1  $\mu$ s. Door gebruik te maken van schrijf- en wispulsen van 10 ms, kan een AAN/UIT verhouding van  $10^3$  bereikt worden met een goede herhaalbaarheid van het schakelproces. Deze verandering wordt waargenomen in diodes met een Al of een Pd top elektrode en wordt geïnterpreteerd in termen van geleiding die plaatsvindt via eigenlijk één, smal kanaal van ZnO deeltjes. Dit kanaal kan geblokkeerd worden door één enkele lading.

In Hoofdstuk 7 wordt aangetoond dat de schakelmogelijkheid van polymeer-aluminium oxide diodes hoofdzakelijk het gevolg is van de aluminium oxide laag. Bij het maken, kan de opbrengst aan werkende, schakelbare vaste-fase geheugens kan toenemen tot ongeveer 100 % door het opzettelijk toevoegen van een dunne, gesputterd  $\text{Al}_2\text{O}_3$  laag aan de organische diodes. Voordat het geheugen gebruikt kan worden, moet het gevormd worden door een elektrisch veld van  $10^9$  V/m, wat correspondeert met een "zachte doorslag" van  $\text{Al}_2\text{O}_3$ . Na de vorming laten de cellen een uitgesproken negatieve differentiële weerstand (NDR) zien en het lokale maximum in de stroom van deze NDR schaal met de dikte van de oxide laag. Het schakelen kan plaatsvinden in honderden nanoseconden, maar de herhaalde pulssequentiemetingen van Hoofdstuk 8 laten een "dode tijd" van ongeveer 3 ms zien. Dit is een tijd waarin het programmeren van de volgende schakeling wordt tegengehouden. Deze dode tijd, die bekend is voor bulk oxides, verklaart de enorme variatie aan gerapporteerde schakeltijden voor 'organische' geheugens.

In Hoofdstuk 9 is het schakelen in weerstand ook aangetoond in diodes gebaseerd op gespincoate lagen van verschillende metaal oxide nanodeeltjes en een halfgeleidend polymeer, geplaatst tussen twee elektrodes. Toevoegen van oxide nanodeeltjes resulteert in permanente elektronische geheugeneigenschappen die vergelijkbaar zijn

met degene geobserveerd voor de corresponderende "bulk" oxide. Een groot verschil is dat de nanodeeltjes-lagen geen vormingsstap vereisen. In de afwezigheid van zuurstof wordt het schakelen in weerstand waargenomen in veel metaal oxides. Onder deze verschillende oxides zijn er verschillen in schakelgedrag (unipolair/bipolair), die gerelateerd zouden kunnen worden aan verschillen in elektronische structuur van de materialen. In geval van ZnO deeltjes leidt de modificatie van de laagmorfologie tot een verandering in geheugeneigenschappen (Hoofdstuk 7). Dit geeft aan dat behalve de elektronische structuur ook de geometrie en het aantal gevormde filamenten belangrijk is in het bepalen van het schakeltype van het geheugen.

In Hoofdstuk 10, is de negatieve differentiële weerstand (NDR) in polymeer- $\text{Al}_2\text{O}_3$  diodes onderzocht door elektrische metingen in tijd- en frequentiedomein en door warmtebeeld weergave. Na de vormingsstap laten de diodes een tijdsafhankelijke NDR zien. In het voltagegebied waar NDR wordt waargenomen, is de capaciteit bij lage frequentie significant hoger dan voor de ongevormde diodes. De geleiding in de gevormde diodes is filamentair van oorsprong. Als verschillende metastabiele ionisatie toestanden van defecten in het oxide en een ruimtelading-gelimiteerde stroom worden aangenomen, kunnen sommige fundamentele aspecten van het schakelen verklaard worden.

Het werk beschreven in dit proefschrift laat schakelingen in de weerstandsniveau voor diodes met verschillende materialen zien. De combinatie van metaal oxides en polymeren is aantrekkelijk, omdat ze een reeks intrigerende schakeleffecten laten zien, die in potentie interessant zijn voor permanente geheugentoepassingen. Een aanzet is gegeven tot het begrip van de oorsprong, het mechanisme en de grootte van het schakelen in termen van een model.



# Curriculum vitae



Frank Verbakel is geboren op 22 december 1979 in Helmond. Na het behalen van zijn diploma aan het St. Willibrord Gymnasium te Deurne is hij in 1998 begonnen met de studie Scheikundige Technology aan de Technische Universiteit Eindhoven. Zijn afstudeeropdracht heeft hij gedaan bij de groep "Polymer Technology" onder leiding van prof. D. Broer. Na in 2004 deze studie te hebben afgerond is hij begonnen met zijn promotie bij de groep "Molecular Materials and Nanosystems" onder leiding van prof. R.A.J. Janssen (TU/e), dr. S.C.J. Meskers (TU/e) en prof. D.M. de Leeuw (Philips). In dit project, dat onderdeel is van het Dutch Polymer Institute (DPI), is er onderzoek gedaan naar de ontwikkeling van polymeren geheugens. De resultaten van dit onderzoek zijn beschreven in dit proefschrift.

Frank Verbakel was born on December 22<sup>nd</sup>, 1979 in Helmond, The Netherlands. After obtaining his gymnasium-diploma (pre-university degree) at the St. Willibrord Gymnasium in Deurne, he studied Chemical Engineering and Chemistry at the Eindhoven University of Technology. His graduation project has been performed at the group "Polymer Technology" under supervision of prof. D. Broer. After completing this study in 2004, he started his PhD project at the group "Molecular Materials and Nanosystems" under supervision of prof. R.A.J. Janssen (TU/e), dr. S.C.J. Meskers (TU/e), and prof. D.M. de Leeuw (Philips). In this project, which is part of the Dutch Polymer Institute (DPI), research towards the development of polymeric memories is performed. The results of this research are described in this thesis.

## List of publications

*Negative differential resistance and resistive switching in polymer diodes*

F. Verbakel, S.C.J. Meskers, L.F. Feiner, D.M. de Leeuw, and R.A.J. Janssen, Manuscript in preparation

*Single electron resistive switching in polystyrene films containing ZnO nanoparticles with partial octanethiol surface coverage close to the percolation threshold*

R.T.M Jakobs, F. Verbakel, J. van Herikhuyzen, S.C.J. Meskers, D.M. de Leeuw, A.P.H.J. Schenning, and R.A.J. Janssen, Manuscript in preparation

*Resistive switching in organic memories with a spin coated metal oxide nanoparticle layer*

F. Verbakel, S.C.J. Meskers, D.M. de Leeuw, and R.A.J. Janssen, Submitted

*Switching dynamics in non-volatile polymer memories*

F. Verbakel, S.C.J. Meskers, M. Cölle, M. Büchel, H.L. Gomes, R.A.J. Janssen, and D.M. de Leeuw, Submitted

*Reproducible resistive switching in non-volatile organic memories*

F. Verbakel, S.C.J. Meskers, M. Cölle, M. Büchel, H.L. Gomes, R.A.J. Janssen, and D.M. de Leeuw, *Appl. Phys. Lett.* **91**, 192103 (2007).

*Switching in polymeric resistance random-access memories (RRAMS)*

H.L. Gomes, A.R. Benvenho, D. M. de Leeuw, M. Cölle, P. Stallinga, F. Verbakel and D.M. Taylor, *Org. Electron.* **9**, 119 (2008).

*Surface modification of zinc oxide nanoparticles influences the electronic memory effects in ZnO - polystyrene diodes*

F. Verbakel, S.C.J. Meskers, and R.A.J. Janssen, *J. Phys. Chem. C* **111**, 10150 (2007).

*Resistive switching and noise in non-volatile organic memories*

L.K.J. Vandamme, M. Cölle, D.M. de Leeuw, F. Verbakel, *SPIE Proceedings* **6600**, 6600-07 (2007).

*Electronic memory effects in diodes of zinc oxide- nanoparticles in a matrix of polystyrene or poly(3-hexylthiophene)*

F. Verbakel, S.C.J. Meskers, and R.A.J. Janssen, *J. Appl. Phys.* **102**, 083701 (2007).

*Printing of Monolithic Polymeric Micro-Structures using Reactive Mesogens*

C. Sanchez, F. Verbakel, M.J. Escuti, C.W.M. Bastiaansen, and D.J. Broer, *Adv. Mater.* **20**, 74 (2008).

*Electronic memory effects in zinc oxide nanoparticle -polystyrene devices with a calcium top electrode*

F. Verbakel, S.C.J. Meskers, and R.A.J. Janssen, *Mater. Res. Soc. Symp. Proc.* **965**, 0965-S09-11 (2007).

*Electronic memory effects in diodes from a zinc oxide nanoparticle-polystyrene hybrid material*

F. Verbakel, S.C.J. Meskers, and R.A.J. Janssen, *Appl. Phys Lett.* **89** (10), 102103 (2006).

*Electronic memory effects in a sexithiophene-poly(ethylene oxide) block copolymer doped with NaCl. Combined diode and resistive switching behavior*

F. Verbakel, S.C.J. Meskers, and R.A.J. Janssen, *Chem. Mater.* **18** (11), 2707 (2006).

*Microstructuring of mesogens using contact printing*

C. Sanchez, C.W.M. Bastiaansen, and D.J. Broer, and F. Verbakel, WO2006006854 (2006).

# Dankwoord

Na de afgelopen jaren met veel plezier aan mijn promotie gewerkt te hebben, komt er met het afronden van het proefschrift een einde aan mijn tijd bij MST, SMO en M2N.

Om te beginnen wil ik René Janssen bedanken voor de vrijheid en het vertrouwen die hij me gegeven heeft in mijn onderzoek. De richting van het onderzoek was voor ons beiden nieuw en na onze gesprekken had ik altijd weer veel energie om verder te gaan. En gaandeweg hebben we veel nieuwe kennis op dit onderwerp gekregen. Ook wil ik mijn tweede promotor Dago de Leeuw bedanken. De mogelijkheden die je me geboden hebt met de productiefaciliteiten van Philips, zijn van onschatbare waarde geweest voor mijn onderzoek. Ook de tijd die we samen hebben doorgebracht met het meten en discussiëren, zal me altijd bij blijven.

Stefan, zonder jou had mijn proefschrift er nooit zo uitgezien. Ik heb veel geleerd van de vele dagen dat we samen gediscussieerd en gemeten hebben. Je vond het altijd leuk om mij te helpen de onverwachte resultaten te verklaren.

Ik wil graag de andere leden van mijn kerncommissie, prof. Paul Heremans, prof. Paul Blom en prof. Bert de With bedanken voor hun deelname en het lezen van mijn proefschrift. Furthermore, I would like to thank prof. Henrique Gomes for participating in my committee. Our collaboration was very valuable and enjoyable to me. The time we spent together performing measurements and discussing the results, while enjoying the nice weather gave me energy to proceed with the research.

Ton van den Biggelaar, zonder jou zouden de laatste hoofdstukken van mijn proefschrift niet bestaan hebben. Heel veel dank voor de vele keren dat je devices voor mij hebt gemaakt en je geduld om ze te veranderen wanneer ik weer net iets anders wilde hebben.

Lode Vandamme, ik wil je bedanken voor de introductie in ruismetingen die je me gegeven hebt. Met veel plezier heb ik op je zolder vol bewondering naar de metingen gekeken. Lou-Fe' Feiner wil ik bedanken voor het begin dat we samen gemaakt hebben om de geheugeneffecten te verklaren.

Jaap, ik wil jou graag bedanken voor jouw introductie in het onderwerp die jij mij gegeven hebt. Ik hoop dat je nog lang met veel plezier bij OCÉ zult werken.

Wiljan, met veel plezier heb ik samen met jou aan de geheugens gewerkt. We hebben er veel van geleerd. Ik wens je veel succes in je carrière.

Martijn Kemerink, bedankt voor de hulp die je mij gegeven hebt met de AFM en de impedantiemetingen. Martijn Wienk en Wijnand Dijkstra, bedankt voor de hulp bij het

maken van de devcies en de metingen. Jullie stonden altijd klaar om mij te helpen wanneer iets kapot was of wanneer ik iets speciaals gemaakt wilde hebben.

O. Henze and Prof. W. J. Feast I would like to thank for generously providing the block copolymers, which are the base of my second chapter.

Edsger, bedankt voor de hulp met de metingen en de tijd die we samen hebben gemeten aan de zink oxides. Veel succes met het afronden van je eigen promotie. Marta, Klara en Simon, ik wil jullie bedanken voor de AFM metingen die jullie voor mij gedaan hebben. Nicole en Jeroen, bedankt voor de SEM en TEM metingen die jullie voor mij gedaan hebben en Patrick voor je hulp bij de synthese van de dotjes. Jullie metingen hebben een grote bedrage geleverd aan mijn proefschrift.

Kristof Lodewijks en Bob Jakobs, ik wil jullie bedanken voor jullie inzet en interesse in het onderzoek, waardoor we samen veel geleerd hebben. Ik wens jullie veel succes in jullie carrière.

Veel plezier heb ik beleefd aan het organiseren van het SMO-uitje samen met Dirk, Nicole, Kelly en Joke. Het was zeer geslaagd! Verder wil ik Joke bedanken voor alle adminstratieve zaken die ze voor mij afgehandeld heeft. Dirk, Nicole en Kelly, veel plezier heb ik gehad op ons beachvolleybal weekend. Jeroen, samen hebben we veel plezier beleefd aan het organiseren van de wintersportvakanties. En ik heb met net zoveel plezier op de pistes rondgeskied. waar ik ook alle wintersporters voor wil bedanken.

Mijn kamergenoten van de eerste jaren, Waldo, Bea, Mark, Bastiaan en Andreea en ook mijn kamergenoten op mijn tweede kamer, Arjan, Wiljan, Johan en Itsuro wil ik bedanken voor de plezierige uurtjes tussen het harde werken door. Waldo, verder ook bedankt voor het doorgeven van al je kennis over zink oxides.

Geert, Annemarie, Willemijn, Kristel en Elly, jullie wil ik graag bedanken voor de interesse die jullie in mij getoond hebben gedurende de periode vanaf de middelbare school. Ik wens jullie allemaal veel succes met jullie eigen carrière en ik hoop dat onze vriendschap nog vele jaren mag duren.

Mijn paranimfen, Martijn en Marieken. Martijn wil ik graag bedanken voor de hulp en de vriendschap die nu al vele jaren duurt. Marieken wil ik verder ook bedanken voor het lezen van mijn proefschrift en het controleren op taalfouten en Engelse grammatica.

En tenslotte wil ik mijn ouders bedanken voor de steun en het vertrouwen dat ze me gegeven hebben in de afgelopen jaren.

**Frank**